ERODIBILITY BEHAVIOUR OF CEMENT-BENTONITE BARRIER MATERIAL CONTAINING PFA AND GGBS

By

MUHAMMAD AKBAR WALENNA

A thesis submitted to the University of Birmingham for the degree of DOCTOR OF PHILOSOPHY

The Department of Civil Engineering
School of Engineering
College of Engineering and Physical Sciences
University of Birmingham

August 2019

UNIVERSITY OF
BIRMINGHAM

University of Birmingham Research Archive

e-theses repository

This unpublished thesis/dissertation is copyright of the author and/or third parties. The intellectual property rights of the author or third parties in respect of this work are as defined by The Copyright Designs and Patents Act 1988 or as modified by any successor legislation.

Any use made of information contained in this thesis/dissertation must be in accordance with that legislation and must be properly acknowledged. Further distribution or reproduction in any format is prohibited without the permission of the copyright holder.

Abstract

Overtopping and internal erosion are two major causes of failure in earth and rockfill dams. Installing cement-bentonite barrier (CBB) is expected to minimise the likelihood of failure. CBB was reported to be susceptible to erosion and the resistance of the barriers against erosion is still poorly understood. This dissertation aims to provide an overview on the past researches pertaining to the methodology employed to assess erodibility behaviour of geomaterials and to improve the understanding the erodibility of CBB by investigating the parameters governed the erosion phenomenon. The previous researches on the erodibility of CBB was found to be problematic for several aspects: hydraulic condition, erodibility parameter, material composition, and test apparatus. This dissertation focuses to study the erodibility behaviour of CBB samples from two main parameters: hydraulic condition (pressure differential, flowrate) and erodibility parameters (hydraulic shear stress, velocity, eroded hole diameter/volume and erosion rate). These parameters were assessed under the varying mix proportion which mainly varying the GGBS percentage and curing duration (from 7 to 90 days). The erodibility parameters obtained from the test were correlated with other characteristics such as strength, moisture content and hydraulic fracture. In addition, the effect of confining pressure to the erodibility behaviour was also explored.

Keywords: Cement, Bentonite, Barrier, Seepage, Internal Erosion

Acknowledgement

First of all, I would like to express my deepest gratitude to my wonderful and very supportive supervisors: Dr. Alexander Royal, Prof. Ian Jefferson and Dr. Gurmel Ghataora for the supervision, helpful advices, constructive criticisms, enthusiasm and continuing support throughout the completion of my PhD study.

Secondly, I would like to express my gratitude to Indonesia Endowment Fund for Education, Ministry of Finance, The Republic of Indonesia for providing financial sponsorship for my doctoral study at The University of Birmingham.

Lastly, but not least, I would like to express my gratefulness for being my strongest support system, my family, especially to my late father, my mother, my brother and my sister who always encourage me to work hard and to finish my study.

Table of Content

Chapter 1 Introduction

1.1 Background I-1
1.1.1 Embankment Dams and Levee I-1
1.1.2 Vertical Cutoff Walls/Barriers I-1
1.2 Problems I-5
1.2.1 Potential Failure in Embankment Dams and Levee I-5
1.2.2 Potential Failure in Cutoff Barriers I-6
1.3 Aim and Objectives I-9
1.4 Thesis Layout I-10

Chapter 2 Literature Review

2.1 Introduction II-1
2.2 Cement-Bentonite (CB) Barrier II-2
2.3 Internal Erosion and Hydraulic Fracturing Mechanism within Soils II-5
2.4 Existing Laboratory Erosion Tests Used to Determine the Internal Erodibility Potential of Soils II-7
2.4.1 The Pinhole, Hole Erosion, Jet Erosion and Rotating Cylinder Tests II-7
2.4.2 Suggested Modifications and Improvements on the Erosion Test Apparatuses II-12
2.5 Erodibility Behaviour of Geomaterials (including concretes, Cement-Bentonite, Untreated and Treated Soil) II-17
2.5.1 Untreated and Non-Cemented Soils II-17
2.5.2 Cemented/Chemically Treated Soils II-20
2.5.3 Concrete and Plastic Concrete II-23
2.6 Erosion of CBB When Compared to other Cemented Soils or Concretes II-25
2.7 Previous Laboratory Studies into Internal Erosion of CB II-26
2.8 Conclusion II-30

Chapter 3 Methodology

3.1 Introduction III-1

3.2 Sample Preparation and Creation III-3

3.2.1 Material Specification III-3

3.2.2 Material Preparation III-5

3.2.3 Procedure III-6

3.2.4 Technical Consideration III-7

3.2.4.1 Curing Procedure III-7

3.2.4.2 Trimming III-8

3.2.4.3 Simulating Concentrated Leak III-10

3.3 Material Strength and Basic Properties Test III-11

3.3.1 Unconfined Compressive Strength III-11

3.3.2 Tensile Strength Test III-13

3.3.3 Hydraulic Fracturing III-14

3.3.4 Moisture Content III-18

3.3.5 Particle Density III-19

3.4 Erosion Test III-19

3.4.1 Concentrated Leak Erosion III-19

3.4.1.1 Introduction III-19

3.4.1.2 Pinhole Erosion Test III-20

3.4.1.3 Hole Erosion Test III-23

3.4.1.4 Technical Procedure III-24

3.4.1.5 Technical Consideration III-30

3.4.1.5.1 Hydraulic Head III-30

3.4.1.5.2 Valve Opening III-31

3.4.1.5.3 Flow and Pressure Reading III-32

3.4.1.5.4 Hole Casting III-33

3.4.1.6 Data Analysis III-34

3.4.1.6.1 Final Flow, Pressure and Hole Diameter III-34

3.4.1.6.2 Data Smoothing III-37

3.4.1.6.3 Hydraulic Shear Stress and Erosion Rate III-38

3.4.2 Modified Triaxial Erosion Test III-41
3.4.2.1 Introduction III-41
3.4.2.2 Technical Procedure III-41
3.4.2.3 Technical Consideration III-44
3.4.2.3.1 Confining Pressure Effect III-44
3.4.2.3.2 Flow and Pressure III-50
3.4.2.4 Data Analysis III-50
3.5 Scanning Electron Microscopy III-51
3.5.1 Technical Procedure III-51
3.5.2 Data Analysis III-51

Chapter 4 Results and Discussion

4.1 Introduction IV-1
4.2 Basic Properties and Material Strength Test IV-1
4.2.1 Particle Density IV-2
4.2.2 Unconfined Strength and Tensile Strength IV-3
4.2.3 Relationship between Particle Density and Strength Characteristics IV-14
4.2.4 Moisture Content IV-15
4.2.5 Relationship between Moisture Content and Strength Characteristics IV-17
4.2.6 Hydraulic Fracturing IV-17
4.3 Erosion Test IV-23
4.3.1 Concentrated Leak Erosion (Hole Erosion Test) IV-23
4.3.1.1 Non-Erodible Test IV-23
4.3.1.2 Juvenile Samples and Entrance Scouring IV-28
4.3.1.3 Pressure, Flowrate, and Hole Diameter IV-30
4.3.1.4 Erosion Data Analysis IV-40
4.3.1.5 Analysis of Erodibility Characteristics IV-45
4.3.2 Modified Triaxial Erosion Test IV-62
4.4 Scanning Electron Microscopy Test IV-67

Chapter 5 Summary

5.1 Conclusion and Future Work V-1

References

List of Table

Table 1.1 Comparison of properties between SB and CB I-4
Table 1.2 Cause or Condition of Failure I-7
Table 2.1 Recommended properties of bentonite-water slurry (Evans, 1993) II-2
Table 2.2 Loading types acting on the cutoff barrier (Wen et al., 2017) II-3
Table 2.3 Proposed approach to quantify the resultant thrust (Sing et al., 2006) II-4
Table 3.1 Summary of research objectives and proposed methodology III-2
Table 3.2 Composition of cement type CEM II/B-V III-4
Table 3.3 Properties of GGBS III-4
Table 3.4 Proportion of cementitious materials, bentonite and water in slurry sample (by weight) (A (Joshi et al., 2008) and (Joshi et al., 2010); B (Royal et al.,2013); C (Opdyke and Evans, 2005); D (Carreto et al., 2015) III-4
Table 3.5 CBB Mix Proportion III-5
Table 3.6 The CB samples sizing detail III-9
Table 3.7 The sample suitability for the hydraulic fracturing apparatus III-18
Table 3.8 The sample suitability for the triaxial modified apparatus III-42
Table 4.1 Particle Density IV-2
Table 4.2 Average Difference for Non-Erodible Sample IV-23
Table 4.4 Critical Hydraulic Shear Stress and Critical Velocity IV-57

List of Figure

Figure 1.1 Example of embankment dam zoning system with a slightly inclined core (typical dam design in Sweden). Zone 1: Core; Zone 2, 3, and 4: fine, medium and coarse filters; Zone 5: support fill (after Sjodahl, 2006) I-2
Figure 1.2 The installation of cutoff wall in the embankment (after USBR, 2014) I-3
Figure 1.3 Illustration of failure mechanisms involved in the failure of cutoff barriers in the dam, a) deformation due to differential water pressure, and b) increased gradients (after Rice and Duncan, 2010b) I-8
Figure 2.1 Schematic diagram of applied force on the barrier (Wen et al., 2017) II-3
Figure 2.2 Pinhole Erosion Test – simplified (redrawn from ASTM D4647) II-8
Figure 2.3 Hole Erosion Test (redrawn from Mehenni et al., 2016) II-8
Figure 2.4 Jet Erosion Test (redrawn from Henensal and Duchatel, 1990) II-11
Figure 2.5 Diagram of Rotating Cylinder Apparatus (after Lim, 2006) II-12
Figure 2.6 Suggested erodibility classification for soil and rock based on hydraulic shear stress (after Briaud, 2008) II-19
Figure 2.7 Suggested erodibility classification for soil and rock based on eroding fluid velocity (after Briaud, 2008) II-19
Figure 2.8 Erosion rate-hydraulic shear stress relationship for lime-treated silt (redrawn from Mehenni et al. (2016)) II-21
Figure 2.9 Erosion rate-hydraulic shear stress relationship for cement-treated silt (redrawn from Mehenni et al. (2016)) II-21
Figure 2.10 The required upstream pressure according to silty soil treatment type and composition (after Mehenni et al. (2016)) II-21
Figure 2.11 Erosion rate-hydraulic shear stress relationship for silty sand treatment using cement and lignosulfate (redrawn from Indraratna et al. (2008)) II-23
Figure 3.1 Unconfined Compressive Strength of Slag-Cement-Bentonite with variation on cementitious material proportion (10%, 15%, and 20%) and slag replacement (after Opdyke and Evans, 2005) III-5
Figure 3.2 The mixed CB slurry were transferred to acrylic moulds and temporarily III-6

Figure 3.3 CB samples submerged in water III-7
Figure 3.4 Samples covered by biofilm during curing III-8
Figure 3.5 Trimming apparatuses III-9
Figure 3.6 CB sample after 21 days curing III-10
Figure 3.7 Sample cross-section with hole in the centre and casted hole (using super glue) III-11
Figure 3.8 Typical UCS test result (CB with GGBS 80%) III-12
Figure 3.9 (a) Sample during UCS test, (b) and (c) Sample after failure III-13
Figure 3.10 Sample during tensile strength test (left) sample with hole (right) sample after fail III-14
Figure 3.11 Typical tensile test result (CB, 90 days old) III-14
Figure 3.12 The schematic diagram of hydraulic fracturing test apparatus III-16
Figure 3.13 (a) Testing was running, (b) Silicone grease was spread at both ends of sample to prevent leaking (c) The sample fails after hydraulic fracturing test, both ends were partially lost as they are attached/glued to the silicone grease (b) when the sample failed, the membrane expanded III-17
Figure 3.14 Typical data analysis for hydraulic fracturing test III-18
Figure 3.15 The schematic diagram of PET (after ASTM (2013)) III-20
Figure 3.16 The schematic diagram of PET used for this study III-22
Figure 3.17 PET results for CB sample (21 days curing) III-22
Figure 3.18 PET results for CB sample (21 days curing) III-22
Figure 3.19 The hardened cast of the eroded hole III-23
Figure 3.20 The schematic diagram and photographs of HET apparatus III-27
Figure 3.21 The relationship between pressure differential and flow rate against time (CB with GGBS 80%, 7 days curing) III-28
Figure 3.22 Turbidity observed at the downstream pipe III-28
Figure 3.23 Entrance sides of sample was flushed away by high upstream pressure III-28
Figure 3.24 Typical pressure differential and flow rate readings for no erosion III-29

Figure 3.25 Sample (a) before testing (b) after testing (c) suffered back-cuts at the downstream side III-29
Figure 3.26 (a) The cast of the eroded hole (b) Uniform hole
(c) Non-Uniform hole III-30
Figure 3.27 The relationship between hole diameter with flow rate
and pressure III-33
Figure 3.28 The results of wax casting on non-erodible hole sample III-33
Figure 3.29 Flowrate and pressure differential plotted against time
(CB, 90 days curing) III-34
Figure 3.30 The relationship between final differential pressure and curing age (CB without GGBS), 5-6 samples for each curing age III-35
Figure 3.31 The relationship between final flow rate and curing age (CB without GGBS), 5-6 samples for each curing age III-35
Figure 3.32 Hole diameter at intermediate time (CB without GGBS, 90 days) III-36
Figure 3.33 The relationship between final hole diameter and curing age (CB without GGBS), 5-6 samples for each curing age III-36
Figure 3.34 The readings from data loggers and smoothed data (CB with GGBS 80%, 7 days) III-38
Figure 3.35 The relationship of hydraulic shear stress, velocity and erosion rate during the test (CB without GGBS, 14 days) III-40
Figure 3.36 The relationship of erosion rate against hydraulic shear stress and velocity (CB without GGBS, 90 days) III-40
Figure 3.37 The modified triaxial erosion apparatus III-43
Figure 3.38 Double layer of membrane III-44
Figure 3.39 The sample after testing (fail due to buckling) III-44
Figure 3.40 the membrane expanded during the test III-45
Figure 3.41 Measurement of confining pressure (water) and air pressure from the bladder for the confining pressure of 50 kPa III-46
Figure 3.42 Measurement of upstream pressure, downstream pressure and pressure differential for the confining pressure of 50 kPa III-47

Figure 3.43 Measurement of confining pressure (water) and air pressure from the bladder for the confining pressure of 100 kPa III-47
Figure 3.44 Measurement of upstream pressure, downstream pressure and pressure differential for the confining pressure of 100 kPa III-48
Figure 3.45 Measurement of confining pressure (water) and air pressure from the bladder (Top), Measurement of upstream pressure, downstream pressure and pressure differential (Bottom) III-49
Figure 3.46 The sample failed during the test inside the membrane III-50
Figure 3.47 Result from the cryo-SEM test (CB with GGBS 80%, 56 days) III-51
Figure 4.1 Typical failure surface of the crack IV-3
Figure 4.2 The typical failure of the sample for (a) tensile strength (CB with GGBS 80%, 21 Days), (b) UCS (CB with GGBS 40%, 14 Days) IV-5
Figure 4.3 Stress-strain relationship for UCS test, CB with GGBS 40%
(3 representative results for each curing day) IV-6
Figure 4.4 Stress-strain relationship for Tensile Strength test, CB with GGBS 80%
(3 representative results for each curing day) IV-7
Figure 4.5 Average UCS and tensile strength test results (5-6 samples tested per curing period) IV-8
Figure 4.6 The relationship between unconfined compressive strength and tensile strength IV-8
Figure 4.7 The sequence of reaction between water, cementitious materials and bentonite (after Carreto et al., 2016) IV-10
Figure 4.8 Average UCS and tensile strength test results (5-6 samples tested per curing period) for samples with 3 mm hole in the centre IV-11
Figure 4.9 Impact of 3 mm hole/simulated crack in strength IV-12
Figure 4.10 Strain at failure/peak stress for strength test IV-13
Figure 4.11 Relevant UCS results from past studies IV-14
Figure 4.12 The relationship between particle density and strength IV-15
Figure 4.13 The oven-dried CB samples (CB without GGBS, 90 Days) IV-15
Figure 4.14 Moisture Content of CB samples with varying GGBS replacement (3 samples tested per curing period) IV-16

Figure 4.15 The relationship between moisture content and strength IV-17
Figure 4.16 Typical results for Hydraulic Fracturing test IV-18
Figure 4.17 Typical fracture after the hydraulic fracturing test: (A) cracks at the upper half of the sample (B) sample lost its lower half during sample extraction IV-20
Figure 4.18 Hydraulic fracture test for CB with GGBS 60%, 28 days IV-21
Figure 4.19 Comparison with past study by Ng (2009) IV-22
Figure 4.20 Average Difference for 3, 4, 5, and 6 mm Non-Erodible Hole (test repeated 2 times) IV-24
Figure 4.21 Average Difference for 8, 10, and 12 mm Non-Erodible Hole (test repeated 2 times) IV-25
Figure 4.22 The relationship between ΔP and Q IV-25
Figure 4.23 The relationship between differential pressure and flowrate for sample with hole diameter of 3, 4, 5, and 6 mm IV-26
Figure 4.24 The relationship between differential pressure and flowrate for sample with hole diameter of 8, 10, and 12 mm IV-27
Figure 4.25 The typical failure occurred at the entrance section for the test conducted under high upstream pressure to the juvenile (7-14 days) samples IV-29
Figure 4.26 Pressure differential measurement from pressure sensors (CB with GGBS 80%, 7 Days) IV-30
Figure 4.27 The relationship between peak pressure differential (A-C), final pressure differential (D-F), and curing age IV-31
Figure 4.28 The relationship between strength characteristics and peak/final ΔP (average values) IV-33
Figure 4.29 The relationship between curing duration and final flowrate/hole diameter (5-6 samples tested for each curing duration) IV-35
Figure 4.30 The relationship between final hole diameter and final flowrate/ΔP (average values) IV-36
Figure 4.31 The relationship between final flowrate and final ΔP IV-36
Figure 4.32 Casted eroded hole IV-37
Figure 4.33 The casted eroded hole (uniformly shaped and consistent hole diameter) IV-38

Figure 4.34 The casted eroded hole (inconsistent diameter size) IV-39
Figure 4.35 The casted eroded hole (deviation from the initial straight pre-casted hole) IV-39
Figure 4.36 Comparison of hole diameter from pre-determined testing duration and theoretical analysis (CB without GGBS) IV-41
Figure 4.37 Comparison of hole diameter from pre-determined testing duration and theoretical analysis (CB with GGBS 40%) IV-42
Figure 4.38 Comparison of hole diameter from pre-determined testing duration and theoretical analysis (CB with GGBS 60%) IV-43
Figure 4.39 Comparison of hole diameter from pre-determined testing duration and theoretical analysis (CB with GGBS 80%) IV-44
Figure 4.40 The relationship between hydraulic shear stress/velocity and erosion rate (CB without GGBS, 14 Days) IV-46
Figure 4.41 The impact of drilling method in the erosion test result (after Mehenni et al., 2016) IV-47
Figure 4.42 The erodibility parameters analysis for CB without GGBS,14 Days IV-48
Figure 4.43 The erodibility parameters analysis for CB without GGBS,28 Days IV-49
Figure 4.44 The erodibility parameters analysis for CB with GGBS 40%,7 Days IV-50
Figure 4.45 The erodibility parameters analysis for CB with GGBS 40%,56 Days IV-51
Figure 4.46 The erodibility parameters analysis for CB with GGBS 60%,14 Days IV-52
Figure 4.47 The erodibility parameters analysis for CB with GGBS 80%,7 Days IV-53
Figure 4.48 The erodibility parameters analysis for CB with GGBS 80%,18 Days IV-54
Figure 4.49 The erosion classification based on hydraulic shear stress (Briaud, 2008) IV-56
Figure 4.50 The erosion classification based on velocity (Briaud, 2008) IV-56
Figure 4.51 The relationship between curing age and critical hydraulic shear stress/velocity (5-6 sample per curing age) IV-58

Figure 4.52 The relationship between critical hydraulic shear stress and critical velocity IV-59
Figure 4.53 The relationship between unconfined compressive strength or tensile strength and critical hydraulic shear stress IV-59
Figure 4.54 The relationship between unconfined compressive strength or tensile strength and critical velocity IV-60
Figure 4.55 The relationship between moisture content and critical hydraulic shear stress or critical velocity IV-60
Figure 4.56 The relationship between critical hydraulic shear stress or critical velocity and eroded volume IV-61
Figure 4.57 The comparison of the current and past studies on the relationship between critical velocity and eroded volume IV-61
Figure 4.58 The modified triaxial erosion test result for CB with GGBS 40%, 21 Days IV-63
Figure 4.59 The modified triaxial erosion test result for CB with GGBS 40%, 56 Days IV-64
Figure 4.60 The impact of applied confining pressure in the peak differential pressure IV-64
Figure 4.61 The impact of applied confining pressure in the final differential pressure IV-65
Figure 4.62 The typical after test sample condition IV-66
Figure 4.63 CB without GGBS, 56 Days IV-67
Figure 4.64 CB with GGBS 40%, 56 Days IV-68
Figure 4.65 CB with GGBS 60%, 56 Days IV-69
Figure 4.66 CB with GGBS 80%, 56 Days IV-70

Chapter I
Introduction

1.1 Background

1.1.1 Embankment Dams and Levee

Embankment dam and levee are both structures that mainly function to retain water. Levee retains water from river or lake and its purpose is to protect the land from the potential hazard that can occur especially during the flood and storm (Osouli et al., 2014). Earth and rock materials are the major components used to build an embankment dam. There are two kinds of embankment dams based on the material selection: earthfill dams and rockfill dams. Earthfill dams are constructed by a single low permeability earth material, however this type of dam is commonly plagued with stability problem and it is therefore rarely chosen for designing high dam. The material used to build rockfill dams is dominated by crushed rock. Unlike earthfill dams, rockfill dams are comprised of several layers/zones (as seen in Figure 1.1) and mainly categorised into three based on their properties and function as seen in Figure 1.1 (Sjodahl, 2006):

- Core. The low permeability material such as clay, clayey sands and silty sands is usually chosen for this zone. The main function is to control water seepage through the dam.
- Filters. This zone prevents the material to mobilise from the core and also to prevent the pore water pressure build up at the downstream side of the core by draining the water seeping to the core. Gravelly sand and sandy gravel usually chosen for this zone.
- Support fill. The dam stability is maintained by this layer and mainly constructed using crushed rock.

1.1.2 Vertical Cutoff Walls/Barriers

The principal use of vertical cutoff walls or barriers in civil engineering structures such as embankment dam or levee is to manage the mobilisation of groundwater and contaminants that move horizontally (Evans, 1993). Cutoff barriers are commonly installed as modifications to the existing dam or levee, but it can also be incorporated as

a part of the structure design (USBR, 2014). Due to the difficulty to observe the completed barriers as they are placed in the subsurface region, the seepage control scheme should not only rely on the walls installation, but they should be design along with appropriate The design criteria of the walls should be tailored with their objectives. If the walls aim to deal with contaminant movement, the impact of the contaminant to the walls and the rate and the mode of contaminant's movement to the wall should be the major concerns considered in the design, whereas the hydraulic condition in the embankment should be adequately understood if the walls aim to minimise the groundwater movement (Evans, 1993). If the walls are expected to be structurally solid during excavation, it is commonly designed with reinforced concrete (Xanthakos, 1979).

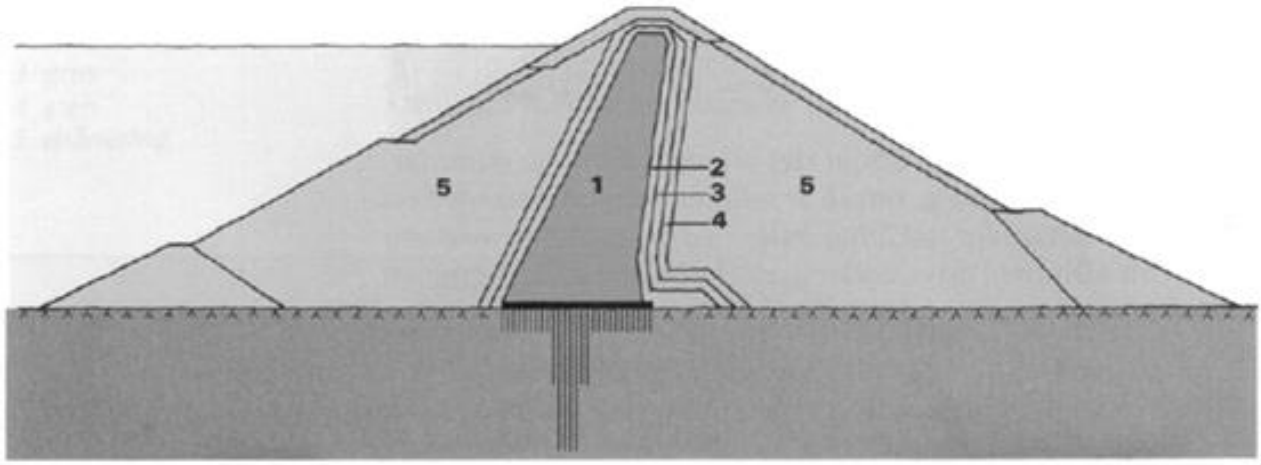
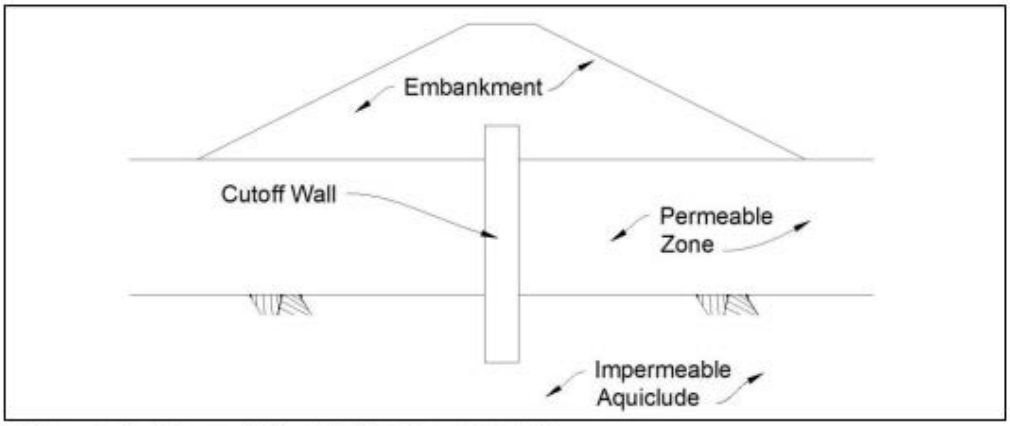


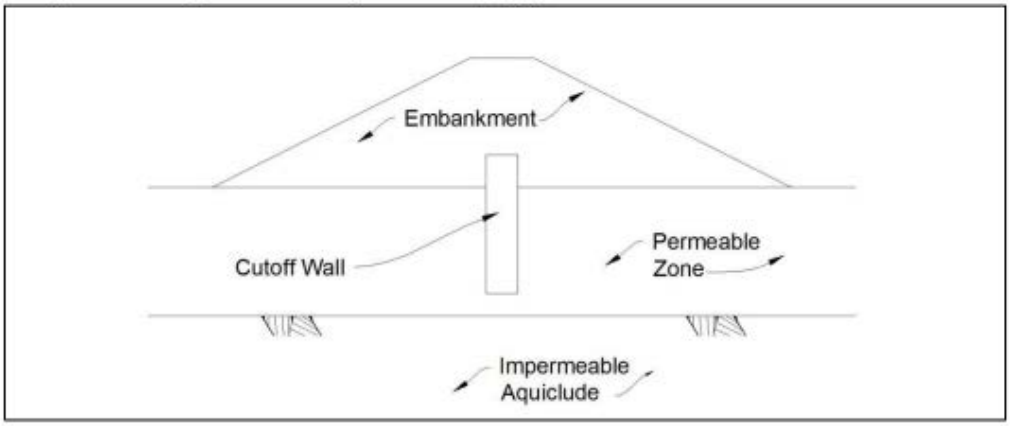
Figure 1.1 Example of embankment dam zoning system with a slightly inclined core (typical dam design in Sweden). Zone 1: Core; Zone 2, 3, and 4: fine, medium and coarse filters; Zone 5: support fill (after Sjodahl, 2006)

Cutoff walls are recommended to fully penetrate the pervious strata to achieve its optimum effectivity, however in certain circumstance it is designed to only partially penetrate (USBR, 2014). As seen in Fig 1.2, the fully penetrating cutoff walls principally aims to blocks the seepage path whereas, the partially penetrating one is to lengthens the seepage path. An estimate of 20% of seepage quantity can be reduced if the cutoff walls penetrate 50% of the pervious stratus. The hydraulic gradients at the wall interface

and around the end of the wall must be adequately understood as the increase of gradients should be expected at the end of cutoff walls.



Fully penetrating cutoff wall (blocks seepage)



Partially penetrating cutoff wall (lengthens seepage path)

Figure 1.2 The installation of cutoff wall in the embankment (after USBR, 2014)

The vertical cutoff barriers commonly have low hydraulic conductivity and they are categorised based on the construction method: slurry trench method, grouting method, and composite techniques (Evans, 1993). This thesis focuses on the walls constructed via slurry trench method in which a bentonite-water slurry is poured into the excavated trench. Depending on the material added to the slurry, the finished wall can vary such as soil-bentonite (SB), cement-bentonite (CB), plastic concrete, and structurally reinforced concrete. Specifically, CB barrier is the main concern of this thesis. As detailed in Table 1.1, several advantages of CB compared to SB are the structural strength, less working construction area, and less solids content (Opydke and Evans, 2005). The size of CB

barriers can vary depending on the design consideration, they are typically 0.6 m and 12 m in width and depth, respectively. For example, CB barrier installed in Diamond Creek Dike in Wyoming is 0.61 m wide and 47.5 m deep (6 m penetrated the bedrock) while the CB barrier in A.V. Watkins Dams in Utah is 0.76 m and 20 m in width and depth, respectively (USBR, 2014). If the deeper excavation required, the wall construction is conducted in a double phase because the bentonite slurry is used to maintain the trench stability before CB fill the trench (Jefferis, 1997).

Table 1.1 Comparison of properties between SB and CB (after Opdyke and Evans, 2005)

Element	SB	Slag-CB
Barrier composition	SB	CB
Hydraulic conductivity	$<10^{-7}$ cm/s	$<10^{-7}$ cm/s after 90 days
Solids content	~70%	~20%
Unconfined compressive strength	~0	>100 kPa @ 28 days
Strain to failure	Plastic	Brittle
Time dependency	Consolidation: Rapidly (within a few days)	Initial set: Within one day, Complete hydration reactions: 90 days or more
Construction stages	Two phase	One phase
Excavation equipment	Backhoe, clamshell	Backhoe, clamshell
Depth (typical)	20 m	15 m
Width (typical)	0.75 m	0.6 m
Length (typical)	>1 km	<1 km
Working space needed	Large for slurry plant and backfill mixing	Small for slurry plant and excavation spoil disposal
Material assessment	Hydraulic conductivity, compatibility	Hydraulic conductivity, strength, strain at failure, compatibility

The cementitious materials other than cement such as pulverized fuel ash (PFA) or ground granulated blastfurnace slag (GGBS) or pulverized fuel ash are commonly added to the bentonite-water slurry and this is widely used barrier type in the UK. In the US, there has been a trend to shift from the SB to CB barrier containing slag or GGBS (Evans and Opdyke, 2005). Jefferis (1981 and 1997), Guner (1978), Evans (1994) and Opdyke and Evans (2005) reported that incorporating GGBS in the CB mixture by replacing 65-80% contributed to the reduction of hydraulic conductivity and the improvement in

strength. They also suggested that the cementitious material and bentonite incorporated should be approximately at 20% and 3-4% respectively to achieve optimum improvement of the material.

1.2 Problems

1.2.1 Potential Failure in Embankment Dams and Levee

The common types of failure that causes the most safety concern in dam, levee or any water retaining structures are overtopping and internal erosion (ICOLD, 1995; Foster et al., 2000; Bonelli and Benahmed, 2011; Eddleston and Wan, 2014; Fell et al., 2018). A significant proportion of embankment (used to control water) and earth dam failures: 31% and 48 %, respectively (ICOLD, 1995; Foster et al., 2000), have been attributed to internal erosion (often piping, but also via suffusion or via the formation of sink holes). Internal erosion is considered to be the second largest cases of earth dam failures after overtopping, with both failures' modes dominate over 60%-70% the failure cases (Singh, 1996; Xu and Zhang, 2009).

Although the risk of dam failure associated with flooding and overtopping has been well studied and researched in the past, improving the understanding of the failure due to internal erosion or piping failure is still considered critically important (Bonelli and Benahmed, 2011). Richards and Reddy (2007) suggested that the absent of an understanding on the seepage mechanism and material zonation for filter system in dam as the causes of the failure for dams constructed dated back to 19th and 20th centuries, however this led to the improvement in material selection and design for the dam construction.

The failure of dam, levee, and any water-retaining structures has continually caused concerned due to the damage it caused. For a large dam situated in densely populated are such as West London, the damage is estimated to cost over £1 billion (Warren, 2011). The failure also poses substantial threat to life of people, especially those who are in the close proximity to the dam such as in the United Kingdom where these dams are located nearby the densely populated industrial area (Charles and Boden, 1985). Teton Dam

failure caused the death of 11 people and property damage amounted to 400 millions dollars (USBR, 2016). The hydraulic fracture was responsible for the crack formation in the dam core that led to failure due internal erosion in the case of Teton Dam in 1976 (Chang, 2012). The reservoir safety legislation was introduced in the UK in 1930 despite the major dam failure occurred over half century ago, Dyle Dam at Sheffield, killing 244 people and followed by other failures in Dolgarrof and Skelmorlie in 1925. Despite its introduction, the dam failure still becomes a crucial issue that require appropriate preventive measure to minimise its likelihood in the future.

Understanding the cause of the dam and embankment failure is critically important as it helps in identifying the necessary design and construction steps that should be considered as well as anticipating the possible source of failure. There are many factors that can lead to the failure of dam and those factors, in general, can be categorised into several causes: the construction material selection, construction monitoring and quality control, maintenance scheme, loading condition, landslide phenomenon, and the fluctuating hydrological and environmental condition (Warren, 2011; Chang, 2011). Warren (2011) suggested that the water movement through the crack and fissures that occur within embankment dam is the main trigger for its failure. The defects in soil used for embankment or levee construction, regardless of the type, should be expected considering its exposure to change, extreme to some extent, in weather and stress condition. Identifying the cracks/defects can be challenging especially if they occur inside the dam and the failure has already been progressing; this is precisely the reason that the failure can only be dealt with after it is happening. Therefore, it is crucial for the engineers to have an understanding on the possible defects in the dam in order to help them designing the appropriate maintenance and monitoring scheme for the constructed dam.

1.2.2 Potential Failure in Cutoff Barriers

Despite its function to maintain and improve the performance of embankment dam or levee, past studies (e.g. Rice and Duncan, 2010a, 2010b; Hinchberger et al. 2010; Wen et al., 2017; Guyer, 2019) suggested that cutoff barriers are susceptible to cracking under

certain hydraulic condition and causes as detailed in Table 1.2. They suggest that the change of hydraulic and loading condition in the structure system caused the barrier to crack and it potentially leads to internal erosion.

Table 1.2 Cause or Condition of Failure

Author	Cause or Condition of Failure
Rice and Duncan (2010a, 2010b)	- The change in pore pressure regime - The crack can form when the tensile stresses are larger than the tensile of the barrier - The increase of hydraulic pressure and gradients causes cracking - The crack can lead to erosion of barrier material or surrounding material, fill material and foundation materials
Hinchberger et al. (2010) and Wen et al. (2017)	- During the construction and reservoir filling stage, the loads (dam structure and water) acting on the dam compress the barrier and the barrier experience significant plastic straining that lead to crack formation - The crack, as small as 1 mm, can cause to the increase (up to 2-3 orders of magnitude) of hydraulic conductivity of barrier and the erosion potential
Guyer (2019)	- The increase brittleness of the barrier can cause the increase susceptibility to crack formation - The cracking is likely to form under bending strains and seismic loading - The cracking decreases the erosion resistance of the barrier

Figure 1.3 shows the mechanism introduced to the barrier when installed in the dam. The construction of the barrier causes a dramatic increase in the differential water pressure between upstream and downstream of the structure which cause the water pressure to concentrate on the wall, surrounding soils and bedrocks leading to the straining and deformation of the material. The difference in stiffness between the barrier material and surrounding structure's material and bedrock cause the high bending moments and large tensile stress in the barrier (Rice and Duncan, 2010b).

Past studies had investigated the other factors causing the crack formation in cutoff barrier, CB in particular, such as hydraulic fracturing (Ng, 2009), desiccation (Jefferis, 2012; Royal et al., 2018), chemical weathering (Joshi et al., 2010), etc. Ng (2009) suggested that the crack formation in the CB is governed by the confining pressures,

injection rate, stress condition, curing and mix proportion. However, the investigation was only limited to old CB samples (> 90 days), hence the susceptibility of barrier at younger age to the hydraulic fracturing should be investigated. Furthermore, as suggested in the previous paragraph, the crack formation and erosion phenomenon occur sequentially, this raises a question on how parameters governed the potential of hydraulic fracturing impacting the erosion phenomenon.

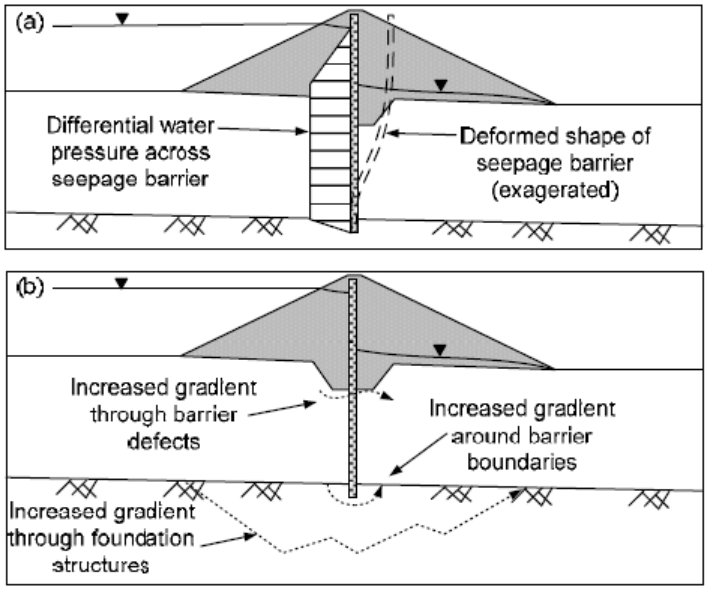


Figure 1.3 Illustration of failure mechanisms involved in the failure of cutoff barriers in the dam, a) deformation due to differential water pressure, and b) increased gradients (after Rice and Duncan, 2010b)

Erosion of CB barrier has been investigated by several studies (e.g. Beier and Strobl, 1985; Garand et al., 2006; Braithwaite, 2013, Wang et al., 2017). Beier and Strobl (1985) suggested that calcium leaching is the principal mechanism to represent erosion phenomenon in CB barrier, however they neglected the role of hydraulic forces of the eroding fluid in the erosion process. Garand et al, (2006) and Braithwaite (2013) investigated the effect of mix proportion on the relationship between eroded mass with time and hydraulic condition. Both studies suggested that under the applied water velocity and testing time of the studies, the CB material would erode but did not take into account the change of velocity due to the change of eroded hole size in the hole during the erosion

process and how it impacted the erosion behavior of the barrier material. While the previous studies did not consider the effect of incorporating GGBS in CB barrier on its erosion resistant characteristics, Wang et al. (2017) studied how the change of GGBS proportion affect the erodibility of CB barrier. However, the study suffered from then lack of hydraulic condition variation applied to the tested barrier material (all samples were tested under the flowrate of 3 L/min). Furthermore, the test did not also consider the change of eroded hole throughout the test that could change the hydraulic condition. All past studies did not also consider the role of shear stress of caused by the interaction between the material surface and eroding fluid in the erosion process. In conclusion, the past studies leave several critical questions regarding the erodibility of CB behaviour remain unanswered:

- How the curing duration and the incorporation of GGBS in the CB barrier mixture affect the erodibility behaviour of CB?
- How the change of hydraulic condition and parameters during the erosion phenomenon affect the erosion resistance of CB?
- How the change of stress condition (e.g. confining pressure) around the barrier affect the erodibility characteristic of CB?

In addition to the questions above, it is also crucial to investigate the relationship between basic properties/the strength characteristic and the erodibility characteristics in order to have better understanding of the CB material behaviour.

1.3 Aims and Objectives

As discussed previously, cracking and erosion are both critical issue that should be expected to occur in the installation of cutoff barrier in the dam. Previous relevant studies are deemed not representative in characterising the erodibility behaviour CB barrier due to the varying CB mixture proportion, the lack of consideration on curing period, the problem in apparatus model the erosion process, and the use of non-representative erodibility. Therefore, the aim of this study is:

To investigate the erodibility of CB barrier containing PFA and GGBS under the varying mix proportion and curing period

In view of concern and problem described in Section 1.2, there is a need to investigate the erodibility behaviour of CB material and to expand this understanding using more representative erosion test method and apparatus. To achieve the aim of this research, the several objectives were formulated:

- Conducting literature review on the erosion process, particularly concentrated leak erosion, relevant laboratory-scale works, and analysing the extent of the research for the relevant geomaterials.
- Developing an understanding on the effect of curing period and changing mix proportion to the CB basic properties and strength by performing series of laboratory standard test.
- Developing a laboratory apparatus for investigating the hydraulic fracturing phenomenon in CB
- Developing a laboratory apparatus for the erosion test for measuring and obtaining erosion parameters which are used to represent the erodibility characteristics
- Evaluate the effect of curing period and changing mix proportion to the erodibility characteristic of CB
- Developing a laboratory apparatus for investigating the effect of confining pressure during the erosion test
- Establishing relationships between basic properties, strength, hydraulic fracture to erodibility characteristic of CB
- Summarising and making conclusions based on the results

1.4 Thesis Layout

This dissertation is divided into 5 chapters and a brief description of each chapter is described as follows:

Chapter 1 gives the background information and the aim/objectives of this research work

Chapter 2 focuses to provide a literature review on the past research pertaining to internal erosion, hydraulic fracturing, existing laboratory apparatus used in erosion test, and the erodibility behaviour of relevant geomaterials

Chapter 3 describes the methodology used in basic properties, strength, and erodibility test. The procedure, technical consideration, and technical difficulties encountered during the apparatus development and laboratory testing are discussed in this chapter. The limitation and assumption adopted for this research is explained and justified.

Chapter 4 provides the results obtained from the test. The results are analysed in order to understand how they are correlated to each other and to analyse how they help to improve the understanding on the erodibility behaviour of CB materials.

Chapter 5 summarises this thesis and recommends future work

The appendices include all the detailed results of the laboratory test: basic properties, strength, erodibility and microstructure. The analysis of the erodibility test results is also presented in this section.

Chapter 2

Literature Review

2.1 Introduction

Internal erosion of geotechnical structures used to control groundwater flow, or retain surface water (such as earth dams, levees, etc.) is a significant geohazard. A significant proportion of embankment (used to control water) and earth dam failures: 31% and 48 %, respectively (ICOLD, 1995; Foster et al., 2000), have been attributed to internal erosion (often piping, but also via suffusion or via the formation of sink holes). Internal erosion is considered to be the second largest cases of earth dam failures after overtopping, with both failure modes dominate over 60%-70% the failure cases (Singh, 1996; Xu and Zhang, 2009). In the UK, there are 2120 large earth dams registered under the Reservoir Act of 1975. Large is defined as dam with retaining capacity of at least 25,000 m3 of water according to Reservoir Act of 1975 or any dam with height over 15 meters or height between 10-15 metres with the capacity and the maximum flood discharge at least 1,000,000 m3 and 2000 m2/s respectively (ICOLD, 2011). These dams have been constructed over a significant period of time (some of these dams predate and there are hundreds of them in the UK which were constructed during the Victorian period according to British Dam Society) and using varying designs and construction techniques. Over time these earth structures may degrade, reducing the ability to retard the movement of groundwater and hence increasing the risk of failure via internal erosion. Draining the reservoir and demolishing the existing earth dam before constructing a new dam is likely to be an unsustainable solution in many instances, therefore cement-bentonite barriers (CBB) have been installed within existing earth dams to introduce a new low permeability structure and hence reduce the risk of internal erosion (Rice, 2007; Rice and Duncan, 2010; ICOLD, 2013).

2.2 Cement-Bentonite (CB) Barrier

Cutoff barrier, in general, have some practical application if it is designed as a part of embankment dams or canal levees structures and according USBR (2014) cutoff barriers are grouped into 6 categories:

1. Earth-backfilled slurry trench cutoff barrier (SB)
2. CB cutoff barrier and soil-cement-bentonite (SCB)

3. Concrete cutoff walls including plastic concrete cutoff barriers
4. Geomembrane cutoff barriers
5. Deep soil mixing (DSM) cutoff barriers
6. Others: includes secant pile, sheet pile, and jet grouted cutoff barriers

Although all types of cutoff barrier are expected to serves as positive seepage cutoff, the design and the selection of the barrier type should consider in situ foundation conditions, hydraulic gradients, constructability issues, groundwater conditions, and economic conditions (USBR, 2014). For the focus of this thesis, this chapter focus on the CB barrier. As discussed in the previous chapter (Section 1.1), CB cutoff barrier is installed as means to control and reduce the seepage by dissipating seepage energy at the upstream side of the dam at which the high pore water pressure and high seepage gradients are expected (USBR, 2014). CB barrier containing GGBS is more commonly used in the UK as an option for seepage barrier, but the use of slag has seen an increasing trend in the US (Opdyke and Evans, 2005).

The recommended properties of bentonite-water slurry for CB is detailed in Table 2.1. According to BGS (2019), at the depth of 100 m, the mean ground temperature can vary about 7-15 degree Celsius. Depending on the season, the ground temperature is higher and lower than air temperature during winter and summer, respectively. As CB walls are set in subsurface, the curing temperature is contingent upon the ground temperature.

Table 2.1 Recommended properties of bentonite-water slurry (Evans, 1993)

Parameter	Bentonite slurry		Cement-Bentonite slurry	
	as-mixed	during excavation	as-mixed	during excavation
Density (g/cm^3)	1.01-1.04	<(**β** backfill -0.25)	1.1-1.24	1.1-1.4
Viscosity, apparent (Seconds Marsh)	32-40	38-68	40-45	38-80
Filtrate loss, ml	<25		100-300	
pH	7.5-12	10.5-12	12-13	
Bentonite content, % by weight	4-7	~6	4-7	
Other ingredients, % by weight	sand, <1	sand, <5	cement, 15-30	

To understand the behaviour of cutoff barrier, it is important to consider the response of the barrier against the horizontal and vertical loads (Wen et al., 2017). Table 2.2 and Figure 2.1 detailed the loading types acting on the cutoff barrier and the mechanism associated with them. Wen et al. (2017) suggested that a considerable amount of differential settlement should be expected due to the difference on the degree of compressibility between wall and surrounding soil which lead to the significant shear force at the interfaces. According to Dascal (1979), the vertical stresses acting on the barrier are attributed to the shear stress up 85%.

Table 2.2 Loading types acting on the cutoff barrier (Wen et al., 2017)

Loading type	Source	Associated Mechanism
Horizontal	Water head pressure	Seepage flow
	Lateral earth pressure	Horizontal displacement
		Dam location
		Dam compaction
Vertical	Self-weight of the wall	
	Vertical earth pressure	Pressure from the filling at the top of the wall
	Vertical water pressure	
	Shear force	Settlement
		Lateral earth pressure

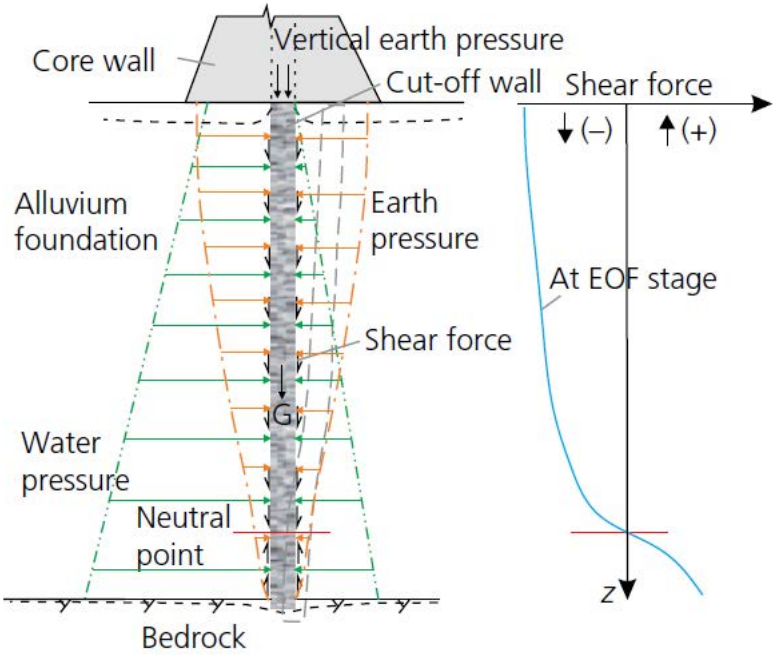


Figure 2.1 Schematic diagram of applied force on the barrier (Wen et al., 2017)

Singh et al. (2006) proposed an approach to quantify the resultant thrust acting on the barrier and Table 2.3 specified the steps and equations to estimate it.

Table 2.3 Proposed approach to quantify the resultant thrust (Sing et al., 2006)

Type	Equation
Active Thrust	$W-(C_F+T_1)\sin\theta-\bar{N}_1\cos\theta+F_S\cos\alpha=0$ (1)
	$\bar{N}_1\sin\theta-(C_F+T_1)\cos\theta-\bar{P}_a+R+F_S\sin\alpha=0$ (2)
Passive Thrust	$W+(C_F+T)\sin\theta-\bar{N}\cos\theta-F_S\cos\alpha=0$ (3)
	$\bar{P}_p-\bar{N}\sin\theta-(C_F+T)\cos\theta+F_S\sin\alpha=0$ (4)
Unbalanced Water Force	$F_{uw}=F_1-F_2$ (5)
Resultant Thrust	$T_r=F_{uw}+(P_a-P_p)$ (6)

where W= the weights, Fs= seepage force, α = angle made by seepage force with vertical, Pa = resultant of distributed stresses between the soil and barrier acting on the upstream side, Pp = resultant of distributed stresses between the soil and barrier acting on the upstream side, F1 and F2 = forces developed due to the water pressure in the upstream and downstream side.

Singh et al. (2006) estimated that the resultant thrust acting on the barrier can vary from approximately 103.3 kN/m to 235.9 kN/m with the variation of water level at the upstream about 10-20 m for the selected material properties. Ng (2009) suggested that the range of confining pressure applied to the CB barrier for the hydraulic fracturing test is varying from 45 – 150 kPa.

CBBs have been used due to the relatively simple construction methods used to install them within the existing earth structure, resulting in comparatively rapid installation against other remediation techniques (Dinchak, 1985; ICE, 1999; Jefferis, 1997, 2012); the self-supporting nature of the barrier whilst the cementitious materials harden; and the low hydraulic conductivities achieved once cured. However, a potential uncertainty with all cement-treated materials is their durability, especially when applied in chemically aggressive environments (Fratalocchi et al., 1996, 2006). The performance of cut-off barrier should satisfy three important design criteria throughout its engineering life, it must achieve and maintain: a low hydraulic conductivity, acceptable deformation characteristics and continued permanence (i.e. the performance of the barrier should be sustained corresponding to the life of structure, in this case earth dam or leeve) (Millet et al., 1992). It is important that the walls are not only impermeable and possess

appropriate strength, but also resistant to erosion and chemical weathering (Brandl, 1996).

Deterioration of man-made assets is a fundamental concept in engineering (hence the use of engineering life during design) and CBBs clearly will deteriorate over time, yet the deterioration of Cement Bentonite (CB) in situ is poorly understood. Hence, the resilience of CBB has been a concern for engineers: the potential susceptibility of CBB to shrinkage cracking with drying/desiccation (Jefferis, 2012; Royal et al., 2018), hydraulic fracturing (Ng, 2009), internal erosion (Rice and Duncan, 2010; ICOLD, 2013; Braithwaite, 2013) and chemical weathering (Joshi et al., 2010) raises concern due to the increase potential for deterioration (and if used in an hydraulic structure, such as an earth dam, potentially increased susceptibility to erosion). If CBB is used in earth dams to improve the safety of the structure against internal erosion, the vulnerability of CBB against internal erosion should also be considered.

The research pertaining to the erodibility of CBB is not comprehensive, although erosion of other materials used in geotechnical applications (e.g. silts, clays, sands, etc.) have been extensively studied (e.g. Haghighi et al., 2013; Mehenni et al., 2016; Fattahi et al., 2017) and it is possible that knowledge gained from this research effort could be applied to understanding how CBB may resist internal erosion. This paper, therefore, reviews the existing understanding of internal erosion mechanisms of soil to determine if lessons learned could be applied to help understanding of the CBB erodibility.

2.3 Internal Erosion and Hydraulic Fracturing Mechanism within Soils

Internal erosion takes place when water seeps through a soil and has been extensively studied in the field of earth embankments and dams (e.g. Burns, 2006; Rodney, 2008; Mattsson et al., 2008; Flores-Berrones and Lopez-Acosta, 2011; Chang, 2012; Sharif, 2013). There are three key factors that trigger internal erosion: hydraulic condition (e.g.

hydraulic gradient, flow velocity), stress condition, and material properties (e.g. plasticity, particle size) (Garner and Fannin, 2010). The mechanism of internal erosion initiation can involve suffusion, concentrated leak erosion (piping), backward erosion, and contact erosion (Fell and Fry, 2013). Piping involves the flowing fluid eroding a stable void, or pipe, within the soil. This mechanism is reliant on the surrounding soil arching to ensure load transfer within the soil changes so that the pipe does not collapse; in so doing the fluid flowing in the pipe losses far less energy than it would do so seeping through unaffected soil, hence the shearing capacity of the fluid increases significantly. Suffusion involves the removal of the smaller sized particles from the soil fabric; the larger particles remain in place and load distribution continues to be transferred through the modified soil skeleton but the hydraulic conductivity of the affected soil increases, potentially increasing the fluid flow through the soil. Both these mechanisms often propagate backwards from an initiating point within the soil: for example, at the interface between two soils of markedly different permeability. Contact erosion takes place at interfaces between two soil types (i.e. high and low permeability soils) forming a void (i.e. at the interface between low permeability core and filter drain) that may propagate backwards to form piping/suffusion.

Marot et al. (2012) and Reggazoni and Marot (2013) suggest that internal erosion of soil is triggered by “the power dissipated by the fluid flow throughout the porous solid phase”. The erosion process involves the removal of particles from the soil skeleton via hydraulic shear stresses created by the flow of the eroding fluid at the rock-water interface. Especially for turbulent flow, greater and more localised shear stresses can be generated (Nearing, 1991). However, it is suggested that the erodibility of soil and rock should be related to the relationship between erosion rate and shear stress rather than erosion and velocity. This is because the velocity within the pore is non-uniform, and as such varies in direction and intensity in the flow field (and thus is difficult to quantify within the pore space) (Briaud, 2008). The susceptibility of soils to erosion is also linked to their tensile strength. This is because, at the soil-water interface, the resisting force of soils required to withstand the pulling/detachment force (i.e. hydraulic shear stress) from eroding fluid depends on their tensile strength (Nearing, 1991). Therefore, tensile failure is an important mechanism in particle detachment.

Hydraulic fracturing has been attributed as one of the potential causes in dam's failure and it involves the development of tension cracks within cohesive soils (or cemented soils) when the water pressure within the soil exceeds the tensile strength of the soil and has been investigated for the earth dam and shallow drilling applications (Wang et al., 2009; Tedd et al., 2011; Fell and Fry, 2013; Ghanbari and Rad, 2015; ICOLD, 2015; Chang and Huang, 2015). The case of hydraulic fracturing in CBB had been investigated by Soga et al. (2013) and suggested that the fracture in CBB should be expected when it is subjected to fluid pressure (Pf) which is calculated as (Mitchell and Soga, 2005):

$$P_f = 2\sigma'_{3_i} + u'_0 + \sigma_t' \quad (7)$$

σt, σ3, and uo represents tensile capacity, initial minor principal effective stress and pore pressure of soil. Therefore, the hydraulic fracturing phenomenon in CBB is mainly governed by its stress condition and tensile strength. Furthermore, as the consequence of hydraulic fracturing, the risk of water to seep through the crack and expand the crack size should be anticipated (Soga et al., 2013).

Therefore, the flow rate of the eroding fluid, the hydraulic shear stress, the tensile strength and contact shear strength of the soil are key parameters with respect to the erodibility behaviour of geomaterials.

2.4 Existing Laboratory Erosion Tests Used to Determine the Internal Erodibility Potential of Soils

2.4.1 The Pinhole, Hole Erosion, Jet Erosion and Rotating Cylinder Tests

The common laboratory based tests for internal erosion are usually based on the Pinhole Erosion Test (PET: developed by Sherard et al.,1976), the Hole Erosion Test (HET: developed by Wan and Fell, 2002), the Jet Erosion Tests (JET) (JET and Mobile JET developed by Hanson (1991, 1992) and Henensal and Duchatel (1990), respectively), and the Rotating Cylinder Test (RCT) by Lim (2006).

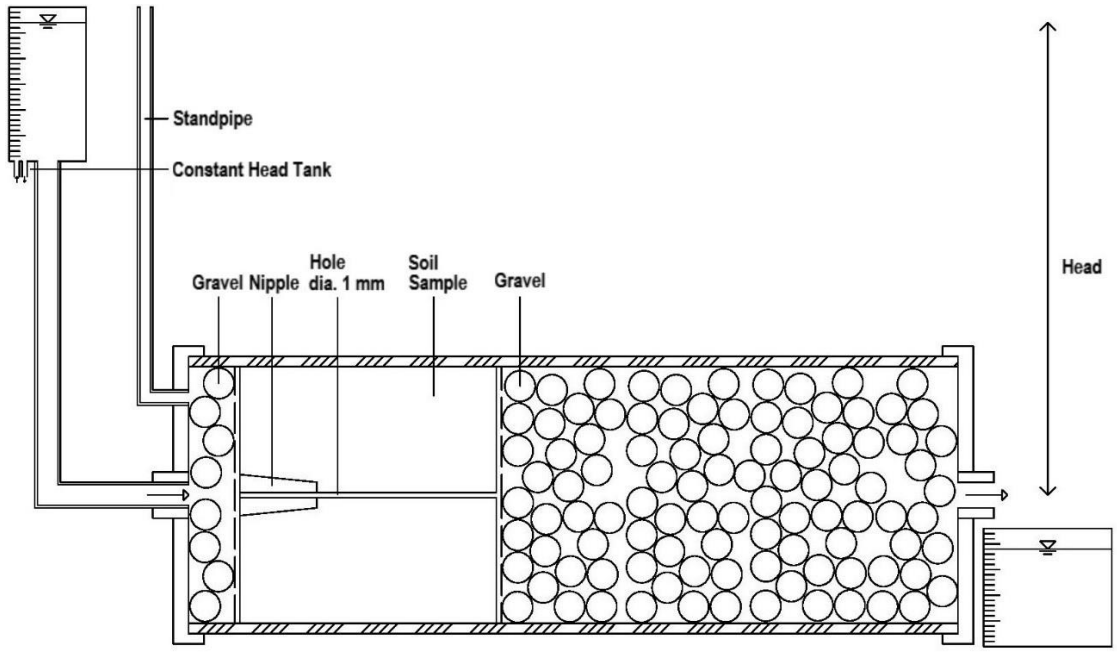


Figure 2.2 Pinhole Erosion Test – simplified (redrawn from ASTM D4647)

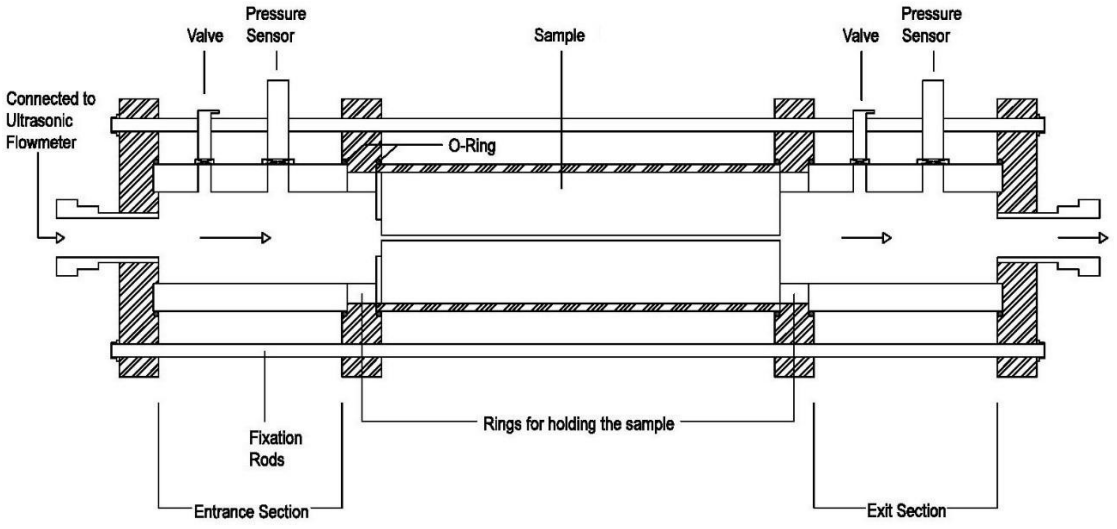


Figure 2.3 Hole Erosion Test (redrawn from Mehenni et al., 2016)

Both PET and HET simulate the erosion occurring due to fluid flow in concentrated leak in the soil sample (Figure 2.2 and Figure 2.3). The main objective of PET is to qualitatively assess the effect of varying eroding fluid hydraulic head to the turbidity or cloudiness of water exiting the sample; the high turbidity, indicated by darker colour of water, suggests a weak resistance to erosion (ASTM, 2013). However, other researchers had attempted to employ alternative approaches in their analysis:

studying the enlargement of predrilled hole due to erosion and erosion progression

using resistivity measurement (Burns, 2006), investigating the relationship between varying hydraulic head and flow discharge to erosion rate (Nadal-Romero et al., 2011). If the objective is to investigate the hydraulic condition required to initiate the erosion on the sample with high resistance to erosion, PET is not suitable as the applied hydraulic heads at the upstream is limited by the maximum height of standpipe; ranging from 50 mm to 1080 mm (e.g. Sherard et al, 1976; Fauzilah et al, 2008). Therefore, PET is only recommended to be used for dispersive material. Unlike PET, HET is more quantitative in investigating the erosion phenomenon. Wan and Fell (2004) focused on two main parameters: hydraulic shear stress τ (Pa) (Equation 8) and erosion rate ε (kg/s/m^2) (Equation 9).

$$\tau = \rho_w g \left(\frac{\phi_t}{4}\right) i \quad (8)$$

$$\varepsilon = \frac{\rho_d}{2}\frac{d\phi_t}{dt} \quad (9)$$

$$\phi_t = \left(\frac{16 Q_t f_{L_t}}{\pi \rho_w g i}\right)^{\frac{1}{3}} \text{(laminar)} \quad \phi_t = \left(\frac{64 Q_t^2 f_{T_t}}{\pi^2 \rho_w g i}\right)^{\frac{1}{5}} \text{(turbulent)} \quad (10)$$

where ρ_w is water density, ρ_d is sample dry density, g is gravity acceleration, i is hydraulic gradient across the sample, ϕ_t is diameter of pre-drilled hole at time t, Q_t is flow rate at time t, and f_{Lt} and f_{Tt} are friction factors for laminar and turbulent flow at time t. Unlike PET which only measure hydraulic head at the upstream side, HET measured the hydraulic head difference at both ends of the sample. Although HET setup used by Wan and Fell (2004) only employed standpipes, thus restricting the maximum hydraulic heads measured, other researchers such as Haghighi et al. (2013) Mehenni et al. (2016) replaced them with pressure transducers and allowing the test to run under considerably higher flow rate and pressure.

JET (Figure 2.4) aims to simulate erosion phenomenon by the means of hydraulic attack (i.e. subjecting soil sample with vertical water jets under controlled and varying pressure and flow) to initiate scour or particle detachment on the surface of sample. Similar to HET, the JET test mainly aimed to find the relationship between erosion rate and hydraulic stress. Soil texture, plasticity, compaction and water content were found to be significant parameters in the soil's erodibility characteristic (Hanson and Cook,2004; Hanson and Hunt, 2007). There has been research that attempted to compare the results from several types of erosion test apparatus. Marot et al. (2011) compare the erosion rate index, critical shear stress and specimen's erodibility

classification obtained from silt and clay with low and high plasticity examined by HET and JET. The results indicated that the erosion index and critical shear stress from HET is higher than those recorded from JET. According to the erodibility system employed by both tests, the samples were also classified slightly differently. The proposed energy model by Marot et al. (2012) enables the relationship between the dissipated energy and erosion to be established. Using this proposed model, the samples tested both HET and JET lie on the same category.

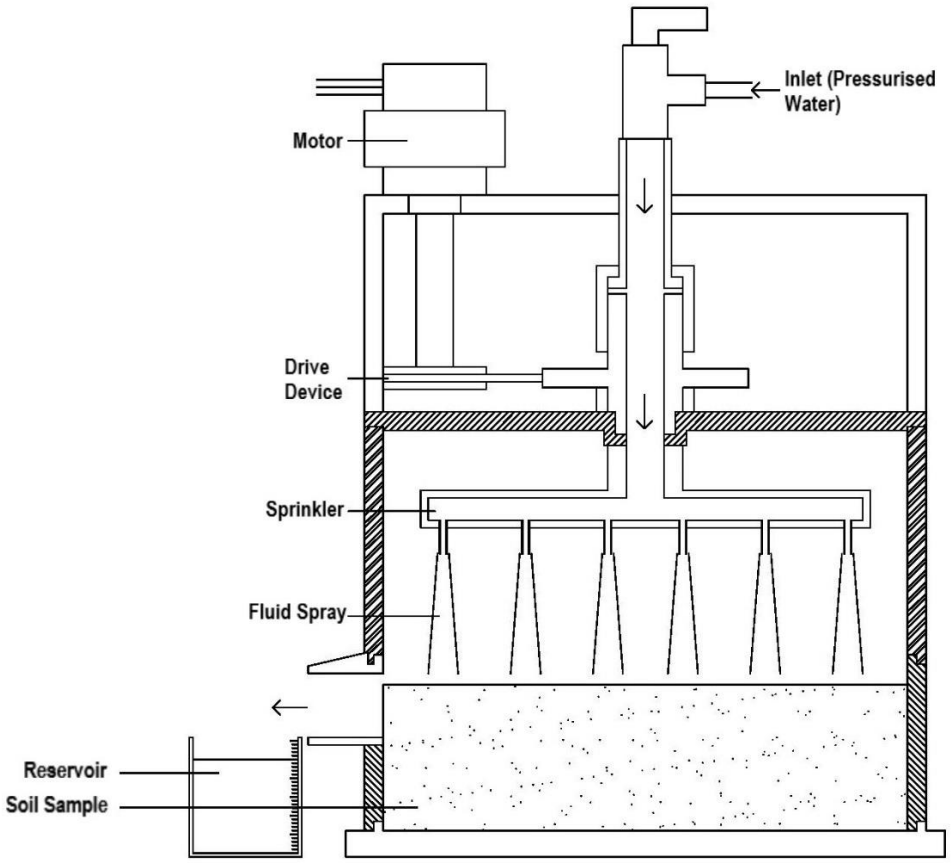


Figure 2.4 Jet Erosion Test (redrawn from Henensal and Duchatel, 1990)

Unlike HET and JET that aim to initiate erosion by controlling the hydraulic parameters (e.g. flow rate, flow pressure) of the eroding fluid, RCT triggers particle detachment by rotating a soil sample under a controlled rotation speed in a cell filled with water (Figure 2.5) (Lim, 2006). Shear stresses generated from a contact between rotating soil sample and water trigger particle detachment on the sample. RCT, like HET and JET, also analysed the erodibility from two main parameters: erosion rate and hydraulic shear stress.

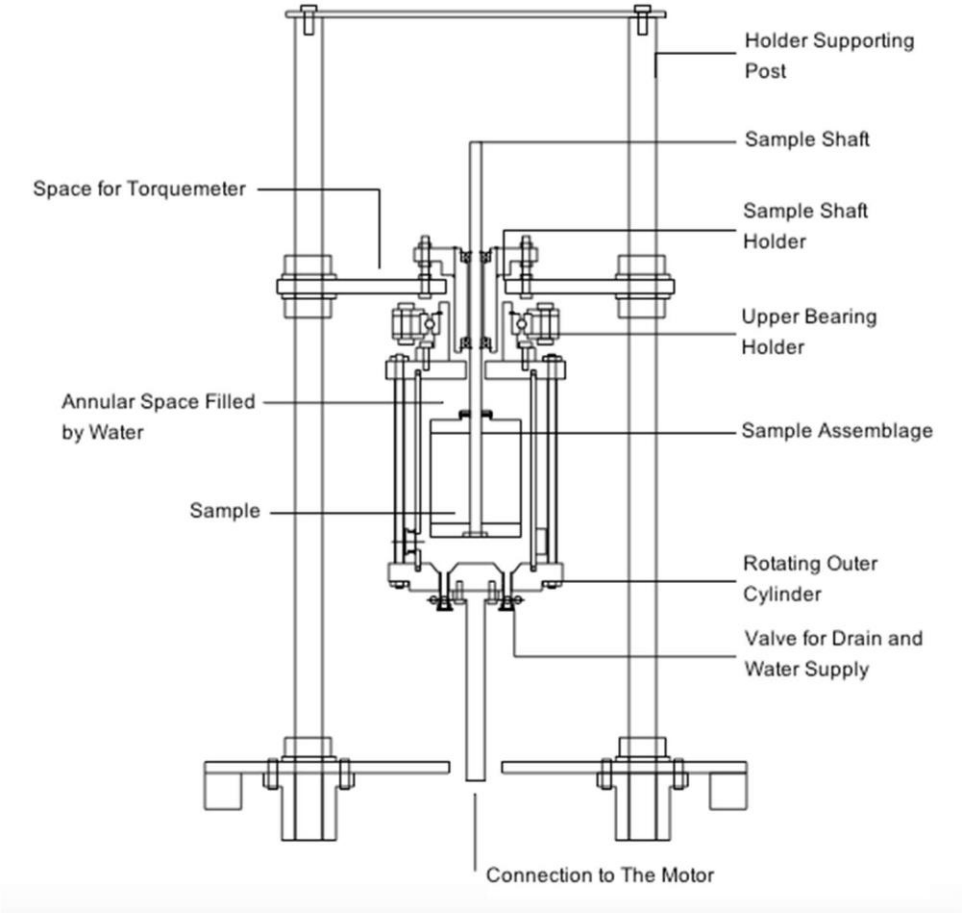


Figure 2.5 Diagram of Rotating Cylinder Apparatus (after Lim, 2006)

2.4.2 Suggested Modifications and Improvements on the Erosion Test Apparatuses

Improvements to these concentrated-leak erosion tests has been progressive rather than transformatory. For example, Beier and Strobl (1985) used the PET to investigate the erosion of metastable soils via calcium leaching (deteriorating the cemented bonds and as such reducing the critical shear stress for erosion of the soil). Garand et al. (2006) and Braithwaite (2013) utilized modified PET apparatus to control water velocity in an attempt to study the relationship between eroded mass with time and the effect of different flow velocities. However, as noted previously, whilst the velocity is an obvious parameter to consider it is less than ideal when considering erodibility due to difficulties in comparing the measured velocity of the water entering and/or exiting the test apparatus with the velocities within the pores (which is unlikely to be constant but likely to vary geospatially within the pore structure). That said, investigation of velocity (of fluid entering or exiting the text apparatus) can still be used to develop an approximate relationship between global velocity and erodibility with time. This set up

offers the advantage that the apparent change in rate of erosion with velocity can be approximated.

Haghighi et al. (2013) improved the measurement accuracy of HET by incorporating turbidity metres placed at the downstream section. This allows for quantification of the mass of soil being eroded during the tests (real-time) without the need to wait for the test to end nor having to terminate the test. This improvement was proposed due to inaccuracy caused by the assumptions adopted in the procedure used by Wan and Fell (2004). Haghighi et al. (2013) pointed out four key problems: (1) friction factors at the start and the end of the test are assumed to change linearly corresponding with the change of flow regimes (i.e. laminar, transitional, turbulent) yet the notion that the coefficient of erosion changes linearly with time has not been supported with physical or numerical basis. According to the Moody chart (Moody, 1944) the curves of friction factor flatten with the increase of Reynold number, therefore suggesting that they do not vary linearly. (2) the application of Bernoulli's law on, what is assumed to be fully established turbulent flow with a constant relative roughness factor, was also considered to be problematic. (3) the hydraulic gradient obtained from the piezometric reading at the entrance and exit chamber did not take into account the losses occurred at the inflow and outflow of the hole, which Haghighi et al. (2013) suggest could be a considerable proportion of the losses (depending upon the experimental layout of the apparatus, especially changes in diameter between inlet pipe and the hole within the sample), as the drop in piezometric head attributed to the transformation of potential into kinetic energy have been overlooked in the previous method. Therefore, it is crucial to not only consider the head loss across the pre-drilled hole h_f but also the head loss at the entrance and exit, h_{ent} and h_{est}, in order to obtain more realistic hydraulic head difference ΔH (Equation 11, Fattahi et al. (2017). (4) as HET uses a pre- drilled hole, it is argued that the initial friction can hardly be considered as ideal nor representative of a naturally occurring crack.

$$\Delta H = h_{ent} + h_{est} + h_f \quad (11)$$

Luthi et al. (2012) considered the approach used by the traditional HET method with a focus on the downstream chamber; the recorded head difference obtained at the sidewall was previously deemed sufficient to represent the energy head loss yet this

assumption was contested as the flow recirculation and hydraulic head drop, at the sidewall, were observed. Marot et al. (2011) suggested that the hydraulic head difference obtained from HET is more dependent on the energy loss due to change of section, approximately up to 75%, between upstream and/or downstream section to hole of sample (i.e. contraction and expansion) than on the friction loss due to eroding fluid-sample contact. Aiming to measure the total energy head loss, Luthi et al. (2012) modified HET by placing pitot static tube at the downstream to measure velocity exiting the sample and downstream energy head. This modification offers two improvements:

(1) replacing hydraulic head difference with total energy head difference in hydraulic gradient calculation, therefore improving accuracy of calculated hydraulic shear stress.

(2) eliminating the use of friction factors in estimating hole diameter change as the velocity, exiting the hole, measured is used in the calculation. Riha and Jandora (2015) also agreed that energy head loss is more representative than hydraulic head loss and suggested that using hydraulic head loss in calculating hydraulic shear stress lead to overestimation because it does not take into account entrance losses and velocity head losses.

Therefore, Riha and Jandora (2015) proposed a modified equation of hydraulic gradient *i* (Equation 12 (Wan and Fell, 2002) and 13) incorporating the energy head loss and coefficient of kinetic energy in the equation to calculate hydraulic gradient along the hole:

$$i = \frac{h_1 - h_2}{L} \quad (12)$$

$$i = \frac{h_{pu} - h_{pd} - (\xi_1 + \alpha_h)\frac{v_h^2}{2g}}{L} \qquad h_{pu} = \frac{p_u}{\rho g} \qquad h_{pd} = \frac{p_d}{\rho g} \quad (13)$$

Where *h1* and *h2* correspond to the piezometric heads at the upstream and downstream section of the sample, *hpu* and *hpd* are the pressure heads at the downstream and upstream, *ξ1* is entrance loss factor (the value is between 0.05-0.80 and contingent upon the shape of entrance hole; Boor et al., 1968; Munson et al., 1998), *αh* is coefficient of kinetic energy for the preformed hole, *vh* is mean velocity in the hole, and *L* is length of hole. Riha and Jandora (2015) investigated the results of testing using Equation 12 and 13. There are three key findings discerned (Riha and Jandora, 2015): (1) the former yields a greater hydraulic gradient than the modified version. (2) calculation with the modified equation produces identical hydraulic gradient regardless of the entrance shape. (3) The result of numerical analysis using computational fluid dynamics would appear to agree with this finding.

The latest study by Fattahi et al. (2017) confirmed the effect of hydraulic consideration on the calculated $\boldsymbol{\tau}$. The apparatus and hydraulic consideration used in the test was identical to Luthi et al. (2012). While Luthi et a. (2012) did not include hydraulic head loss at upstream $\boldsymbol{h_{ups}}$ (Equation 16; proposed by Riha and Jandora, 2015) in calculating the energy head loss $\Delta \boldsymbol{H}$ (Equation 15), the study included it. The study also attempted to compare the results using the equation adopted by Wan and Fell (2004) (Equation 14).

$$\Delta \boldsymbol{H} = (\boldsymbol{h_u}) - (\boldsymbol{h_d}) \qquad \boldsymbol{h} = \frac{p}{\rho_w g} \quad (14)$$

$$\Delta \boldsymbol{H} = (H_u) - (H_d) \qquad H = \frac{p}{\rho_w g} + z + \frac{v^2}{2g} \quad (15)$$

$$h_{ups} = K_{ups}\left(\frac{v^2}{2g}\right) \quad (16)$$

h_u and h_d are the observed hydraulic head at the standpipe, H_u and H_d are total energy head, and K_{upc} is the head loss coefficient at the entrance. The study discovered that τ calculated using hydraulic consideration by Wan and Fell (2014) is higher than those calculated by Luthi et al. (2012) and Fattahi et al. (2017); indicating the former is overestimating τ. The ratio of calculated τ between Fattahi et al. (2017) and Wan

and Fell (2014) was ranging from 0.39 and 0.87, with the mean of 0.5. The difference was greater for higher hydraulic shear stresses, i.e. higher applied flowrate and pressure. Whereas, the ratio compared with Luthi et al. (2012) was 0.7-0.99 which was expected as the hydraulic consideration is the same except h_{upc}. From this study, it was learned that HET using hydraulic consideration by Wan and Fell (2004) is not suitable for soils or geomaterials that require high τ (> 10 Pa) to initiate erosion and it is recommended to follow the set-up and hydraulic consideration by the other authors (e.g. using turbidity meter (Mehenni et al., 2016) or pitot-static tube (Fattahi et al., 2017))

Khanal et al. (2016) argued that the accuracy of the method used to determine critical shear stress (i.e. Indraratna et al.,2009) was problematic. Depending on the chosen model (non-linear and linear models have been considered) may lead to the major discrepancy on the estimated critical shear stress. Historically, it would appear that the

linear model is preferred due to its practicability, although as it is determined by graph-fitting method the linear model may be considered to overestimate the critical shear stress and erosion coefficient.

It is clear from the findings of the previous research that both PET and HET tests are limited in their scope, that perhaps they should be considered more akin to an index test rather than those investigating inherent response of the materials under *in situ* conditions. That said, studying erosion response in naturally occurring fractures within soils, in either the laboratory or field settings, is inherently problematic. The principal advantage of these erosion tests is that they allow for parametric analysis in a relatively consistent and repeatable approach, as such fundamental understanding of possible soil response to the action of eroding fluids can be developed. It has been suggested that installing turbidity measurement at the outflow section of the HET (Haghighi et al., 2013) or incorporating pitot-static tubes (Luthi et al., 2012) could help mitigate issues raised above. Nevertheless, despite offering improved accuracy, the errors during testing should be anticipated as Braithwaite (2013) reported that the use of turbidity meter to investigate erosion in CBB is not suitable as during the test the cement paste and bentonite block the sensor thus disabling to measure the turbidity of eroding fluid. Luthi (2011) also discovered that the pitot static tube could be clogged by the eroded particles, thereby the energy head at the downstream could not be computed. This is inevitable as the tube is placed at the centre of the pre-casted hole where the eroding fluid and eroded particles exiting the sample, thus the possibility of particle clogging is high.

2.5 Erodibility Behaviour of Geomaterials (including concretes, Cement-Bentonite, Untreated and Treated Soil)

2.5.1 Untreated and Non-Cemented Soils

The erodibility of uncemented soils has been previously studied in the laboratory using HET (e.g. Wan and Fell, 2002; Haghighi et al., 2013; Mehenni et al., 2016) and Pinhole apparatus (e.g. Sherard et al., 1976; Head, 1982; Leonards et al., 1991; Tosun, 1997; Botschek, 2002; Batog et al., 2007; Fauzilah et al., 2008; Nadal-Romero et al., 2011). Wan and Fell (2002), Haghighi et al. (2013) and Mehenni et al. (2016) studied the erodibility of silt under HET and found that the critical hydraulic shear stress τ_c and erosion coefficient k_{er} for the silty soils varied from 152 Pa up to 615 Pa and 1.13 x 10^{-4}s/m

up to 3.04 x 10^{-4} s/m respectively (Mehenni et al., 2016; Haghighi, 2013). Briaud (2008) suggested the critical hydraulic shear stress and velocity for untreated silt are ranging approximately from 0.4 Pa to 10 Pa and 0.3 to 2 m/s respectively, while for untreated clay are from 1 to 80 Pa and 0.6 to 6 m/s respectively (as shown in Figure 2.6 and 2.7). These ranges vary according to the plasticity and particle size of the soil. Chevalier et al. (2012) proposed a higher range: critical hydraulic shear stresses of 400 Pa to 500 Pa for untreated silt. Mehenni et al. (2016) attributed the fine particle proportion and dry density of the silt samples investigated to control the erosion resistance of silty soil; with lower fines content and greater dry densities resulting in increased resistance. Benahmed and Bonelli (2012) attributed five key parameters controlling the erodibility behaviour of untreated soil: (1) dry density, (2) water content, (3) clay mineralogy, (4) degree of saturation and (5) degree of compaction. Water content, according to Wan and Fell (2004), is one of the key parameters the erodibility characteristic but Benahmed and Bonelli (2012) argued that when dealing with clay soils this parameter should not be considered in isolation, as the clay mineralogy of the soil will significantly influence how the soil erodes with changing water content. In addition, it is suggested that the properties (e.g. chemical composition, mineral concentration) of the fluid flowing through the soil will impact on the erosion process because mineral types and concentration interact differently with soil, for example clay is more resistant to erosion if the eroding fluid contains higher salt concentration. (Briaud et al., 2001; Briaud, 2008).

Bennabi et al. (2012), Haghighi et al. (2013) and Mehenni et al. (2016) studied the impact of partial clay (e.g. Kaolinite, Illite) replacement in sand and silts towards the erodibility characteristic of the parent soil. Bennabi et al. (2012) and Haghighi et al. (2013) concluded that the treatment of sand with partial clay replacement could decrease the erosion rate of the treated soil, although it was found that the minerology of the clay used has an impact upon the relative performance of the modified soil. For example, 9% Kaolinite replacement is required to achieve the equivalent improvement of 2% Bentonite treatment (Mehenni et al. 2016; Benahmed and Bonelli, 2012). Mehenni et al. (2016) argued that the improvement due to partial clay replacement is exclusive to the reduction of erosion rate as no improvement on critical shear stress was observed. For example, the critical hydraulic shear stress of a Kaolinite-Sand mixture with equal proportion is approximately 10 Pa; increasing the proportion of

Kaolinite up to 70% increased the critical hydraulic shear stress up to 25 Pa (Haghighi et al. 2013). With 30% Kaolinite, the critical hydraulic shear stress of the sand-Kaolin sample increase from 0.2-1.3 Pa to 5 Pa (Bennabi et al. 2013). In conclusion, the type of clay mineral and its proportion used for treatment influences the magnitude of erosion resistance improvement.

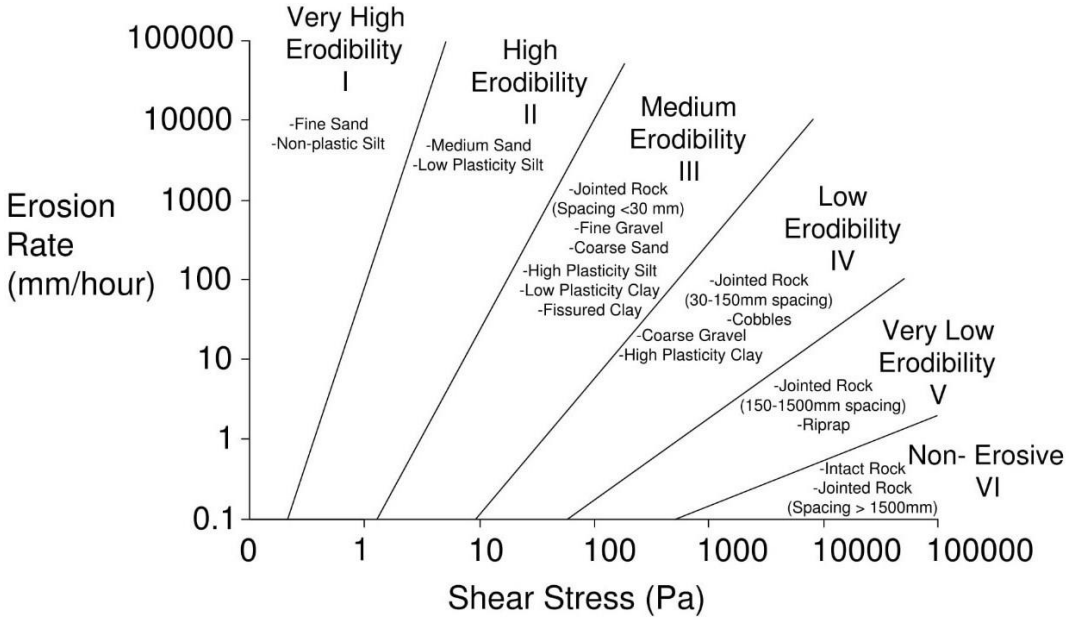


Figure 2.6 Suggested erodibility classification for soil and rock based on hydraulic shear stress (after Briaud, 2008)

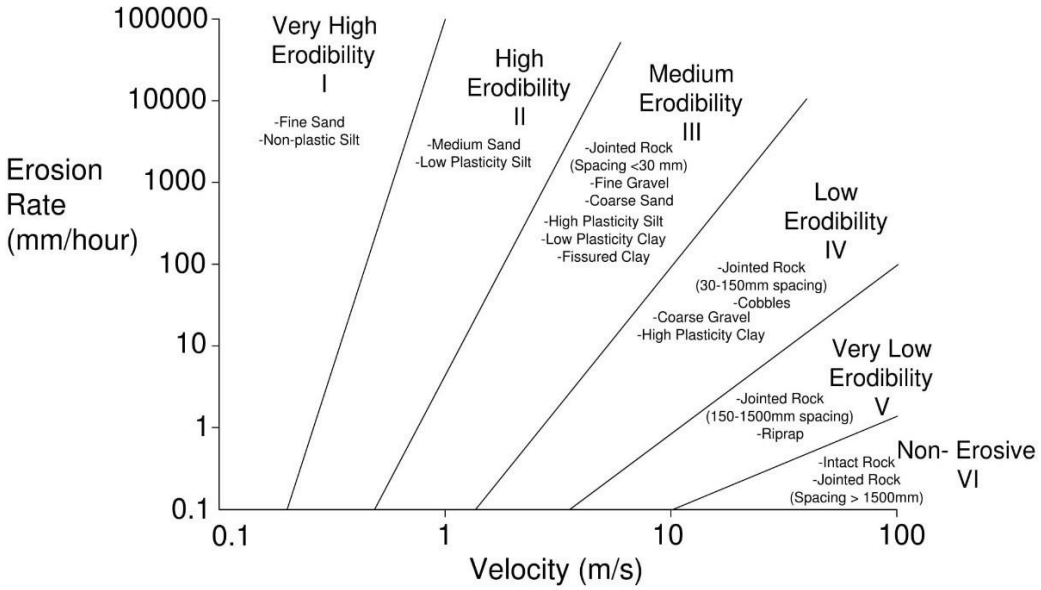


Figure 2.7 Suggested erodibility classification for soil and rock based on eroding fluid velocity (after Briaud, 2008)

Unlike cohesive soil, the erodibility of granular material is controlled by the properties of soil mass. Briaud et al. (2001) highlighted two key erodibility characteristics for granular soils (e.g. sand, gravel): (1) erosion occurs in sliding and rolling motion, (2) electromagnetic and electrostatic forces are absent and negligible during erosion process. Benahmed and Bonelli (2012) suggested three governing parameters controlling the erodibility characteristic of granular material: (1) dilatancy, (2) permeability and (3) undrained shear strength. From the laboratory testing using Erosion Function Apparatus (EFA), Briaud et al. (2001) obtained a critical hydraulic shear stress of 3 Pa and 0.26 for coarse sand and fine sand-silt. Although required higher hydraulic shear stress to initiate erosion, once erosion starts coarse sand erodes in higher rate than the mixture of fine sand-silt (1000 mm/hour/Pa and 21 mm/hr/Pa, respectively). According to the study of erosion in cohesionless soil, to study its erodibility behaviour it is necessary to consider the hydraulic loading (i.e. hydraulic gradient, hydraulic shear stress and velocity) applied to the soil particle as the phenomenon is governed by two key conditions: solid-fluid interaction and hydrodynamic condition (Marot et al., 2016). The test on cohensionless soil by Marot et al (2016) using modified triaxial erosion apparatus suggested that the hydraulic shear stress <1 Pa and velocity <1 m/s are required to initiate the erosion and the rate of erosion appeared to increase with the increase in the hydraulic shear stress. The finding corresponded well with the range of hydraulic shear stress suggested by Briaud (2008), as seen in Figure 2.5.

2.5.2 Cemented/Chemically Treated Soils

Cement and lime have been utilised as chemical additives for improving the geotechnical properties of soil for many years (e.g. Jiang et al., 2004; Sezer et al., 2006; Nerincx et al., 2016). The results of previous research on the effect of lime and cement towards the erodibility characteristic of treated soil appear to have been positive; the incorporation of the cementing agent increases the erosion resistance (Muttuvel, 2008; Indraratna et al., 2008; Chevalier et al., 2012; Mehenni et al., 2016). Both lime treatment and cement treatment increase the critical hydraulic shear stress of the treated soil. For cement treatment, the cement setting and the increase of cementitious products that promote strong interparticle bonds are responsible for the improvement on erosion resistance. The effect is time-dependent (in the short term) as the strength of cementation improves with curing; it is also a function of the

proportion of cementing agent incorporated into the soil. For lime treatment, changes in erosion resistance is attributed to the flocculation-aggregation in the short term, and if the soil is susceptible to chemical reaction with the lime, cementation of the soil. A silty soil treated with 3 % lime was observed to experience an increase in critical hydraulic shear stress from 1200 Pa to 1700 Pa in 7 days; while 6 % cement treatment was observed to increase approximately from 5900 Pa to 9800 Pa for the same duration (as shown in Figure 2.8 and 2.9). The inlet/upstream pressure required to initiate erosion for the treated silty soil increase from 70-80 kPa for the non-treated up to 300 kPa for 3% lime treatment and 650 for 6% cement treatment, respectively (as shown in Figure 2.10). Cement treatment also contributes in reducing the erosion rate whereas lime treatment was not observed to replicate the same impact (in the time frame considered). This was attributed to lime-treatment changing both the soil deformation response and changing the particle size distribution (increasing coarse grain content). Consequently, the mode of soil detachment changes from individual particles to aggregates detachment (Mehenni et al., 2016).

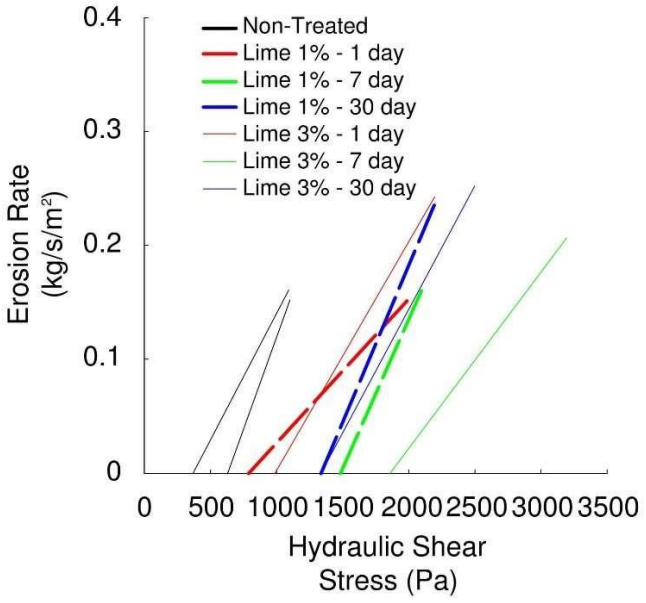


Figure 2.8 Erosion rate-hydraulic shear stress relationship for lime-treated silt (redrawn from Mehenni et al. (2016))

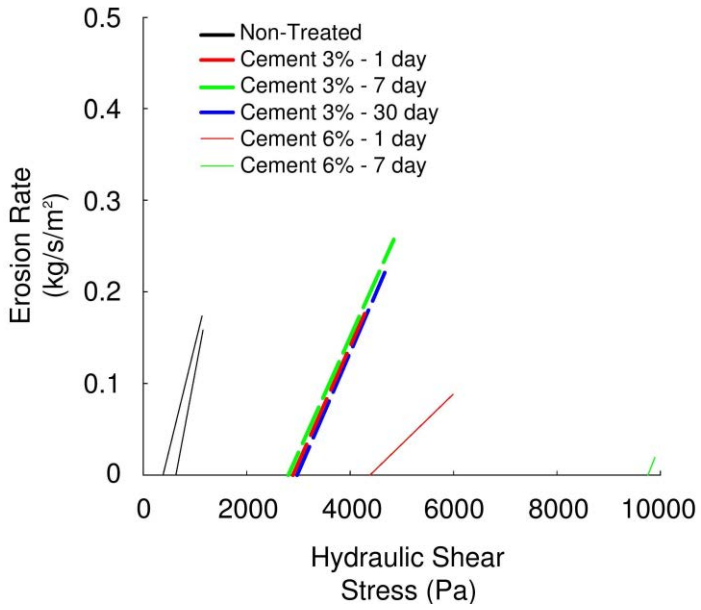


Figure 2.9 Erosion rate-hydraulic shear stress relationship for cement-treated silt (redrawn from Mehenni et al. (2016))

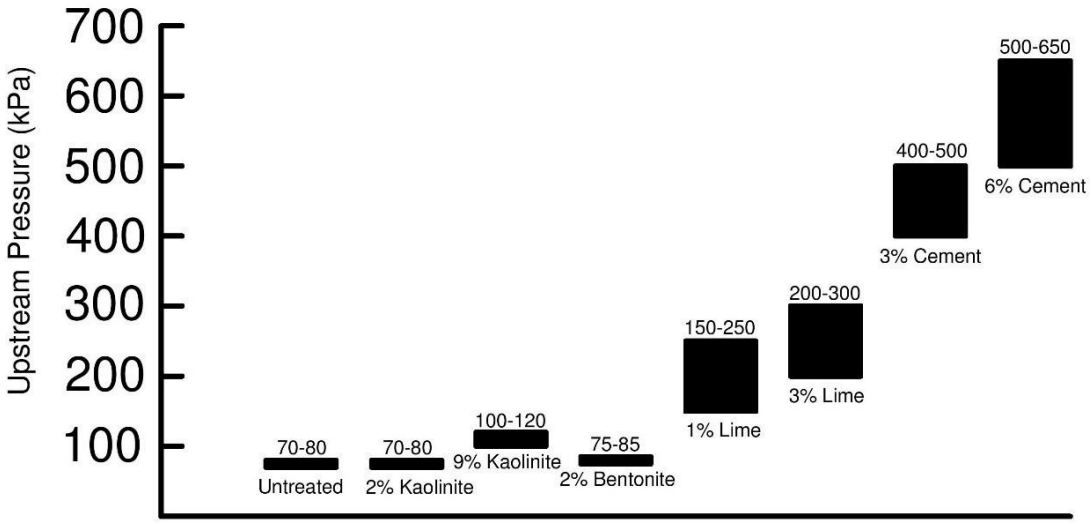


Figure 2.10 The required upstream pressure according to silty soil treatment type and composition (after Mehenni et al. (2016))

Indraratna et al. (2008) and Muttuvel (2008) studied the effect of lignosulfate and cement treatment on the erodibility of silty sand. Lignosulfate treatment was found to be more effective than cement treatment in improving the erosion resistance of the samples (i.e. increasing critical shear stress and slowing the erosion rate): it only required 0.6 % lignosulfate to acquire the equivalent or greater impact of 2 % cement replacement (as shown in Figure 2.11). Furthermore, Muttuvel (2008) and Indraratna

et al (2008) studied that the higher compaction and water content coupled with chemical additives treatment contributes to higher critical hydraulic shear stress. Conversely, Muttuvel (2008) observed the opposite relationship for soils containing clays; cement treatment was found to be more effective for dispersive clay mainly because cement, when mixed with clay, is able to transform the mineral structure of the clay (if the chemical conditions are favourable, i.e. pH level, etc.) while lignosulfate only acts as binder.

The erodibility behaviour of chemically treated soils would appear, in the main, to be controlled by the effect of cementation rather than the properties of the host soil (prior to addition of the binding agent) (Muttuvel, 2008; Indraratna et al., 2008; Chevalier et al., 2012; Mehenni et al., 2016).

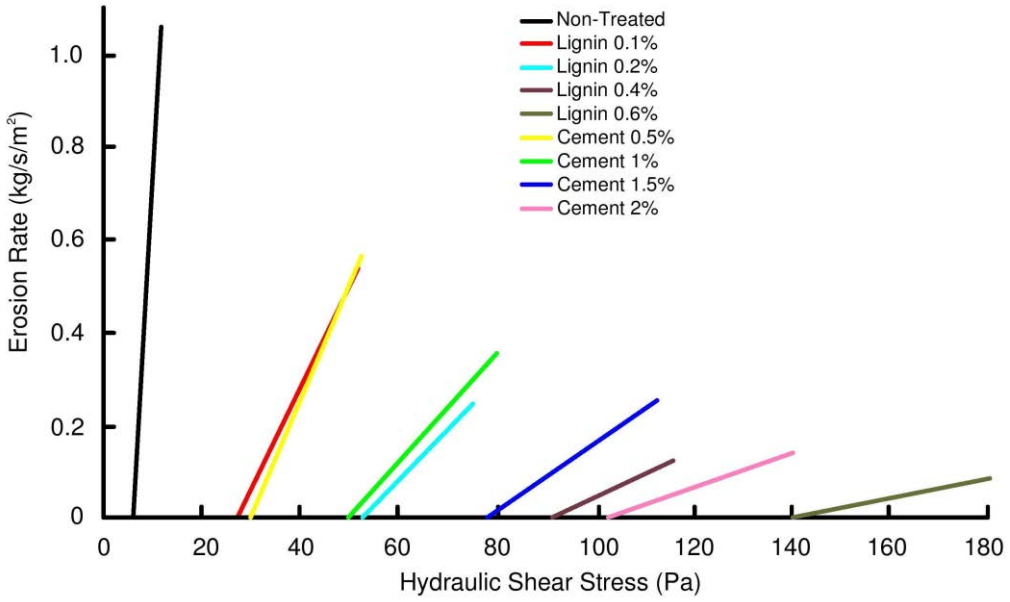


Figure 2.11 Erosion rate-hydraulic shear stress relationship for silty sand treatment using cement and lignosulfate (redrawn from Indraratna et al. (2008))

2.5.3 Concrete and Plastic Concrete

Garand et al. (2006) and Braithwaite (2013) and studied various cemented materials (e.g. plastic concrete, conventional concrete, CB) using an apparatus which function and set -up is similar to HET. Braithwaite (2013) discovered that under the experimental conditions considered (at the approximate velocity up to 10 m/s and applied for 8 days), the conventional and plastic concretes were found to be non-

erosive (i.e. the eroded particle is not beyond 1% of sample weight). Garand et al. (2006) also investigated the erosion resistance of plastic concrete using PET and Controlled Water Velocity (CWV) apparatus under the applied velocity range of 3-12 m/s (applied for 20-24 hours) and maximum hydraulic head of 6500 mm. It observed that it did not erode significantly; with the total eroded mass was mostly less than 100 grams (sample diameter of 150 mm and length of 300 mm). The applied velocity was within the expected velocity range suggested by Briaud (2008) to erode intact rock, however it was not clear whether such velocity range exist in the earth dam/embankment/levee after the erosion start or not. The cement paste was observed to erode during the tests, although the sands and/or gravels in the concrete and plastic concrete samples did not. It was argued that the aggregates created an 'armouring effect' that hindered the erosion process (Braithwaite, 2013) and the same phenomenon observed by Garand et al. (2006) citing that the eroded materials were mainly dominated by cement and bentonite binder. Thus, it was suggested that incorporating coarse material or aggregates in barrier mixtures could improve the erosion resistance. Although offering a prospect of barrier performance tantamount to intact rock, such improved erosion resistance results in increased costs. The same concern should be considered in deciding to use conventional concrete for the seepage barrier. Garand et al. (2006) also discovered that the increase of bentonite ratio in plastic concrete could increase the erosion resistance. However, Garvin and Hayles (1999) suggested that increasing the bentonite proportion (in CB rather than plastic concrete) makes the slurry thicker and more difficult to mix and pump. Hence, the idea of increasing bentonite content is not ideal option either to improve the erosion resistance.

A small amount of erosion was observed in the concrete materials and this was mainly attributed to the formation of loose blocks of material during sample splitting prior to testing. The plastic concrete investigated by Garand et al. (2006) was observed to erode in the first 5 to 60 minutes and this was attributed to sample disturbance associated with splitting or placement of metal pin for PET, although there was no observation on the mode of erosion (e.g. erosion in form of fine particle, small to big lump, wedge/block, etc) or the relationship between eroding fluid and erosion rate of the deformities. It was crucial to quantify the erosion rate, especially if the flowrate and pressure of eroding fluid remain constant after the erosion is initiated, to understand

and predict the time required before the breach occur. Whilst it was argued that these materials were not susceptible to internal erosion, with any erosion observed being attributed to material damaged inflicted sample preparation, this does highlight the need to undertake quality assurance procedures when constructing these barriers as any defects within the structure may be a potential weakness that could conceivably be subject to internal erosion – especially if the barrier experiences strains.

2.6 Erosion of CBB When Compared to other Cemented Soils or Concretes

Cement-bentonite, comprising cement (and cement replacement materials), bentonite and water, may appear to be similar in nature to other cemented soils (or considered a very weak concrete) and hence it might appear desirable to apply the lessons learned from previous research into the internal erosion of these materials when attempting to determine how CB may respond to eroding fluids. However, Alzayani et al. (2017) notes that CB does not appear to exhibit the same physical responses as cemented soils (there is a significant range of behaviour reported in the literature, and whilst some responses will be similar to CB it is difficult to identify which without first characterising the CB, hence reducing the value of such comparisons), concretes or plastic concretes. Therefore, it is difficult to determine which, if any, responses observed in the cemented soil or concretes are directly applicable and thus research must be conducted into the internal resistance of CB if these barriers are to be used in situations where internal erosion of a CBB could compromise the geotechnical structure (such as a CBB installed in an earth dam to remediate an aging low hydraulic conductivity core).

A few studies have been undertaken in an attempt to assess the internal erosion resistance of CB (reported below), although much is still poorly understood and requires further investigation. For example, the impact of the constituent components within the mixture (including cement replacement materials that can have a significant influence on the material properties of the CB) has on the internal erosion resistance, nor is the impact of curing on the material response. Uncertainty also surrounds the modes of erosion involved and the effect of hydraulic parameters on the erosion rate (pressure differential, seepage velocity, etc.), hence the response of CB in terms of critical hydraulic shear stress and erosion rate is also poorly defined.

2.7 Previous Laboratory Studies into Internal Erosion of CB

It has been suggested that there are four main elements attributed to the erodibility of cut-off barrier materials, these being: the properties of the eroding fluid (including the chemical properties, which can have a significant role in the erosion process); the hydraulic gradient acting across the barrier; the loading environment acting on the barrier; and the material properties (mixture proportions, hydraulic conductivity and compressive strength, etc.) of the barrier (Beier and Strobl, 1985; Braithwaite, 2013). Garand et al. (2006) states that the hydraulic gradient and mixture proportions of the cut off material are the main factors determining its erodibility characteristics.

There is limited information regarding the modes of erosion in CB materials; it is not yet clear whether the erosion in CB takes the form of abrasion of individual particles or via the failure of blocks, created with the shearing of the cementitious products surrounding the block, it is also uncertain how much of an impact changes in pore chemistry has on the erodibility of these materials. A few, somewhat limited, studies have been undertaken that investigate aspects of CB internal erosion and these are summarised below.

Braithwaite (2013) investigated a type of CB (cured for 28 days) that was found to be susceptible to internal erosion. It was observed that the test run for 6-9 days under the eroding fluid with velocity ranging from 0.3-0.7 m/s, and pressure differential across the sample ranging from 5000-12000 Pa eroded the CB material 11.76 -19.14 % by specimen weight: the initial crack of 1-2 mm widened to 17-26 mm. The effect of increasing the applied pressure differential yielded higher erosion percentage. According to the critical velocity range by Briaud (2008), the applied velocity range in Braithwaite (2013) test was classified as high to very high erodibility and the erodibility is equivalent to sand and low plasticity silt. Compared to the other barrier materials tested (e.g. soil-cement-bentonite, plastic concretes) by Braithwaite (2013), CB was highly erosive. Conventional concrete, plastic concrete and soil-CB did not erode even under critical velocity 10 to 15 times that of CB. It should be noted that this CB could be considered a relatively unusual mixture, from a UK view point, as it only contained a cement (14.5 % of relative weight) and a bentonite (4.8 % of relative weight), and had a quoted 28-days strength of 22 psi (which is approximately 150 kPa); as such it may not achieve the specification requirements for barrier walls in the UK. CB mixtures

tend to contain ground granulated blast furnace slag, GGBS, or pulverised fuel ash, PFA, to achieve the strength and hydraulic conductivity requirements whist maintaining an economical mix (Opdyke and Evans, 2005) and the inclusions of these materials may change the material response to internal erosion, as noted below. However, the mixture investigated by Braithwaite (2013) was found susceptible to internal erosion, with the simulated crack developing into a void, although the mode of erosion during the test was not reported, nor was the relationship between eroding fluid (fluid velocity and/or pressure) and rate of erosion reported. This point of discussion is vital as it provides overview on the severity of CB erosion after it reaches a critical stress. Due to the very weak nature of the CBB investigated it is not clear how representative this material was of other CB mixtures.

Ryan (2015) investigated the erodibility of CB, mixture composition per litre of water: 40 grams bentonite, 40 grams cement and 160 grams GGBS) under 2-3 L/min flowrate (with the initial hole diameter of 1.6 mm, the initial applied velocity was ranging approximately from 16.6 m/s to 25 m/s) and up to 2 hours testing duration. There are three parameters analysed in the study: 1) effect of applied flowrate, 2) effect of testing duration, and 3) effect of sample curing age. As suggested in Figure 2.6 by Briaud (2008), under such range of velocity, the erosion should be expected for material with strength greater than intact rock. Although the author did not quantify the extend of the erosion (i.e. the final eroded hole diameter), it was visually observed that the increase of flow rate and longer testing duration led to increase of erosion. After erosion was initiated, the hole enlarged which caused the applied pressure and velocity to decrease, if the flow rate was kept constant. The fact that the erosion was initiated at 2 L/min flowrate, indicating that the critical velocity of the CB sample was below the initial applied velocity. However, it was unknown whether the particle detachment occurring constantly and uniformly or only occurring at certain period during the testing duration. The older age sample was observed to be more resistant to erosion that the juvenile sample and this was expected as the hydration process continued until 90 days (ICE, 1999). Despite these findings, erodibility characteristic of CBB is still poorly understood as the critical velocity and hydraulic shear stress to initiate erosion are still not known. This is crucial as the engineer should understand and be aware of the safe range for the velocity and pressure of water that should exist in the dam/embankment/levee. In addition to that, the erosion resistance of CBB sample

older than 28-days is not yet properly understood, therefore it is imperative to investigate this matter.

Beier and Strobl (1985) conducted erosion tests on various CB mixtures: 1) bentonite 2.4%, cement 11%, rock-flour 48%, and water 40.6%, 2) bentonite 3.5%, cement 17%, electro filter-ash 9%, and water 70.5%, 3) bentonite 1%, cement 5%, rock-flour, clay, sand, gravel 74%, and water 20%. It was postulated that the erosion process of these materials could be related to the stability of the calcium silicate hydrate (CSH) gels formed during curing. The stability of the CSH gels is a function of the environmental conditions (pH, flowing water destabilising the equilibrium of the pore water chemistry, etc.) and hence the calcium leaching was assumed to influence the erodibility characteristic of the materials. Thus, the leaching factor and limit gradient of calcium were established for each of the mixtures in separate batch tests; from this it was suggested that the seeping fluid could result in Portlandite (calcium hydroxide) dissolution with the released calcium ions being flushed from the pore spaces. In so doing it was argued that the equilibrium is disrupted, which could lead to increased rates of internal erosion. Beier and Strobl (1985) supported this hypothesis with scanning electron microscopy (SEM) analysis of the CB samples before and after the erosion tests. The long and thin CSH fibres (along with the noticeable voids) were observed before the test; the frequency of these fibres was observed to reduce after the test, which also indicates that there should have been an associated reduction in strength of the samples (Beier and Strobl, 1985). Nevertheless, the study by Beier and Strobl (1985) appeared to neglecte the role of hydraulic degradation in the erosion process, hence it is not clear if the chemical equilibrium of the material is a more significant factor in erosion process than the velocity or pressure of the eroding fluid and certainly merits additional research. In addition, Jefferis (2012) permeated CB samples with multiple pore volumes of water and noted that the pH of the CB reduced towards 8 (from around 12.5) and suggested that as the pH approached 8, carbon dioxide dissolved within the permeating fluid interacted with calcium within the pore fluid resulting in the precipitation of calcium carbonate. Therefore, if the chemistry of the CB is being affected by the eroding fluid (i.e. dissolution of some compounds, precipitation of others, and removal of ions from the pore water), and this is an important mechanism in the long-term vulnerability of CB to internal erosion, then the physico-chemical degradation of these materials when exposed to eroding fluids

merits additional research. In addition, the CB mixture used can result in very different cemented structures being created. Opdyke and Evans (2005) observed that CB containing significant proportions of GGBS (as a cement replacement material; 70 % or greater) did not produce CSH 'needles' but a much finer 'foil like' structure, and Royal et al. (2013 and 2018) note that changing the mixtures can result in significant changes in physical properties, then these factors may influence physico-chemical degradation of the CB material when exposed to a seeping fluid and necessitate bespoke testing of specified CB mixtures to determine the potential vulnerability to internal erosion prior to it being used *in situ*.

It is difficult to draw substantial conclusions on the generic susceptibility of CB to internal erosion from the studies above due to the variety of potential mixtures that could be used *in situ*. For example, the study by Beier and Strobl (1985) used CB samples containing electro-filter ash (9 %) along with bentonite (3.5 %) and cement (17 %, all percentages quoted being relative weight), whereas Braithwaite (2013) examined CB samples containing mixture of cement (14.5%), bentonite (4.8%) and water (80.7%). Opdyke and Evans (2005), Jefferis (2012), Soga et al. (2013) and Royal et al. (2018) have incorporated GGBS in their mixtures and obtained improved CB performance. The CB 28-days UCS compressive strength from Braithwaite was approximately 150 kPa whereas this value was below the suggested values from Soga et al. (2013) and Royal et al. (2018), that are 360 kPa and 529 kPa respectively. This suggests that it is not ideal to assume that the CB material used in the two previous erosion studies could properly represent the CB erodibility behaviour.

While the improvement of CB performance with GGBS replacement has been reported previously, it would appear that no consideration has been given to the associated magnitude of improvement to the CB erosion resistance. The comparison between CB material with and without other cementitious replacement material (e.g. GGBS, PFA, etc.) has not yet been established. This point is crucial as this may help the engineer and designer to design the proper CB composition in the field with high erosion resistance.

Other researches have attempted to compare CB with other barrier material such as plastic concrete containing gravel and sand with combined proportion up to 83 % and soil-CB containing approximately 70 % sand (Garand et al., 2006; Braithwaite, 2013). However, as noted by Alzayani et al. (2016), it is difficult to compare the physical response of these cemented materials as they have fundamentally different physical responses; therefore, attempting to apply the lessons learned from the study of the resistance of internal erosion of one material to the others may result in an unsatisfactory outcome. Whilst it could be argued that a high strength concrete will give better resistance to internal erosion than a CBB; the concrete panel wall may not be an appropriate design solution on engineering, economic, logistical grounds and as such the CBB is required and such comparisons become moot.

2.8 Conclusion

The failure of embankment and dams is still mainly dominated by piping erosion with considerably high percentage, 31% and 48 % (ICOLD, 1995; Foster et al., 2000). The cement-bentonite barrier is a potential solution to this problem as the barrier can be installed into an existing earth dam, that is considered vulnerable to internal erosion, and it will cure to form a cut-off wall that will renovate the low hydraulic core of the barrier and thus reduce the risk of dam failure via internal erosion. For the CBB to be used in such an application (or for environmental protection purposes when attempting to control contamination plumes), then it is important that these walls are resistant to internal erosion.

Laboratory based investigation using one of several techniques has proven a relatively simple way of assessing of the internal erosion resistance of various soils, including CB. However, insufficient research has been dedicated to furthering the understanding of how this material (CB) withstand the internal erosion. Therefore, it is important to investigate the erodibility of CB especially focusing on the hydraulic shear stress that is required to initiate erosion and the rate of erosion after the erosion commence. Further understanding on the behaviour of CB older than 28-days is also important in order to assess the resistance of CB against erosion over the time.

Chapter 3
Methodology

3.1 Introduction

This chapter mainly addresses the methodology used to produce the material studied in this investigation, the range of apparatuses used and developed to investigate the behaviour of the studied material, and the testing program. Detailed specification and procedures used to produce CB samples are described in Section 3.2. The design and procedure of the laboratory testing investigating the strength and erodibility characteristics of CBB samples are discussed in Section 3.3 and 3.4, respectively. A brief explanation on the test investigating the microstructure of CBB is included in Section 3.5. A summary of this chapter is given in Section 3.6.

Table 3.1 detailed the steps undertook in this research and the methodology approach taken to manifest the objectives set at the start of this research.

Table 3.1 Summary of research objectives and proposed methodology

No	Objectives	Methodology/Testing	Outcome
1	Conducting literature review on the erosion process, particularly concentrated leak erosion, relevant laboratory-scale works, and analysing the extent of the research for the relevant geomaterials	Literature and systematic review	Chapter 2
2	Developing an understanding on the effect of curing period and changing mix proportion to the CB basic properties and strength by performing series of laboratory standard test.	Basic properties test, strength test	Particle density, moisture content, UCS, tensile strength
3	Developing a laboratory apparatus for investigating the hydraulic fracturing phenomenon in CB	Apparatus that can apply internal and confining pressure to the CB sample	The internal pressure required to trigger fracture under varying confining pressure, the effect of the curing period and variation of mix proportion
4	Developing a laboratory apparatus for the erosion test for measuring and obtaining erosion parameters which are used to represent the erodibility characteristics	Erosion apparatus that can simulate concentrated leak erosion and to apply varying hydraulic condition to the CB sample during the erosion process	Hydraulic conditions required to trigger erosion (e.g. differential pressure, flowrate, hydraulic shear stress, velocity), the effect of curing periods and variation of mix proportion
5	Evaluate the effect of curing period and changing mix proportion to the erodibility characteristic of CB	Plotting the hydraulic conditions obtained from the testing and analyse the trend with the changing curing period and mix proportion	Analysis on the effect of curing period and mix proportion
6	Developing a laboratory apparatus for investigating the effect of confining pressure during the erosion test	Apparatus that can conduct erosion test with the application of confining pressure	The effect of confining pressure on the erosion process
7	Establishing relationships between basic properties, strength, hydraulic fracture to erodibility characteristic of CB	Plotting the hydraulic conditions obtained from the erosion testing against the basic properties and strength of the sample	The relationship between erodibility and basic properties/strength characteristic

3.2 Sample Preparation and Creation

3.2.1 Material Specification

This research deliberately investigated specimens produced from laboratory prepared batches with manufactured cracks due to several major obstacles: the limitation to obtain CBB sample from the field, the difficulty in preparing 'naturally cracked' samples for erosion testing, and variability in barrier properties when cast in situ (Joshi et al., 2010). There are three major components in the creation of CBB samples: the cementitious materials, bentonite, and water. Both bentonite and cementitious material, in dry form, used were industry sourced. Berkbent™ 163 Bentonite, sodium carbonate activated type with the percentage of weight retained on 150 μm of 5%, was used (TOLSA 2008). The cement used was CEM II/B-V type, supplied by CEMEX, with composition specified in Table 3.2 (BS EN 197-1 2011). GGBS used was sourced from Hanson Cement and its properties are summarised in Table 3.3 (Hanson 2015, BS EN 15167-1 2006). GGBS is considered pozzolanic at low temperatures (i.e. at 10 °C or less (Escalante-Garcia and Sharpe, 2004), material and its primary elements are silicates, alumina-silicates, and calcium alumina-silicates (Talefirouz et al., 2016).

The mix proportion and preparation method of cement-bentonite slurry sample have been established by several past researches (Table 3.4). The 20% of cementitious materials was chosen as this mix proportion produces sample with higher strength than those with 10% and 25% of cementitious materials (Figure 3.1). The proportion of bentonite is recommended not to exceed 4% as the percentage above that may result in the undesirable slurry thickness thus it raises problem during mixing and pumping (Garvin and Hayles, 1999).

Table 3.2 Composition of cement type CEM II/B-V

Constituents	%
Clinker	65-79
Fly ash (siliceous)	21-35
Other minor constituents	0-5

Table 3.3 Properties of GGBS

pH	10-12
Density	2.4 - 3 g/cm^3
Chemical Compositions	
CaO	40%
SiO_2	35%
Al_2O_3	12%
MgO	10%
Fe_2O_3	0.2%

Table 3.4 Proportion of cementitious materials, bentonite and water in slurry sample (by weight) (A (Joshi et al., 2008) and (Joshi et al., 2010); B (Royal et al., 2013); C (Opdyke and Evans, 2005); D (Carreto et al., 2015)

Materials	A	B	C	D
Water	84%	81%	83%	81-84%
Cement	2.50%	16%	2.60%	13-16%
Bentonite	3.30%	3%	3.10%	3-4%
Slag/GGBS	10%	-	10%	-

Table 3.5 CBB Mix Proportion

No	Sample Type	GGBS Replacement (%)	Sample Composition Water (mL)	Bentonite (gr)	Cement (gr)	GGBS (gr)
1	CB with GGBS	40	1000	40	120	80
2	CB with GGBS	60	1000	40	80	120
3	CB with GGBS	80	1000	40	40	160
4	CB without GGBS	0	1000	40	200	-

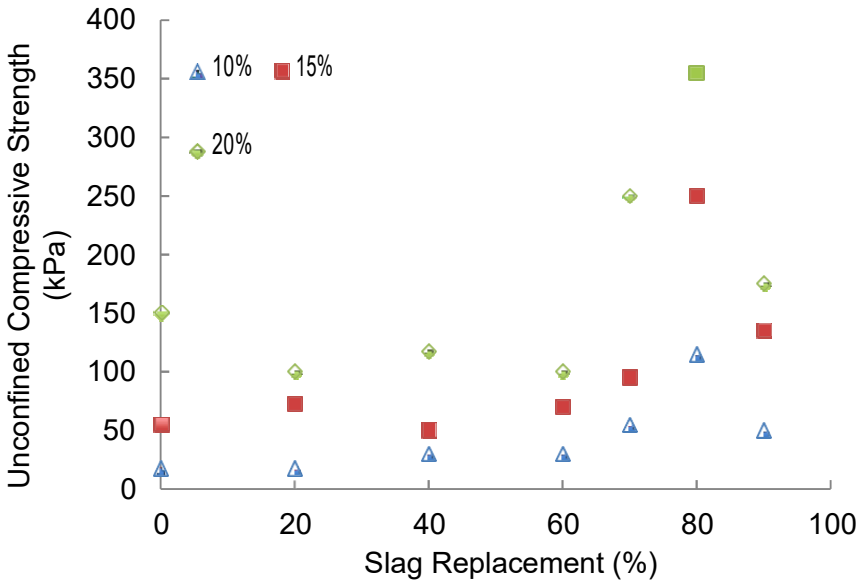


Figure 3.1 Unconfined Compressive Strength of Slag-Cement-Bentonite with variation on cementitious material proportion (10%, 15%, and 20%) and slag replacement (after Opdyke and Evans, 2005)

3.2.2 Material Preparation

Both cementitious materials (cement and GGBS) were prepared in dry condition. The bags used to store those materials were sealed in order to ensure they were not affected by temperature and humidity condition of the laboratory environment which tend to change over the year. The distilled water used was sourced from chemically filtered machine, which maintain its chemical purity, stability, composition, acidity and cleanliness, in the laboratory.

3.2.3 Procedure

In general, the procedure to produce CBB samples used in this study was mainly adopted from past relevant studies (e.g. Garvin and Hayles, 1999; Royal et al., 2017; Wang et al., 2017; Walenna et al., 2019). The procedure used is as follow:

1. The initial stage of sample preparation was mixing the dry bentonite with water for 25±3 minutes using a commercial food mixer under controlled speed. Some dry bentonite usually stuck to the wall of mixer bowl; hence it is highly recommended to check the bowl every 10 minutes, scrape the wall using spatula and put them back into the bentonite slurry for further mixing.
2. The bentonite-water slurry was left to hydrate for 24±1 hour at room temperature. The bowl was covered with plastic wrap to prevent dust or other material to get into the bowl.
3. Before the cementitious material was mixed with bentonite-water slurry, they were sieved beforehand to ensure there was no big lump of cement or GGBS mixed in the mixture. The duration of mixing for cementitious material with bentonite-water slurry is 5-7 minutes.
4. After the mixing, CB slurry was poured into the cylindrical moulds (See Figure 3.2). For samples used for erosion test, moulds with 3mm in diameter acrylic rod placed in the centre to simulate a crack/hole. The rod was attached to the plastic caps that close both ends of the mould.



Figure 3.2 The mixed CB slurry were transferred to acrylic moulds and temporarily

5. The samples were placed on the vibrating table for 10-15 minutes to allow entrapped air in the slurry to escape (Royal et al. 2013). All samples were cured in moulds at temperature-controlled room (5-7 °C) and suitable with the typical ground temperature (BGA, 2019). For this study, the curing days were set at 7, 14, 21, 28, 56 and 90 days.
6. After samples were cured for the assigned curing days, both tube caps and acrylic rod were removed, and the sample was partially extruded from the mould to be trimmed to the desired length.

3.2.4 Technical Consideration

3.2.4.1 Curing Procedure

CB samples used for strength testing were extruded from the moulds after 7 or 14 days curing. The material was still soft for curing age less than 7 days, especially for the samples without GGBS, hence they were extruded at 14 days. The extruded samples were transferred to container filled with water and were submerged for the rest of curing duration (see Figure 3.3). Samples used for erosion test were cured inside the mould. Although it was technically possible to extrude and reinsert the samples to the mould, during the reinsertion the samples were heavily disturbed (e.g. crack along the edges, shear failure) by the procedure. Hence, it was decided to cure the samples inside the mould.

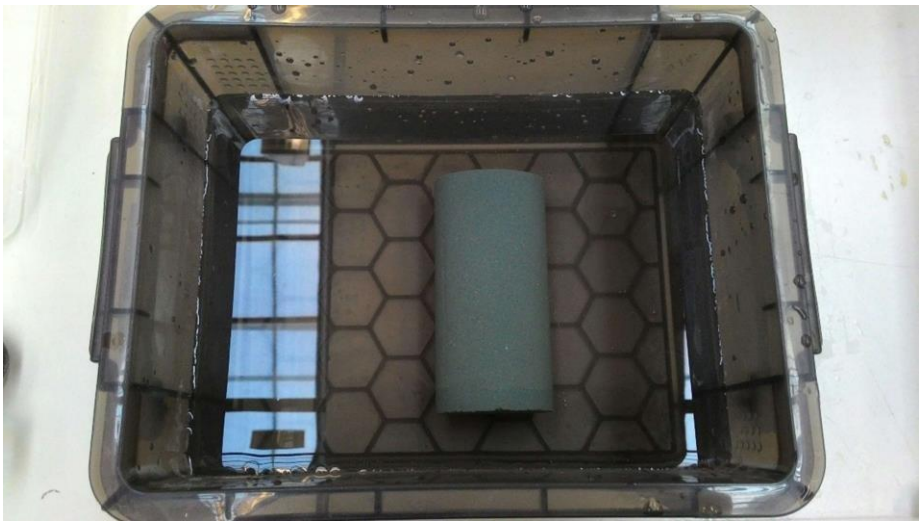


Figure 3.3 CB samples submerged in water

The water used to submerge the samples were the same water used to produce the CB slurry. During the curing, some samples were covered by white-translucent layer biofilm. The samples covered by the biofilm (see Figure 3.4) were weaker in strength (unconfined compressive and tensile strength) compared to those biofilm layer removed as soon as the noticeable layer was observed. The water should be regularly (weekly) changed in order to prevent the biofilm layer to form.



Figure 3.4 Samples covered by biofilm during curing

3.2.4.2 Trimming

Before the samples were used for testing, they should be trimmed to the desired length using the trimming apparatus (see Figure 3.5 and Table 3.6). The cross-sectional surface of the sample should be flat and smooth. This is particularly critical as the flat surface ensure uniform load distribution from through the top and bottom cap. Spirit level was used to check the flatness and evenness of the sample surface. Juvenile samples, 7-14 days old in particular, were still really soft therefore the trimming should be done carefully by cutting the height in steps instead of cutting the large part directly. During curing, the CB slurry hardened and experienced a shrinkage (Jefferis, 2012). After shrinking, the thin unhydrated layer was formed (as seen in Figure 3.6). This layer usually had a noticeable different in colour (light grey) in comparison to the dominant sample colour and weaker in strength. Hence, this layer should be trimmed first in order to ensure this weak layer would not affect the testing result.



Figure 3.5 Trimming apparatuses

Table 3.6 The CB samples sizing detail

Test	Size (mm)		
	Sample Diameter	Hole Diameter	Height
Material Strength Tests			
Unconfined Compression Strength	50	-	100
Hydraulic Fracturing	50	5	75
Tensile Strength	50	-	35-37.5
Tensile Strength (with centre hole)	50	3	35-37.5
Erosion Test			
Hole Erosion Test	52	3	100-115
Modified Triaxial Test	50	3	100



Figure 3.6 CB sample after 21 days curing

3.2.4.3 Simulating Concentrated Leak

For erosion test samples, a crack should exist to simulate the initial condition before the erosion phenomenon was started (Rice and Duncan, 2010). There are two suggested methods to simulate a crack in sample: artificially fail the sample or form the crack via other means. Rice and Duncan (2010) suggested that the formation of crack in CB sample is due to the tensile stress imposed is larger than its tensile strength, therefore failing sample through tensile strength test could be an option. Nonetheless, there were several technical issues considered for this method:

- The crack orientation and post-failure sample form/shape could hardly be controlled. As sample would be tested inside the mould therefore it is important to ensure the samples did not deform drastically.
- The sample surface roughness would always vary which could result in high variability of initial friction coefficient.
- Although it is not considered major technical issue, this method will form rectangular shape erosion channel and larger erodible surface. They will become problem as post-erosion test sample are usually not uniform (e.g. Mehenni et al., 2016; Hark, 2019) and the larger the erodible surface will potentially increase this risk.



Figure 3.7 Sample cross-section with hole in the centre and casted hole (using super glue)

Considering above issues, it was decided that the circular shape erosion channel was better option as the above technical difficulties could be avoided. The circular erosion channel could be formed by drilling and casting. Drilling exposed samples to too much disturbance (e.g. thrusting force from drill bit, vibration during drilling) and it put sample into a higher risk of failure. Moreover, drilling procedure could also influence the erosion test result as the drilling control the degree of disturbance the erodible surface would have. Therefore, casting the circular channel using rod was chosen. Acrylic rod was used as it did not rust like metal during curing and the hole formed was more uniform than using wire. In addition, it did not stick to the CB making extraction relatively straightforward. The orientation and shape of the hole created by the rod was checked by pouring super glue or paraffin wax to the hole and let it set and harden (as seen in Figure 3.7)

3.3 Material Strength and Basic Properties Test

3.3.1 Unconfined Compressive Strength (UCS) Test

The procedure of UCS test used in this study was in accordance with British Standard (BS) 1377-7: 1990. The maximum compressive force per unit area that trigger failure is defined as the strength of the sample. Equation 2 was used to calculate the strength σ (in kPa):

$$\varepsilon = \frac{AL}{L_0} \quad (1)$$

$$\sigma = \frac{P\,(1-\varepsilon)}{Æ_0} \cdot 1000 \quad (2)$$

ε, ΔL, L_0, P, and A_0 represent axial strain, change in sample length (mm), initial sample length (mm), compressive force (N), and initial cross-sectional area of sample (mm^2).

After the sample fail, the test was continued until the force applied to the sample decreased dramatically (Figure 3.8). The orientation of sample after failure was documented and further analysed (Figure 3.9). There were total of 206 samples tested for UCS this test.

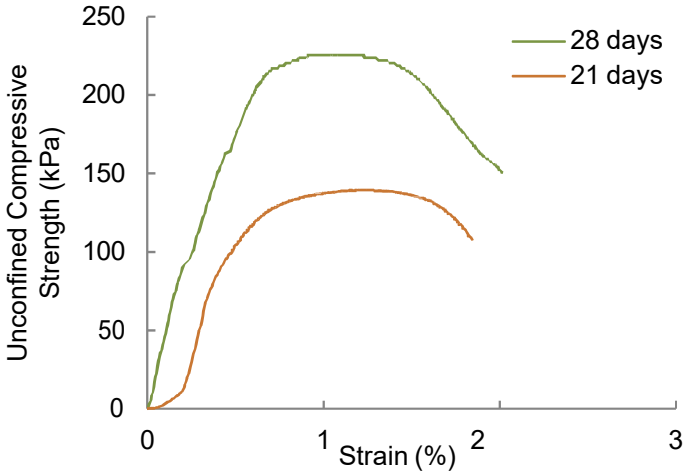


Figure 3.8 Typical UCS test result (CB with GGBS 80%)

All the tested samples had the same dimensions: 100 mm in height and 50 mm in diameter. The test was conducted under the deformation rate of 1 mm/min (suggested range 0.5-2%/min). The test for the same sample characteristic was repeated for 5-6 times to determine if the result obtained was repeatable or not and how big the encountered variation was (as a material cast from slurry, variation in properties is a known issue). The noticeable appearance of these samples is discussed in Result and Discussion chapter.

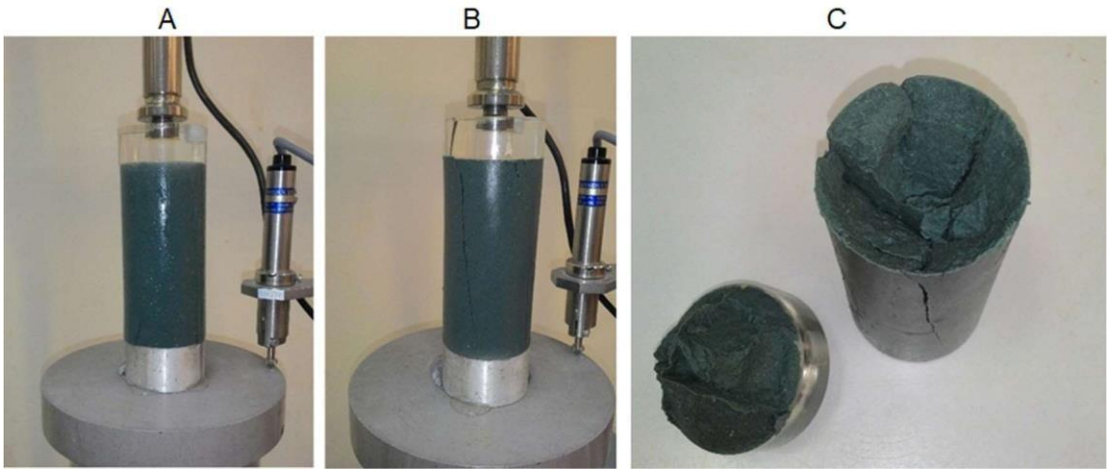


Figure 3.9 (a) Sample during UCS test, (b) and (c) Sample after failure

3.3.2 Tensile Strength Test

The test procedure used was following the detail specified in American Society for Testing and Materials (ASTM) D3967-16. Similar to UCS, the tensile strength is defined as the maximum compressive load per unit area that sample can receive until it fails. The difference mainly lies on the sample placement (perpendicular to the direction of load, as seen in Figure 3.10) and its size. As the sample was placed on flat platen, Equation 3 was used to calculate the tensile strength σt (in kPa):

$$\sigma t = \frac{2P}{\pi DH} \quad (3)$$

P, H, and *D* represent maximum applied load (N), sample thickness and diameter (mm).

After sample fail, the load applied to sample usually dropped dramatically and the test ended (as seen in Figure 3.11). Samples with 3 mm hole were tested in order to study its influence the effect of centre hole to the tensile strength.



Figure 3.10 Sample during tensile strength test (left) sample with hole (right) sample after fail

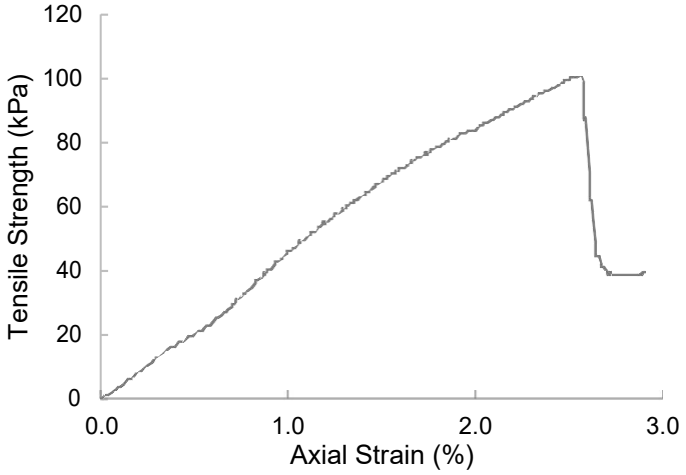


Figure 3.11 Typical tensile test result (CB, 90 days old)

According the standard, the thickness to diameter ratio should be within the range of 0.2-0.75. Therefore, as the sample diameter is 50 mm, the sample thickness is ranging from 35-37.5 mm. The strain rate and the repeatability procedure used were similar to UCS test: 1 mm/min and additional 5-6 times repeated test. There are total of 205 samples tested for UCS this test.

3.3.3 Hydraulic Fracturing

The hydraulic fracturing test aimed to study the resistance of CB sample to failure against fluid pressure. Ng (2009) studied the susceptibility of CB samples to hydraulic fracturing using hollow cylinder test apparatus (cavity

expansion and leak-off test). Several parameters should be considered to understand the hydraulic fracturing in CB samples: confining pressure, injection rate, stress condition, curing age, and mix proportion (Ng, 2009). As the previous study only examined the sample older than 90 days, this test attempted to examine the hydraulic fracturing phenomenon in younger CB samples. The apparatus detail is illustrated in Figure 3.12.

For hydraulic fracturing test, the test was conducted under unconsolidated undrained condition. The nozzle size was the same with the one used in PET and both ends of the sample should be drilled using countersink in order to ensure the nozzle could perfectly be inserted inside the sample. Before the testing commenced, the system (sample hole, upstream and downstream channels) was de-aerated (to ensure there was no air bubbles) and filled with water. The cell was filled with water to apply confining pressure and internal pressure (pressure inside the sample hole). Firstly, the confining pressure was set to desired value (25 – 150 kPa) while the internal pressure was kept below 10 kPa. The internal pressure was increased at the controlled rate (increase of 25 kPa per 30 seconds) until the sample failed. The sample failure was indicated by visual observation of crack and the expansion of membrane (Figure 3.13). The membrane expansion was due to the pressure inside the hole which was higher than the confining pressure. This phenomenon will be further discussed in Section 3.4.2.

Due to the sample preparation that exposed the sample with considerable disturbance, some samples were considered not suitable as they were still soft/weak therefore could easily be destroyed during the sample preparation. For CB samples without GGBS replacement, although cured for 90 days, they were still easily disturbed. The suitability of CB samples for this test is specified in Table 3.7.

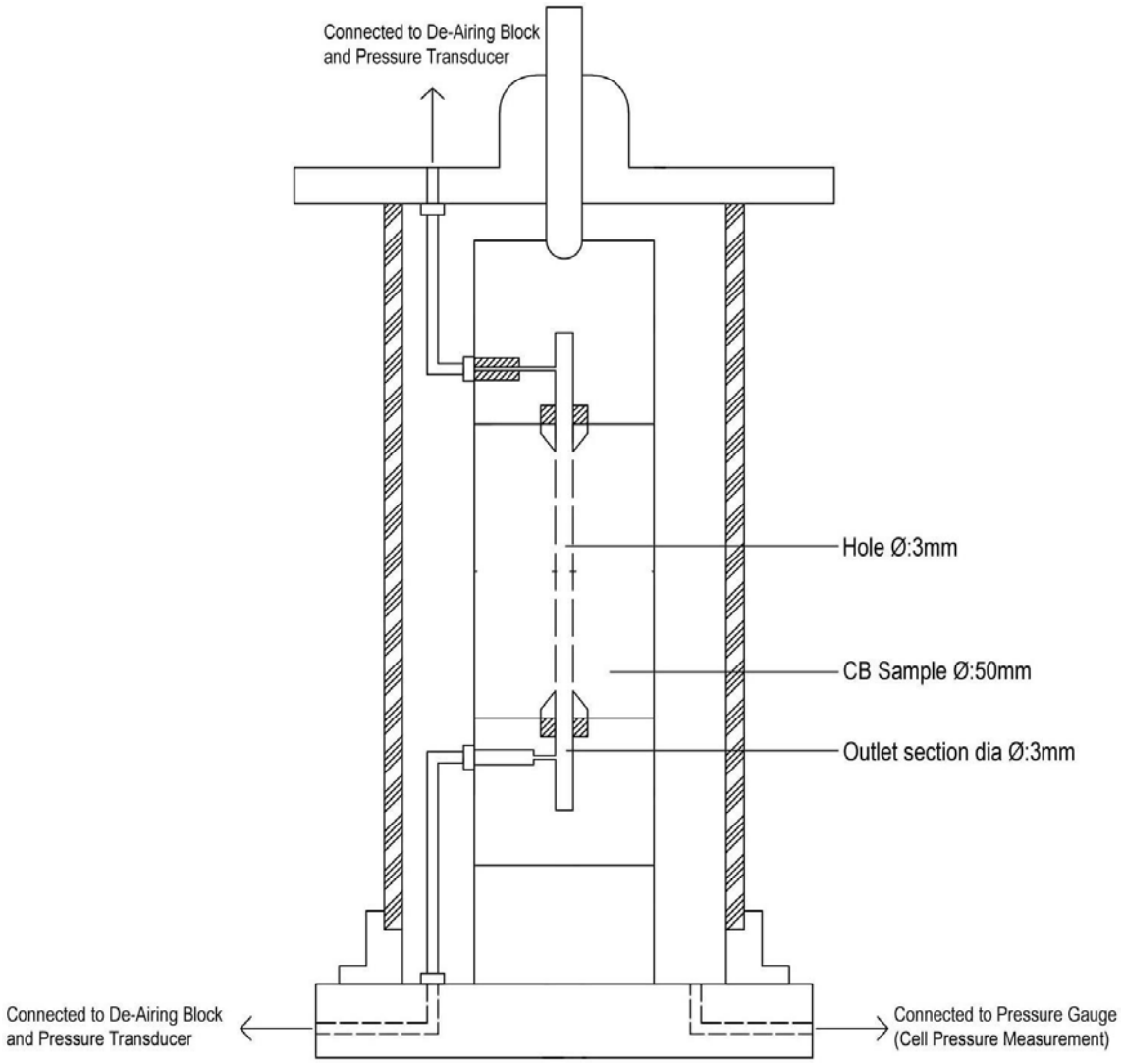


Figure 3.12 The schematic diagram of hydraulic fracturing test apparatus

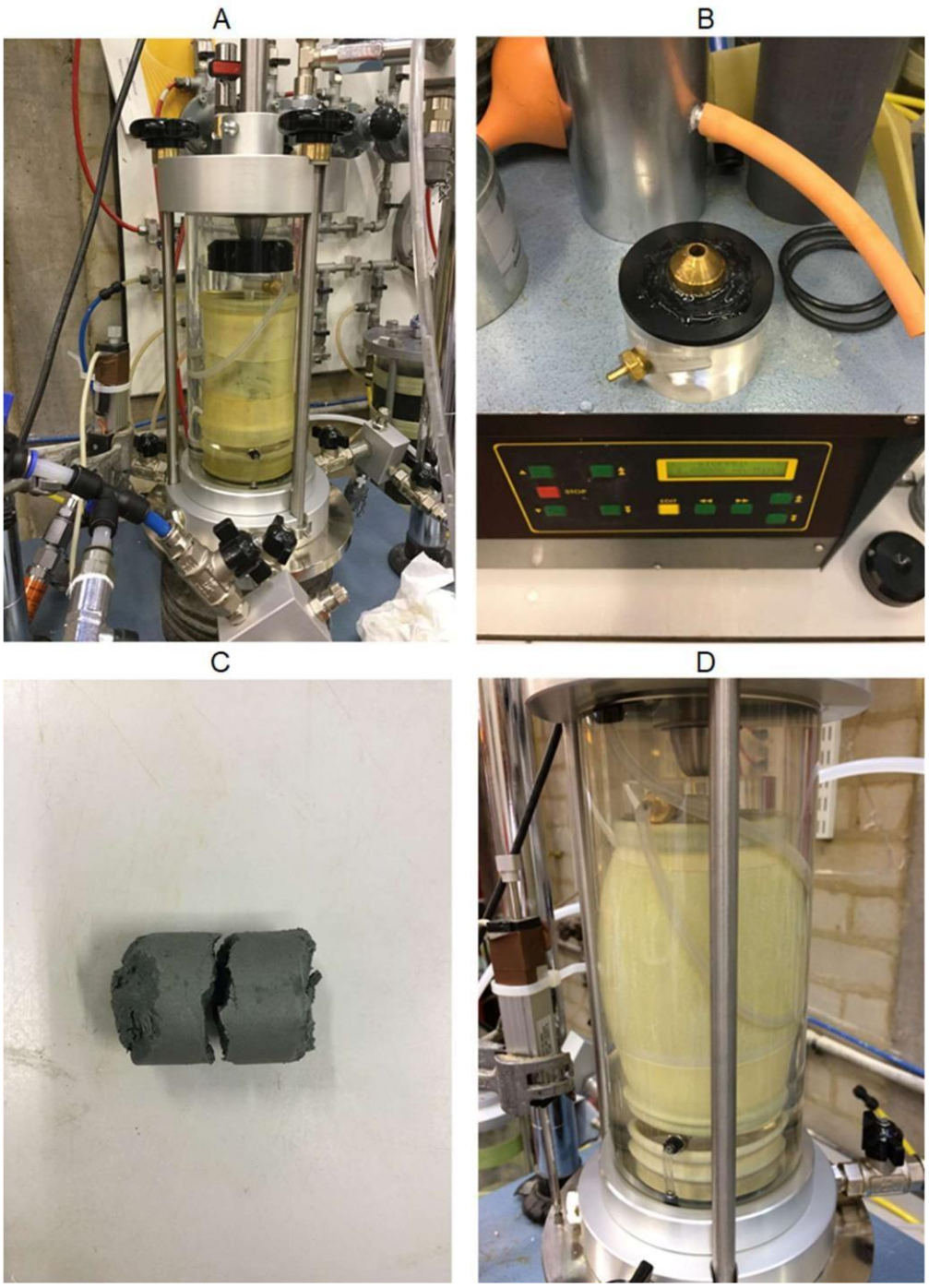


Figure 3.13 (a) Testing was running, (b) Silicone grease was spread at both ends of sample to prevent leaking (c) The sample fails after hydraulic fracturing test, both ends were partially lost as they are attached/glued to the silicone grease (b) when the sample failed, the membrane expanded

Table 3.7 The sample suitability for the hydraulic fracturing apparatus

Type	% GGBS Replacement	Age					
		7	14	21	28	56	90
CB	0	No	No	No	No	No	No
CB with GGBS	40	No	No	**Yes**	**Yes**	**Yes**	No
CB with GGBS	60	No	No	**Yes**	**Yes**	No	No
CB with GGBS	80	No	**Yes**	**Yes**	No	No	No

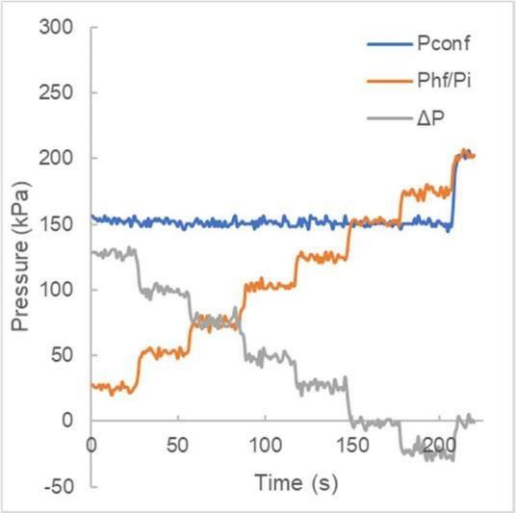


Figure 3.14 Typical data analysis for hydraulic fracturing test (CB with GGBS 60%, 21 days) – P_{conf}, P_{hf}/P_i, and ΔP represent confining pressure, internal pressure, and pressure differential.

3.3.4 Moisture Content

The procedure to determine the moisture content of soil is specified in BS 1377-2:1990. The weight of CB sample before and after the oven-drying (at 100° C for 24 hours) were recorded. Equation 4 was used to determine the moisture content ω:

$$\omega = \frac{m_{wet} - m_{dry}}{m_{dry}} \quad (4)$$

m_{wet} and m_{dry} represent mass, in gram, of sample before and after the oven drying, respectively.

3.3.5 Particle Density

The procedure used to conduct particle density test was based on BS 1377-2:1990. CB samples was dried in oven for 24 hours at the temperature of 100° C. The dried samples were ground in order to pass a 2 mm sieve. As the particle size of the ground sample was finer than 2mm, small pyknometer method was chosen. The results differences should be maintained +/- 0.03 Mg/m^3, otherwise the results should be discarded, and the test was repeated until it obtained the difference less than that. Equation 5 was used to determine particle density ρ_s:

$$\rho_c = \frac{M_2 - M_1}{(M_4 - M_1) - (M_3 - M_2)} \quad (5)$$

m_1, m_2, m_3 and m_4 represent mass of bottle, mass of bottle and dry soil, mass of bottle, soil and water, and mass of bottle and water.

3.4 Erosion Test

3.4.1 Concentrated Leak Erosion Test

3.4.1.1 Introduction

The test mainly aims to study the erodibility characteristics of the CB sample. Initially, there were two types of concentrated leak erosion test to be performed:

1. Pinhole erosion test (PET)
2. Hole erosion Test (HET)

The main difference between these two tests are their entrance section and the parameters analysed. The size of PET entrance section is the same with the initial hole diameter of the sample while the diameter of HET section is always bigger than the sample hole. In terms of the analysed parameters, PET mainly focus on linking the amount of eroded materials within the certain duration and hydraulic characteristics whereas HET emphasised on understanding the relationship between hydraulic shear stress and erosion rate. Due to several technical considerations (described below), HET was chosen over PET as the former was considered more appropriate to study the CB erodibility and this will be further discussed in the following subchapter.

3.4.1.2 Pinhole Erosion Test (PET)

In principle, PET, first developed by Sherard et al. (1976) is used to identify and classify dispersibility of geomaterial and its detail and procedure are standardised in ASTM D4647 (Figure 3.15). The test is conducted by flowing water through a sample with pre-formed hole under controlled hydraulic head/flow rate. Analysis of the dispersibility is done qualitatively by assessing the effluent turbidity exiting from downstream section of the sample with varying eroding fluid hydraulic head and flow rate. The test is conducted under constant hydraulic head ranging from 50 to 1020 mm. As the dispersibility classification is only available within that range of hydraulic head, if the samples do not erode or disperse at hydraulic head of 1020, it is automatically classified as non-dispersive (non-erodible) (ASTM D4647). CB sample is not dispersive soil as the samples were submerged under water during curing and there was no indication of dispersion observed. According to past relevant studies (Garand et al., 2006; Wang et al., 2017), it required high velocity (e.g. 3 m/s: Garand et al., 2006) of the eroding fluid to initiate particle detachment on CB samples. Therefore, the established classification and its technical limitation was deemed not suitable for this study.

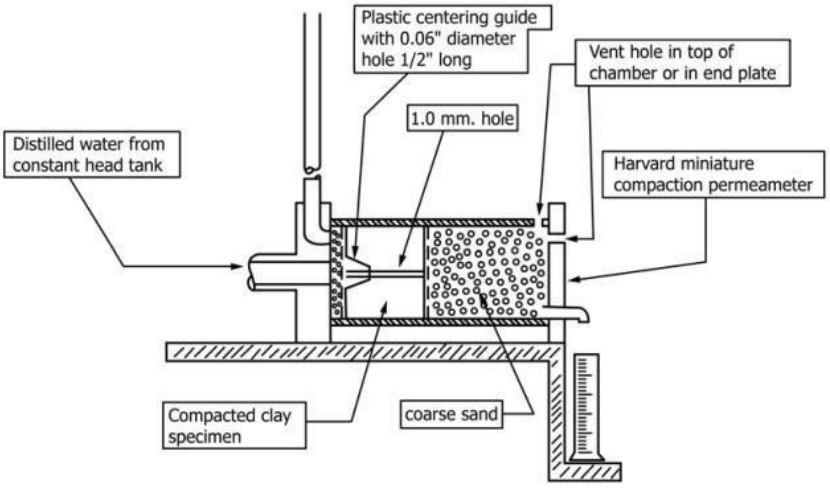


Figure 3.15 The schematic diagram of PET (after ASTM (2013))

The PET apparatus built for this study was equipped with pressure sensors and ultrasonic flowmeter to record the pressure and flowrate during the test. It used entrance size of 3 mm instead of prescribed 1 mm (ASTM, 2013)

because it was not possible to cast perfect hole using 1 mm wire and the metal wire would rust during the curing. However, the problem was not on the size of entrance hole but on the ratio of entrance to sample hole. The apparatus had an initial ratio of entrance to sample hole of 1 (Figure 3.16). As the particle detachment commenced, the entrance size did not experience any change therefore the hydraulic energy exiting the entrance remained the same during the test (Figure 3.17 and 3.18); but would drop upon entry into the eroding sample (which was not determinable using this layout). Whilst changes in downstream flow conditions could be monitored, and (slowly) reducing downstream pressures would suggest that erosion was taking place (as can be seen in Figure 3.18), it was not possible to determine the critical conditions that initiated erosion within the material using PET. Concerns with the characterising the hydraulic characteristics of the sample using PET have been raised previously (Wang et el., 2017) as whether or not the test replicates crack erosion in the field.

Hence if the fluid flow rate and pressure were maintained, the surface of the sample was exposed to the same hydraulic condition during the test. From the test results (Figure 3.17-3.18), the upstream pressure and flowrate remained constant until the end of the test. The downstream pressure dropped at a slow rate; this was due to hole enlargement which indicated erosion had occurred. This condition was deemed problematic as the test was run under the assumption that the sample should erode (i.e. above critical point at which erosion initiated), the critical condition was not possible to be estimated and regardless of the testing duration, the sample would continue to erode, and this was the case from the previous study (Wang et al., 2017). Moreover, when the erosion occurs in the field, the crack enlargement due to erosion causes the change in the hydraulic condition inside the erosion channel which PET does not properly simulate.

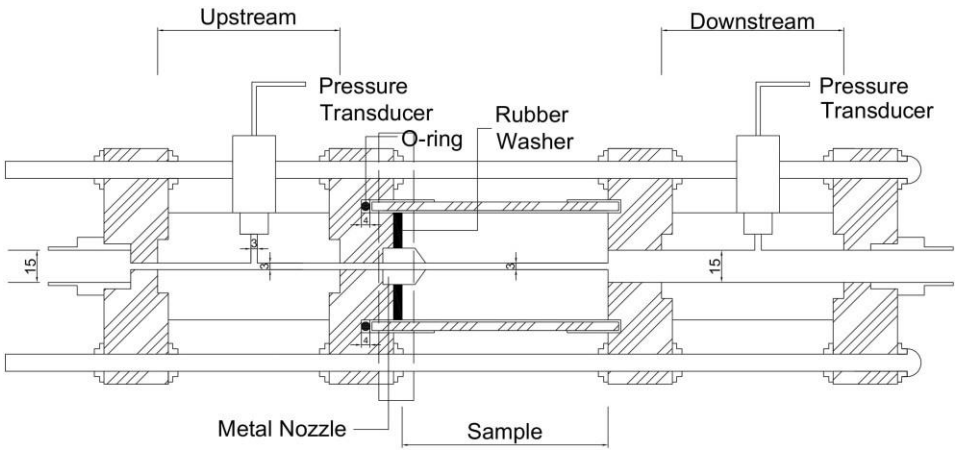


Figure 3.16 The schematic diagram of PET used for this study

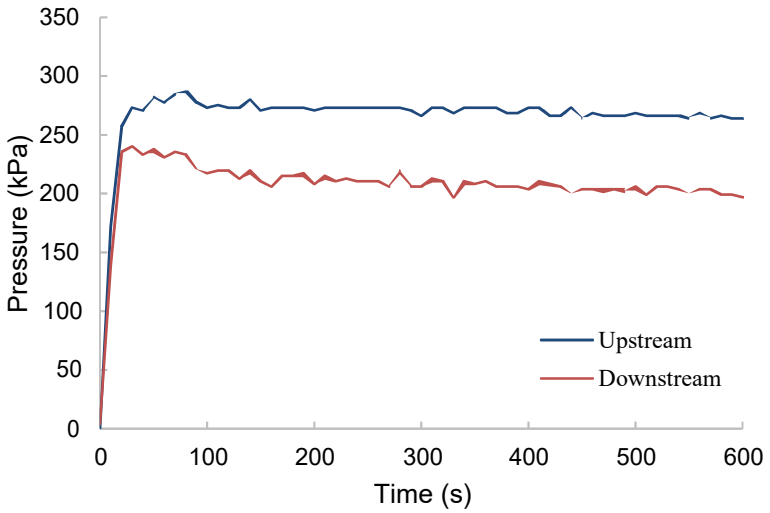


Figure 3.17 PET results for CB sample (21 days curing)

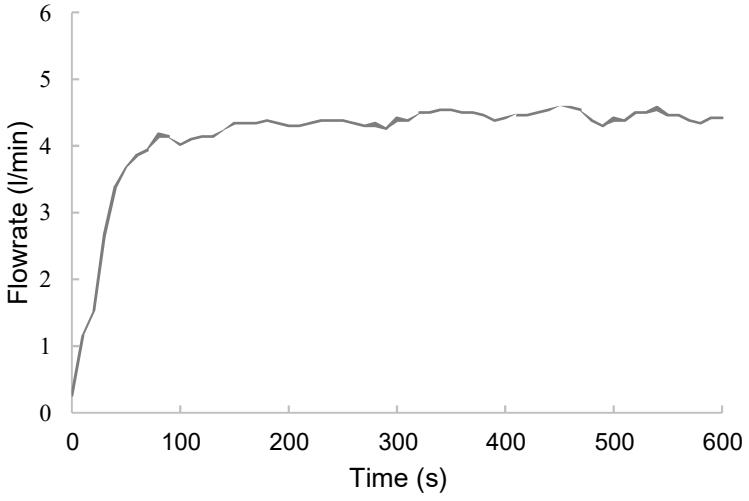


Figure 3.18 PET results for CB sample (21 days curing)



Figure 3.19 The hardened cast of the eroded hole

In addition to the technical issue discussed in the previous paragraph, it also affected the shape of the final eroded hole. As seen in Figure 3.19, the middle part was comparatively bigger than the section closer to the downstream. This was because the energy exiting the upstream were concentrated at that area and the sudden drop of hydraulic energy at the upstream area caused the noticeable difference on the amount of particle detachment at the downstream. In addition, this added complexity in interpreting the final eroded hole due to its non-uniform shape (did not resemble cylinder), therefore its volume could not be accurately estimated. For these reasons, experimentation using PET was terminated and an alternative HET was used.

3.4.1.3 Hole Erosion Test (HET)

First developed by Wan and Fell (2002), HET had been used and modified by several researchers (e.g. Luthi, 2011; Haghighi et al., 2013; Mehenni et al., 2016) to study and improve the understanding of geomaterials erodibility. Unlike PET, the HET test has a larger entry diameter within the housing than of the crack under investigation so the issues regarding the change in flow conditions as the water erodes the sample (and the crack diameter becomes larger than the entry diameter) do not arise. However, the test relies on the erosion being uniform along the length of the sample if the assumptions used to characterise the flow conditions are to be valid, hence non-uniform samples

(such as that displayed in Figure 3.18) are deemed not ideal when considering the flow conditions (Mehenni et al., 2016). This is a limitation in the test, but one that is accepted herein as it offered a method to systematically investigate the difference in response of the CB with changing mixture and curing age. This limitation is considered once again later in the following subchapters.

The HET method ultimately aims to analyse the relationship between hydraulic shear stress (τ) across the simulated crack and its corresponding erosion rate (ε). From the relationship, critical hydraulic shear stress (τc) is obtained which is used as threshold value for the particle detachment to occur. The test is conducted by flowing the eroding fluid inside the simulated crack and its flowrate and pressure are controlled during the test. The erosion occurs when the pressure differential (ΔP) between upstream and downstream starts to drop and the flowrate (Q) increases dramatically. Unlike PET, HET apparatus allows for changing hydraulic condition across the sample, that depend on the evolution of the simulated crack diameter. When the crack size enlarges to the point where the hydraulic condition is closer to, or below, the threshold of the critical point, the erosion ceases.

3.4.1.4 Technical Procedure

Pressure transducers are located at both ends (upstream and downstream) of the sample and the ultrasonic flowmeter at the entrance side measured and recorded the fluid pressure and flowrate at predetermined time interval. As shown in the schematic diagram of testing apparatus (Figure 3.19), the pressure differential is mainly controlled by gate valve at both ends. The internal diameter of the pipe where the flowmeter is installed is 18 mm and it decreases to 15 mm at the gate valve. The size of sample is 52 mm in diameter and 100mm in height with initial hole/crack diameter of 3 mm (inlet to crack diameter ratio of 5, as opposed to 1 in the PET). The diameter of both upstream and downstream is 15 mm. Although the o-rings were placed at both ends of the acrylic tube to seal it, both ends of sample were cushioned by rubber washers to provide extra protection against leaking. The clear acrylic tube was placed at the downstream side to visually observe the eroded

material and camera was installed to record the erosion process during the testing. After sample was placed, all parts of the apparatus are tightened by wing nuts.

The technical procedure of HET is as follow (using the procedures outlined by Wan and Fell, 2004):

1. Once the sample is installed within the housing and this is inserted within the apparatus the system is filled (closing the downstream valve) with water under low pressure and velocity to prevent any particle detachment. The air vents at both upstream and downstream as well as upstream valve are closed gradually as the system is filled with water and the air is displaced. The water used for the test (tap water) is not previously de-aired therefore it is not possible to diminish all the air bubbles completely. However, excessive amount of air bubbles should be avoided. The booster pump (Figure 3.20) was turned on to completely fill the pipe with water thus allowing the flowmeter to undertake measurements. The maximum rated pressure of the booster pump is 350 kPa and the maximum flowrate could be pumped to the system is 30 litres/min.
2. The gate valves at upstream and downstream were opened slowly until the pressure transducer pick up the measurement and pressure differential below 5 kPa was reached. The data logging feature on both pressure transducers and flowmeter was activated and the recording interval was set to per second. The camera used to record the downstream side was also turned on at the same time.
3. The test was started by slowly opening the upstream gate valve. As there was a time lag between pressure and flow measurement, it is important to carefully opening the valve so both measurements could be synchronised. There are 3 phenomenon which indicated that the erosion had commenced:
    - Pressure differential dropped and did not increase even as the valve continues to open

- Flowrate increased dramatically as the pressure differential dropped (Figure 3.21);
- Visual observation from acrylic pipe at downstream side (Figure 3.22)

4. The initial upstream pressure should be started at very low levels, especially for juvenile samples. If the upstream pressure is too high, it risks the sample being damaged (Figure 3.23)
5. The valve continues to be turned until the pressure differential continued to drop dramatically. The test was then continued to run under the constant flow rate for the desired duration. Maximum duration of the testing is ranging from 500 to 900 seconds.
6. For the case of no erosion, there was no drop of pressure differential under the maximum pressure differential that the system could generate (ΔP of 320 kPa) (Figure 3.23)
7. After the test was finished, the apparatus was de-watered and disassembled. The sample tube was released and transported to the sample extruder. The sample was extruded carefully from the tube and air-dried. The sample was then dried especially inside the hole. After it was dried, the melted paraffin wax was poured into the hole and was left until hardened (it took up to 7-10 minutes). The sample was trimmed carefully to take the cast out from the sample (Figure 3.26). As the shape of eroded hole could be either uniform or non-uniform, the measurement of diameter was undertaken every 10 mm along the cast using calliper. As the length of the sample was 100-115 mm, there would 10-11 diameter measurements and the diameter of the eroded hole used was the average of the measurements. Sample with back-cuts at the downstream side was discarded as it affected the pressure differential measurement (Figure 3.25c). However, the occurrence was recorded in order to analyse the likelihood of back cuts in regard to the mix proportion and curing time.

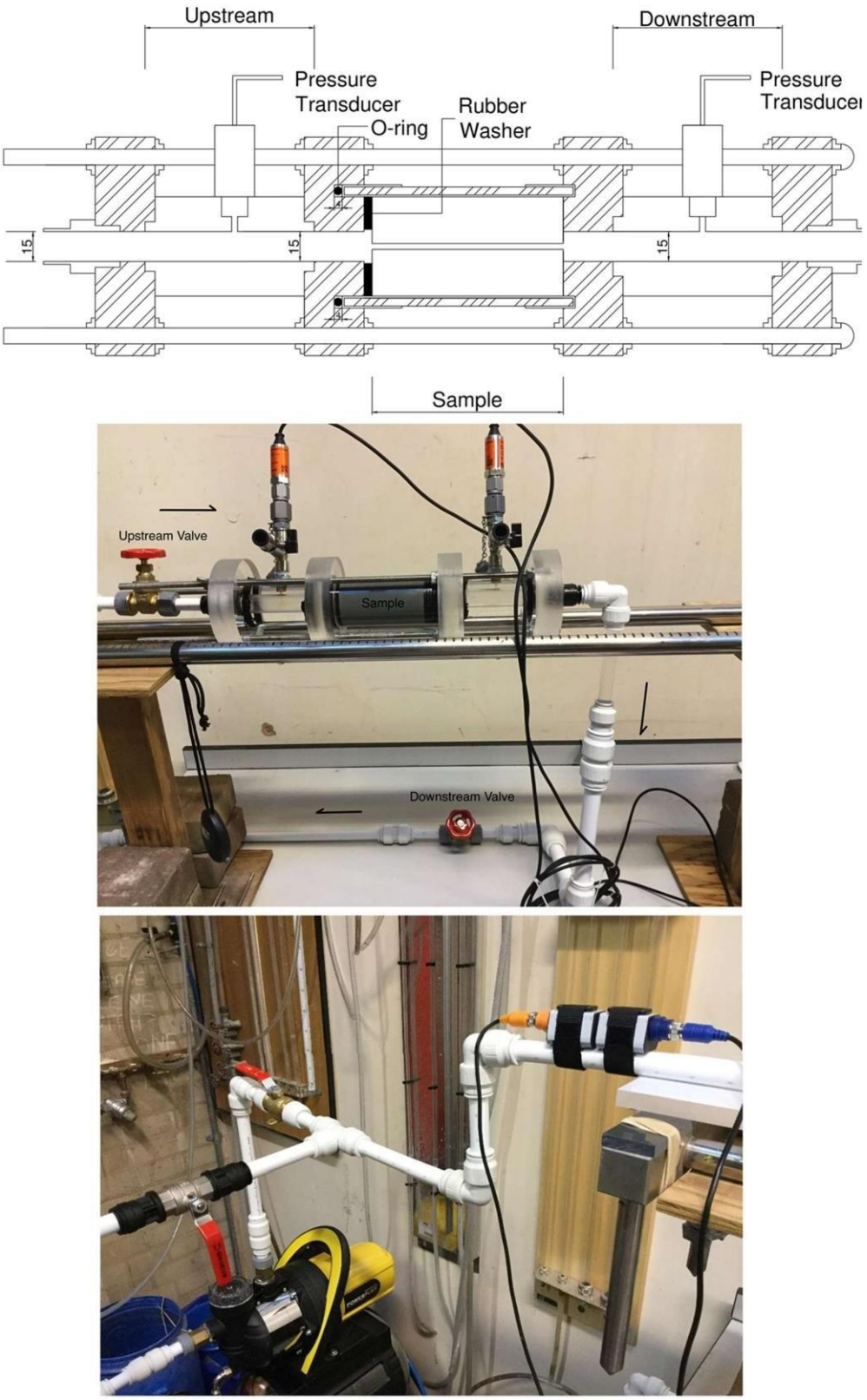


Figure 3.20 The schematic diagram and photographs of HET apparatus

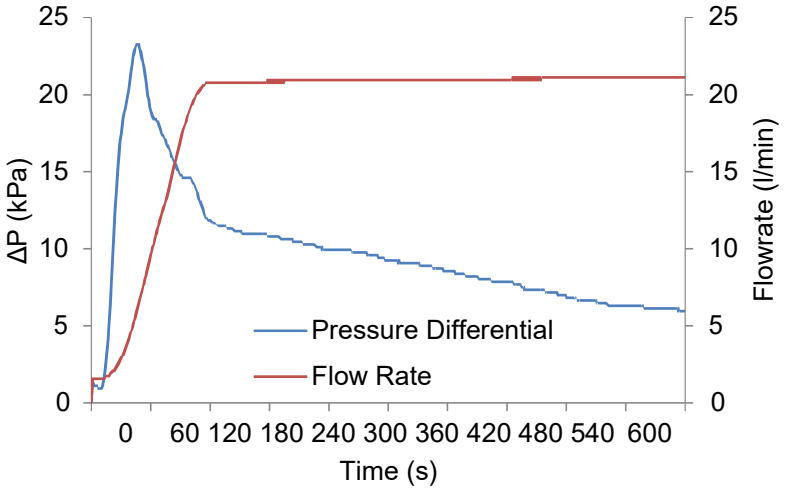


Figure 3.21 The relationship between pressure differential and flow rate against time (CB with GGBS 80%, 7 days)



Figure 3.22 Turbidity observed at the downstream pipe

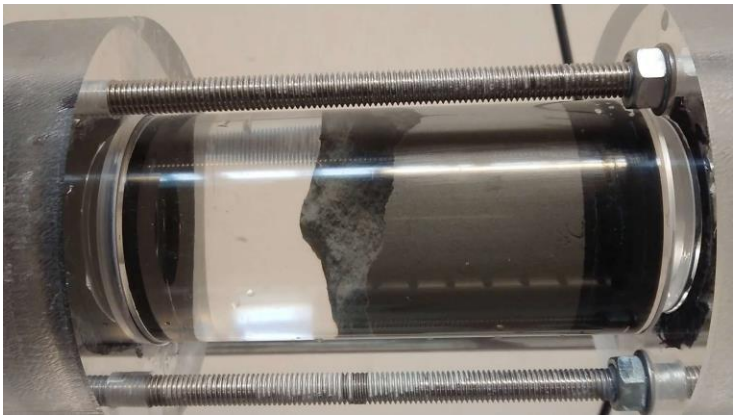


Figure 3.23 Entrance sides of sample was flushed away by high upstream pressure

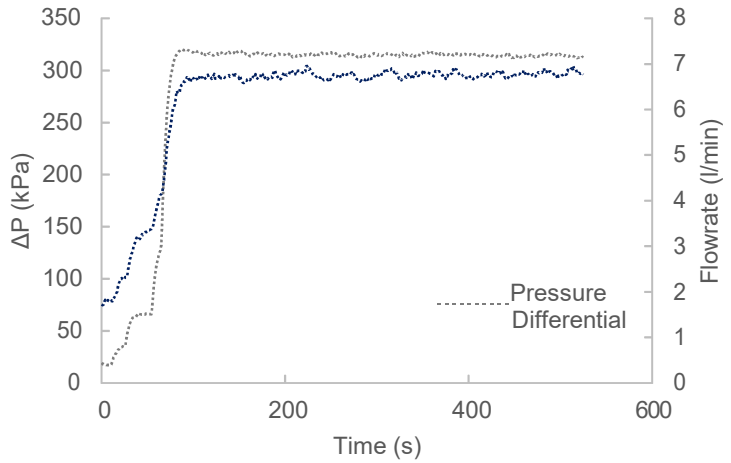


Figure 3.24 Typical pressure differential and flow rate readings for no erosion

Erosion was considered to commence from 100-150 seconds, depending whether it reached the peak or not. Note that the pressure differential took time to establish due to the requirement to open the value slowly enough not to shock the sample and damage it (Figure 3.23)

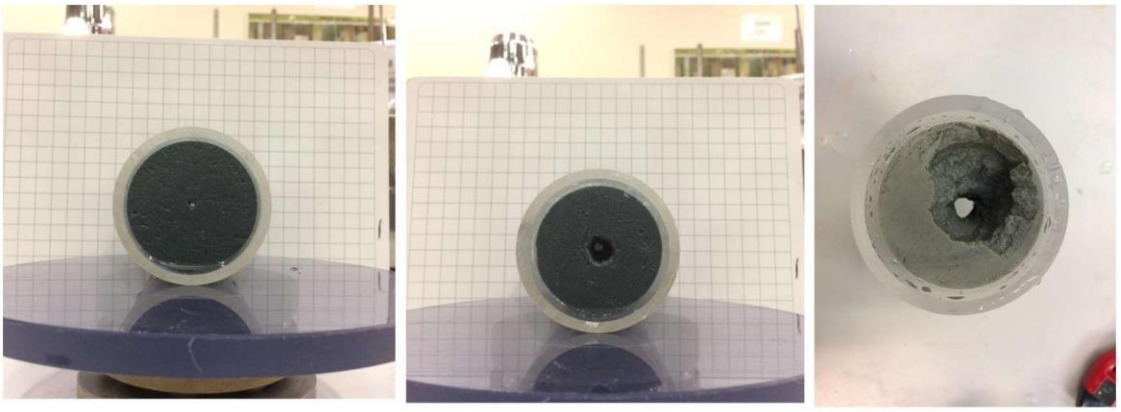


Figure 3.25 Sample (a) before testing (b) after testing (c) suffered back-cuts at the downstream side



Figure 3.26 (a) The cast of the eroded hole (b) Uniform hole (c) Non-Uniform hole

3.4.1.5 Technical Consideration

3.4.1.5.1 Hydraulic Head

The apparatus used by Wan and Fell (2002) had a limited range of hydraulic head (from 50 to 1200 mm) which affected the range of hydraulic shear stresses that could be applied to the sample. However, a previous study (Mehenni et al., 2016) had improved on this by using pressurised tank to produce higher upstream pressures, thus generating higher hydraulic gradients. There had been several modifications done to improve the hydraulic head estimation. Luthi (2011) and Fattahi et al. (2017) used pitot-static tube to measure velocity at the exit section of the sample. However, it could lead to flow disturbance at the downstream side and could affect the accuracy of reading. The risk of clogging should also be considered especially for the sample with high proportion of fine-grained material (Luthi, 2011). Measuring the flowrate at the downstream using ultrasonic flow meter was not possible as the flow meter could only pick up measurement if the flowing water did not contain soil particles. Turbidity was used to improve the method to estimate hole enlargement (Haghighi et al., 2013; Mehenni et al. 2016), but the option was not considered for this study due to the limitation of available funding. The turbidity sensor should be kept clean to ensure the accuracy of

the reading, this potentially raised an issue if the sensor were covered by the eroded material during the test (Braithwaite, 2013).

It is acknowledged that positioning the pressure transducers in positions where the pipe diameter is 15 mm, rather than after the step-down where it becomes 3 mm, is not going to provide accurate data on the hydraulic conditions within the simulated crack. Hence the stated values are an estimate. This is a limitation of the approach, although as noted above it is one known to the scientific community. Positioning the sensors where they can gain accurate readings (i.e. in flow or as near as possible to the entrance and exit) is likely to influence the flow conditions established within the samples and hence potentially change the erosion response. Clearly neither is desirable, and the decision was taken not to place the sensors too close; in fear of changing/artificially influencing the erosion processes to the entrance and exit, and accept that the hydraulic conditions recorded are an approximation. As this study focuses upon changing internal erosion resistance with material mixture and duration of curing (i.e. focusing upon the geotechnical response of the material), and the limitations of measuring the hydraulic conditions are constant across the tests, then this was deemed an acceptable (if undesirable) limitation to the work.

3.4.1.5.2 Valve Opening

As mentioned in 3.4.1.4, the flow rate and pressure were controlled by gate valve, and at the start of the test this had to be opened to create the desired pressure difference acting across the samples. This was a manual operation that had to take place over a given time (10-20 seconds) if damage to the samples were to be avoided; opening it too swiftly resulted in the potential for sample damage (presented in Chapter 4). Opening of valve resulted in a (comparatively) rapid transitory change in the flow conditions within the apparatus (Figure 3.21), changes that were difficult to accurately quantify with the equipment available. Once the desired pressure difference was achieved, then the valve was left in position and the changes in hydraulic conditions occurred at a rate that could be accurately recorded. Therefore, at the beginning of each test there is a period of rapid change in pressure where the

erosion (if any) processes are difficult to quantify due to this rapid transitional phase. Once again, in order to protect the samples from damage by applying the desired pressure too quickly to the samples, the adopted procedure contains unavoidable limitations (with the equipment available), although this was also deemed acceptable (if not ideal) as once the desired pressure differential was achieved the hydraulic conditions could be determined (estimated, as noted in the previous section).

3.4.1.5.3 Flow and Pressure Readings

In order to understand how the change in hole diameters affected the measured flow rate and pressure differential, non-erodible samples (CB with GGBS, at cement replacement proportions of 80%, cured more than 90 days) with varying hole diameters (3-12 mm: cast in place using different diameter plastic rods) were tested under different hydraulic conditions (the results are presented in Chapter 4). The relationship between hole diameter with maximum flow rate and pressure (the upstream valve fully opened) (Figure 3.26) indicated that the hole enlargement resulted in the increase of flow rate and the decrease of pressure differential. The increase of flow rate was mainly because the increase in diameter meant increase in volume therefore more volume of water could flow inside the hole while the decrease in pressure differential was attributed to the increase of pressure at downstream. The error range for flow rate measurement increased from +/- 0.1 to 0.3 l/min with the hole enlargement while there was no noticeable trend for the pressure reading and the recorded error was within the range of 10 to 14 kPa. The relationship of measured flow rate and pressure for certain size of hole diameter suggested that an increase in flow rate lead to a decrease of pressure differential

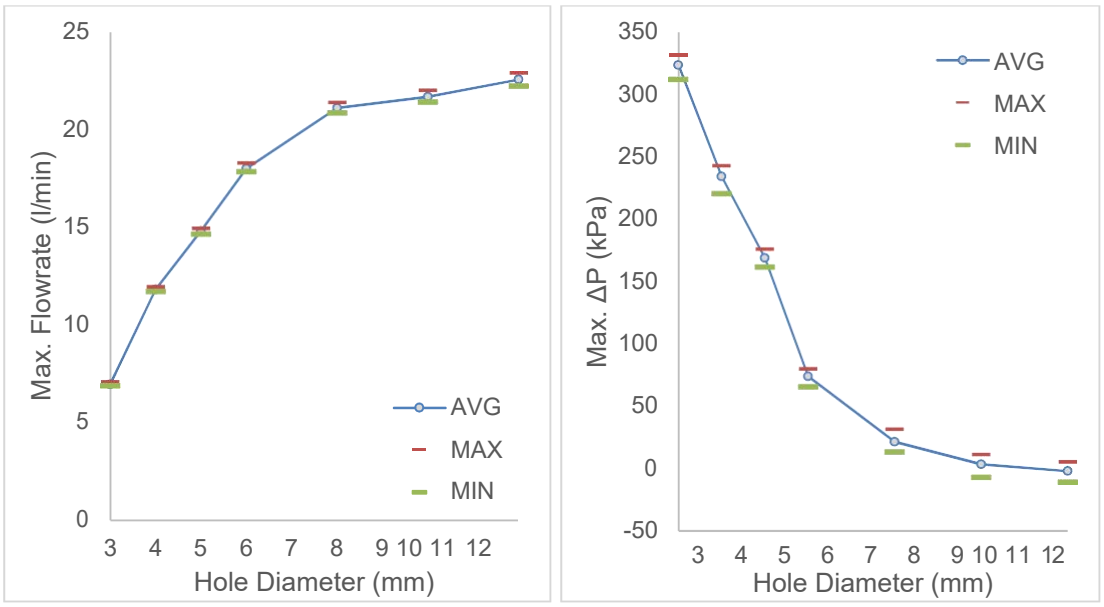


Figure 3.27 The relationship between hole diameter with flow rate and pressure

3.4.1.5.4 Hole Casting

The eroded hole was cast using paraffin wax and was left to harden at room temperature. In order to investigate the degree of error from the wax casting, non-erodible samples were used for this purpose. From the results (as seen in Figure 3.28), the error was ranging from 0.1-0.2 mm. This could be attributed to the shrinkage of wax during hardening process, or variation within the diameter of the plastic rods used to simulate the cracks. In either situation, this was deemed an acceptable (if undesirable) level of error.

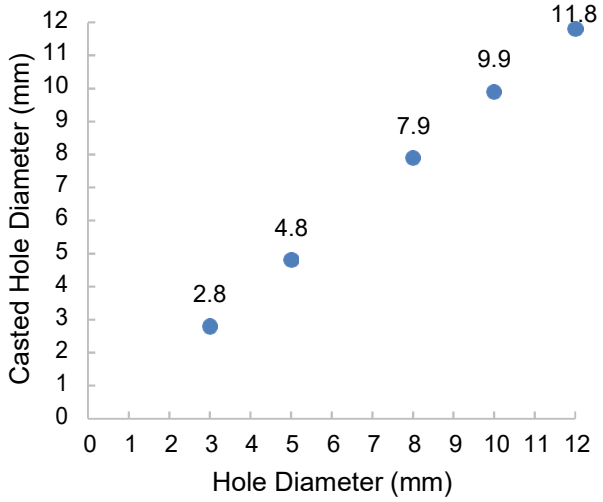


Figure 3.28 The results of wax casting on non-erodible hole sample

3.4.1.6 Data Analysis

3.4.1.6.1 Final Flow, Pressure, and Hole Diameter

The set of data obtained from data loggers reading comprised of flow rate and pressure. The initial and final hole diameter were also known (by measurement of the diameter of the plastic rods before use and the wax casts post testing). The flow rate and pressure differential were plotted against time (an example is presented in Figure 3.29). In doing so, analysis of the change of both parameters during the test could be undertaken. Both were used in estimating hydraulic shear stress and erosion rate (further discussed in Section 3.4.1.6.3).

The final flow rate and pressure differential were plotted against curing age and mix proportion (Figure 3.30 and 3.31). The objective was to investigate how the curing duration and difference in mix proportion affected the erosion resistance of CB samples.

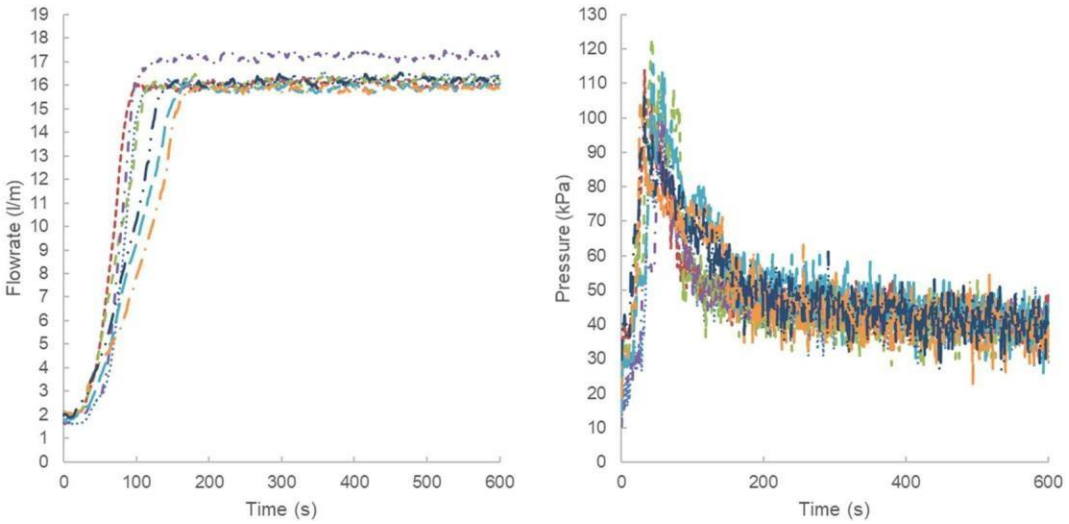


Figure 3.29 Flowrate and pressure differential plotted against time (CB, 90 days)

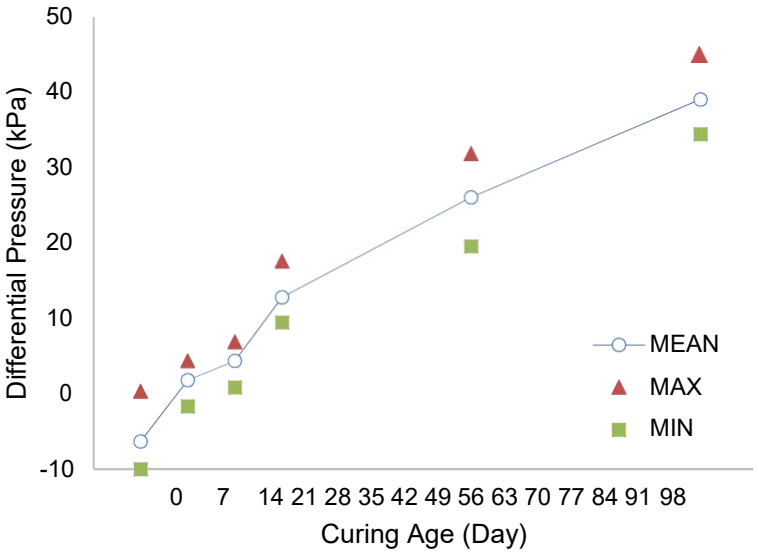


Figure 3.30 The relationship between final differential pressure and curing age (CB without GGBS), 5-6 samples for each curing age

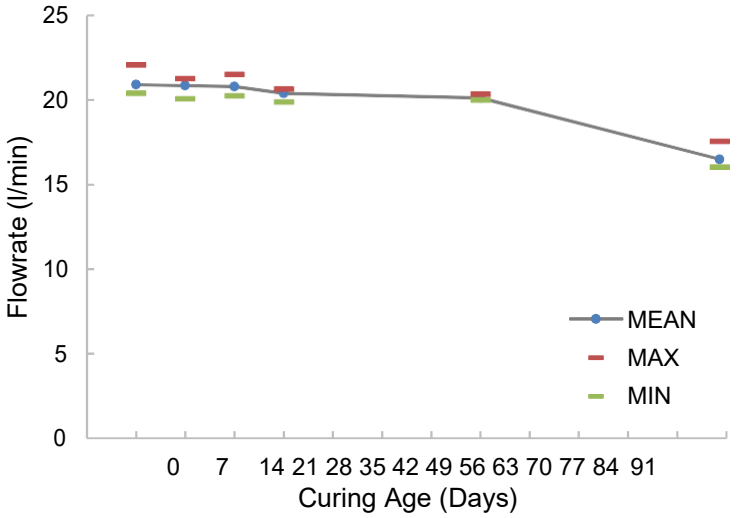


Figure 3.31 The relationship between final flow rate and curing age (CB without GGBS), 5-6 samples for each curing age

The single test usually lasted for 600 seconds and in order to investigate how the hole diameter changed during the intermediate time, the tests were repeated but stopped at desired time (e.g. 150, 300, 450, and 525 seconds) (Figure 3.32). The measured diameter was then plotted against time. In addition, final hole diameter was plotted against curing duration and mix proportion (Figure 3.33).

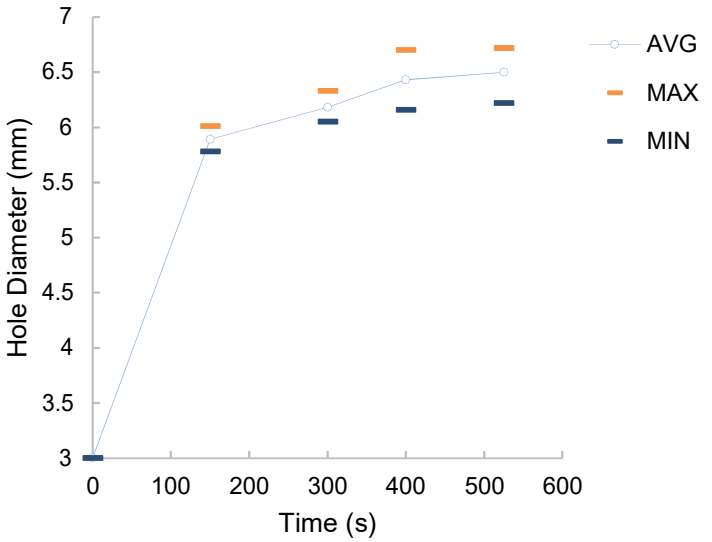


Figure 3.32 Hole diameter at intermediate time (CB without GGBS, 90 days)

Note that tests were not terminated before 100s due to the time required to open the upstream valve (approximately 60s); as noted above it was not possible to describe (or accurately control the valve opening process) the behaviour within the sample before opening was completed.

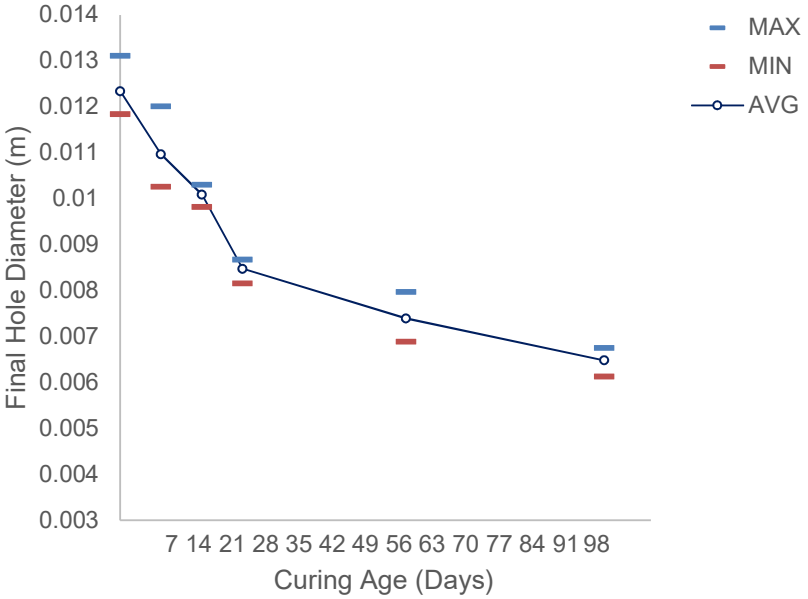


Figure 3.33 The relationship between final hole diameter and curing age (CB without GGBS), 5-6 samples for each curing age

The equations developed for the HET theoretically allow for back calculation of the erosion rate, internal hole diameter, etc., at various stages of the test. However, these equations were developed for non-cemented soils, and not cemented clay suspensions (such as CB), therefore it is still inconclusive to whether this practice be applied to CB data. To determine this, back calculation was undertaken using the equations from the end point of a standard test (duration of 600 s) and the hole diameters observed for the tests terminated before 600 s was mapped onto the projected trends to determine if back calculation is feasible.

3.4.1.6.2 Data Smoothing

Estimating the hole enlargement during the test (via back calculation) is a function of the change of flow and pressure differential parameters. However, there is noise within these trends (caused by factors such as rotation of the pump's impeller, when used, or flow conditions from the tap water, etc.). Inclusion of this noise during analysis caused inconsistencies for the back calculation of hole enlargement. Before the pressure and flow rate data could be used to analyse the hydraulic shear stress and erosion rate, the noises in the reading should be minimised. The previous studies (e.g. Mehenni et al., 2016; Fattahi et al., 2017) did not report nor confirm the use of data smoothing; this was due to the time interval in the testing program which was longer (per 10 or 60 s) than the current study, therefore the trend of pressure differential drop and its associated flowrate was not affected by the fluctuation caused by the apparatus (e.g. pump). As the test used time interval of a second and the reading results were subjected to fluctuation caused by the pump, therefore, the approach to apply smoothing functions to the data before undertaking back analysis was adopted.

The data smoothing undertaken herein used data analysis feature of Excel and exponential smoothing was chosen. The exponential smoothing emphasised the smoothing data of the recent observation/data set and the weight of the previous data decreased exponentially as the observation moves forward with time. The smoothed value was calculated using Equation 6 proposed by Brown (1963):

$$s_t = \alpha \cdot \chi_t + (1 - \alpha) \cdot s_{t-1} \quad (6)$$

Where s_{t-1}, α, and χ_t represent previous smoothed value, smoothing factor ($0 < \alpha < 1$), and weighted average of current observation.

The typical smoothed data is as seen in Figure 3.34. The smoothing factor (α) of 0.8 was chosen as the amount of eliminated noises was appropriate for the pressure and flowrate data to be used for the analysis of hydraulic shear stress and erosion rate.

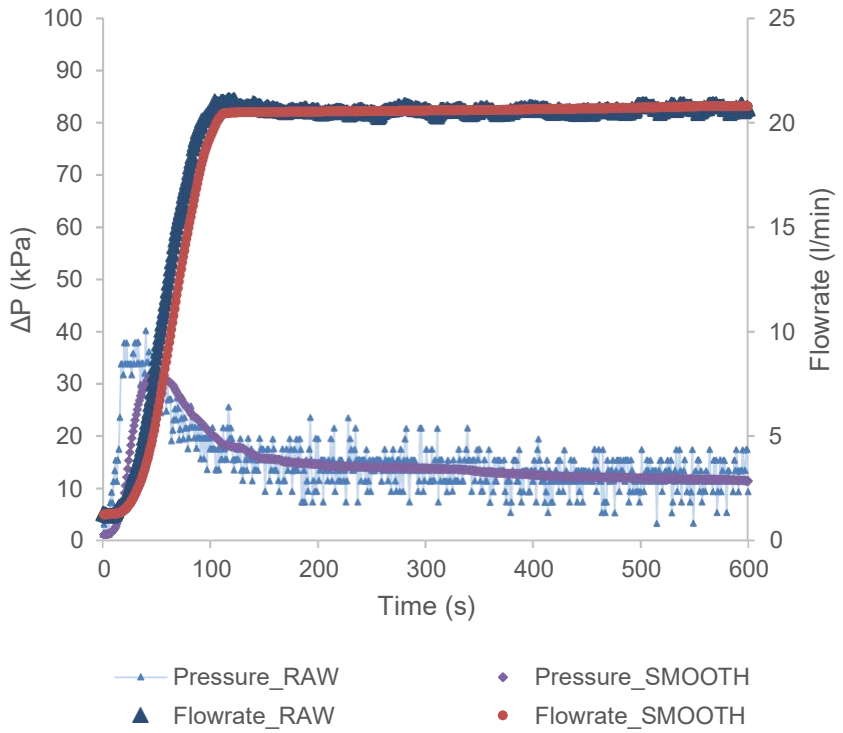


Figure 3.34 The readings from data loggers and smoothed data (CB with GGBS 80%, 7 days)

3.4.1.6.3 Hydraulic Shear Stress and Erosion Rate

The crack diameter enlargement is not known during the course of the test, hence it must be back calculated using the diameter, flow rate, and pressure differential recorded at the beginning and the end of the test. Back calculation can be undertaken using Equations 7-12.

The data analysis procedure mainly followed the method used by Wan and Fell (2002). Firstly, the initial and final flow conditions should be determined,

i.e. whether the flow is laminar or turbulent, by calculating the Reynolds number (Equation 7). After establishing the flow conditions, the initial and final friction factors (f) were computed using Equation 12. The friction factors at intermediate times between the beginning and the end of the test were assumed to vary linearly with time, thus allowing f at time t to be estimated by interpolation. As f, flow rate (Q) and pressure differential (ΔP) were known, the hole diameter at time t (Φt) could be calculated (Equation 11). Hydraulic shear stress (τ) and erosion rate (ε) were estimated using Equation 8 and 9, respectively. Afterwards, τ was plotted against ε. If it exhibited linear relationship, a linear trendline could be generated and critical hydraulic shear stress τc could be estimated (the intersection of the trendline with the axis of hydraulic shear stress). Typical results from the HET test are illustrated in Figure 3.41-3.42.

$$Re = \frac{\phi_t V_t}{\nu} \quad (7)$$

$$\tau = \rho_w g \left(\frac{\phi_t}{4}\right) i \quad (8)$$

$$\varepsilon = \frac{\rho_d}{2}\frac{d\phi_t}{dt} \quad (9)$$

$$i = \frac{\Delta P}{L} \quad (10)$$

$$\phi_t = \left(\frac{16 Q_t f_L}{\pi \rho_w g i}\right)^{\frac{1}{3}} \text{ (laminar)} \qquad \phi_t = \left(\frac{64 Q_t^2 f_T}{\pi^2 \rho_w g i}\right)^{\frac{1}{5}} \text{ (turbulent)} \quad (11)$$

$$f_L = \frac{\pi \rho_w g i \phi_t^3}{16} \text{ (laminar)} \qquad f_T = \frac{\pi^2 \rho_w g i}{64 Q^2}^{\frac{5}{t}} \text{ (turbulent)} \quad (12)$$

The hydraulic shear stress, velocity and erosion rate were then plotted against the results from strength test. This aimed to see how these erodibility parameters related to the strength parameters.

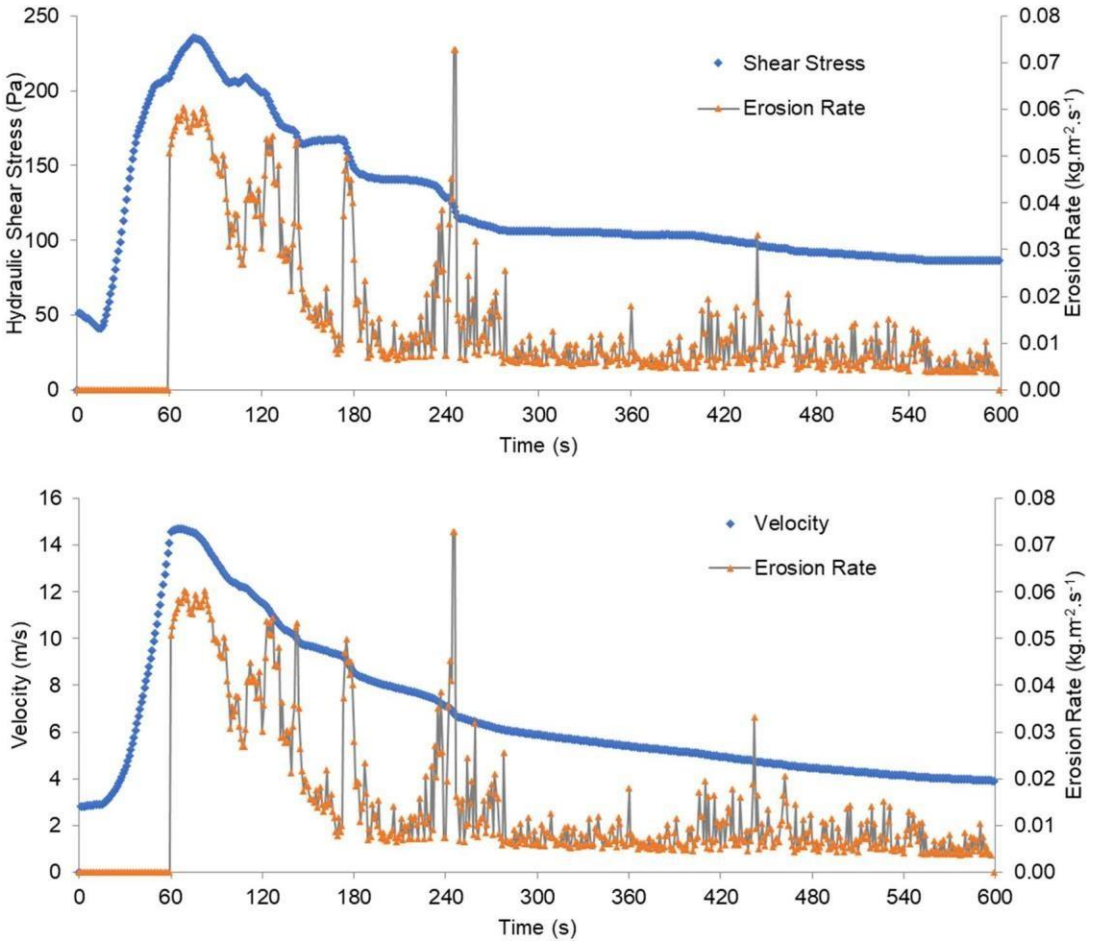


Figure 3.35 The relationship of hydraulic shear stress, velocity and erosion rate during the test (CB without GGBS, 14 days). Note that the erosion rate was not calculated whilst the upstream valve was opened; this is presented as zero on the trends above

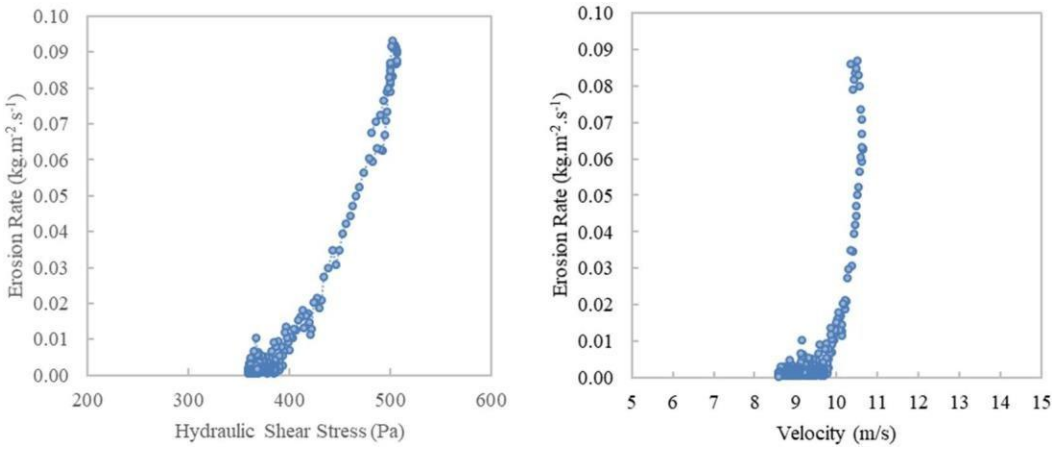


Figure 3.36 The relationship of erosion rate against hydraulic shear stress and velocity (CB without GGBS, 90 days)

3.4.2 Modified Triaxial Erosion Test

3.4. 2.1 Introduction

This modified triaxial erosion test aimed to study the effect of varying confining pressure to the erosion resistance (something lacking in the HET and PET methods) and observe the other phenomena that occur during the test. The modification made to the triaxial apparatus to investigate erosion phenomenon had been done previously by several studies however it was used to study suffusion phenomenon/fine particle migration (e.g. Chang, 2012; Ke and Takahashi, 2014), although not in terms of concentrated leak. Moreover, there has not been any previous study on the erodibility of CB under changing applied confining pressure.

3.4. 2.2 Technical Procedure

For this erosion test, the procedure was similar to HET except the setting of confining pressure. As illustrated in Figure 3.37, the eroding fluid was flowing vertically down through the sample. The ratio of entrance to initial hole diameter is 3.3, which was dictated by the geometry of the triaxial cell used in this study (Triaxial Cell by Controls Group). This was because the outer diameter of the metal rod (commonly used to connect the sample with the loading frame) used to connect the entrance section is already 15 mm and drilling a hole wider than 10 mm inside the rod would potentially break the rod. A double layer of membranes (Figure 3.38) and rubber washers at both ends were used to provide better protection against leaking, however this caused some young samples (from certain mixes) to be crushed during the sample assembly, so care was required during preparation.

Once the sample was installed within the cell, the two halves of the cells clamped together then initially the hole in the centre of the sample, and the associated pipework was filled with water, to displace the air within. Time was taken to look for leaks in the system during this time. Then the cell was filled with water and a confining pressure applied. The confining pressure was set as low as 25 kPa at the beginning and it was increased up to 150 kPa.

In this test arrangement it was found that various CB mixtures/curing ages were too weak to intestate. For example: samples that did not contain GGBS, or only had 40% GGBS replacement but had cured for less than 21 days were too weak/vulnerable and prone to failure during the sample assembly in the apparatus and the sample suitability for this test is specified in Table 3.8

Table 3.8 The sample suitability for the triaxial modified apparatus

Type	% GGBS Replacement	Age					
		7	14	21	28	56	90
CB	0	No	No	No	No	No	No
CB with GGBS	40	No	No	**Yes**	**Yes**	**Yes**	No
CB with GGBS	60	No	No	**Yes**	**Yes**	No	No
CB with GGBS	80	No	**Yes**	**Yes**	No	No	No

The testing was stopped at the predetermined duration or when the sample failed during the test. Unlike HET samples, the erosion tended not to be uniform along the length of the crack, with far more erosion usually observed at the upper part of the sample (where the water entered the sample). Due to this, it was not possible to cast the eroded hole at the end of the test and analyses it using the methodology associated with HET. However, an interesting failure mechanism was encountered that could not be encountered in HET; if the erosion reached a certain point/ leaving relatively thin sample wall thickness, the sample appeared to experience buckling and localised failure (collapse of the material into the eroded crack; Figure 3.39).

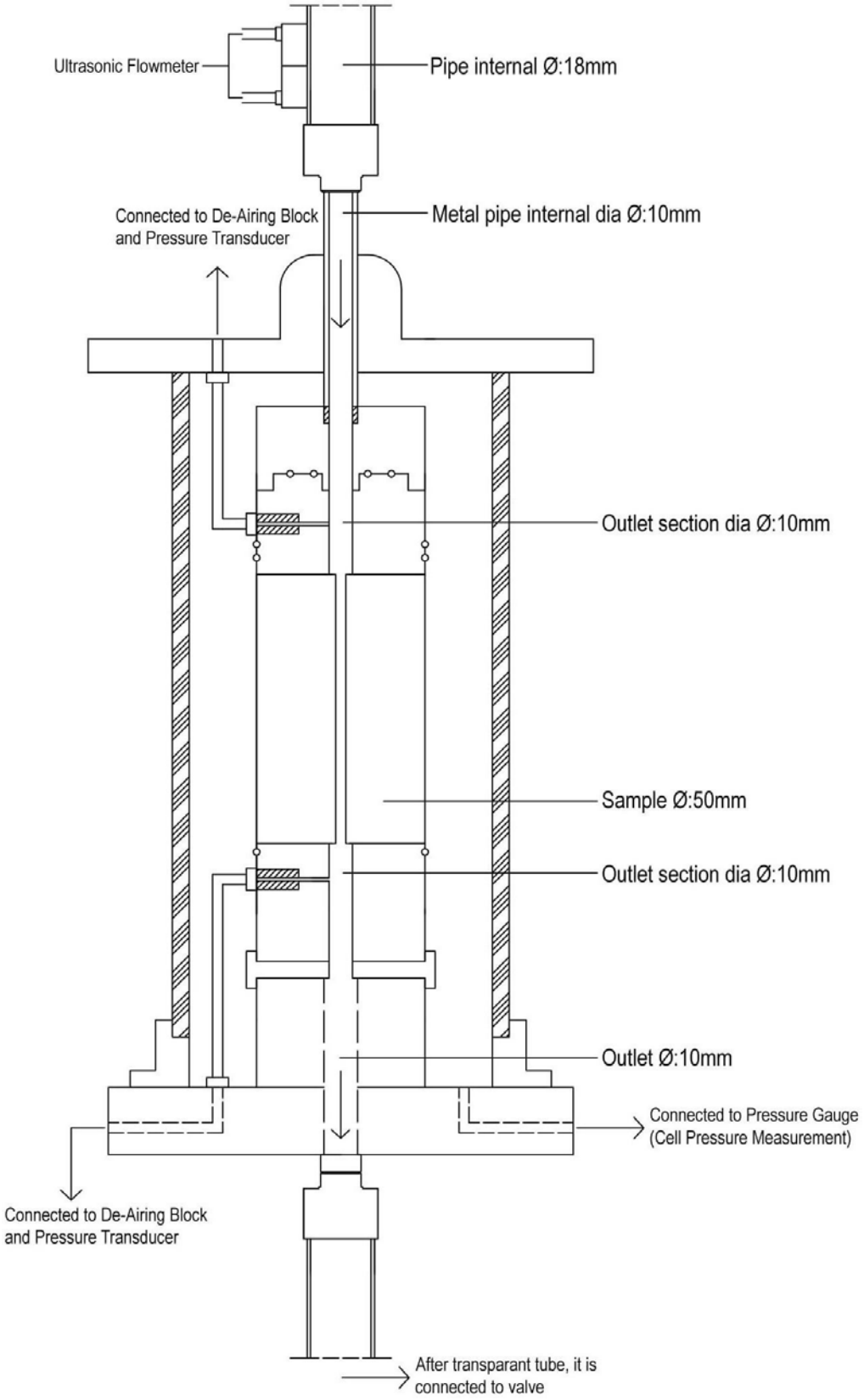


Figure 3.37 The modified triaxial erosion apparatus

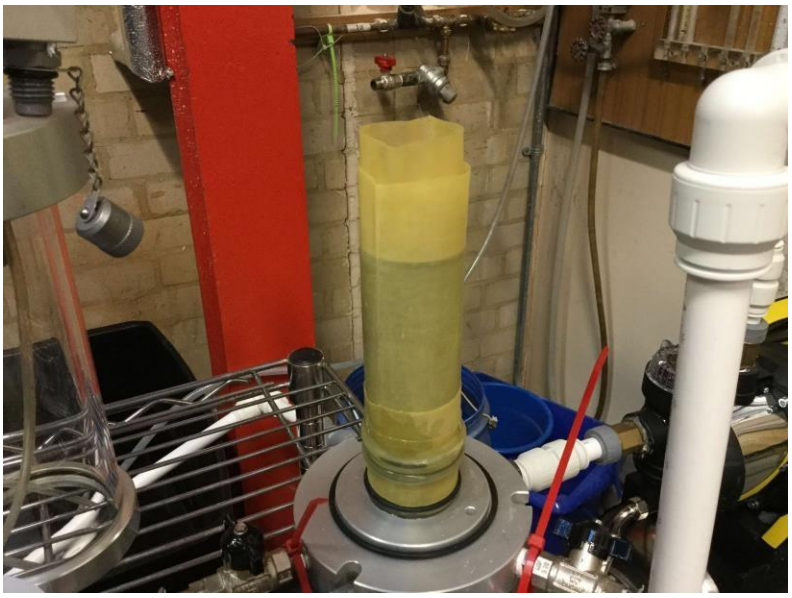


Figure 3.38 Double layer of membrane

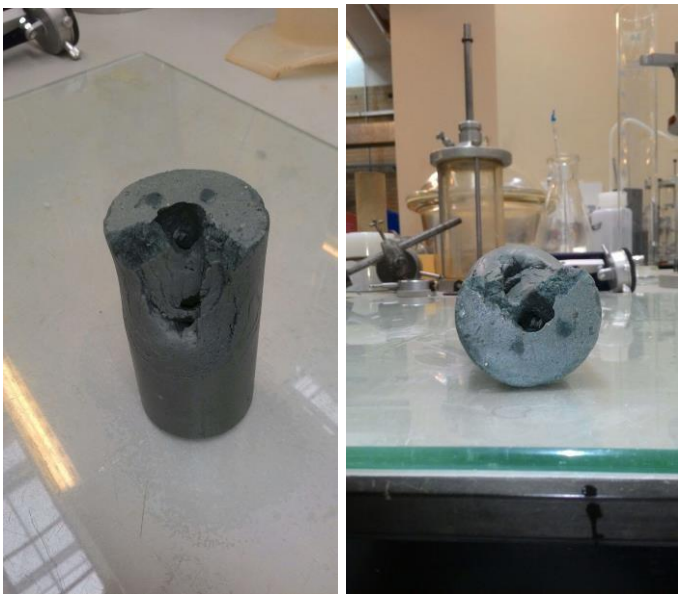


Figure 3.39 The sample after testing (fail due to buckling)

3.4. 2.3 Technical Consideration

3.4.2.3.1 Confining Pressure Effect

There were some technical difficulties encountered when attempting to maintain the applied confining pressure in the triaxial cell:

1. During the test, the sample would form crack especially, and possibly buckle, after the particle detachment commenced, which could be attributed to the circumferential or hoop stress. When these cracks appeared, it opened a pathway for the eroding fluid inside the hole to

be hydraulically connected with the confining fluid. As the pressure generated from the pump was higher than the applied confining pressure, this resulted in the membrane inside the cell expanding (Figure 3.40).



Figure 3.40 the membrane expanded during the test

2. When the membrane expanded, the effect of the confining pressure was lost as the pressure inside the cell became equal with the pressure generated from the pump. Different regulators were trialled (more details given below) to try to maintain the cell pressure but these were found wanting with the existing triaxial set up (funds were not available to purchase a new system). The increasing confining pressure could not be vented quickly enough to prevent build-up of pressure within the cell, limiting the effectiveness of the test post cracking.

In order to investigate the technical limitation of the apparatus, several tests were conducted. The tests aimed to investigate how the pressure regulator responded with the change of confining pressure inside the cell and what eroding fluid pressure was required to diminish the effect of confining

pressure. These tests were conducted at the confining pressures of 50, 100 and 250 kPa. The results from the tests can be seen in Figure 3.41-3.45. The confining pressure of 250 kPa was high enough to prevent the pressure of eroding fluid dominating the pressure of the cell. However, for the confining pressures of 50 and 100 kPa, these pressures could not be sustained with eroding fluid pressures of approximately 300 kPa. The time required for the effect of confining pressure to lose was quicker for the initial confining pressure of 50 kPa. The pressure regulator was not sensitive enough with the change of pressure in the cell as indicated by the unchanged pressure condition inside the bladder. When the pressure from the pump decreased, the rate of confining pressure decrease was comparatively slower which suggested that the regulator could not recover quick enough to the initial pressure condition inside the cell.

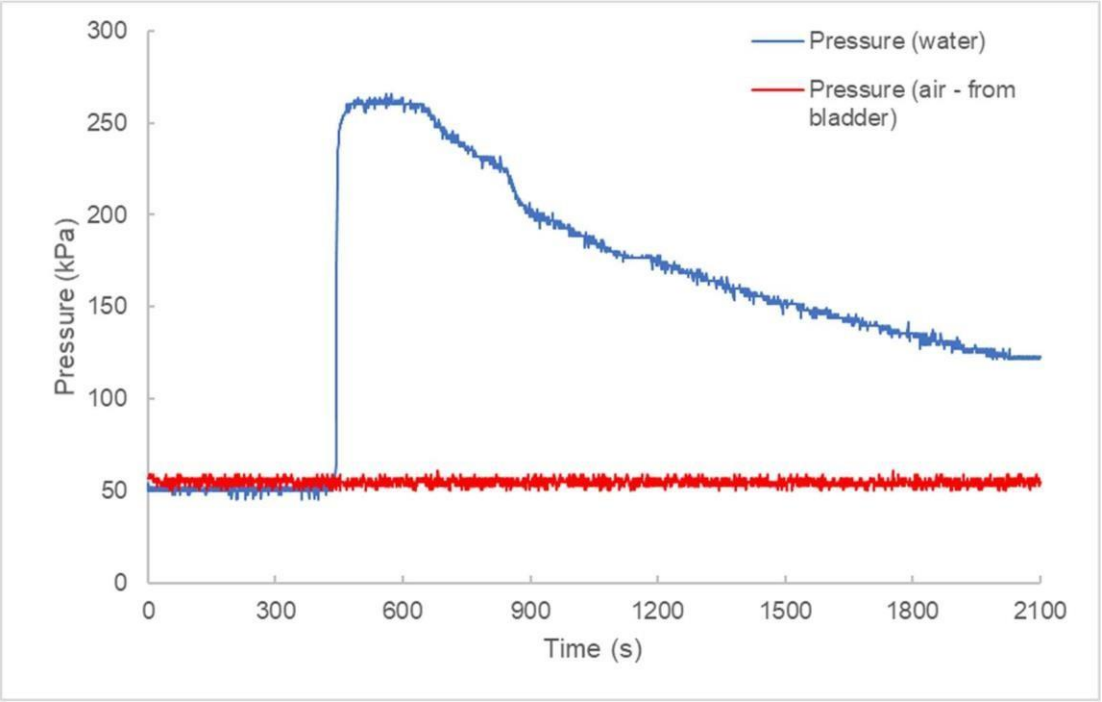


Figure 3.41 Measurement of confining pressure (water) and air pressure from the bladder for the confining pressure of 50 kPa

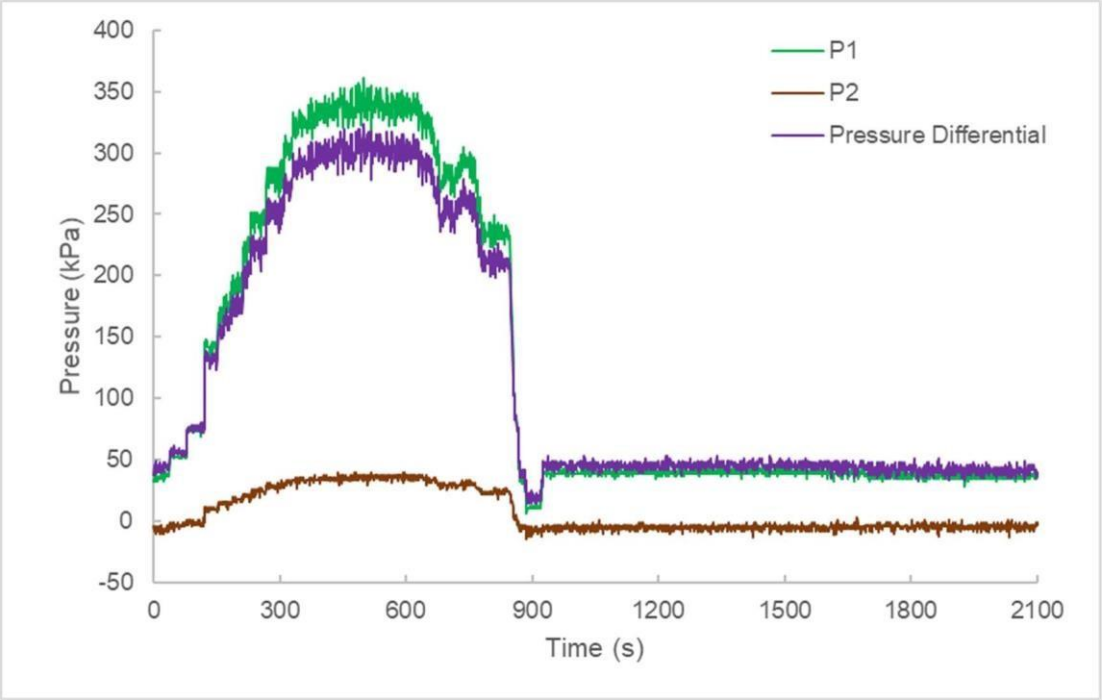


Figure 3.42 Measurement of upstream pressure, downstream pressure and pressure differential for the confining pressure of 50 kPa

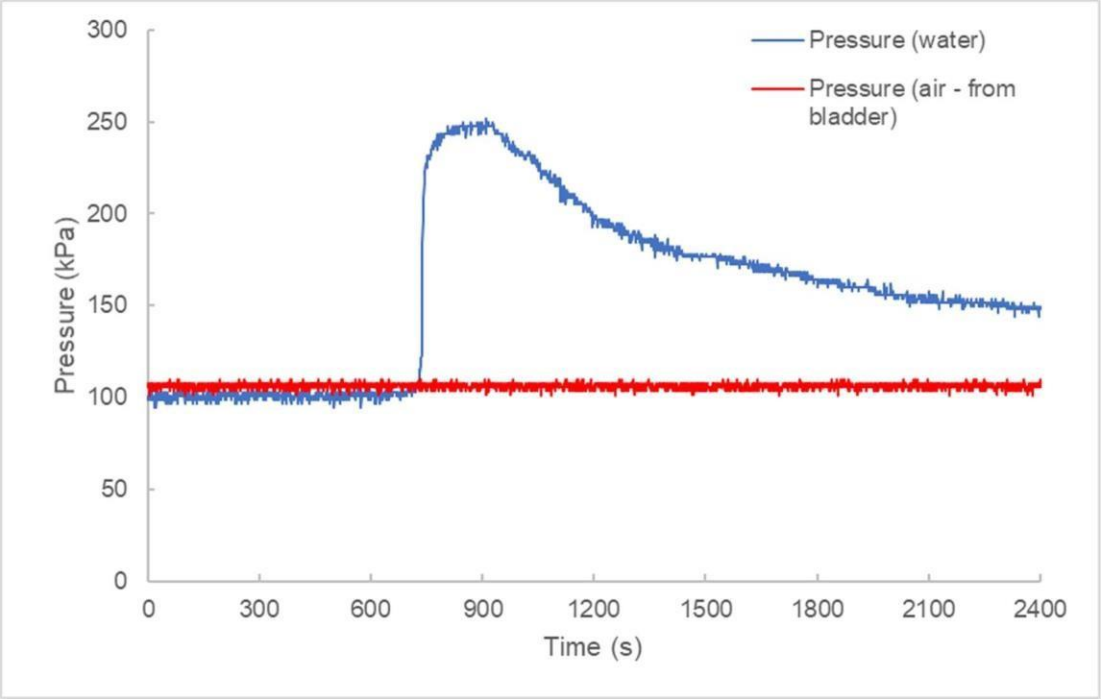


Figure 3.43 Measurement of confining pressure (water) and air pressure from the bladder for the confining pressure of 100 kPa

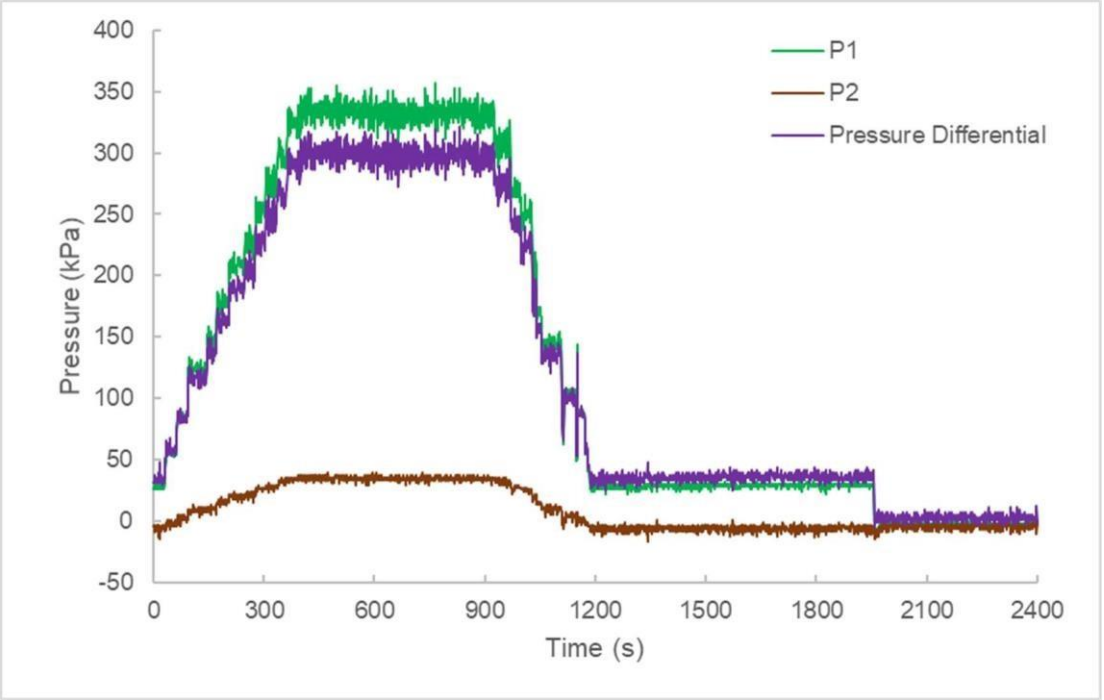


Figure 3.44 Measurement of upstream pressure, downstream pressure and pressure differential for the confining pressure of 100 kPa

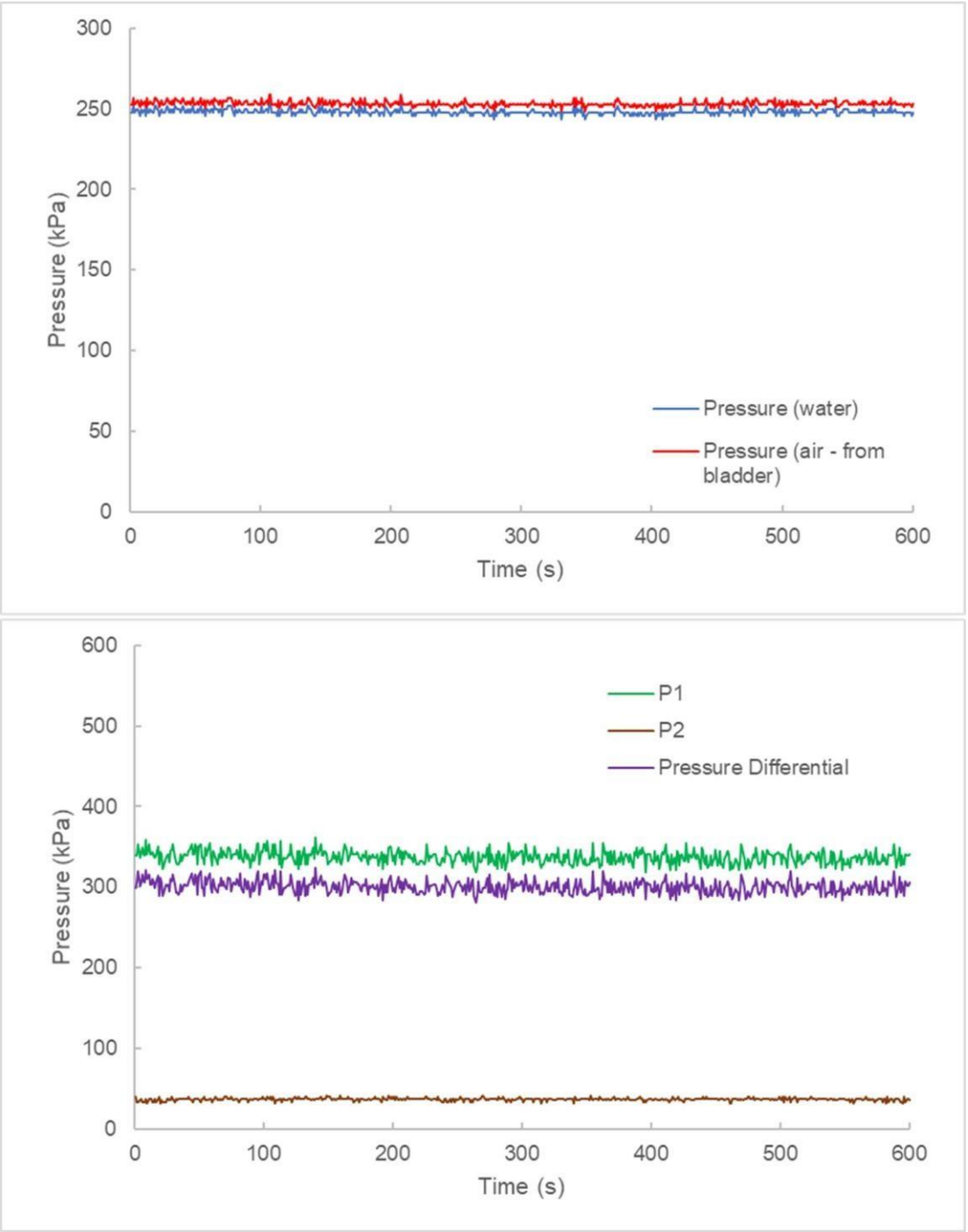


Figure 3.45 Measurement of confining pressure (water) and air pressure from the bladder (Top), Measurement of upstream pressure, downstream pressure and pressure differential (Bottom), for the confining pressure of 250 kPa. P1 and P2 represent upstream and downstream pressure.

3.4.2.3.2 Flow and Pressure

As previously discussed, the outcome of the test was unlike HET as the sample were prone to fail during the test. Therefore, the flow and pressure measurement were terminated when the sign of failure observed and that was considered the end of the test. This meant the test could last less than the prescribed duration of 600 seconds.

3.4. 2.4 Data Analysis

Similar to HET, the set of data obtained from data loggers reading were comprised of flow rate and pressure. The pressure differential and flow rate were plotted against time. Due to difficulties to cast the eroded hole, it was not possible to measure the diameter of the eroded hole. Some samples failed either in shear or tension which also added complexities in interpreting the data (Figure 3.46). Nonetheless, the point at which the sample fail during the test and could indicate other failure mechanism. This would be further discussed in the next chapter.

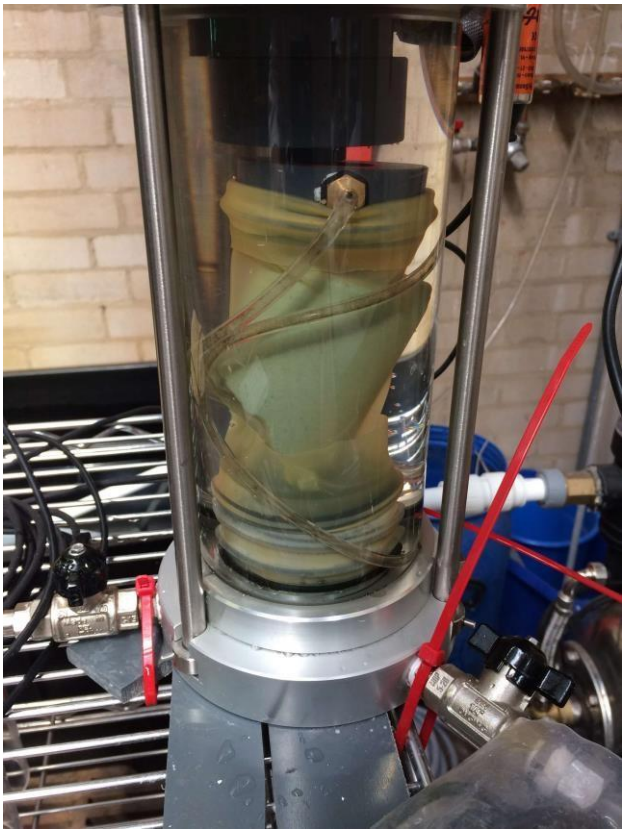


Figure 3.46 The sample failed during the test inside the membrane

3.5 Scanning Electron Microscopy (SEM) Test

3.5.1 Technical Procedure

The SEM test was conducted by the laboratory technician at The Centre of Electron Microscopy within the University. Drying of the CB sample was undesirable due to the likely significant change in fabric with loss of water (Royal et al., 2018), therefore cryo-SEM test was chosen as the method was considered less disruptive (Negre et al., 2004). This method allowed the sample to maintain its original form by rapidly freezing it. Firstly, the CB was plunge-frozen in nitrogen slush at temperature less than -200 °C. The frozen sample was cut in order to expose the surface that would be observed in the microscope and the temperature was increased to trigger sublimation of ice. The temperature was decreased again in order to maintain the stability of the sample microstructure before it was observed. The magnification used was a spatial resolution of 2 μm.

3.5.2 Data Analysis

The data obtained from this test was the visual documentation from the microscope. The analysis was conducted by qualitatively analysed the visual form of the sample microstructure and how they change and differ with the change of curing duration and mix proportion. The typical visual documentation obtained from the test can be seen in Figure 3.47.

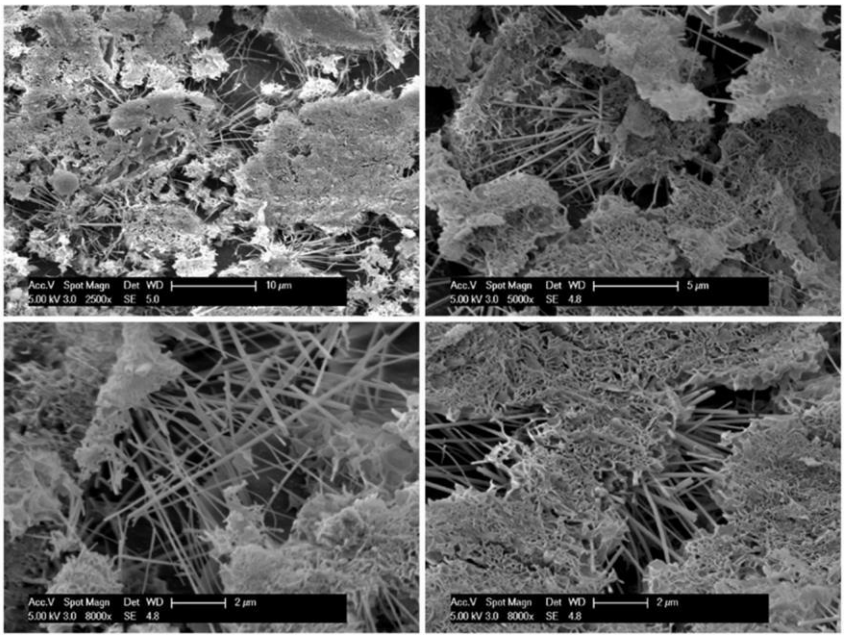


Figure 3.47 Result from the cryo-SEM test (CB with GGBS 80%, 56 days)

Chapter 4
Results and Discussion

4.1 Introduction

This chapter mainly focus to present and analyse the result from the laboratory experiment undertaken to study the behaviour of CBB material. There are three key aspects of CB behaviour that become the focus of this chapter:

1. Basic properties and material strength
2. Erodibility
3. Microstructure

Section 4.2 focuses to analyse the effect of curing duration and GGBS proportion to basic properties (particle density, moisture content) and strength characteristics (unconfined compressive strength, tensile strength) of CB material. The relationship between basic properties and strength characteristics is also investigated. This section also presents the result from hydraulic fracturing test, how the result is related to strength characteristic, and the limitation of the hydraulic fracturing apparatus. This section serves as the preliminary investigation towards the erodibility behaviour of CB material; whether the basic properties and strength characteristics are correlated with the susceptibility of CB material to erosion phenomenon.

Section 4.3 explores the use of hole erosion test and modified triaxial erosion apparatus in examining the erodibility characteristic of CB material. The erodibility parameters are used to analyse the behaviour and their relationship with strength and basic properties are investigated. Technical issue encountered during the test as well as the assumption adopted for the data analysis are also presented

Section 4.4 presents the result from cryo-scanning electron microscopy test. This chapter focus to provide visual observation of CB material microstructure.

4.2 Basic Properties and Material Strength Test

4.2.1 Particle Density

The test was conducted to obtain the particle density (ρ_s) of the materials studied in this research. The samples were dried and ground to meet the minimum particle size specified in the British Standard 1377-2 (BS, 1990). Both individual and mixed material were examined. The particle density of the mixed material was used in the analysis and calculation of erodibility parameters which is presented in this chapter. In order to ensure the accuracy and repeatability, the parallel batch was prepared simultaneously, and the results were compared. For each material type, 2 batches, each comprised of 5 samples, were tested.

Table 4.1 Particle Density

Type	Density (kg/m^3)
Individual	
Cement	2136
Bentonite	2553
GGBS	2918
Mixed Material	
CB without GGBS	2254
CB with GGBS 40%	2443
CB with GGBS 60%	2614
CB with GGBS 80%	2711

The testing results are presented in Table 4.1. For individual material, ρ_s of cement, bentonite, and GGBS are 2137 kg/m^3, 2553 kg/m^3, and 2918 kg/m^3 respectively. ρ_s of bentonite is within the suggested value between 2500-2600 kg/m^3 from the manufacturer supplied the material (TOLSA, 2008). The obtained GGBS ρ_s also falls within the expected range (ECOCEM, 2012). For mixed material, the value of ρ_s increased with the GGBS proportion and this was expected as ρ_s of GGBS is higher compared to cement and bentonite. ρ_s of samples without GGBS is 2254 kg/m^3. The increase of GGBS replacement from 40%, 60% and 80% contributed in the increase of ρ_s to 2443 kg/m^3, 2614 kg/m^3, and 2711 kg/m^3, respectively.

The relationship between ρ_s and strength characteristic of CB samples was further analysed in Section 4.1.5. Its relationship to erodibility was also analysed (presented in the later section) which aimed to investigate whether ρ_s is relevant parameter to be used to understand the susceptibility of CB materials, with varying GGBS composition, against erosive force.

4.2.2 Unconfined Compressive Strength and Tensile Strength

Unconfined Compressive Strength (q) and Tensile Strength (σ) test were conducted to investigate the strength characteristic of CB samples with and without GGBS. Cylinder samples with 100 mm in height and 50 mm in diameter were examined for UCS, whereas the height/thickness of samples used for tensile strength test ranging from 35-37.5 mm. Total of 411 (203 with 3 mm hole) samples examined in both UCS and tensile strength test; the test were repeated for 5 – 6 times for every GGBS proportion and curing day. The peak stress, at which the sample failed/fractured, was used to represent the strength obtained from the test. All samples were cured inside the temperature-controlled room (approximately at 5 °C). After 7 days, the samples were taken out of moulds and they were transferred to a container filled with water for the curing process to continue.

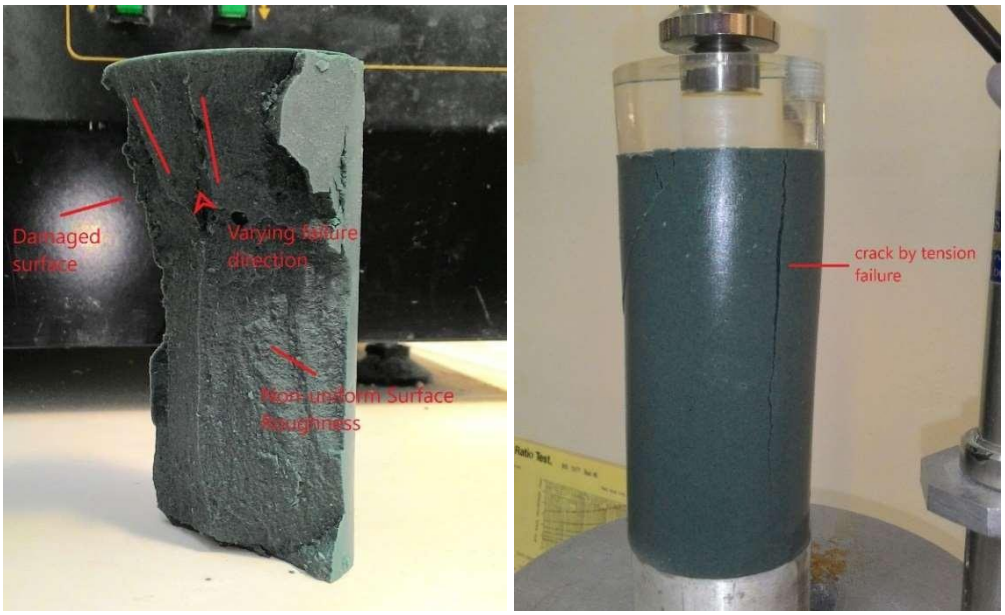


Figure 4.1 Typical failure surface of the crack

The test programme included both solid sample and sample with 3mm hole in the centre. The hole in centre was created purposely which aimed to simulate small/micro cracks in the sample. During the initiation stage of dam/levee failure, the small cracks are commonly associated with the increasing likelihood of failure due to internal erosion (Rice and Duncan, 2010). However, the mechanics involved in the creation of the hole in the sample and micro crack in the dam are completely different. The hole was created by inserting acrylic rod in the centre before the curing process begun, while the micro crack could be formed due to the variety of factors (e.g. stress condition, desiccation, animal burrowing, etc (Fell et al., 2018)). The hole created by the acrylic rod produced a smooth and consistent area of impact, whereas the micro crack can have varying direction of failure, damaged area, surface roughness, etc as illustrated in Figure 4.1. Nonetheless, replicating the micro cracks found in the field and ensuring the homogeneity of the micro crack characteristic for all samples were technically hard and complex. The homogeneity of the hole created by acrylic rod was more consistent and the possibility of sample not meeting the replicability standard was minimised. The hole characteristics used for this test was akin to those used for erosion test, therefore it was more representative to be used to further investigate the relationship between strength and erosion resistance characteristics.

Figure 4.2 shows the typical failure plane for both UCS and tensile strength test. For UCS test, the samples mostly failed in the form of wedge and cone. Similar failure trend observed in the past study by Royal et al. (2018). The angle of cone formation ranging from 30-40 degree. For tensile strength test, the sample failed by the formation of tension crack running mostly across the centre of the sample. The formation of tension crack was also observed from the UCS test, mostly from old samples (i.e. cured 56 days and older) as seen in Figure 4.1

Figure 4.3 and 4.4 show the typical stress and strain relationship obtained from UCS and tensile strength test. After reaching the peak stress, the fracture/crack formed in the sample and the stress decreased due to the crack enlargement or formation of other cracks. For tensile strength test, a significant stress decrease after reaching the peak stress for tensile strength was observed, unlike UCS test in which the drop was gradual. The full report of the results for both tests can be accessed at Appendix B.



Figure 4.2 The typical failure of the sample for (a) tensile strength (CB with GGBS 80%, 21 Days), (b) UCS (CB with GGBS 40%, 14 Days)

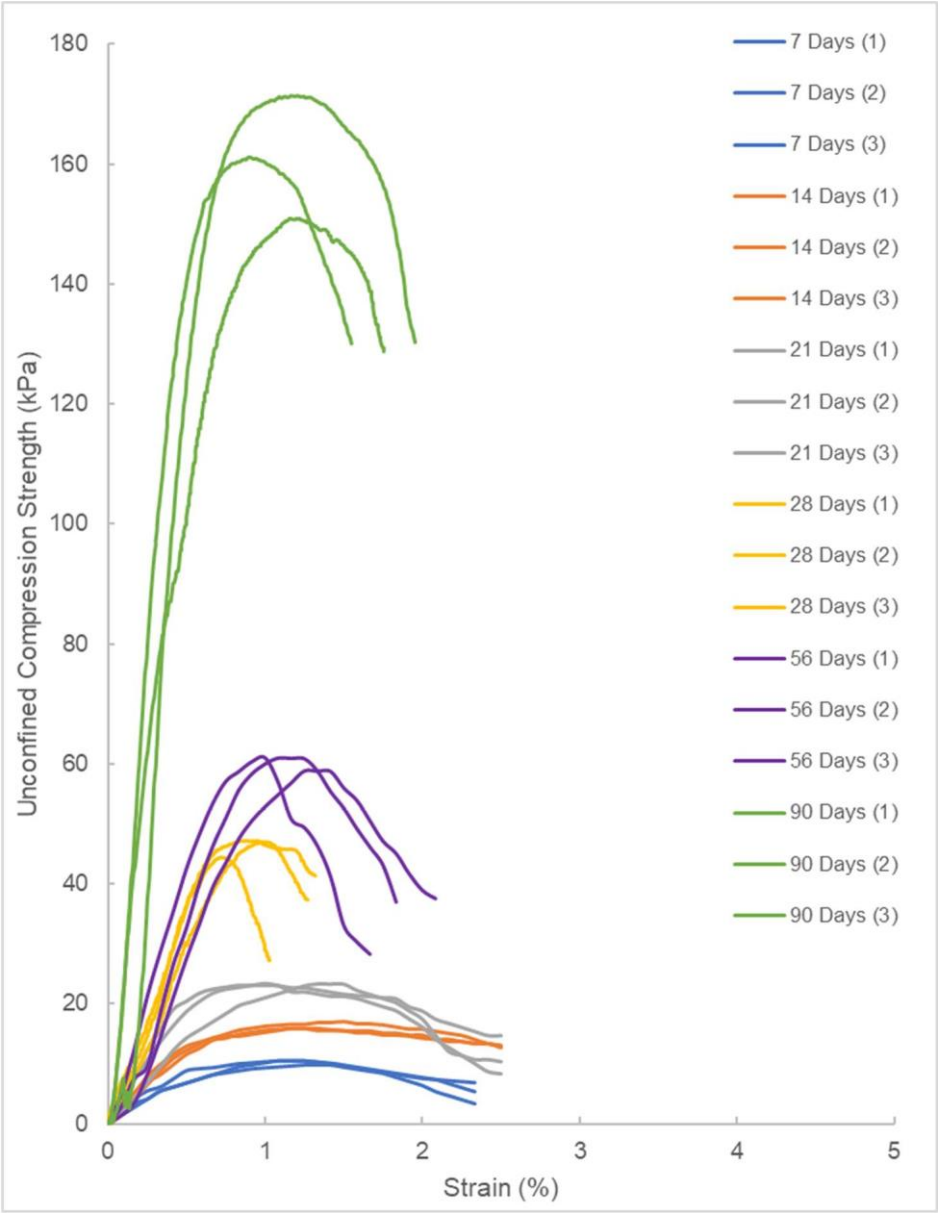


Figure 4.3 Stress-strain relationship for UCS test, CB with GGBS 40% (3 representative results for each curing day)

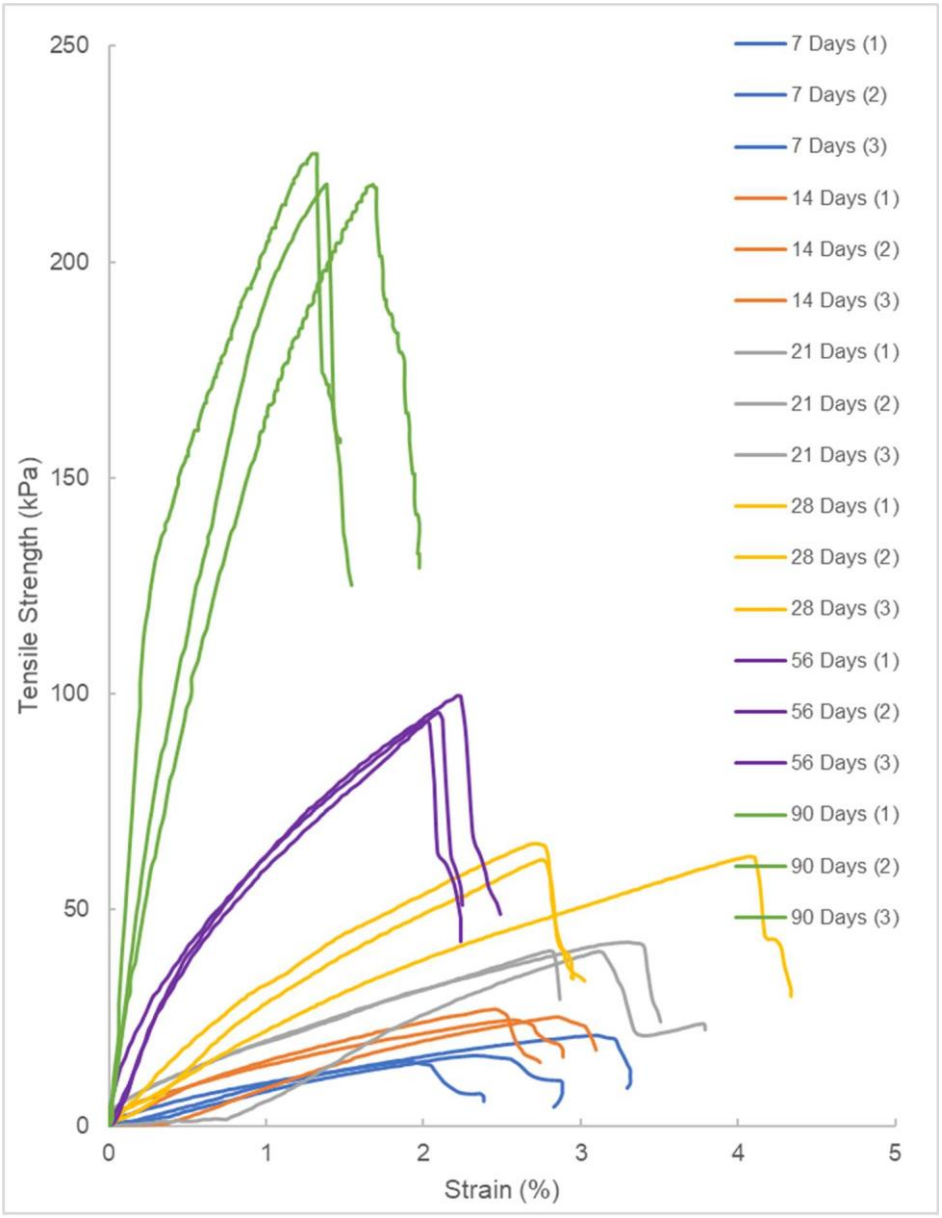


Figure 4.4 Stress-strain relationship for Tensile Strength test, CB with GGBS 80% (3 representative results for each curing day)

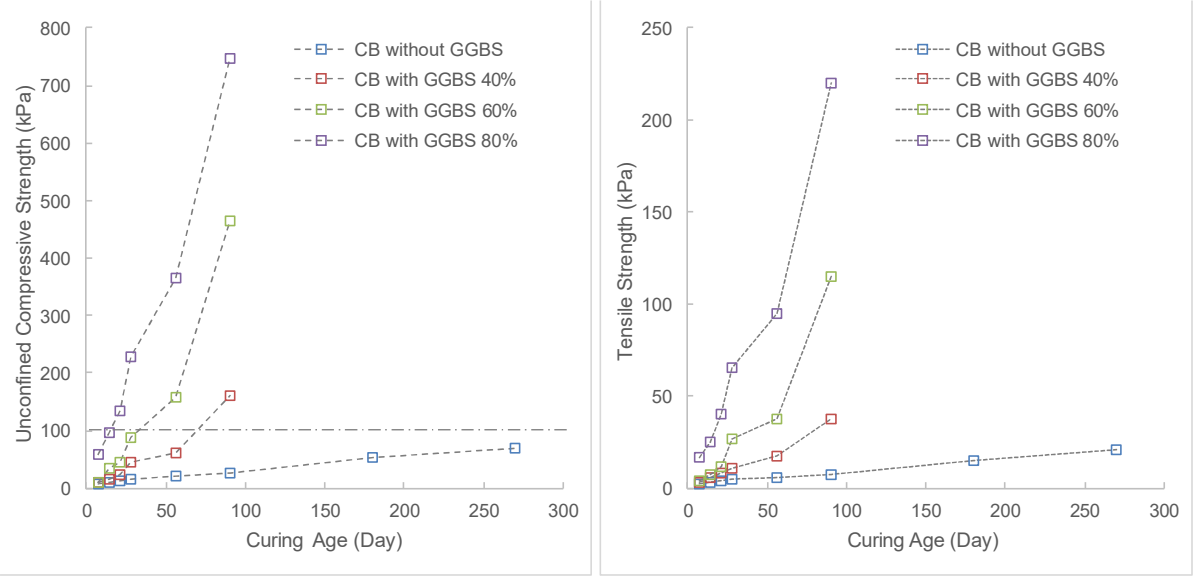


Figure 4.5 Average UCS and tensile strength test results (5-6 samples tested per curing period)

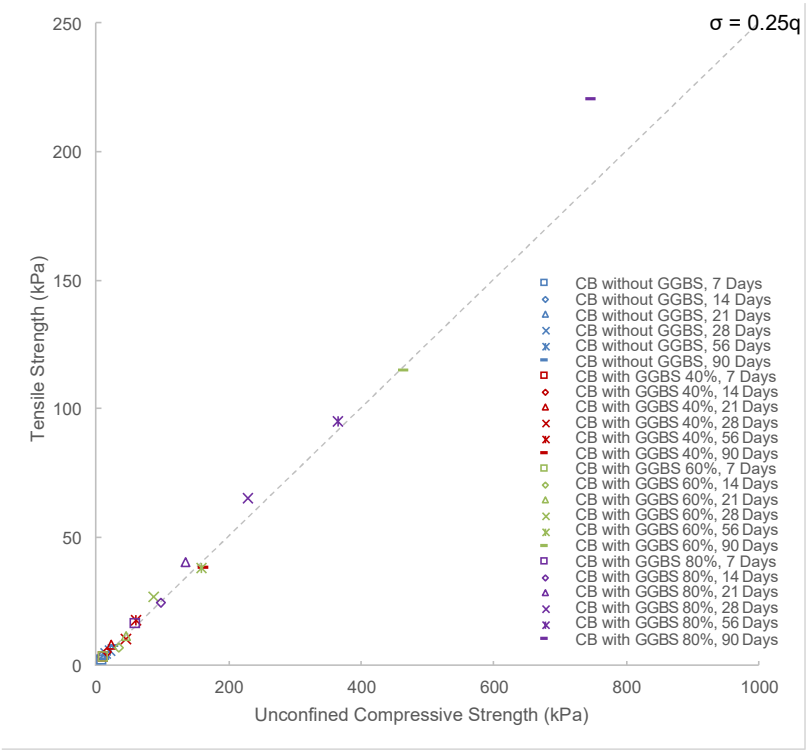


Figure 4.6 The relationship between unconfined compressive strength and tensile strength

Figure 4.5 summarise the result of UCS and tensile strength test for sample without hole. CB without GGBS sample did not meet ICE (1999) specification of 100 kPa despite cured longer than 270 days. CB with GGBS 40% needed 90 days curing to

meet the specification and at least 56 days for CB with GGBS 60%. Only 21 days curing duration required for CB with GGBS 80% to pass 100 kPa UCS value. As summarised in Figure 4.6, the obtained tensile strength values were approximately 25% of UCS values, the exception for CB with GGBS 80% cured for 90 days which yielded 30%.

The rate of strength increase for CB without GGBS was consistent within the range of 20%-50% for the first 28 days curing per 7 days interval to 56 days. The significant increase, approximately over 100%, was recorded at the curing duration from 90 to 180 days. The inclusion of GGBS within the mix contributed to the increase of the strength growth and its growth correlated as well with the curing duration. The most significant strength increase for CB with GGBS 40% and 60% was recorded during the curing duration of 56 to 90 days. The strength increase for CB with GGBS 80% was consistent above 40%-60% and reaching 100%-120% at 56-90 days.

Incorporating 80% GGBS contributed to the strength increase of approximately 600-700% for curing days of 7 days compared to those without GGBS. This trend increases with longer curing days and the strength growth reached approximately 2700% at curing duration of 90 days. Guner (1978) and Jefferis (1997) suggested 2000% increase with 80% GGBS. The GGBS proportion of 40% and 60% also demonstrated similar trend of strength increase except the magnitude was smaller. 40% GGBS generated a strength increase of 40%-50% at 7 days and increased up to approximately 500% at 90 days, whereas 60% generated approximately 50%-70% and 1450%-1700% at curing days of 7 and 90 days, respectively.

As illustrated in Figure 4.7, The main products from CB mix are calcium silicate hydrate (CSH), CAH (calcium aluminium hydrate), and calcium hydroxide (CH) (Carreto et al., 2016). Past studies reported that bentonite left from the CB mix reaction is either in negligible amount or non-detectable (Joshi et al., 2008; Jefferis, 2012). This suggested that the behaviour of CB is mainly influenced by the cementitious products (CSH, CAH) produced from the reaction. Therefore, the strength increase observed from samples with GGBS especially during later stage of curing (56 to 90 days) was attributed to the strength improvement of cementitious products and structure. Due to time constraint, the rate of strength improvement for CB samples containing GGBS

cured longer than 90 days could not be investigated. Hence, for the future work recommendation, it is suggested to investigate the strength improvement trend of CB samples cured older than 90 days. The complete results from strength testing were presented in Appendix B.9 and B.10.

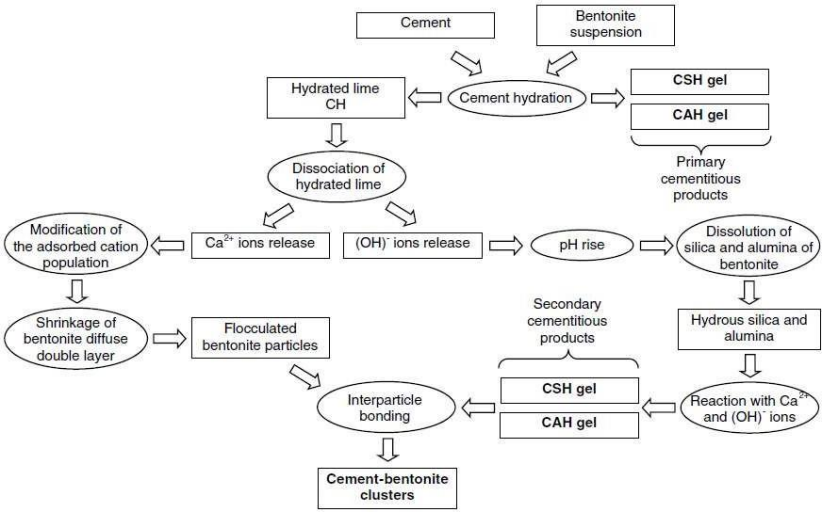


Figure 4.7 The sequence of reaction between water, cementitious materials and bentonite (after Carreto et al., 2016)

Figure 4.8 summarise the strength testing result from samples with 3 mm hole in the centre. In general, the strength dropped due to the formation of the hole. Figure 4.9 shows the rate of strength drop for varying GGBS replacement and curing duration. The strength drop was within the range of 10%-25%. The strength drop indicated a declining trend with the curing duration for CB with GGBS 40% and 60%, and partially for CB without GGBS before it increased after cured longer than 90 days. Due to the hole in the centre, the hoop or circumferential stress should be taken into consideration. In general, this trend suggested that the simulated crack/hole on samples affected the strength of the samples and the concern over the effect of simulated crack towards the performance of the CB samples were confirmed with this strength drop.

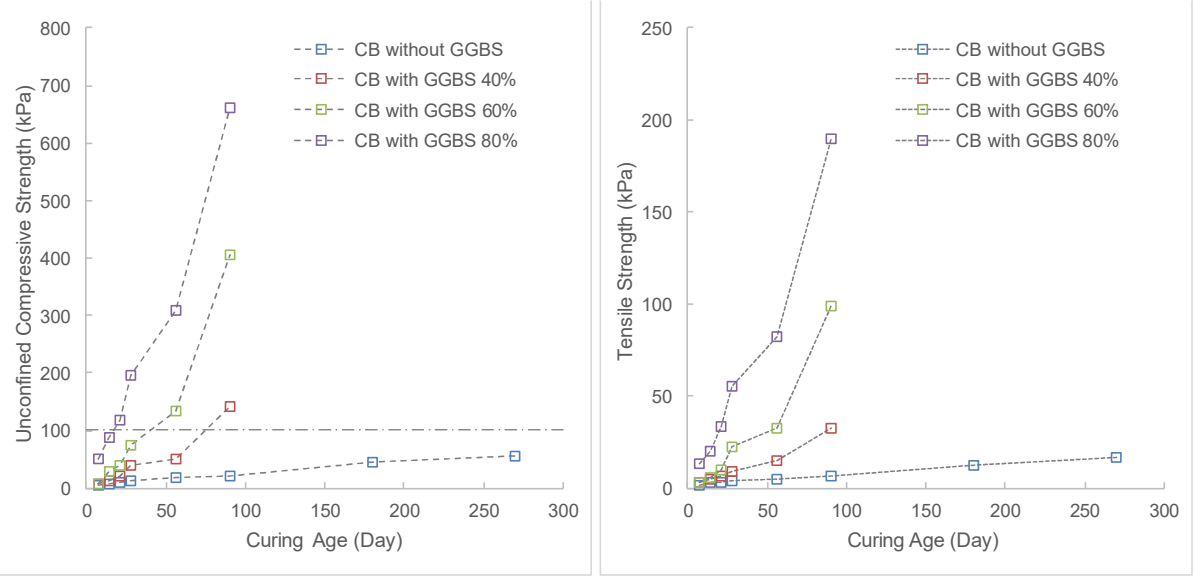


Figure 4.8 Average UCS and tensile strength test results (5-6 samples tested per curing period) for samples with 3 mm hole in the centre

The strain % at which sample failed varied with curing duration and GGBS proportion as seen in Figure 4.10. In general, the strain % at failure for UCS test was within the range of 1%-2%. The strain % were higher for CB without GGBS samples cured for 7 to 21 days. It was observed that the samples were still soft and weak which could lead to an overestimation of the strain % at failure. For tensile strength test, the slight increase was observed with the inclusion of GGBS. The range of strain % was 1%-2.5% for sample without GGBS whereas those with GGBS was within 2%-3.5%, except for sample with GGBS 80% cured for 90 days which recorded 1.5% strain at failure.

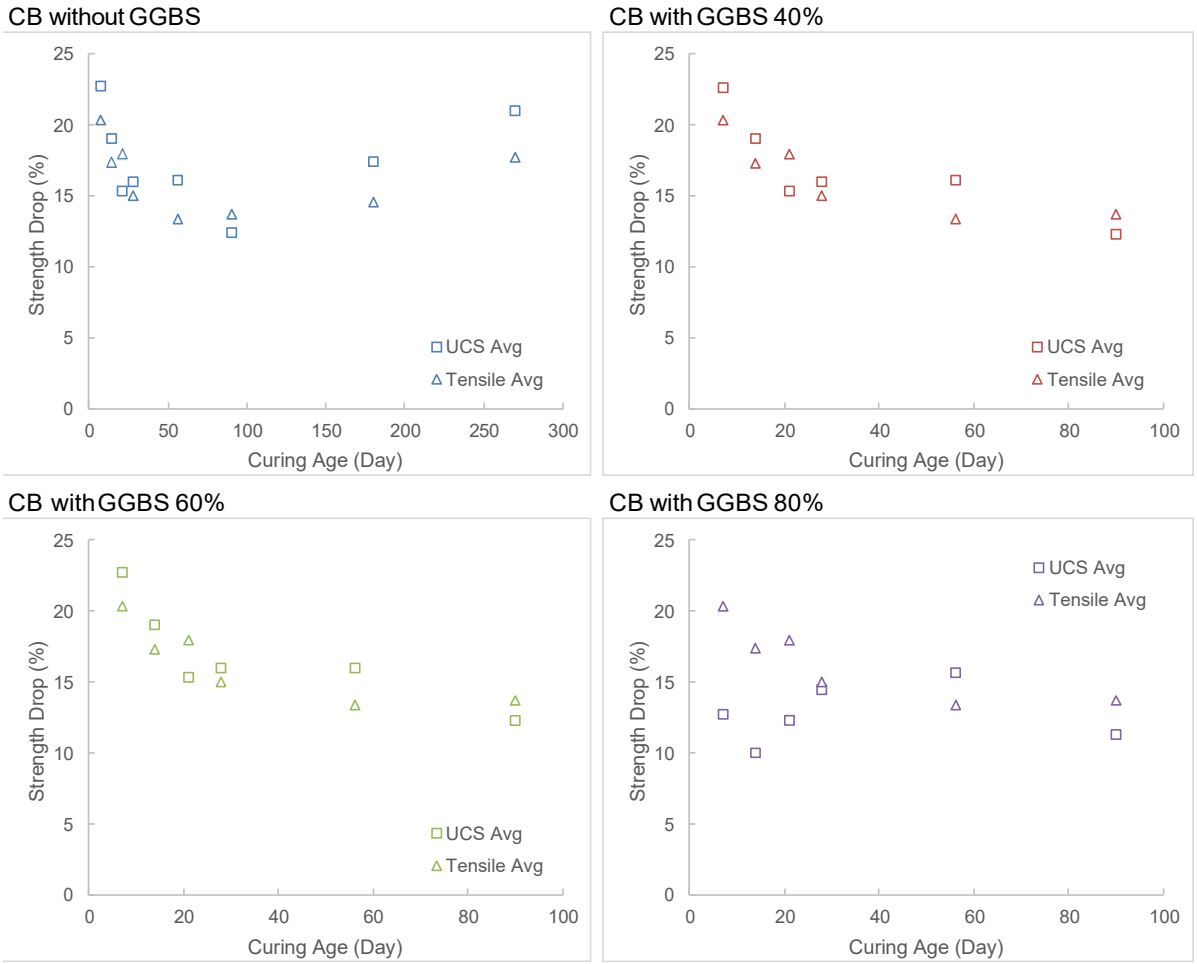


Figure 4.9 Impact of 3 mm hole/simulated crack in the strength

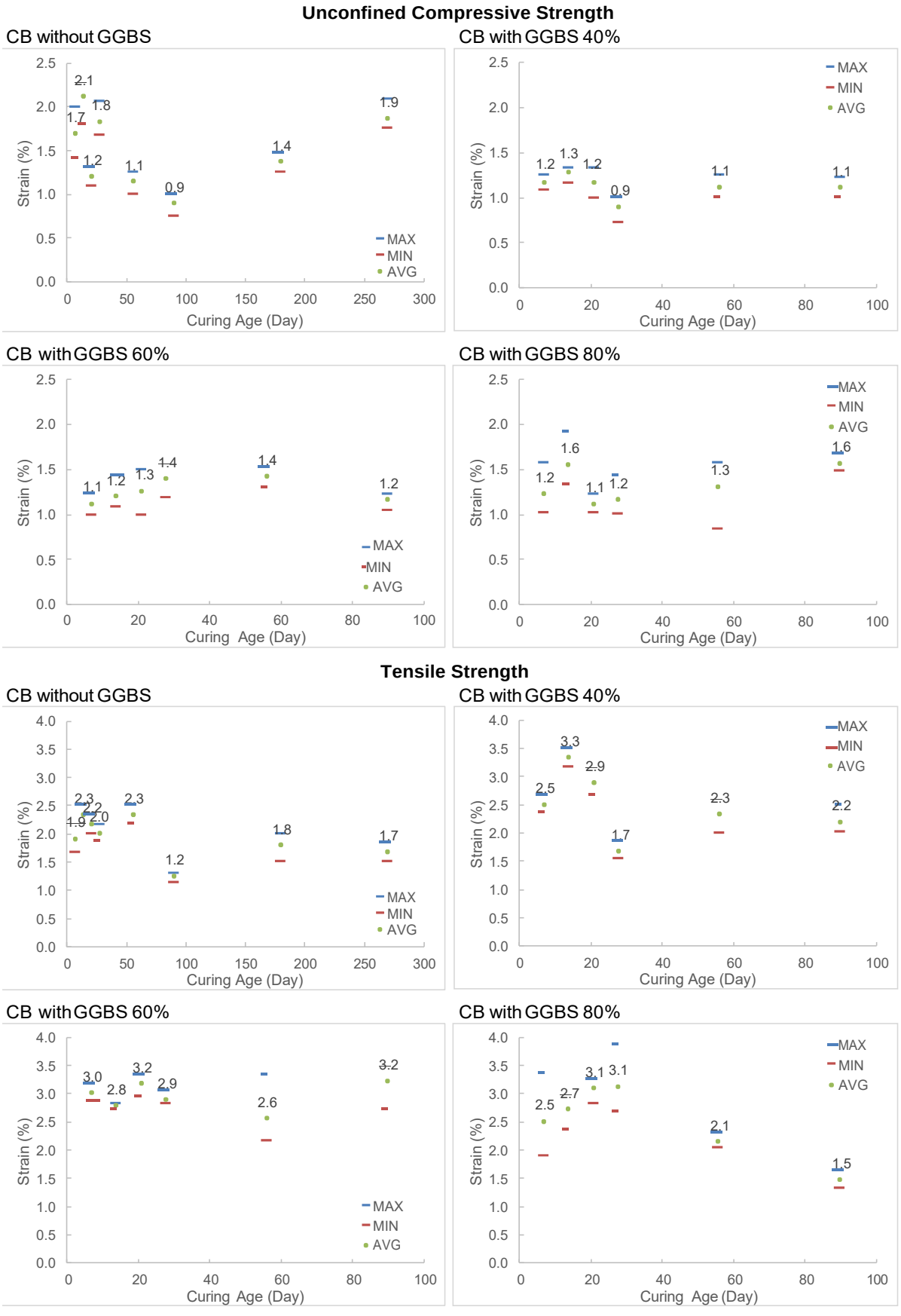


Figure 4.10 Strain at failure/peak stress for strength test

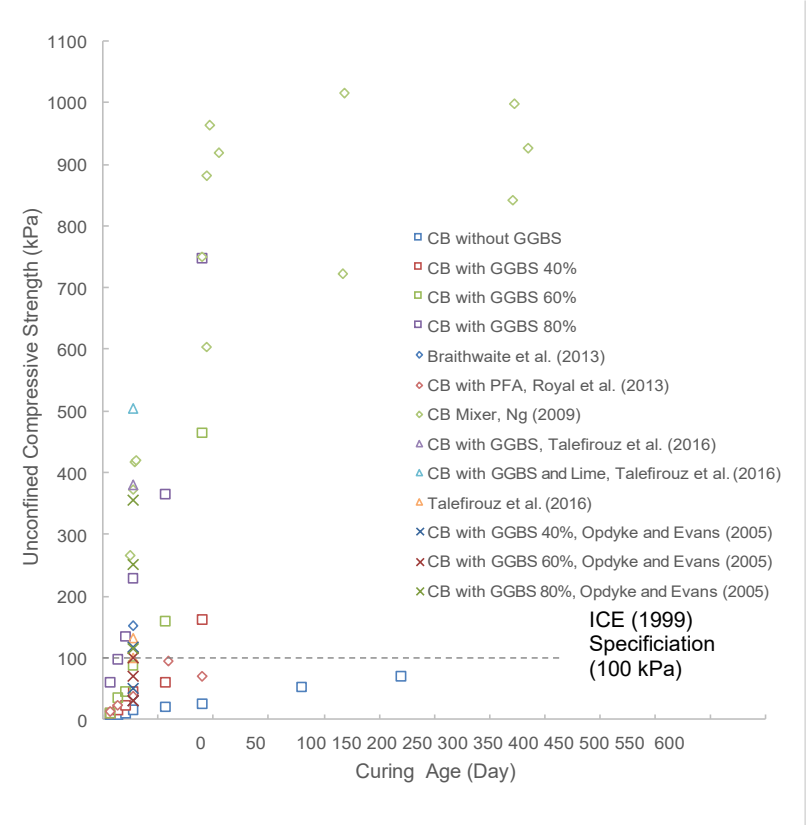


Figure 4.11 Relevant UCS results from past studies

In order to check the relevancy of the samples studied in this research, the results were compared against the other past studies (as presented in Figure 4.11). Samples investigated by Ng (2009) was higher in strength, however this was due to the longer curing period (older than 90 days). The current study, due to the constraint of the erosion apparatus, was only able to test samples cured up to 90 days. Compared to the previous studies, especially those incorporating GGBS (e.g. Opdyke and Evans, 2005; Talefirouz et al., 2016), they have similar UCS values to the current study.

4.2.3 Relationship between Particle Density and Strength Characteristics

This section explores the relationship between the basic properties and strength (UCS and tensile strength) of CB samples (as seen in Figure 4.12). The relationship is represented by the exponential regression line. In general, the trend observed was the strength of CB samples improves with the increase of particle density. However, it is still inconclusive whether the strength values associated with the particle density are only exclusive to CB sample or representative to relevant geomaterials.

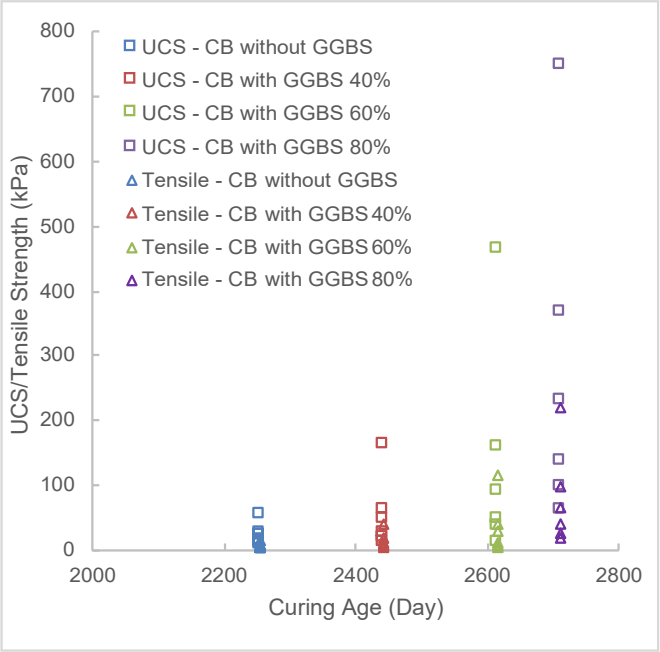


Figure 4.12 The relationship between particle density and strength

4.2.4 Moisture Content

Water took up to 80% of CB samples mix proportion, therefore it is critical to investigate how moisture content of the sample change with the curing duration and varying GGBS proportion. The typical dried sample is presented in Figure 4.13. The result and analysis are presented in Figure 4.13 and Appendix D.



Figure 4.13 The oven-dried CB samples (CB without GGBS, 90 Days)

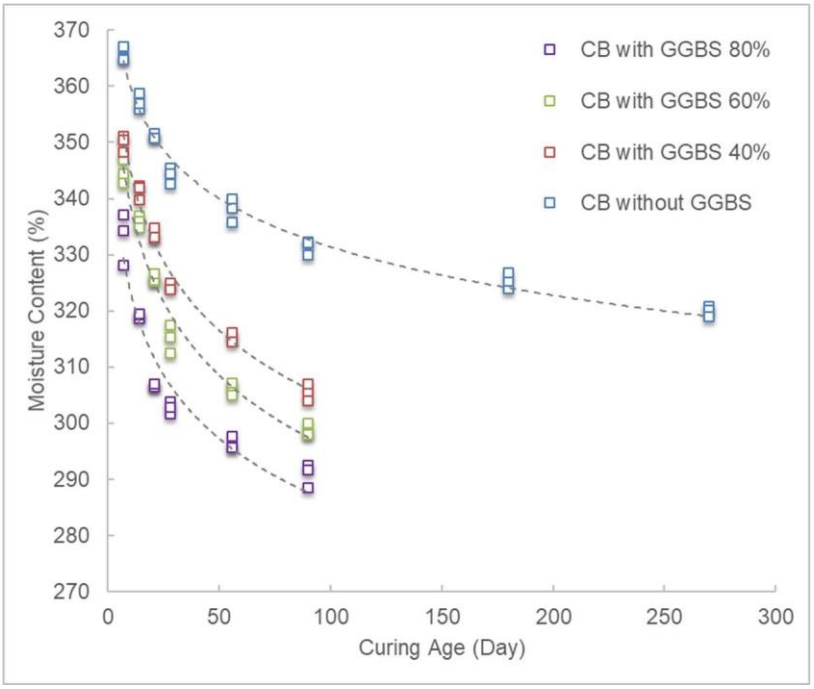


Figure 4.14 Moisture Content of CB samples with varying GGBS replacement (3 samples tested per curing period)

Figure 4.14 shows the relationship between moisture content and curing age. In general, that moisture content of the samples was influenced by both curing age and mix proportion. The rate of moisture content drop was observed to be consistent across the pre-determined curing duration except the CB with GGBS 80% which there was a significant decrease from 12% to 4% between 14-28 curing time frame. For sample with 40% and 60% GGBS as well as without GGBS, the drop was within the range of 5-10%. However, slight increase in the rate of moisture content drop was observed with the addition of GGBS. The moisture content drop rate consistently increased for CB with GGBS 40% and 60%, increasing from 15% to 25% and 20% to 30% at the curing days of 7 to 90 days, respectively. The drop rate increase from 32% at 7 days and reaching 45% at 21 days for CB with GGBS 80%. The drop for became steady from 28 days to 90 days. The cement hydration, which requires water for the reaction, occurs over the time, hence the younger samples were keeping more moisture compared to the older samples. The inclusion of GGBS in the sample mix changed the microstructure of the sample and contributed to the finer structure (Richardson and Groves, 1992) that filled the pore. This caused the less space for water to be trapped inside the pore.

4.2.5 Relationship between Moisture Content and Strength Characteristics

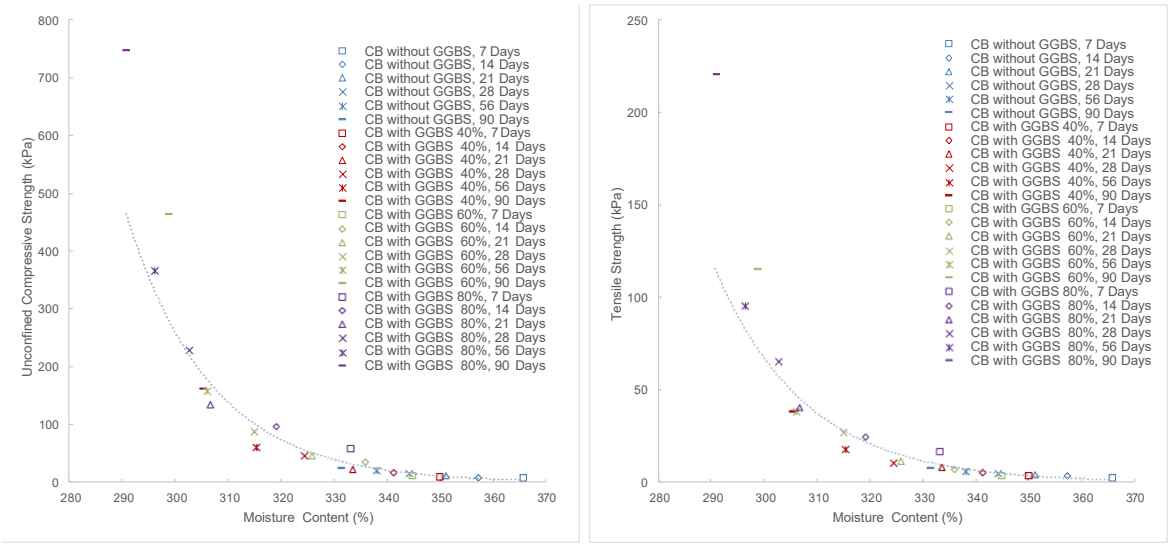


Figure 4.15 The relationship between moisture content and strength

Figure 4.15 shows how, strength characteristics correspond related with the moisture content. The values from both strength parameters follow the trend and mostly fitted with the exponential regression line, however several data points from CB with GGBS 60% and 80%, especially 90 days samples, did not fit into the trend. In general, the decrease in moisture content contributed to the increase in CB strength.

On the next chapter, the correlation between strength characteristic and/or moisture content with the erodibility characteristic is explored. As it is technically easier and simpler to perform strength or moisture content test, it is important to investigate how they relate to each other and whether both strength and moisture parameters can be used to gauge the erosion susceptibility of CB samples.

4.2.6 Hydraulic Fracturing

The hydraulic fracturing test aimed to investigate the CB sample under complex stress condition. As previously explained in Chapter 3, the sample was exposed to two different hydraulic loads: confining pressure and internal pressure. The internal pressure was applied from the 5 mm hole at the centre of sample. Both pressures were controlled independently during the test. The test was performed until reaching a failure point at which a fracture or crack occurred. Total 65 samples were examined, and the test was repeated 2-3 times for each characteristic (e.g. mix and curing time).

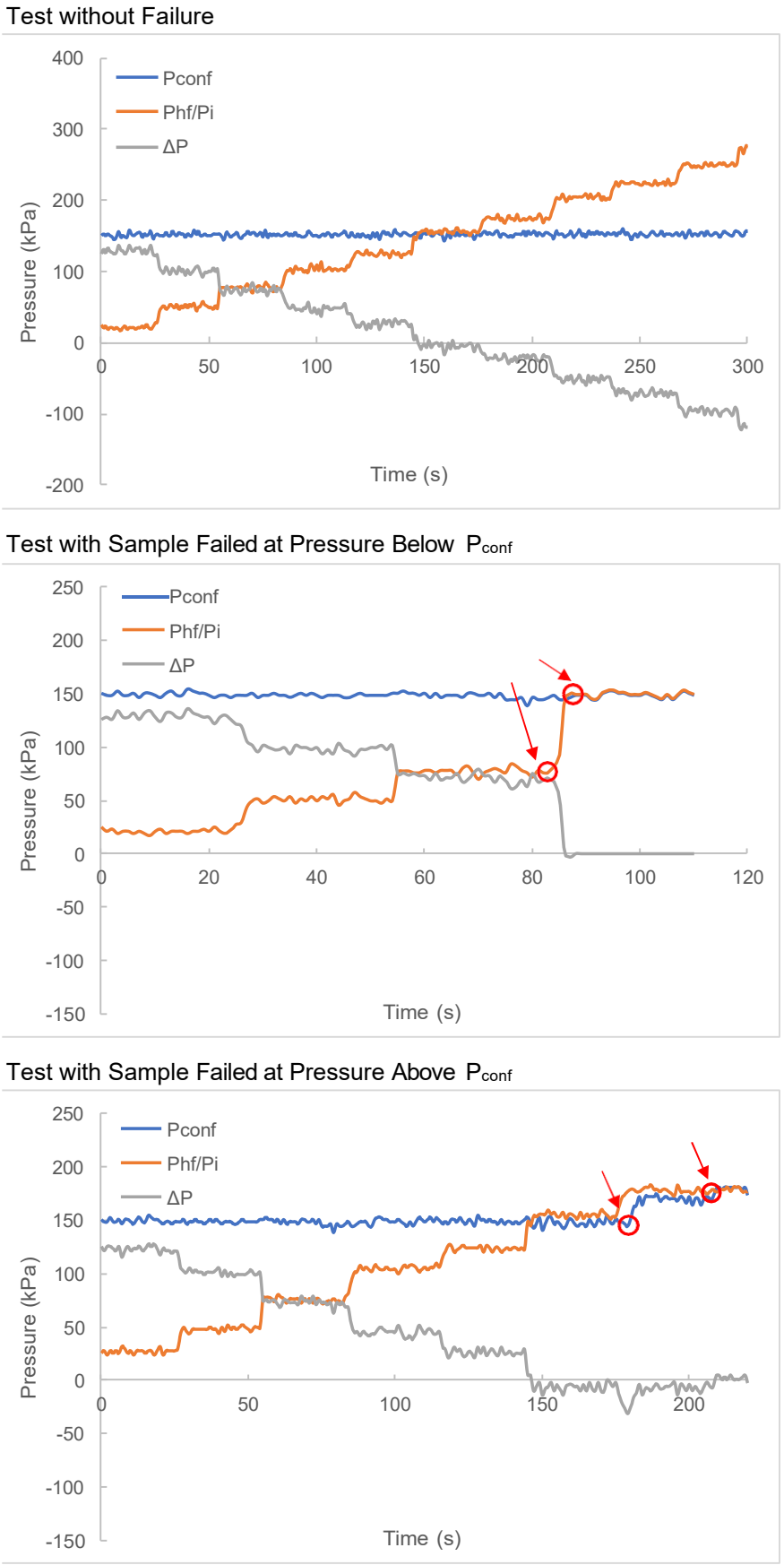


Figure 4.16 Typical results for Hydraulic Fracturing test

The typical result is presented in Figure 4.16 (P_{conf}, P_{hf}/P_i and ΔP represent confining pressure, internal pressure and pressure differential between confining and internal pressure). If the combination of P_{conf} and P_{hf}/P_i did not manage to fracture the sample, the change on both pressures was not observed. If failure occurred, it was either of the pressures that experienced the change. If failure occurred at the condition which the internal pressure was lower than the confining pressure, the sudden rise of internal pressure was observed. If the internal pressure higher than the confining pressure, the sudden rise happened to the confining pressure. The pressure would rise to the point at which the higher pressure applied/existed in the apparatus.

As discussed in Chapter 3, all CB without GGBS were not able to be examined due to technical difficulties encountered in sample preparation. The same issue applied to juvenile samples (7 to 14 days curing age) samples containing GGBS. Mature samples (older than 56 days) were too strong, hence the range of P_{hf}/P_i could be generated by the apparatus used was not enough to trigger fracture.

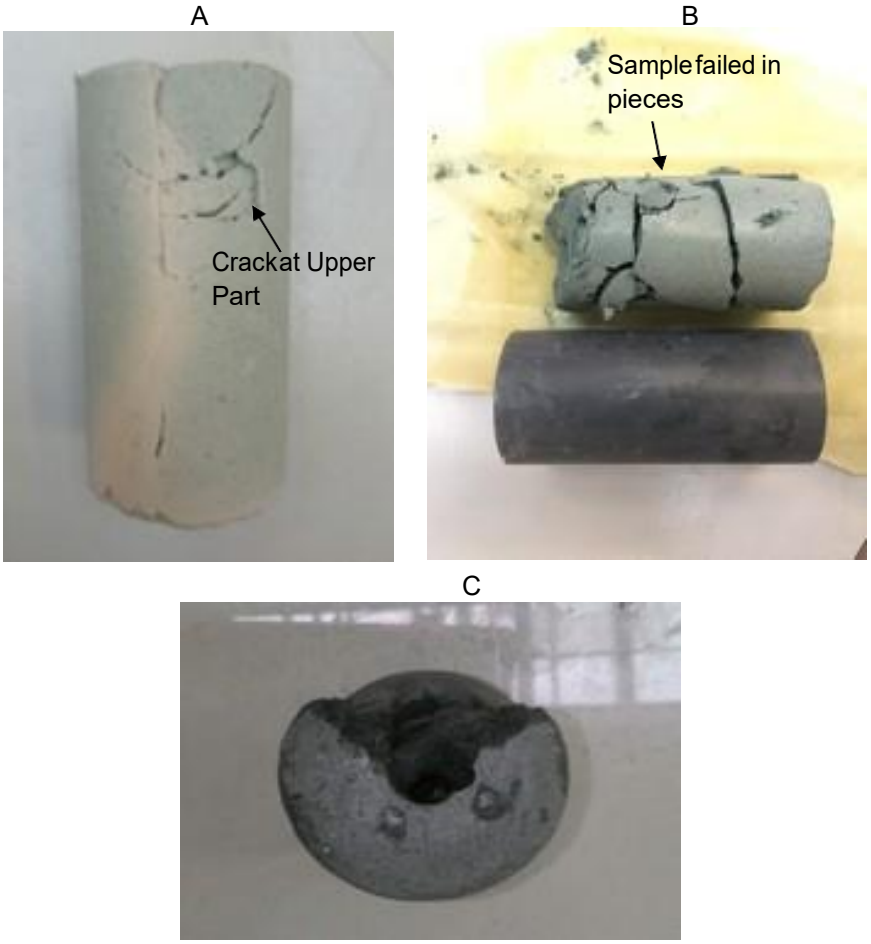


Figure 4.17 Typical fracture after the hydraulic fracturing test: (A) cracks at the upper half of the sample (B) sample lost its lower half during sample extraction

When the failure occurred, the membrane expansion was one of the visual signs that indicate it. The samples after the test were usually hard to extract without being crumbled into pieces because after reaching failure the fluid pressure fractured the sample and only membrane that kept the fractured sampled inside the system. Figure 4.17 showed one of samples that managed to be extracted with minimum damage and the cracks could be observed.

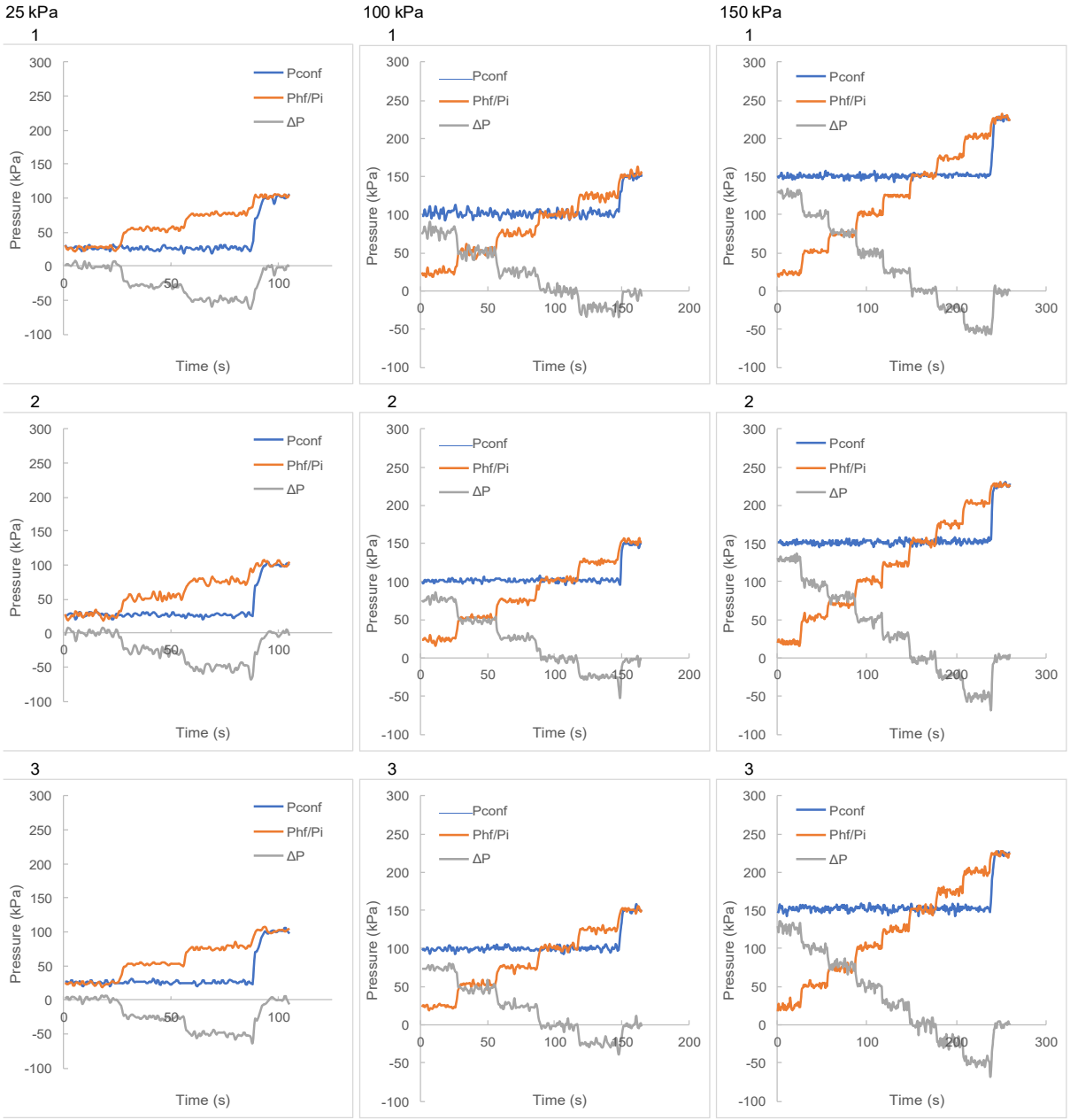


Figure 4.18 Hydraulic fracture test for CB with GGBS 60% (28 days)

Figure 4.18 compiled the test conducted to CB with GGBS 60%, cured for 28 days, samples with P_{conf} ranging from 25 kPa to 150 kPa. It was observed that all the failure occurred on the case which $P_{hf}/P_i > P_{conf}$. P_{hf}/P_i required to fracture samples increased with the higher P_{conf}, it increased from 100 kPa, 155 kPa and 215 with the increase of P_{conf} from 25 kPa, 100 kPa, and 150 kPa. Respectively. This trend generally observed for all GGBS proportions. The incorporation of GGBS also contributed in the increase of P_{hf}/P_i for all applied P_{conf}, the higher GGBS proportion yielded higher P_{hf}/P_i value. The results for the other mix proportion and curing time can be accessed at Appendix

E. Past study on the hydraulic fracture of CB sample aged 3 months, 1 and 10 years by Ng (2009) suggested that the cavity pressure (internal pressure) required to trigger fracture increased with the increase of initial effective confining pressure, in addition to sample types (laboratory produced, in situ, and contaminated). The rate of increase, however, became insignificant at high confining pressure. The internal pressure applied in the study by Ng (2009) was by the means of controlling fluid injection rate, whereas the pressure in this study applied by the pressure regulator. The current study was performed under undrained condition while the apparatus system used by Ng (2009) allowed the back pressure to be applied. Figure 4.19 compares the results from this study and Ng (2009). It suggested that the samples tested under undrained condition failed at lower internal pressure than at drained condition. However, the results included in the figure only represented the samples which could only be examined in the apparatus and they were younger than samples studied by Ng (2009). Hence, the extent of test condition, undrained or drained, to the susceptibility of CB sample to hydraulic fracturing is still inconclusive. In general, due to different method in applying P_{hf}/P_i and test condition, it was deemed not ideal to compare both results.

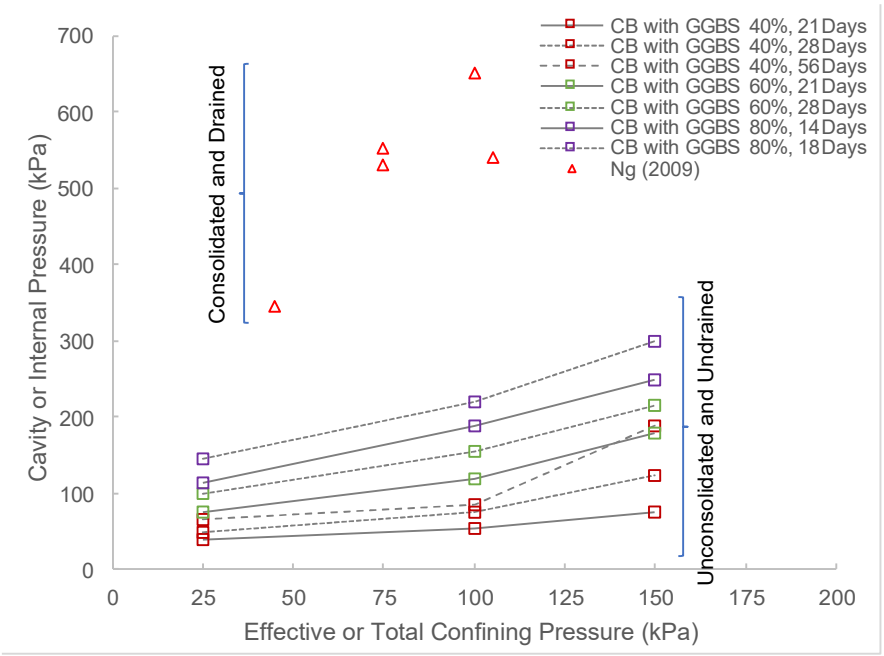


Figure 4.19 Comparison with past study by Ng (2009)

The CB samples tested under consolidated and drained condition in Triaxial apparatus failed at higher strain and stress (under higher confining pressure (e.g. 500 kPa)

sample did not exhibit failure sign), and they also experienced changes in failure mechanism according to Deschênes et al. (1995) and Soga et al. (2013). Comparison of CB strength characteristics under drained and undrained condition by Alzayani et al. (2017) also concluded that the material demonstrated higher strength at drained condition. These suggested that the role of test condition is crucial in the material strength characteristic and it can be a relevant hypothesis to suggest the impact of test condition to the hydraulic fracture behaviour. To better understand the role of test and condition and confining pressure, it is therefore suggested that further study using improved test apparatus should be conducted to investigate the CB material susceptibility to hydraulic under both test conditions for young samples and higher confining pressure ranges.

4.3 Erosion Test

4.3.1 Concentrated Leak Erosion (Hole Erosion Test)

4.3.1.1 Non-Erodible

In order to investigate the fluctuation recorded during the test which were produced by the pump used in the apparatus and the relationship between pressure and flow of the eroding fluid inside the sample hole during the test, series of test using non-erodible samples were conducted. The test was conducted to CB with GGBS 80% cured for 56 days samples with hole diameter of 3, 4, 5, 6, 8, 10, and 12 mm under the target pressure maintained throughout the course of test duration. The tests were repeated 1-2 times to ensure the repeatability of the results.

Table 4.2 Average Difference for Non-Erodible Sample

Diameter (mm)	Pressure (kPa)		Flowrate (l/min)	
	Avg. Max	Avg. Min	Avg. Max	Avg. Min
3	9.3	-10.16	0.14	-0.15
4	6.95	-8.55	0.14	-0.14
5	7.59	-7.24	0.16	-0.16
6	7.1	-6.74	0.23	-0.2
8	6.7	-6.85	0.2	-0.24
10	6.99	-8.23	0.25	-0.29
12	8.14	-9.58	0.28	-0.26

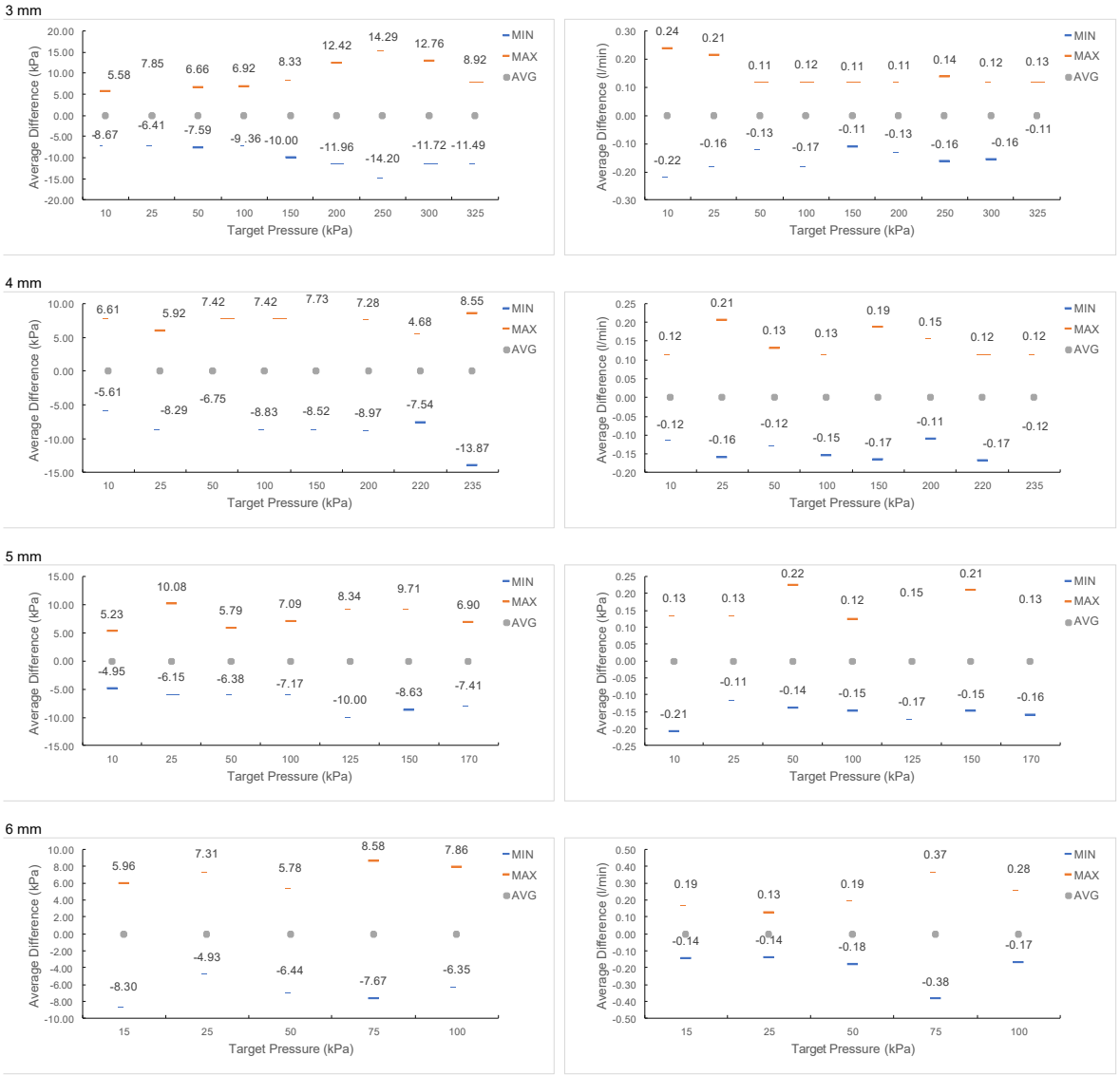


Figure 4.20 Average Difference for 3, 4, 5, and 6 mm Non-Erodible Hole (test repeated 2 times)

Table 4.2 and Figure 4.20-4.21 summarise the average difference range obtained for each target pressure and hole diameter. For the fluctuation recorded in pressure reading, the biggest range was recorded at the test of 3 mm hole, ranging from the average of +9.3 to -10.16. For the rest, they were within the range of 6.95 to 8.14 for the upper threshold and -6.74 to -9.58 for the lower threshold. In general, there was no specific trend observed. The general trend for flowmeter reading: the range was getting wider with the increase of hole diameter. The average upper limit range increased from 0.14 to 0.28 for 3 mm to 12 mm hole, whereas the bottom limit expanded within the range of -0.15 to -0.26, The full results of the average difference analysis including the frequency of the difference are presented in Appendix F.1-F.16.

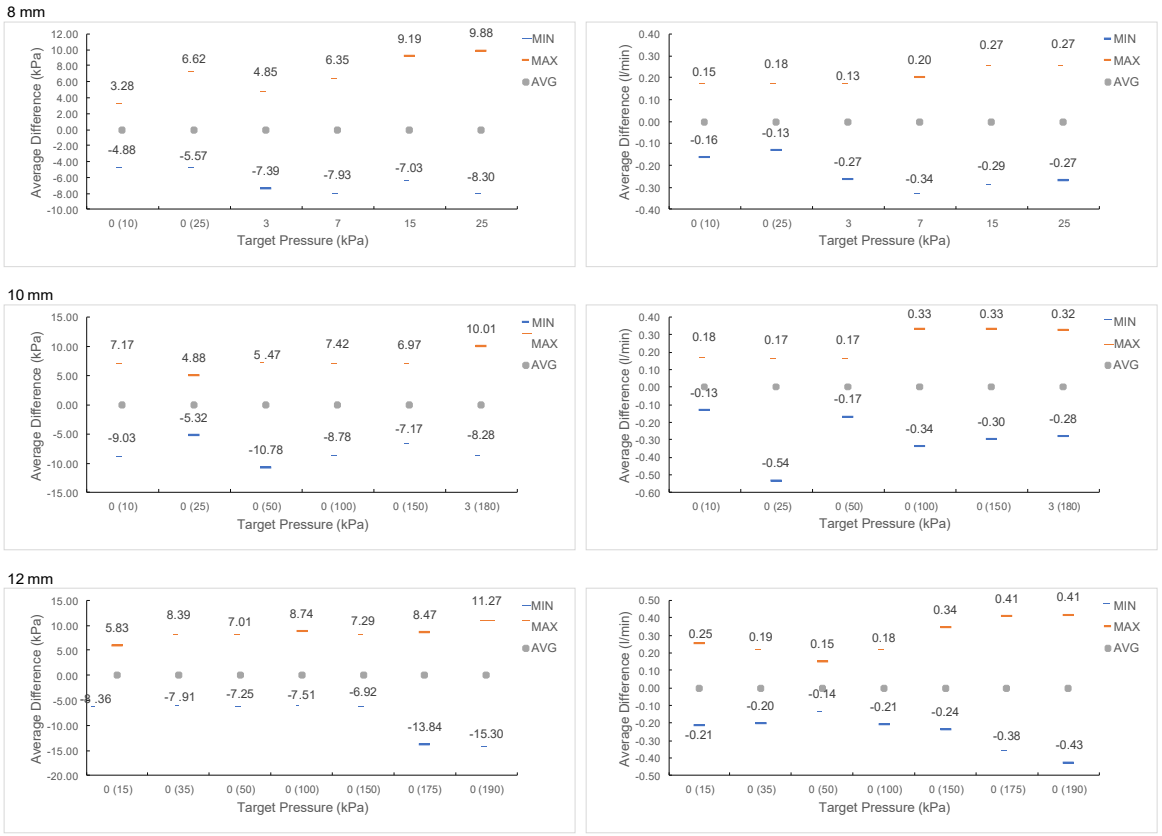


Figure 4.21 Average Difference for 8, 10, and 12 mm Non-Erodible Hole (test repeated 2 times)

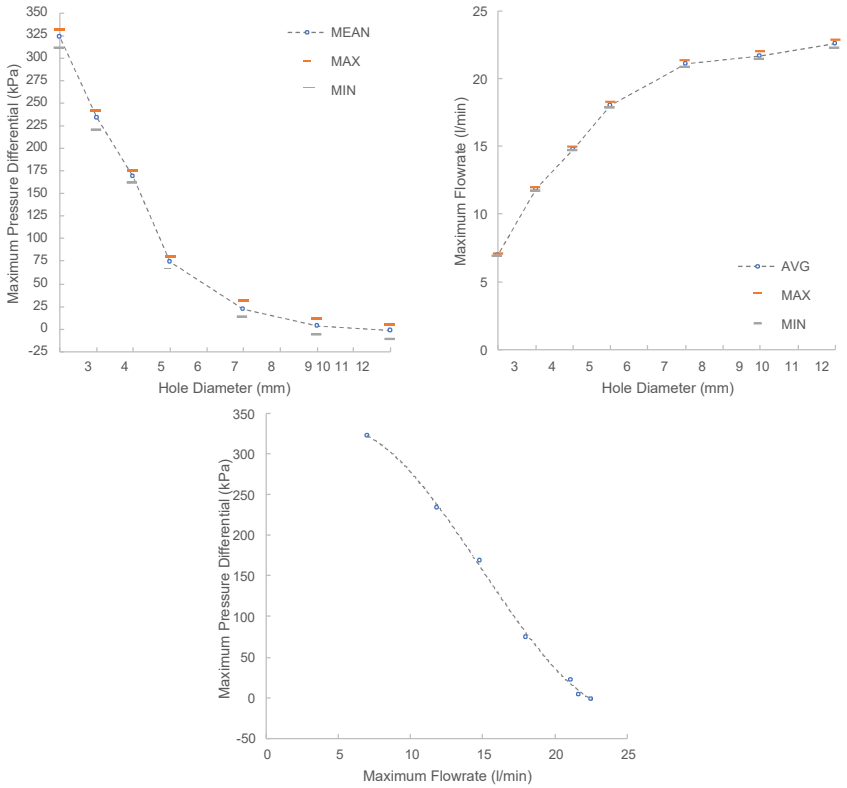


Figure 4.22 The relationship between ΔP and Q

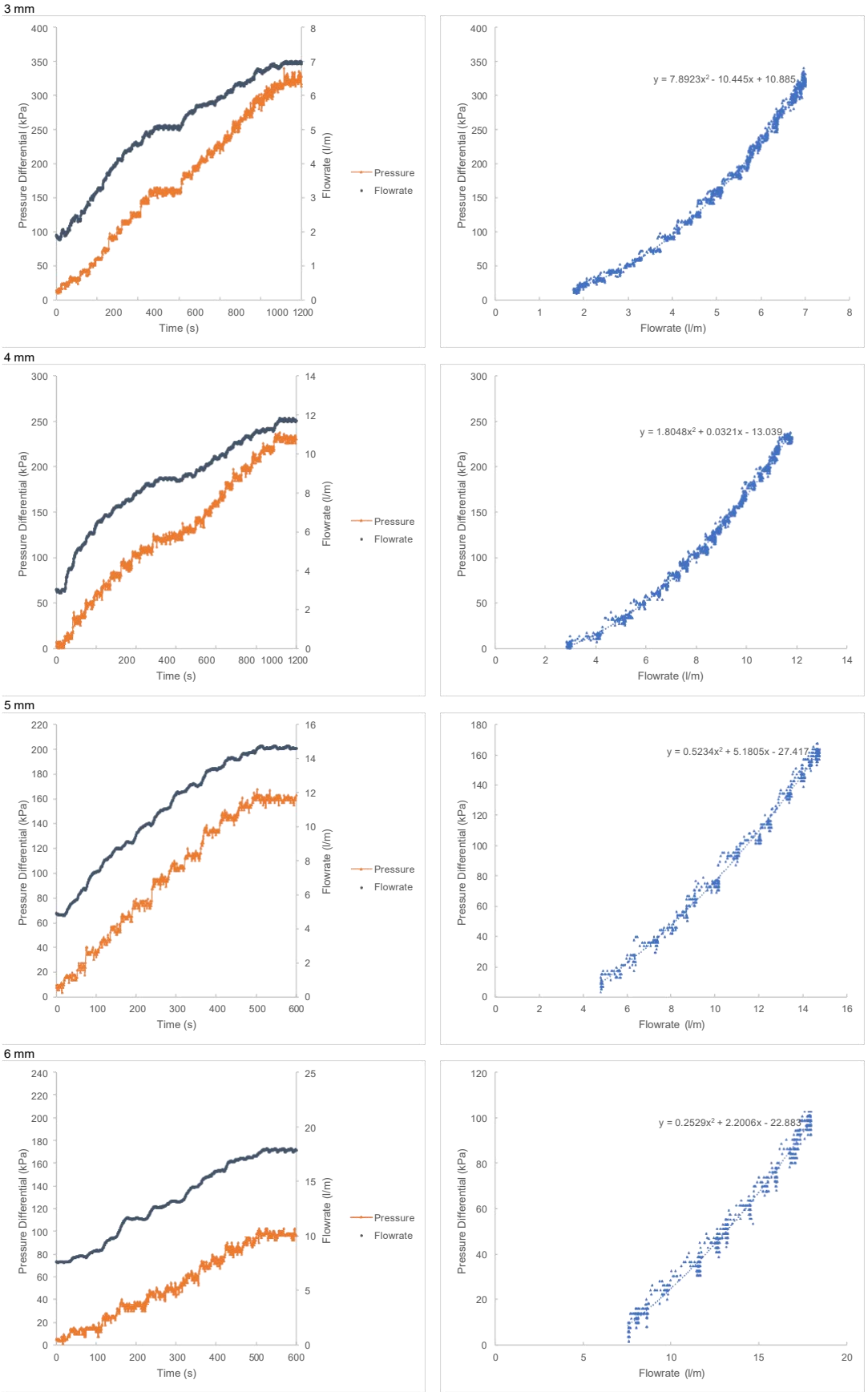


Figure 4.23 The relationship between differential pressure and flowrate for sample with hole diameter of 3, 4, 5, and 6 mm

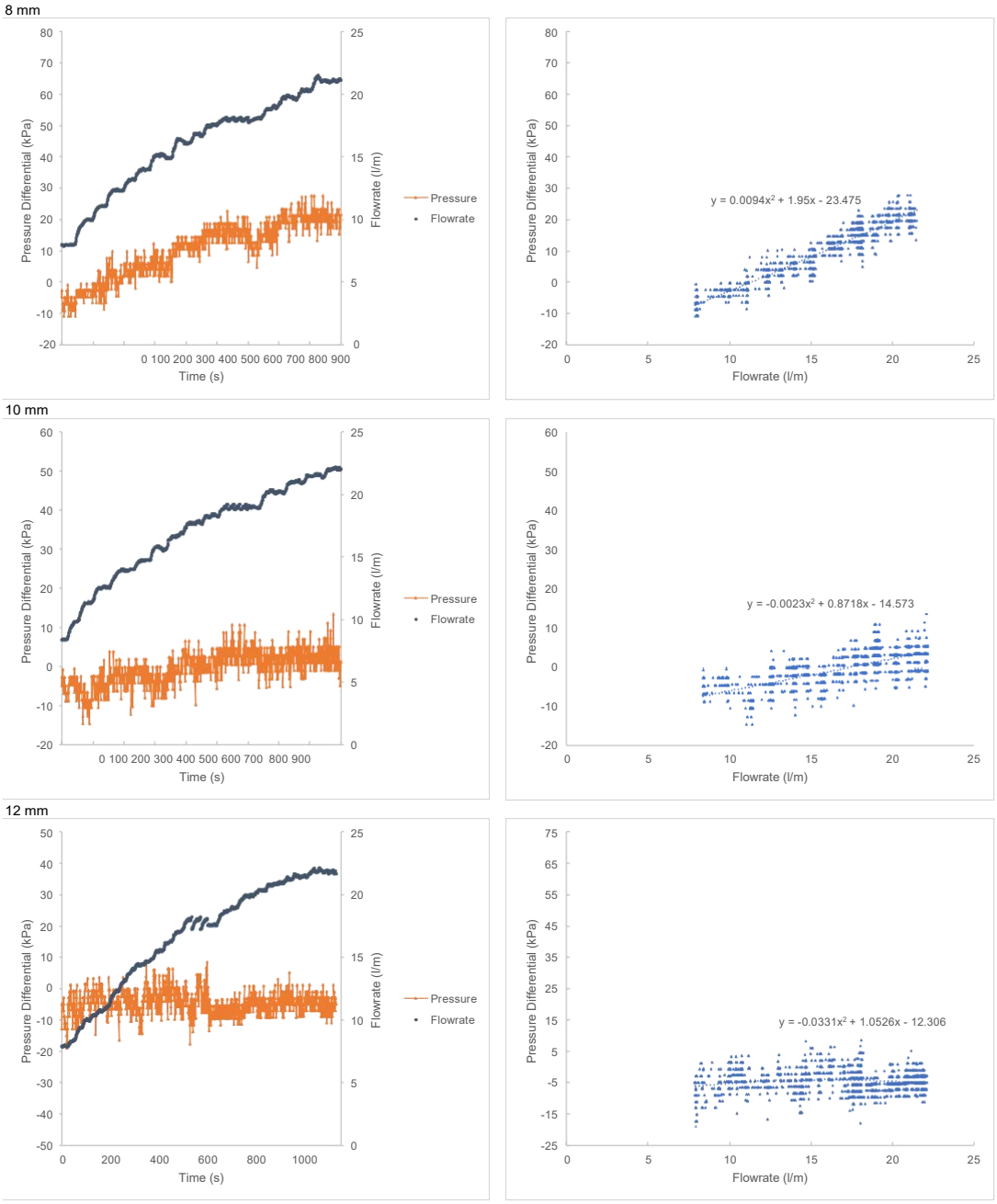


Figure 4.24 The relationship between differential pressure and flowrate for sample with hole diameter of 8, 10, and 12 mm

Figure 4.22-4.24 show the relationship between Pressure Differential (ΔP) and Flowrate (Q). The maximum pressure at which the pump capacity was set at the maximum for each diameter was correlated with the measured flowrate from flowmeter. Due to the pump noise, some differential pressure recorded at 10 and 12 mm reached below 0. They did not indicate the pressure differential pressure was negative, but it suggested that the pressures at the upstream and downstream were equal or there was no pressure lost across the pipe. The recorded pressure decreased with the

increase in hole diameter, while the reverse trend was observed for the flowrate. This trend is in line with Bernoulli's principle:

$$P_1 + \frac{1}{2}\rho v_1^2 + \rho g h_1 = P_2 + \frac{1}{2}\rho v_2^2 + \rho g h_2 \quad (1)$$

The test was performed to hole with smooth surface and uniform diameter; however, these are not always the case for the hole of eroded samples. The eroded hole can vary in terms of surface roughness and symmetricity due to non-uniform response of impacted surface to erosive force which impacted the uniformity of the eroded diameter and shape. The non-uniform surface can affect the friction between eroded surface and eroding fluid, thus impacting the pressure loss across the pipe (i.e. ΔP). The technical difficulty encountered in producing the more representative hole (i.e. non-uniform surface) were the method to produce samples with the desired hole diameter. The current study used melted paraffin wax poured into the hole to estimate the diameter of the hole. The sample should be split in half to retrieve the hardened wax; therefore, the sample could not be used again for the test. This suggested that the possibility to non-invasive measurement method in measuring the diameter of eroded hole should be explored. Despite the limitations, the result provided an overview on the range of data noise should be expected from the apparatus and the relationship of hydraulic parameters.

4.3.1.2 Juvenile Samples and Entrance Scouring Entrance Section

In order to trigger erosion in the hole, it should reach a certain point of pressure difference across the pipe. However, for juvenile samples, the threshold of pressure difference required were too low that instead of eroding the sample inside the hole, the entrance section experienced a formation of cracks followed by a significant scouring of the section. The sequence occurred within the time frame of 10-20 seconds depending the magnitude of ΔP and Q. This type of occurrence was mostly observed from CB without GGBS and CB with GGBS 40% and 60% sample for curing duration of 7-14 days. The longer curing period and higher GGBS proportion diminished the likelihood of this phenomenon to occur. Figure 4.25 demonstrated the effect of the high-pressure application at the upstream that caused the sample to be partially damaged. As soon as the sequence of entrance damage ceased, the test was halted. Due to the damage caused, it was not possible to properly quantify the extent

of the erosion and the test was considered not completed. Nonetheless, this phenomenon suggested that under the high-pressure difference, instead of causing erosion, it led to fracturing and followed by the flushing of the destroyed sample by the eroding fluid.

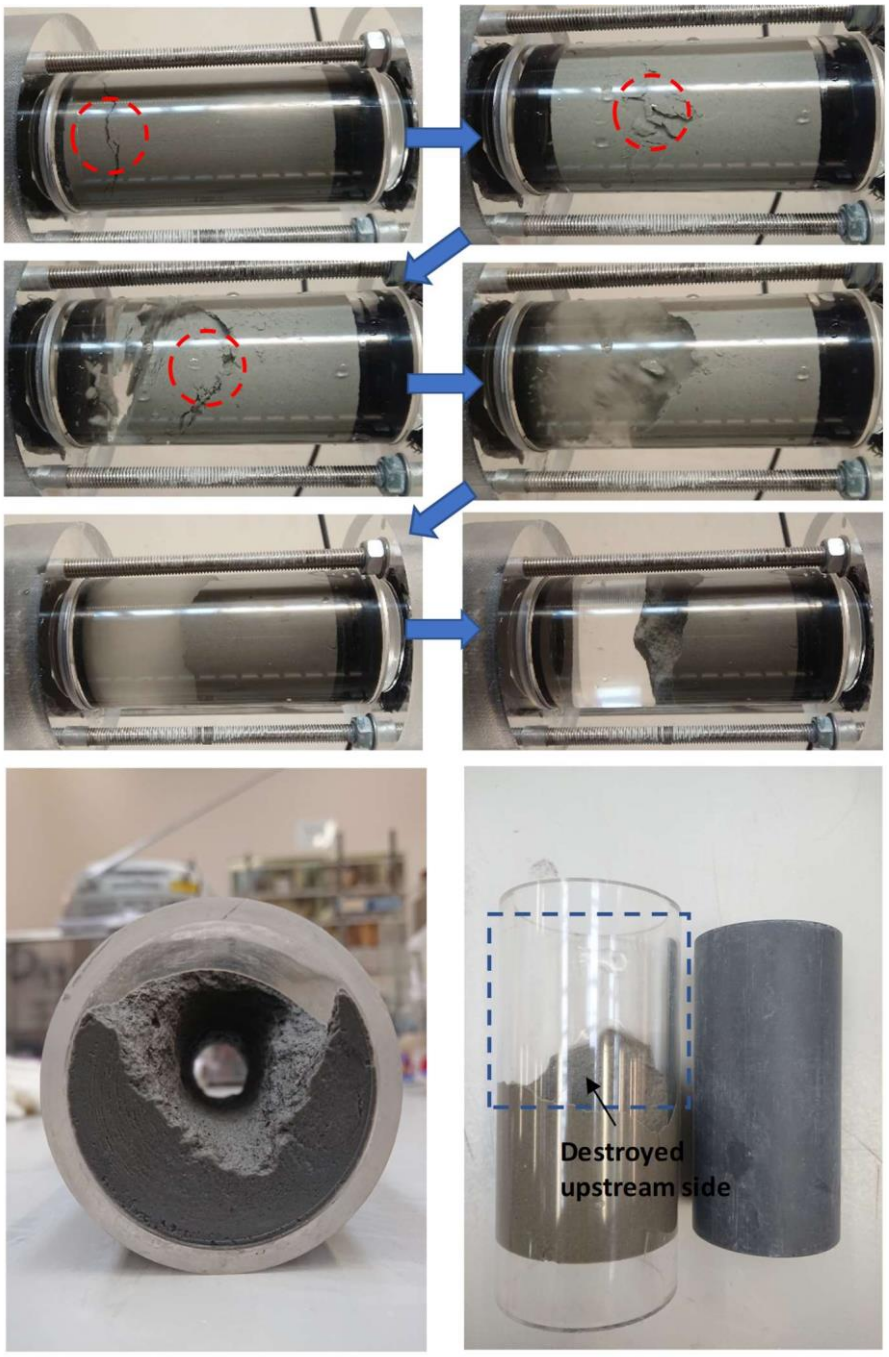


Figure 4.25 The typical failure occurred at the entrance section for the test conducted under high upstream pressure to the juvenile (7-14 days) samples.

4.3.1.3 Pressure, Flowrate, and Hole Diameter

The apparatus used, Hole Erosion Test (HET), for this test mainly aimed to investigate the erosion resistance of CB samples under varying hydraulic parameters and specified testing duration. There were approximately 121 samples tested (each curing period and GGBS proportion, the tests were repeated for 5-6 times). For the initial assessment, there are three parameters obtained from visual observation/calculation, pressure transducers and flowmeter that were investigated:

1. Pressure differential ΔP (peak and final)
2. Flowrate Q
3. Hole diameter

The full result of pressure sensor and flowmeter measurement for varying curing duration and GGBS proportions can be accessed at Appendix F.17-F.20 and F.21-F.24, respectively.

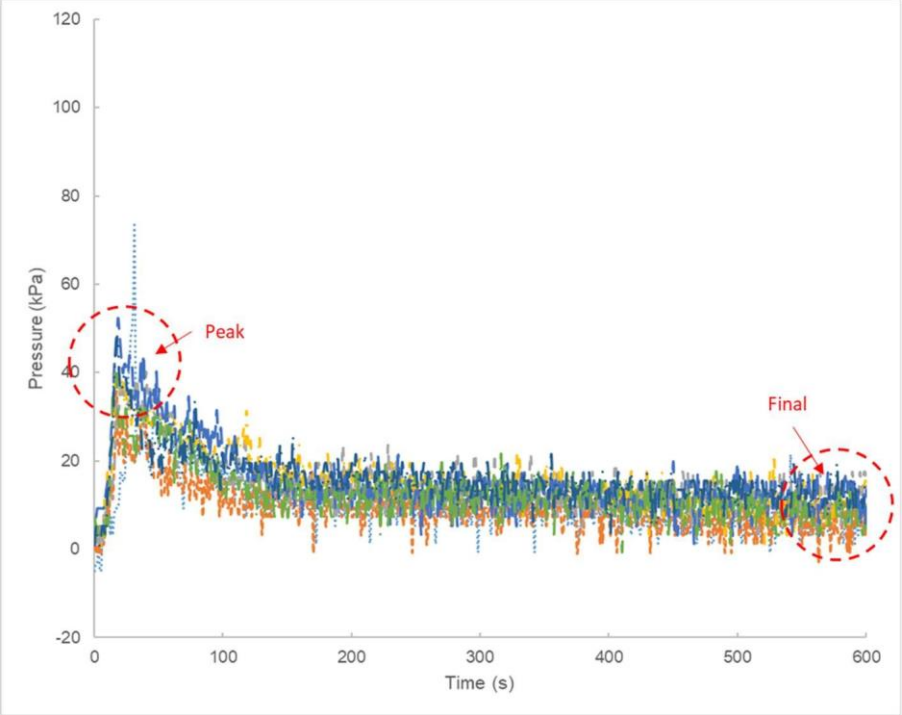


Figure 4.26 ΔP measurement from pressure sensors (CB with GGBS 80%, 7 Days)

Figure 4.26 highlighted the points used to represent Peak and Final ΔP. Peak ΔP represents the highest point reached before the sequence of ΔP drop follows. As it was not possible to precisely determine the exact point of which erosion commenced, the peak ΔP was used to represent the initial point of erosion process. The drop of ΔP caused by the increase of downstream pressure. The decrease of pressure difference

across the pipe can be caused either by the upstream pressure drop or the change in hole size. As the upstream pressure was maintained to be constant throughout the test, ΔP drop was caused by the hole enlargement which indicated the erosion process took place.

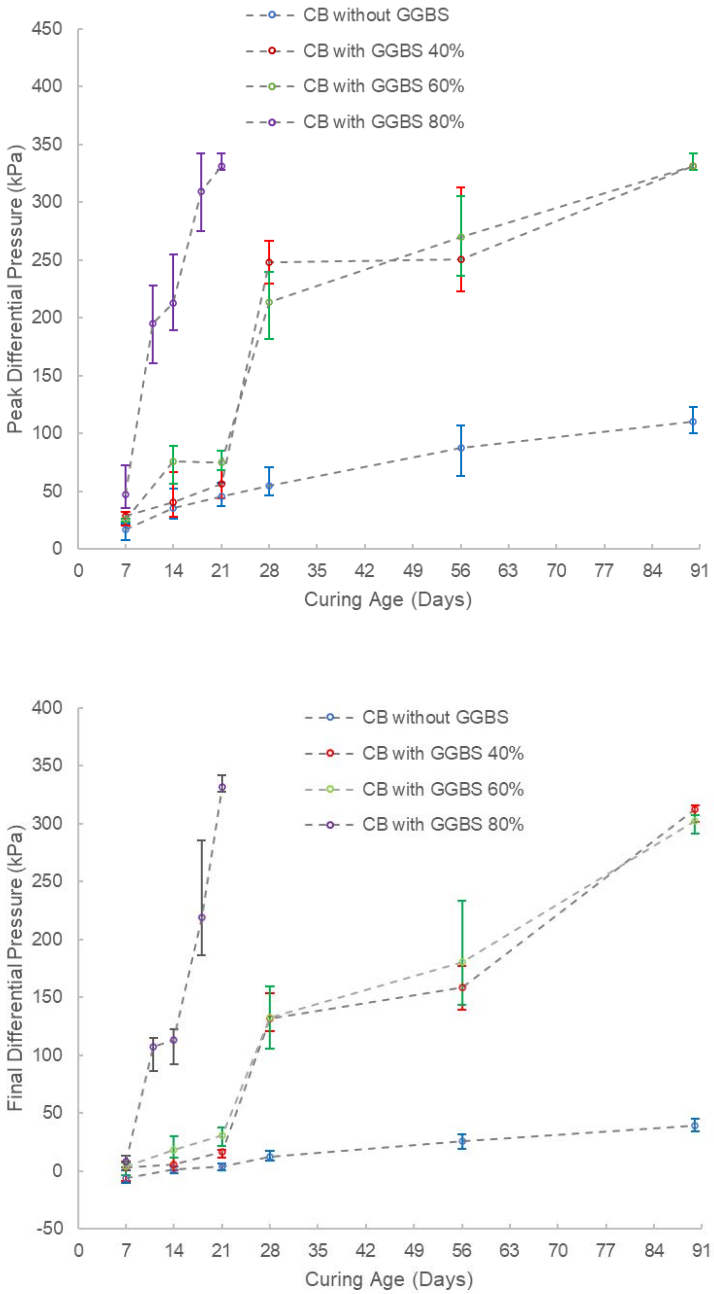


Figure 4.27 The relationship between peak ΔP, final ΔP, and curing age

Figure 4.27 shows the effect GGBS replacement and curing days in peak and final ΔP. CB without GGBS is used as the reference point. The peak ΔP for CB without GGBS increase from 16 kPa to 110 kPa from curing age of 7 to 90 days. The improvement

of peak ΔP obtained with the inclusion of GGBS. Incorporating 40% and 60% GGBS in the CB mix led to the slight increase of peak ΔP for curing period of 7-21 days, the rate of increase was consistent below 100%. Peak ΔP significantly increased

approximately 300-350% after cured a month and maintained 200% peak ΔP increase for the next two months. The sample containing 80% GGBS experienced an increase at greater magnitude: 182%, 500%, and 630% for the curing period of 7, 14, and 21 days. Increasing GGBS replacement to 80% not only significantly improved the peak ΔP but shortened the time required to reach the improvement rate obtained by the samples containing less GGBS. In general, the trend is that the higher GGBS proportion resulted in the better strength improvement rate. In addition, it should be noted that peak ΔP recorded at 'No Erosion' point represented the maximum pressure that could be generated by the apparatus; therefore, it was inconclusive whether the point could represent the peak ΔP for the specified curing period as the increase of peak ΔP value could be higher.

The improvement rate for CB without GGBS peaked at the curing duration of 7 to 14 days at 115% and decreased to below 40% for the following two weeks. Although recorded an increase approximately 60% from the curing period of 28 to 56 days, it was an accumulation from the longer period, hence it was deemed insignificant. The rate of peak ΔP improvement generally lower for the curing duration of 28 to 90 days and 11 to 21 days for samples containing GGBS 40%/60% and 80%, respectively. The highest peak ΔP improvement was recorded at curing period of 21-28 days and 7-11 days for CB with GGBS 40% and 80%, respectively, whereas CB with GGBS 60% reached the highest improvement rate, approximately 180%-190%, at curing period of 7-14 and 21-28 days. In conclusion, the curing duration had a varying impact to the rate of peak ΔP increase.

Final ΔP represents the point at which the test ends. At this point, the rate of ΔP decrease was virtually non-existent, which indicate the erosion process occurs at very slow rate/negligible state. The trend observed for final ΔP was similar to peak ΔP: (1) For GGBS with 40% and 60%, the final ΔP increase rate was insignificant for curing duration 7 – 21 days, however the improvement rate was comparatively higher for samples containing 60% GGBS, and the pronounced increase of final ΔP was recorded at curing period of 28-90 days for both GGBS proportions, (2) the impact of incorporating 80% GGBS not only significantly improved the final ΔP after cured for 14 and 21 days, but also reduced time in reaching 'No-Erosion' point, which other GGBS proportion needed 2 months more to achieve.

Compared to the peak ΔP, the rate of increase achieved in final ΔP was generally higher for all GGBS proportion and curing time frame. Similar to trends observed in peak ΔP: (1) the increase rate was generally lower at late stage of curing duration of (e.g. 28-90 days for CB without GGBS and samples containing GGBS 40%-60%), (2) The highest improvement rate recorded at early stage of curing duration for CB with GGBS 60% and 80% at curing duration of 7-14 and 7-11 days respectively, (3) The increase rate was at highest during the curing period of 21-28 days for samples without and with GGBS containing 40%.

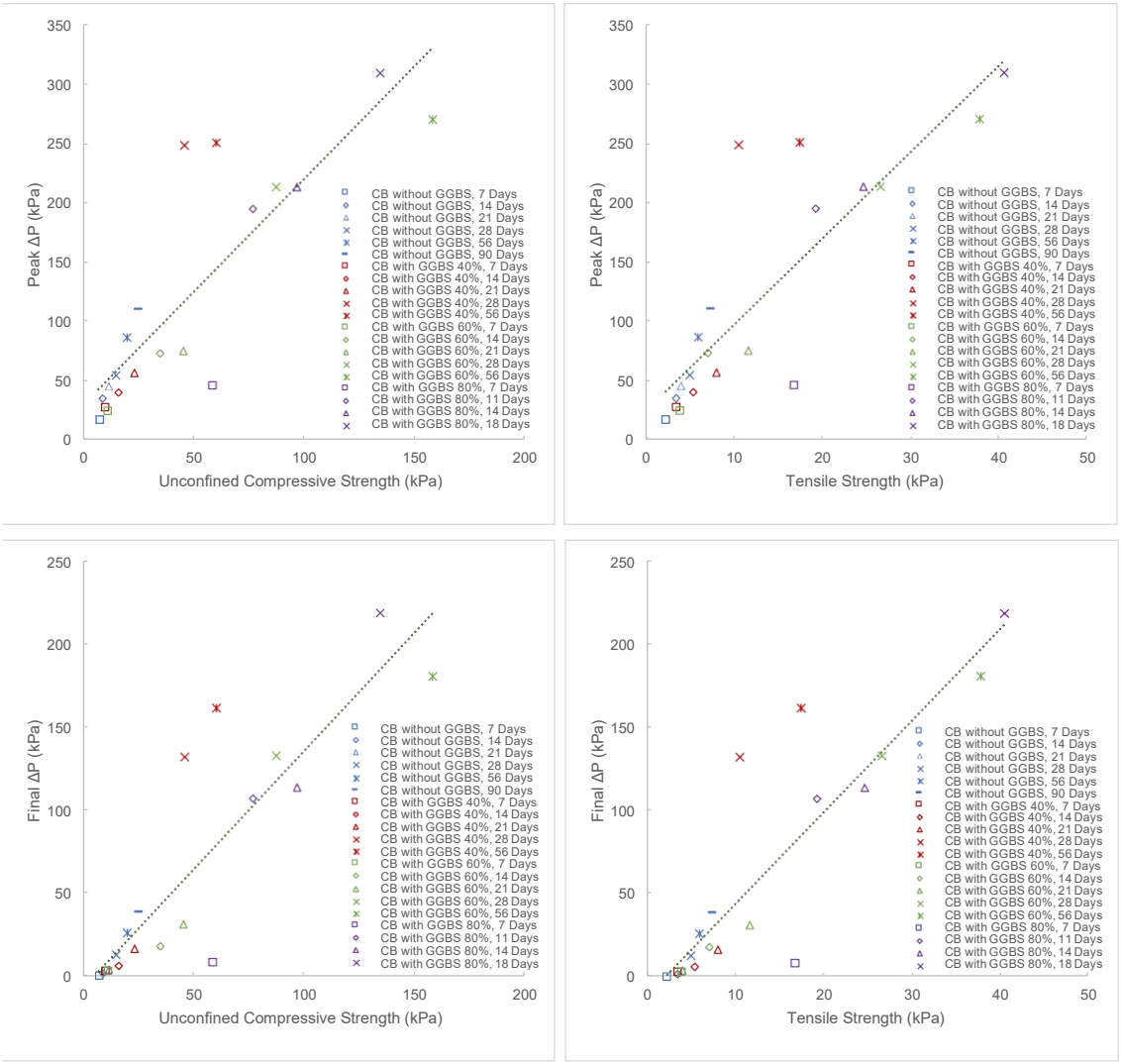


Figure 4.28 The relationship between strength characteristics and peak/final ΔP (average values)

As shown in Figure 4.27, the trend observed in CB strength characteristics was also found in peak/final ΔP: increasing GGBS proportion and curing duration contributed in

the increase of peak/final ∆P. The significant improvement in peak/final ∆P of CB with GGBS with 40% and 60% for curing duration between 21 – 28 days was observed; however, this trend was only relevant to CB with GGBS 60% than 40% as the strength improvement at this curing duration was not observed for the latter. Figure 4.28 shows the relationship between strength characteristics and peak/final ∆P. Linear line was added to analyse how the plotted data fit the line. In general, the relationship was not linear mainly because the spread of the data for all mix proportions. For samples without GGBS, the increase of strength characteristics linearly increased peak/final ∆P. However, samples with GGBS, regardless of its percentage, did not fit with the generated trendline and the data spread was bigger with the increase of curing duration. This suggested that although the general trend between strength characteristics and peak/final ∆P were correlated, the correlation should also consider the material characteristics such as GGBS proportion and curing duration.

Figure 4.29 summarise how final flowrate and hole diameter changed with curing duration and different GGBS proportions. Both final flowrate and hole diameter decreased with the increase of GGBS proportion and curing duration. This indicated an improvement on the erosion resistance as the enlargement of hole diameter are related to the amount of material eroded during the test, therefore the smaller the hole diameter means reduction of eroded material. The reduction of hole volume also affected the amount of eroding fluid flowing through the hole per unit time. For samples containing GGBS, it required 90 days curing duration to reach ‘no erosion point’ for samples with 40% and 60% GGBS whereas only 21 days for 80% GGBS. Akin to the trend in peak/final ΔP, the significant decrease of final flowrate and hole diameter was observed during the curing duration of 21 and 28 days for samples with 40% and 60% GGBS whereas samples with 80% GGBS experienced higher rate of reduction from the early curing age. The minor decrease of the final flowrate and hole diameter between curing duration of 11 and 14 for samples with 80% GGBS can attributed to the shorter time interval (3 days). It can be observed that the rate of decrease for final flowrate differed from the final hole diameter, this is mainly because, as shown in Figure 4.22, both are not correlated linearly. The decrease of flowrate is smaller at bigger hole diameter and flowrate; the decrease of flowrate is more progressive at smaller diameter.

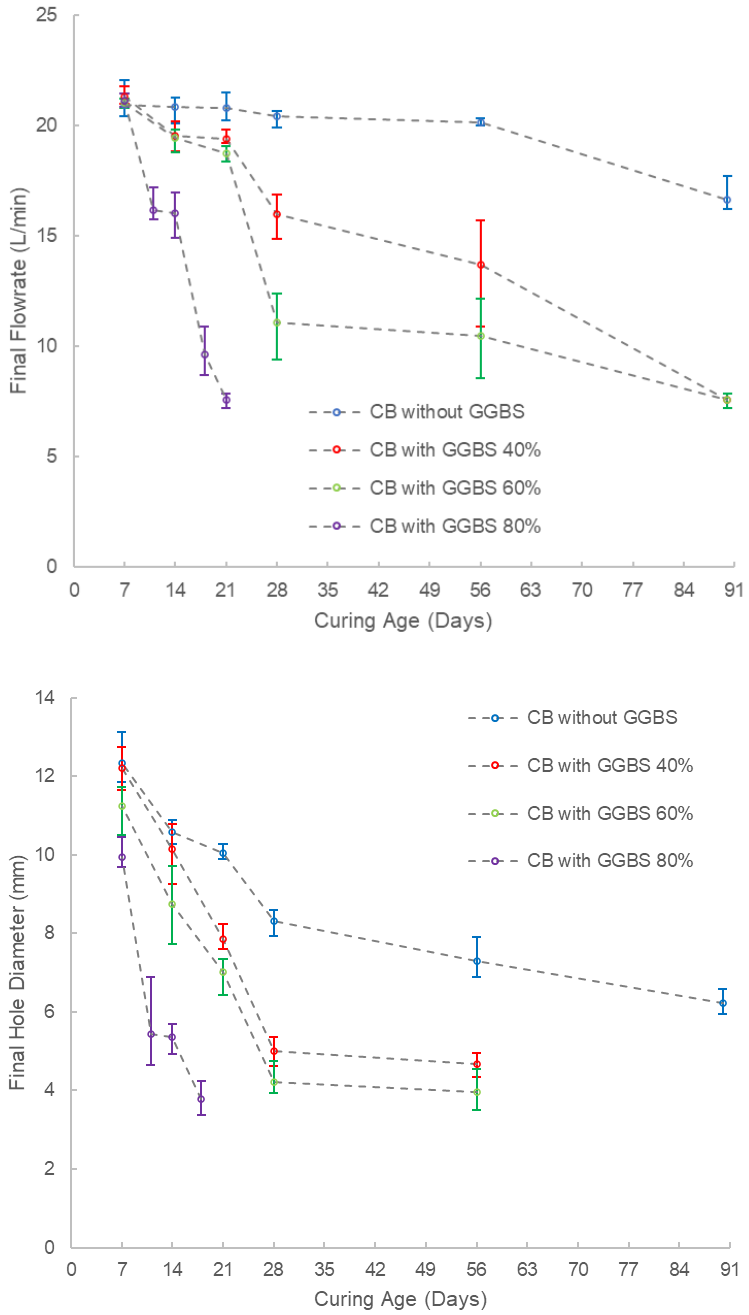


Figure 4.29 The relationship between curing duration and final flowrate/hole diameter (5-6 samples tested for each curing duration)

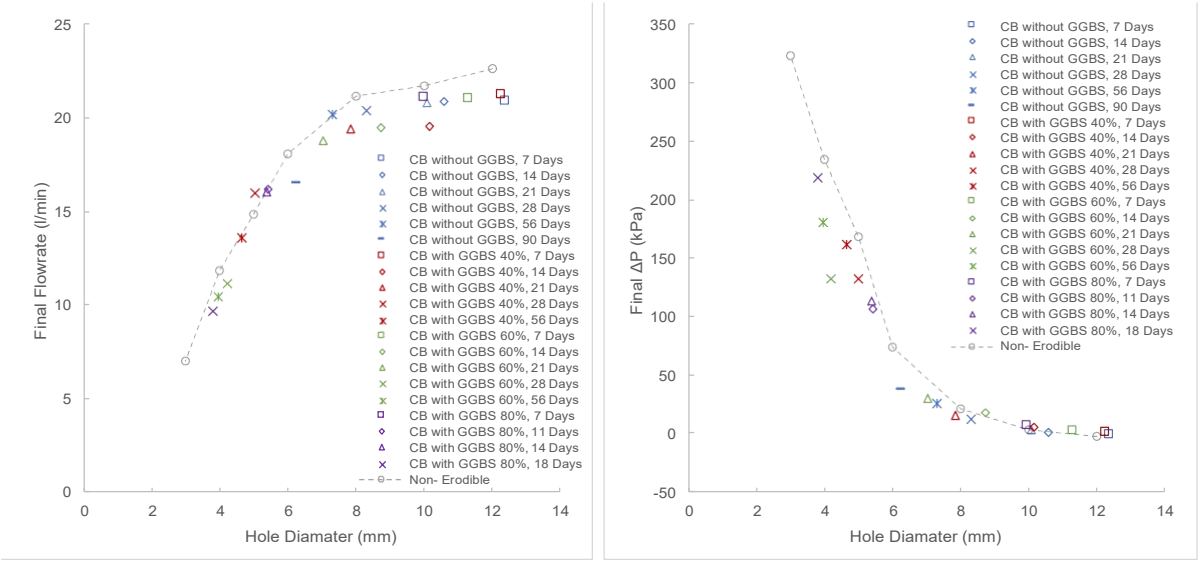


Figure 4.30 The relationship between final hole diameter and final flowrate/ΔP (average values)

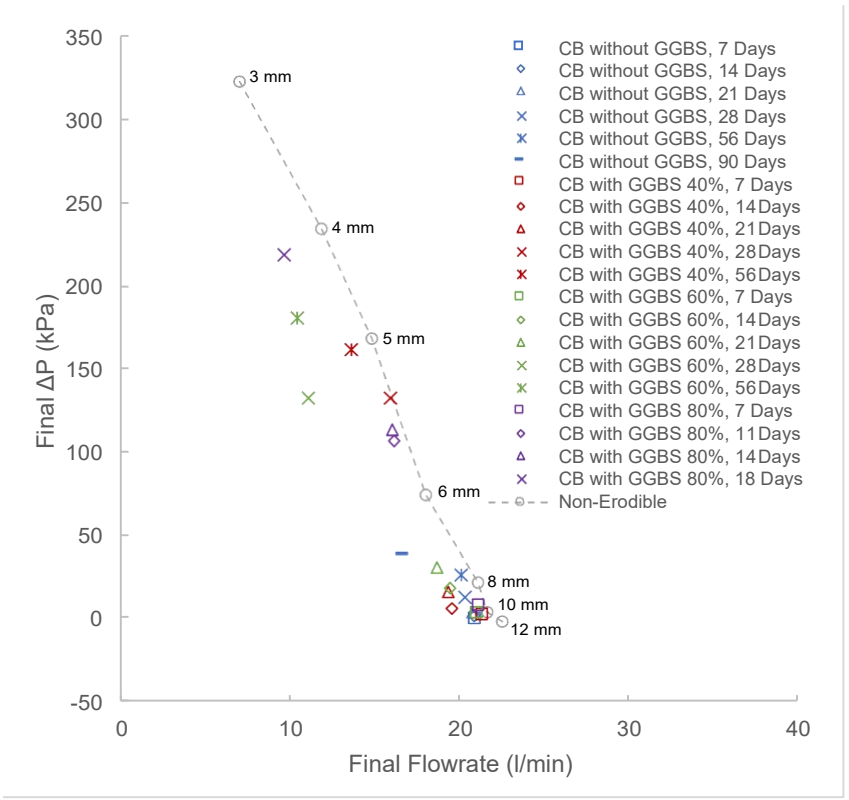


Figure 4.31 The relationship between final flowrate and final ΔP (average values)

Figure 4.30 and 4.31 show a correlation between final hole diameter, final flowrate and final ΔP. Results from non-erodible test was included as the reference. It was observed that the trend between final hole diameter and final flowrate/ΔP as well as between

final flow rate and final ΔP corresponded well with the trend obtained from non-erodible test. The slight deviation of the plotted data from the non-erodible test data was observed, this can be attributed to the different hole characteristics between the non-erodible and erodible sample.

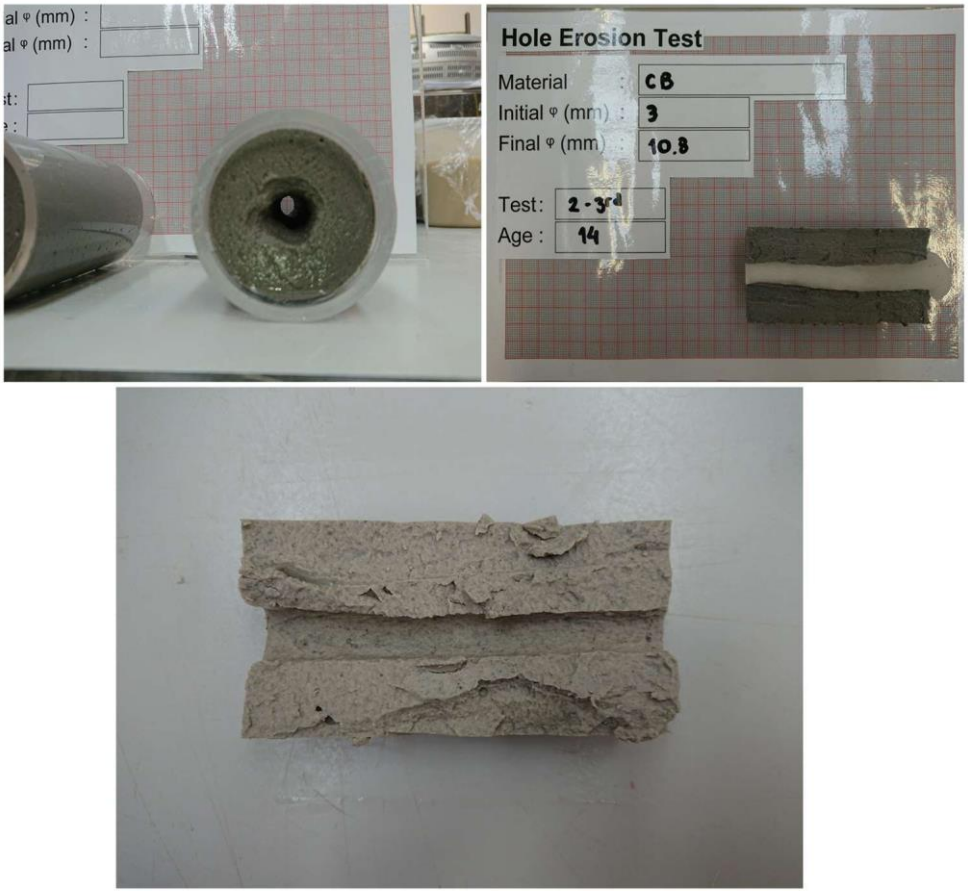


Figure 4.32 Casted eroded hole

Figure 4.32 shows the typical cross-section of eroded hole. After the test, the eroded hole was left to air-dried in room temperature for 4-5 minutes in order to minimise the effect of the moisture inside hole when the melted paraffin wax poured into the hole. In general, there were 3 eroded hole characteristics encountered during the experiment:

1. Uniformly shaped (straight hole) with consistent diameter.
2. Inconsistent size diameter, either bent or straight.
3. Angled or bent eroded hole.

These varying hole characteristics can be attributed to the variation from the hydraulic forces exploring the hole as the turbulent flow was the dominant flow condition inside the hole during the erosion process.



Figure 4.33 The casted eroded hole (uniformly shaped and consistent hole diameter)

The type 1 hole (Figure 4.33) was easier to interpret for its consistent diameter and hole direction. Due to its consistent diameter and hole direction, the hole friction reduced. Figure 4.34 and 4.35 show the hole types with irregular shape and inconsistent hole diameter. The type 2 hole (Figure 4.34) typically had either bigger diameter at upstream or downstream section. The irregularity could also be observed across the hole. The type 3 hole (Figure 4.35) was commonly characterised by the angled hole direction. The result fluctuatuon increased with the increase degree of hole irregularity and angle of hole direction. Hence, not only the pump contributed in the fluctuation of the test results, the hole characteristics should also be considered in interpreting the test results.



Figure 4.34 The casted eroded hole (inconsistent diameter size)



Figure 4.35 The casted eroded hole (deviation from the initial straight pre-casted hole)

4.3.1.4 Data Analysis

From the following data: pressure, flowrate and hole diameter, there are 3 parameters that can be obtained from the analysis (Wan and Fell, 2004):

1. Hydraulic shear stress (τ)
2. Velocity (v)
3. Erosion rate (ε)

As the maximum test time took 600 seconds, the intermediate time test stopped the test at different time interval: 150, 300, 400, and 500 seconds. For several samples containing 80% GGBS, the last interval was shorter than 500 seconds. The test was repeated 4-5 times for each time interval.

At the start of the test, the start of erosion process was mainly indicated by the drop of ΔP, the increase of flowrate and visual observation from the transparent pipe at the downstream section. For juvenile samples (7 and 14 days), the samples were still soft and eroded at low ΔP and flowrate, therefore some materials could be carried by the eroding fluid before reaching the peak ΔP. Due to this technical issue to quantify this, it was assumed that the initial diameter was 3 mm before the test reached peak ΔP and the increase of flowrate was observed.

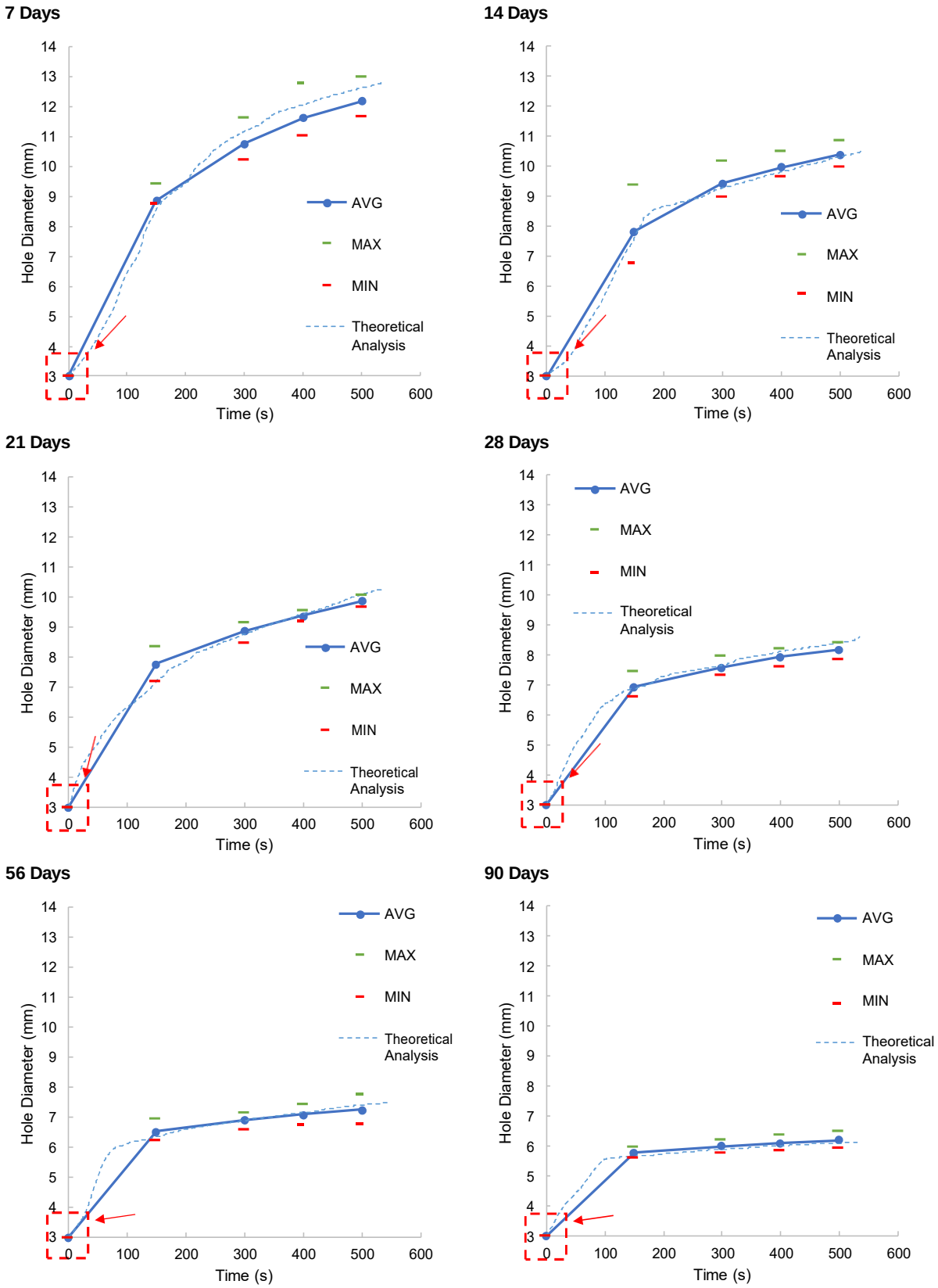


Figure 4.36 Comparison of hole diameter from pre-determined testing duration and theoretical analysis (CB without GGBS) (5-6 data collected for each time interval)

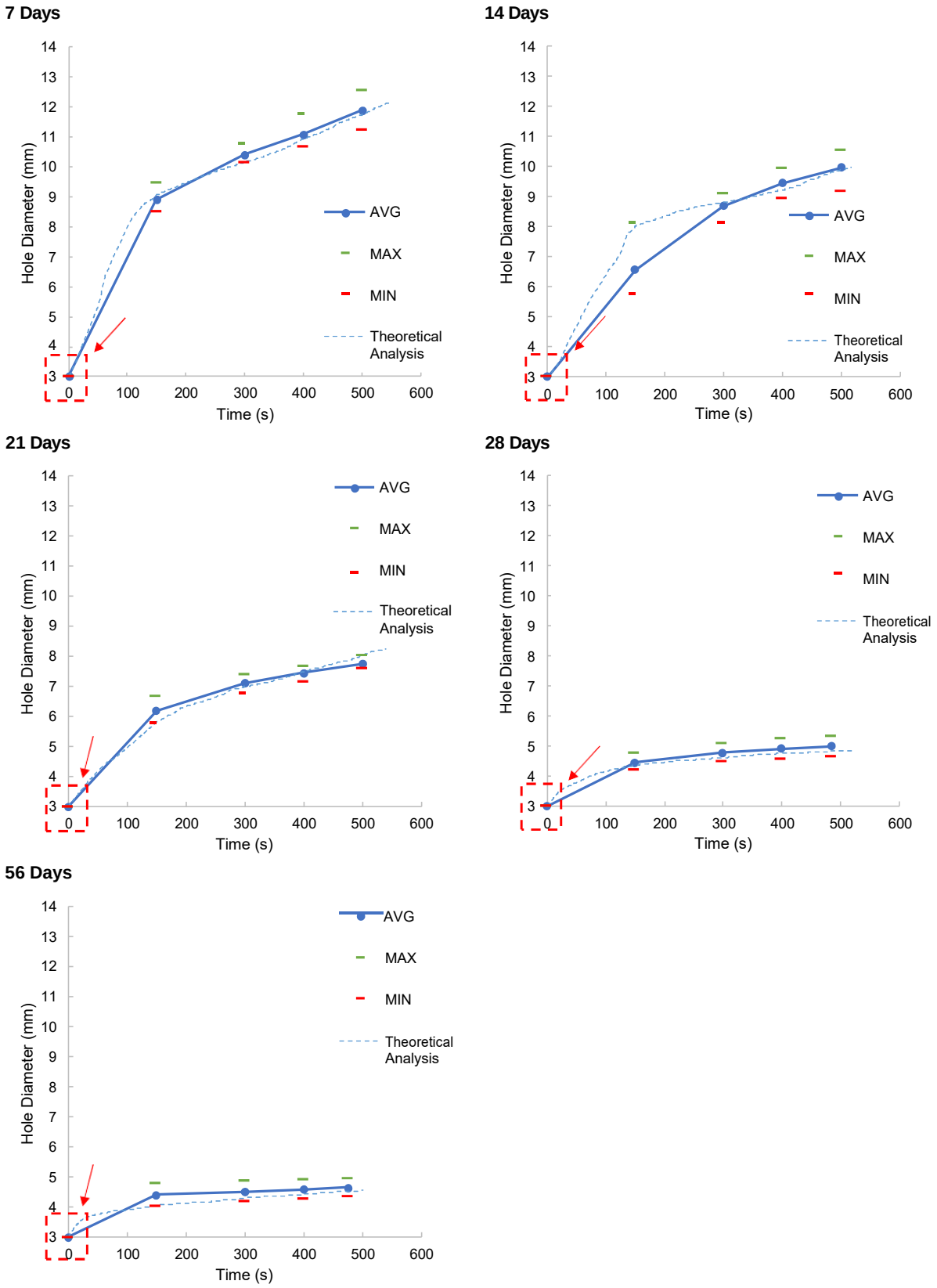


Figure 4.37 Comparison of hole diameter from pre-determined testing duration and theoretical analysis (CB with GGBS 40%) (5-6 data collected for each time interval)

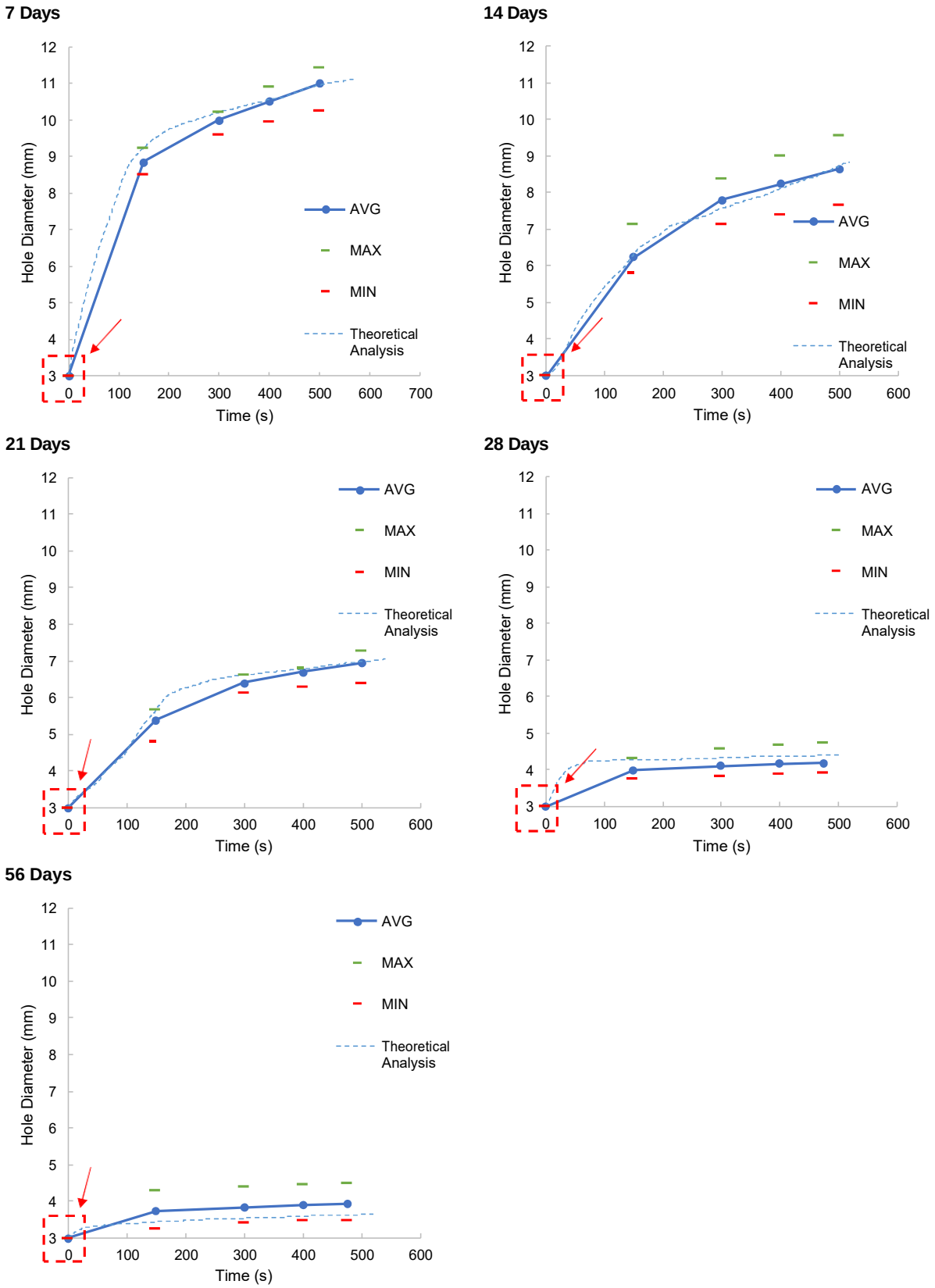


Figure 4.38 Comparison of hole diameter from pre-determined testing duration and theoretical analysis (CB with GGBS 60%) (5-6 data collected for each time interval)

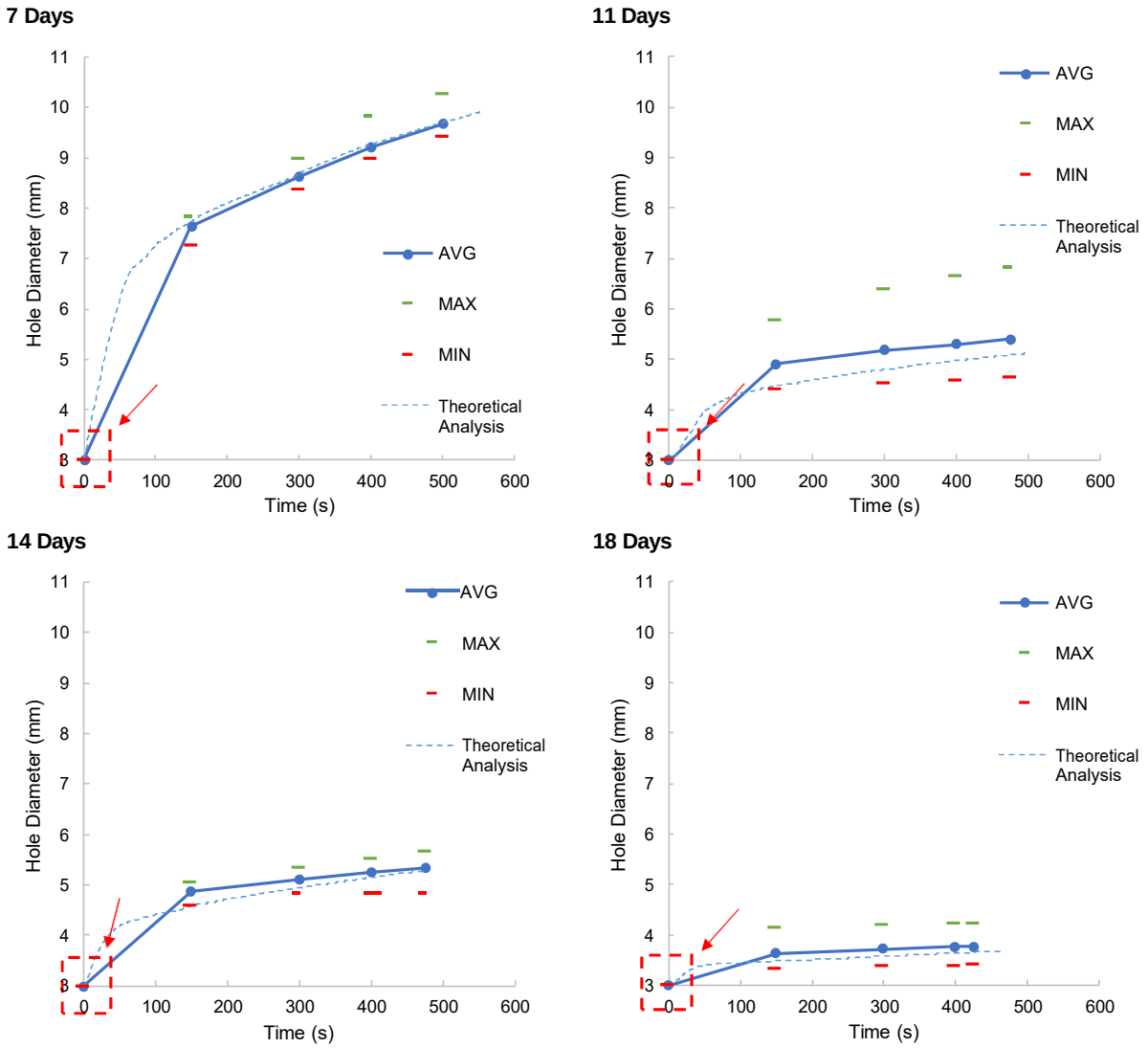


Figure 4.39 Comparison of hole diameter from pre-determined testing duration and theoretical analysis (CB with GGBS 80%) (5-6 data collected for each time interval)

Figure 4.36-4.39 summarise and compare the results from the intermediate time test and the diameter calculation using equation 2 (theoretical analysis). It can be observed that the results from the theoretical calculation were within the range of the maximum and the minimum of the result obtained from the intermediate time test, suggesting the assumption used did not have major impact to the results. Due to absent of results for the test time before 150 seconds, it was not possible to compare the deviation of the theoretical calculation at this time frame with the intermediate time test. Alternatively, recent relevant studies (e.g. Haghighi et al., 2013; Mehenni et al., 2016) employed turbidimeter at the downstream side to quantify the amount of eroded material during the test, thus eliminating the need to calculate the friction factor during the test.

4.3.1.5 Result of Erodibility Parameters

The aim of this section was to analyse the relationship between the hydraulic parameter (e.g. ΔP) and erodibility parameters as well as how they changed during the course of the test. The relationship between erodibility parameters was also explored in this section. The complete results can be accessed from Appendix F.37-F.177.

During the test which lasted approximately 600 seconds in total, it could be categorised into 4 points:

Point A - Peak ΔP reached

Point B - Upstream valve was fully opened

Point C - The rate of ΔP, τ, and v drop significantly decreased

Point D - End or critical point

It was observed at Point A, the peak v was reached when ΔP at its peak point, in contrary, peak τ never corresponded with peak ΔP. Peak τ was reached between Point A and B. The change in erosion rate was contingent upon the rate of ΔP, τ, and v drop during the test. Hence, when reaching Point C, the erosion rate significantly decreased compared to Point A and B. Point C also indicated that the threshold point, Point D, at which the erosion process started was getting closer. Hence, Point D was assumed to be the critical point. The change observed between Point C and D was not as much as the change between Point A and B, indicating that the amount of erosion occurred between Point A and B was higher.

The selected analysis results are presented in Figure 4.42-4.48. The relationship between hydraulic shear stress, velocity and erosion rate were analysed; this ultimately aimed to estimate the critical point of hydraulic shear stress and velocity from the relationship. Past studies (e.g. Haghighi et al., 2013; Mehenni et al., 2016) assumed that the relationship between hydraulic shear stress and erosion is linear, represented by linear trendline, therefore the critical point is estimated from the linear line equation. The problem with this method was it simplified the spread in the data plot as well as the other trend existed in the plot. Due to this simplification, in order to generate the linear relationship, only data that fitted in the linear line that were considered. As seen in Figure 4.40 (red line), there were more than one relationship could be interpreted from the data plot. Nonetheless, it is not possible to accurately determine the critical point using the apparatus used in this study, this assumption was still adopted for this study. In addition, if there were more than a trend observed in the data plot, the values of hydraulic shear stress and velocity obtained at the end of the test were used as the critical point.

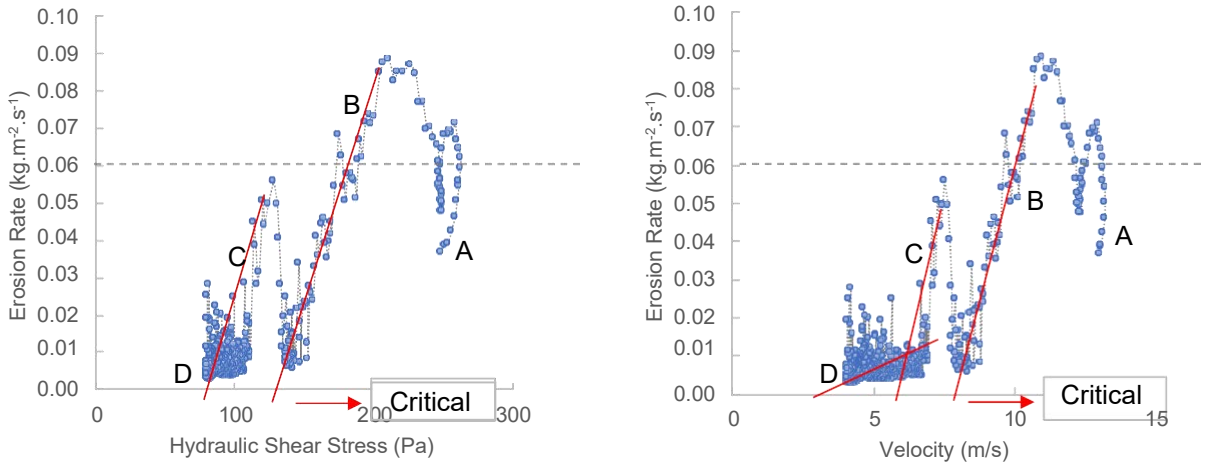


Figure 4.40 The relationship between hydraulic shear stress/velocity and erosion rate (CB without GGBS, 14 Days)

In general, the increase in erosion rate corresponded with the amount of hydraulic shear stress and velocity drop; the bigger the drop per unit time, the higher the erosion rate. The higher hydraulic shear stress and velocity are associated with the higher erosion rate, this indicated that the amount of erosion was higher when the erosion energy was higher. However, the trend was not consistent during the test; the same erosion rate could be yielded by different hydraulic shear stress. As seen in Figure

4.40, the grey dash line shows that for erosion rate of 0.06 kg/m^2/s was associated by different hydraulic shear stress and velocity. This could be attributed to the change of hole characteristics during the test. At the beginning of the test, the hole was smooth and consistent in size. This characteristic changed as the erosion commenced as the turbulent flow caused the hydraulic energy from the eroding fluid to be irregular and random, leading to the irregular or angled eroded hole. The change in hole characteristics caused the change in the response of the hydraulic parameters (pressure and flowrate); the irregularity of the hole surface affected the friction between the sample surface and eroding fluid.

The hole creation method also contributed to the change in response of the hole surface to eroding fluid. The hole created by inserting acrylic rod in the centre and the rod was taken out before the test. When the rod was taken out from the hole, it caused friction between rod and hole surface, thus it inevitably disturbed the sample. Consequently, the initial hole surface was weaker compared to the unaffected part of the sample. Mehenni et al. (2016) also discovered that different method of hole creation method affected the relationship between hydraulic shear stress and erosion rate; the hole created by drilling caused a damage (small cracks) on the surface the hole, this lead to higher erosion rate at lower hydraulic shear stress followed by higher hydraulic shear stress for the corresponding erosion rate (as shown in Figure 4.41)

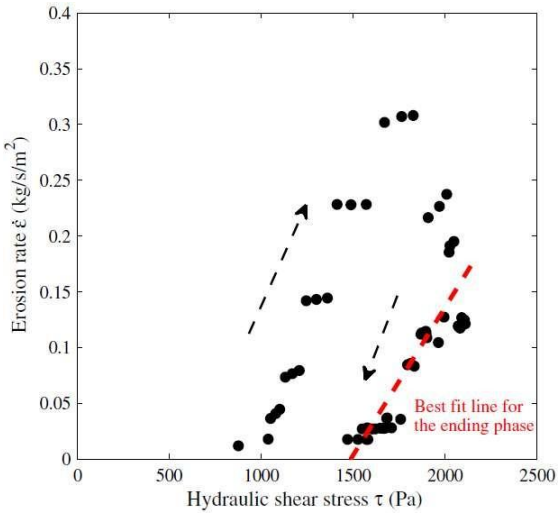
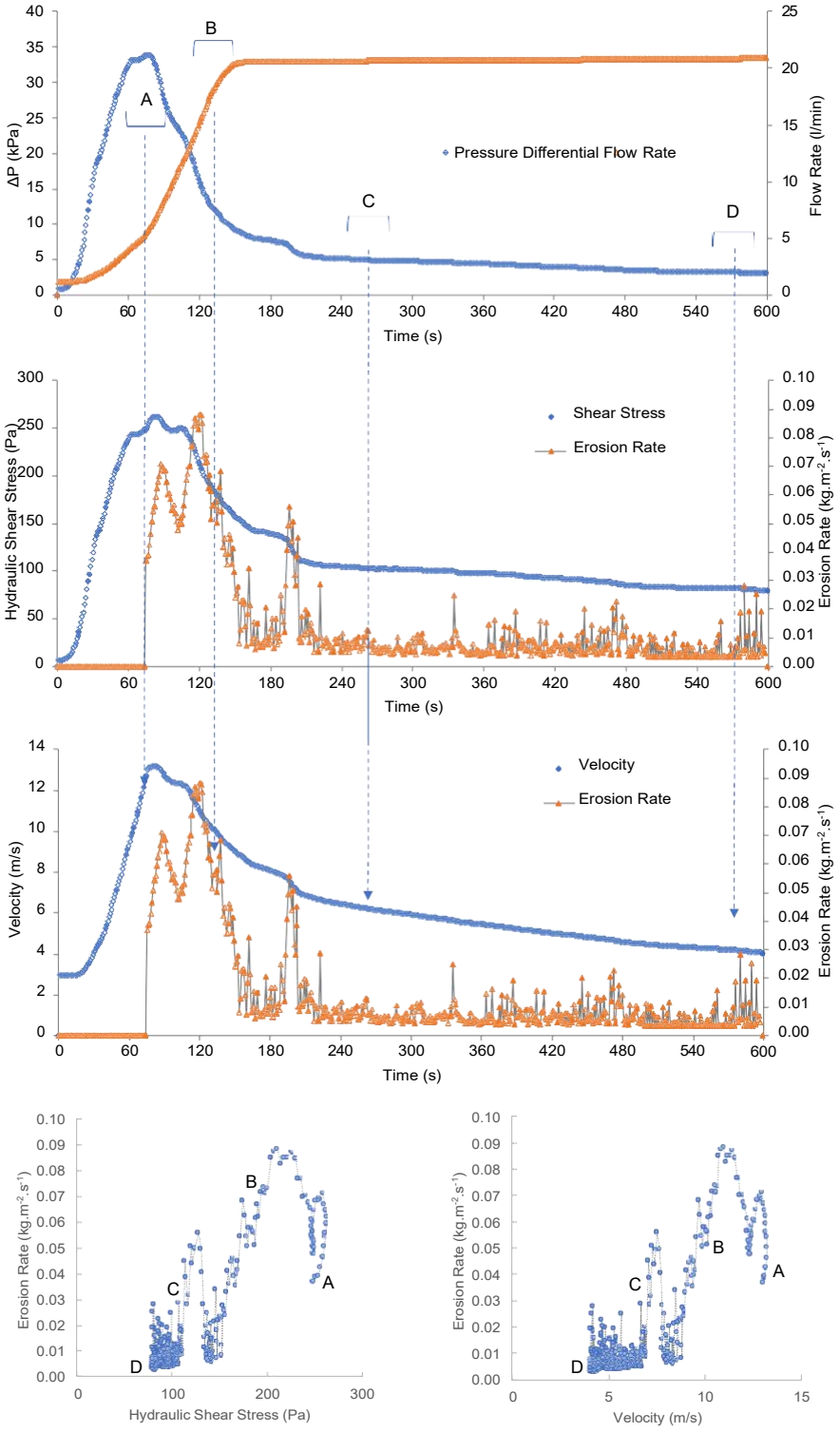
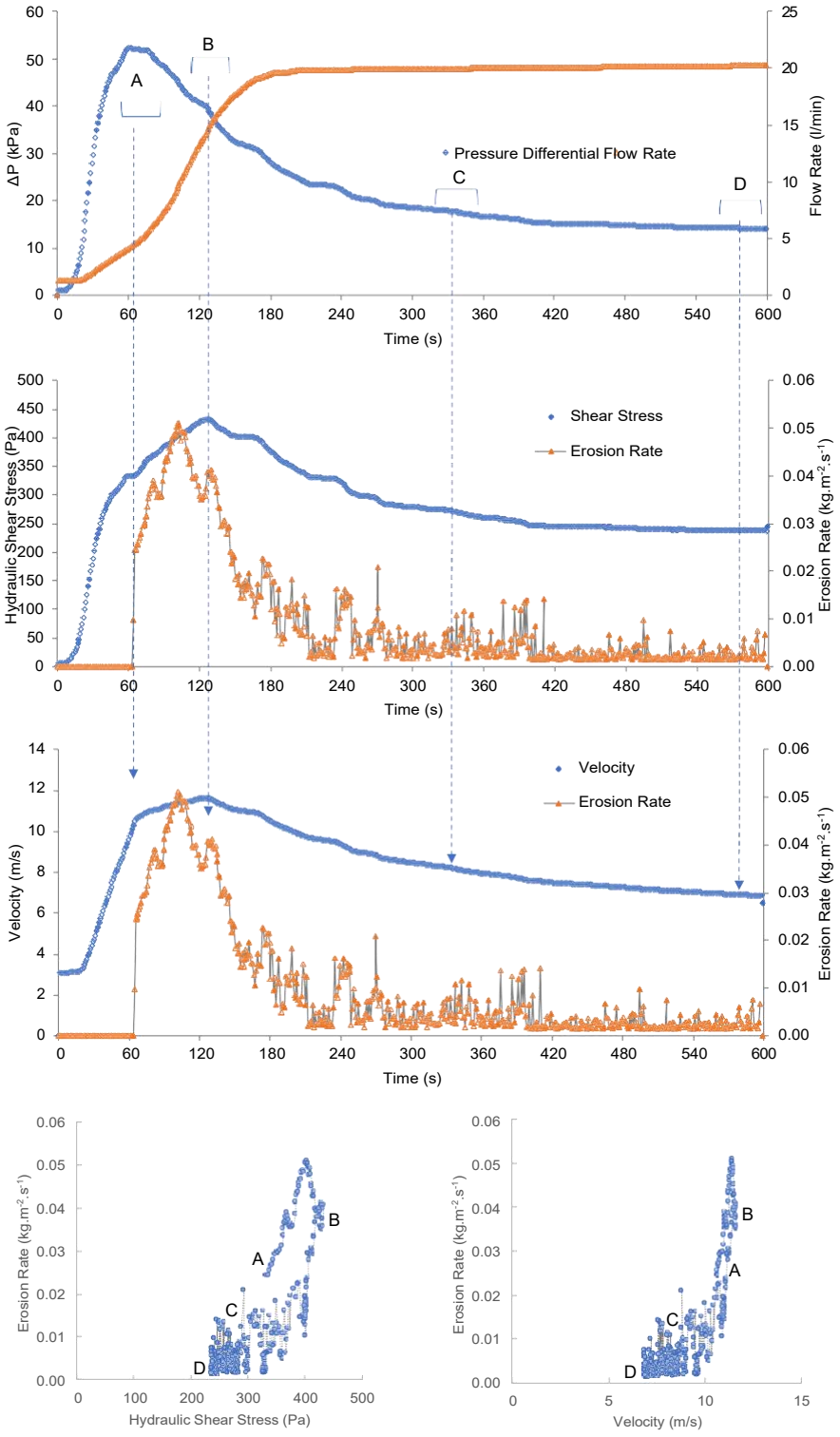


Figure 4.41 The impact of drilling method in the erosion test result (after Mehenni et al., 2016)



A - Peak Differential Pressure
B - Upstream Valve Fully Opened
C - Rate of Differential Pressure, Hydraulic Shear Stress, Velocity, and Erosion Rate Drop Decrease
D - End/Critical Point

Figure 4.42 The erodibility parameters analysis for CB without GGBS, 14 Days



A - Peak Differential Pressure
B - Upstream Valve Fully Opened
C - Rate of Differential Pressure, Hydraulic Shear Stress, Velocity, and Erosion Rate Drop Decrease
D - End/Critical Point

Figure 4.43 The erodibility parameters analysis for CB without GGBS, 28 Days

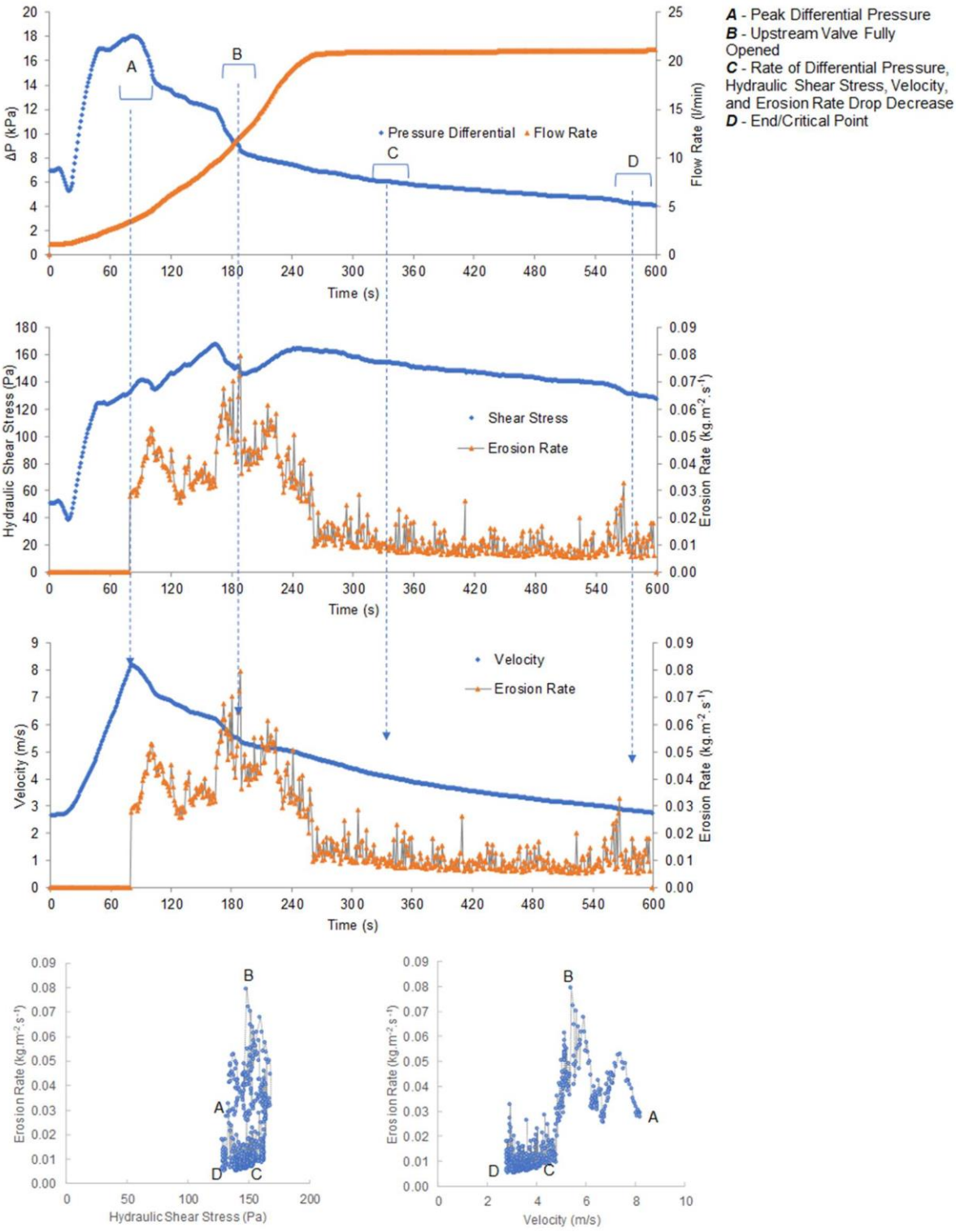
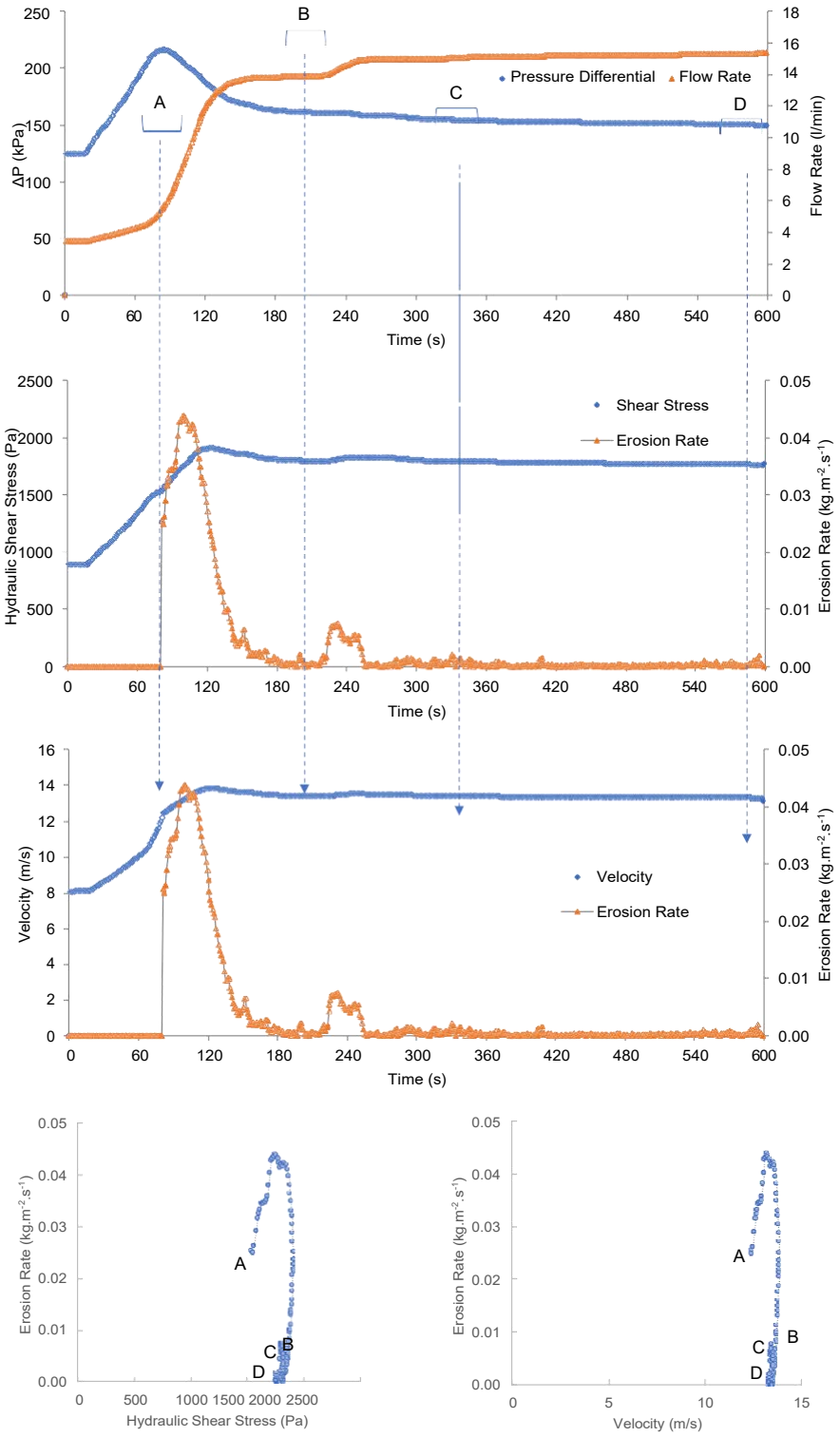
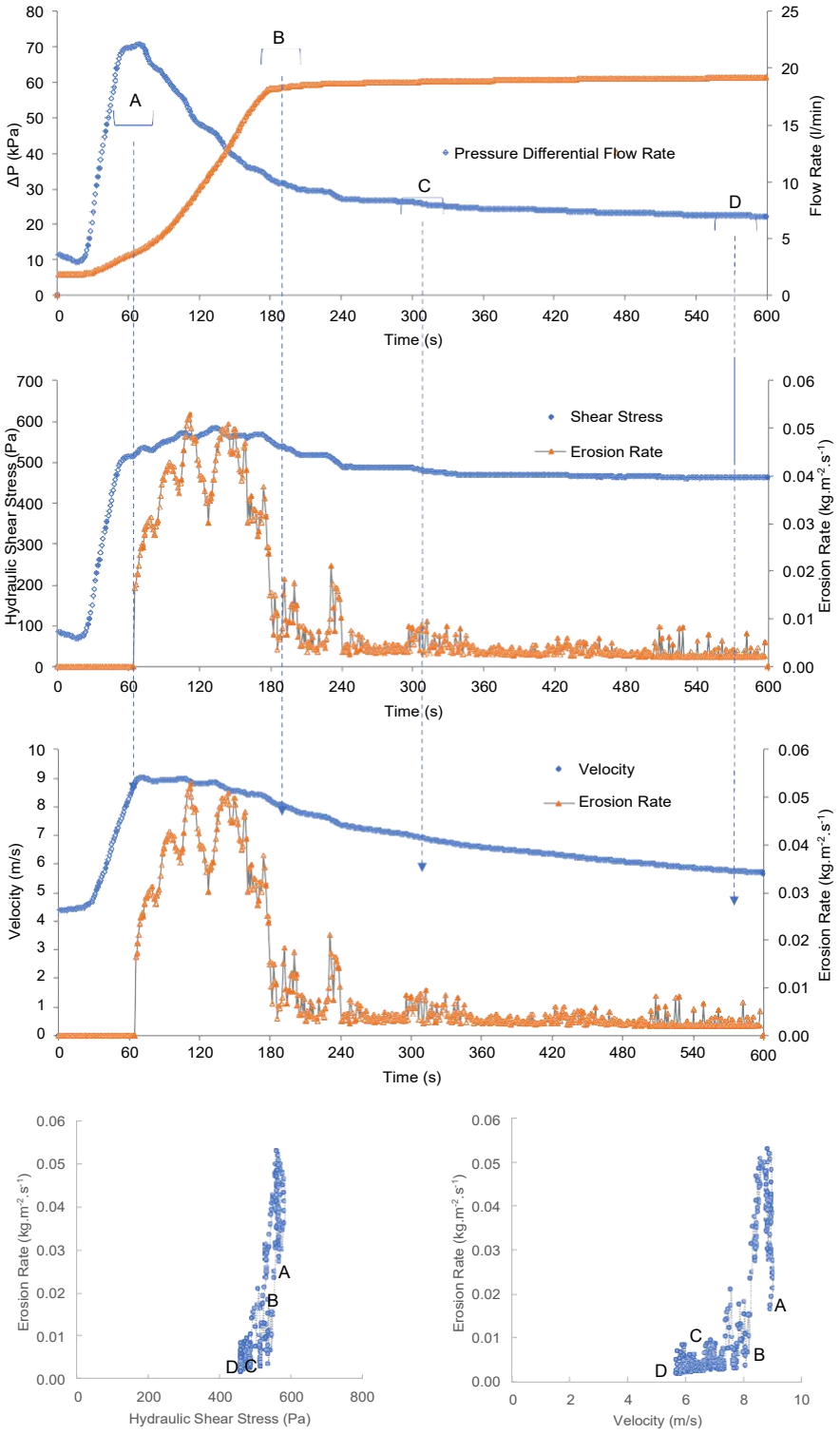


Figure 4.44 The erodibility parameters analysis for CB with GGBS 40%, 7 Days



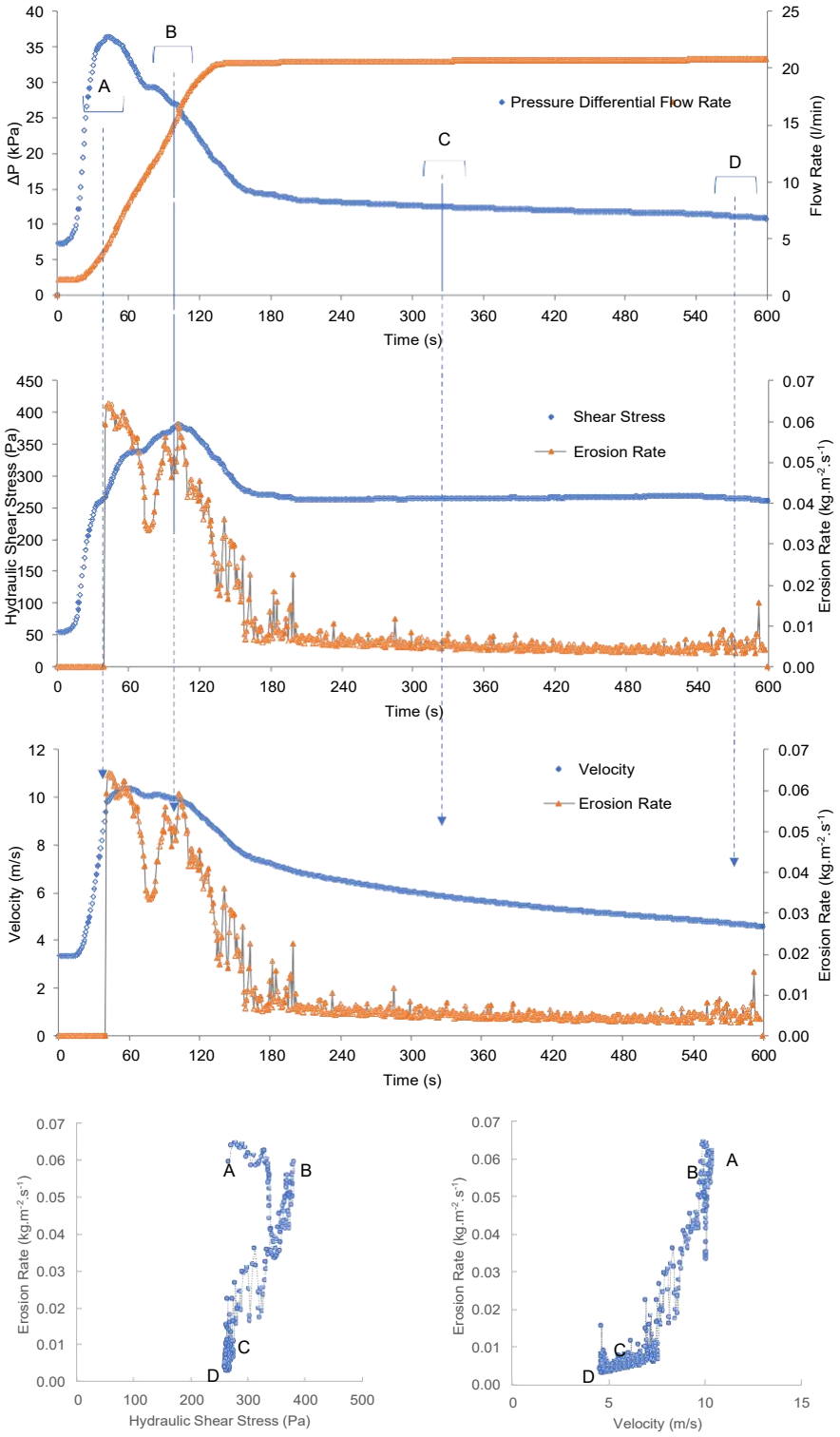
A - Peak Differential Pressure
B - Upstream Valve Fully Opened
C - Rate of Differential Pressure, Hydraulic Shear Stress, Velocity, and Erosion Rate Drop Decrease
D - End/Critical Point

Figure 4.45 The erodibility parameters analysis for CB with GGBS 40%, 56 Days



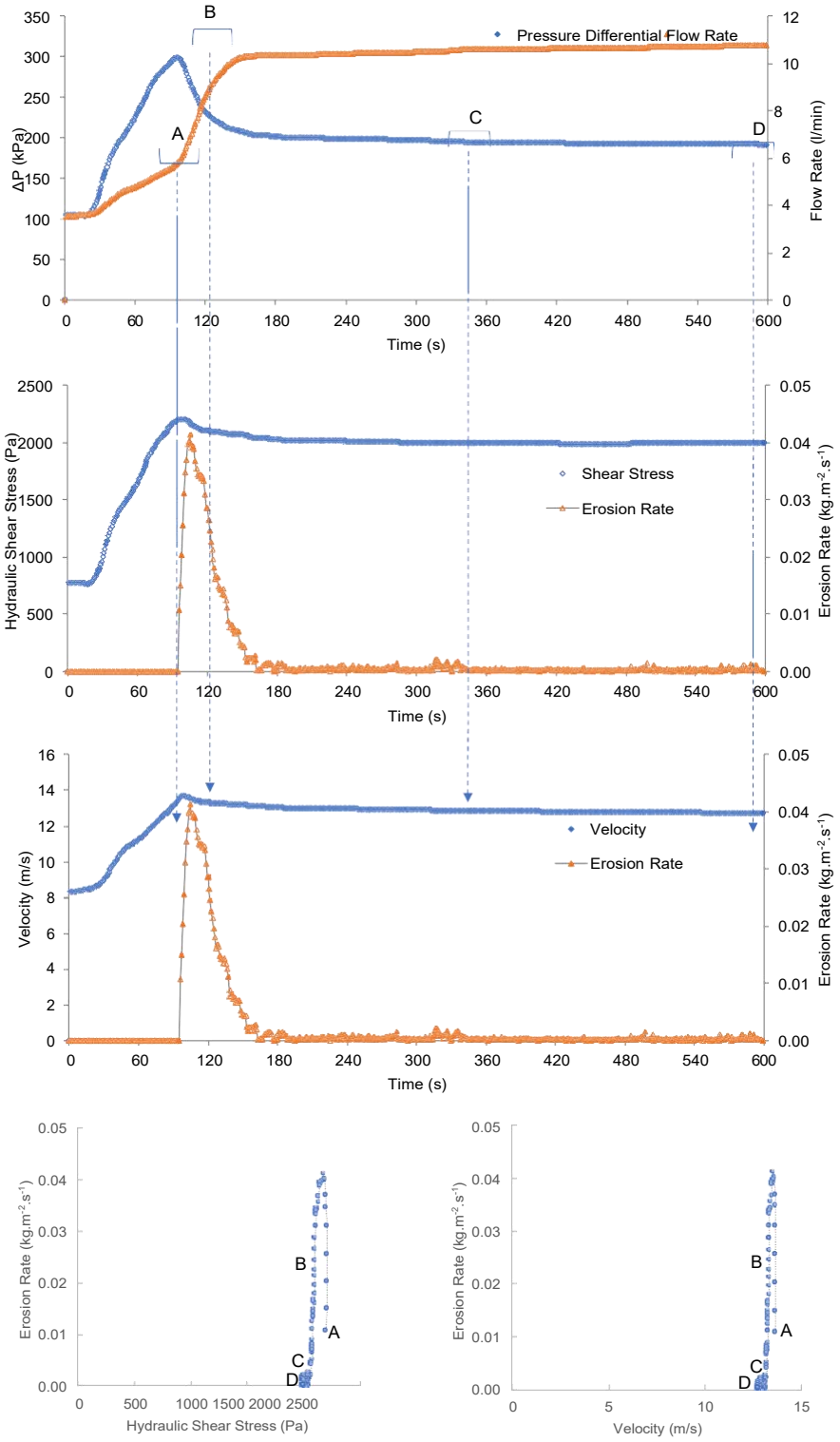
A - Peak Differential Pressure
B - Upstream Valve Fully Opened
C - Rate of Differential Pressure, Hydraulic Shear Stress, Velocity, and Erosion Rate Drop Decrease
D - End/Critical Point

Figure 4.46 The erodibility parameters analysis for CB with GGBS 60%, 14 Days



A - Peak Differential Pressure
B - Upstream Valve Fully Opened
C - Rate of Differential Pressure, Hydraulic Shear Stress, Velocity, and Erosion Rate Drop Decrease
D - End/Critical Point

Figure 4.47 The erodibility parameters analysis for CB with GGBS 80%, 7 Days



A - Peak Differential Pressure
B - Upstream Valve Fully Opened
C - Rate of Differential Pressure, Hydraulic Shear Stress, Velocity, and Erosion Rate Drop Decrease
D - End/Critical Point

Figure 4.48 The erodibility parameters analysis for CB with GGBS 80%, 18 Days

Figure 4.45 and 4.48 show that the range of hydraulic shear stress and velocity values existed during the test was smaller than the associated erosion rate. This trend generally found from the samples containing GGBS; older than 28 days for CB with

40% and 60% whereas older than 14 days for CB with 80%. For Figure 4.48, this trend indicated that for the relatively same hydraulic shear and velocity (2000 Pa and 13 m/s, respectively), this rate of erosion caused could range from 0.001 to 0.04 kg/m^2/s. It was inconclusive whether this trend change in the relationship between hydraulic shear stress/velocity to erosion rate with curing period should attributed to the very small change in diameter or the limitation of the apparatus used. Nonetheless, this phenomenon should be interpreted as if the said hydraulic shear stress or velocity existed in the dam/levee, the associated range of erosion rate should be expected

Figure 4.49 and 4.50 shows the classification of erodibility, proposed by Briaud (2008) based on the results from the analysis of erodibility parameters (hydraulic shear stress, velocity and erosion rate). Only representative results were included in the classification graph for each mix proportion and curing duration. Due the discrepancy of the unit used for erosion rate, the unit was changed from kg/m^2/s to mm/hour. In general, the classification of CB samples tested in this study was ranging from medium to very low erodibility, depending upon the GGBS proportion and curing proportion. For CB without GGBS, the early stage curing (7-14 days) were classified in medium erodibility, the curing stage between 21-28 days were in between the medium and low erodibility, and the latter stage (56-90 days) were all categorised as low erodibility. Incorporating 40% GGBS contributed led to the sample cured for 21-28 days, both to be classified as low erodibility. Increasing the GGBS proportion to 60% contributed the change in classification for 14 days sample from medium to low erodibility, however this was only relevant for hydraulic shear stress. For CB containing 80% GGBS, the classification for 7 days changed from medium erodibility to in between medium to low erodibility. This trend suggested that the increasing GGBS proportion and curing age contributed in the improvement in the erodibility classification (i.e. more resistant to erosion). It was observed that the classification system used by Briaud did not manage to properly classify the old age (28-90 days) CB samples. For example, CB with GGBS 60% sample cured for 28 days, the plotted results classified it as low erodibility for higher erosion rate but also classified it as very low erodibility for lower erosion rate. This inconsistency could be attributed to either the distinct erodibility characteristic of old age CB samples containing GGBS or the fact that the classification by Briaud (2008) were developed from and based on the erodibility characteristic of soil (fine and coarse type).

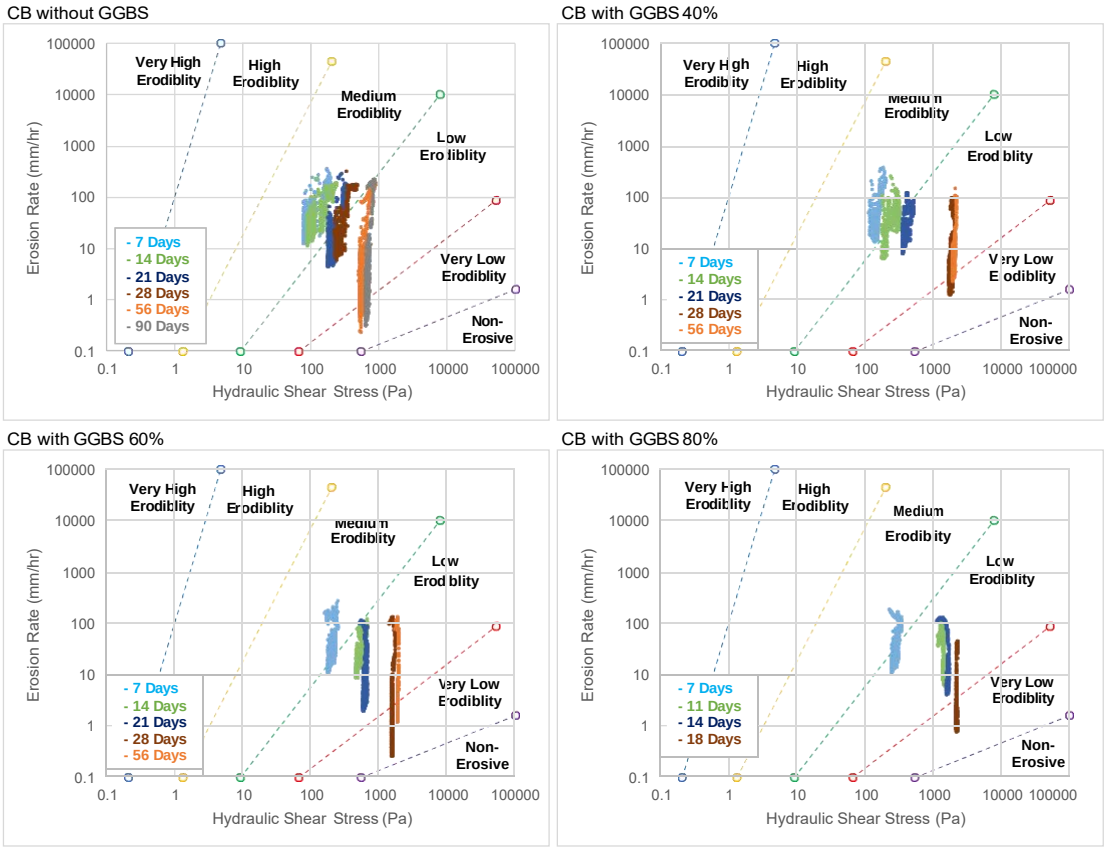


Figure 4.49 The erosion classification based on hydraulic shear stress (Briaud, 2008)

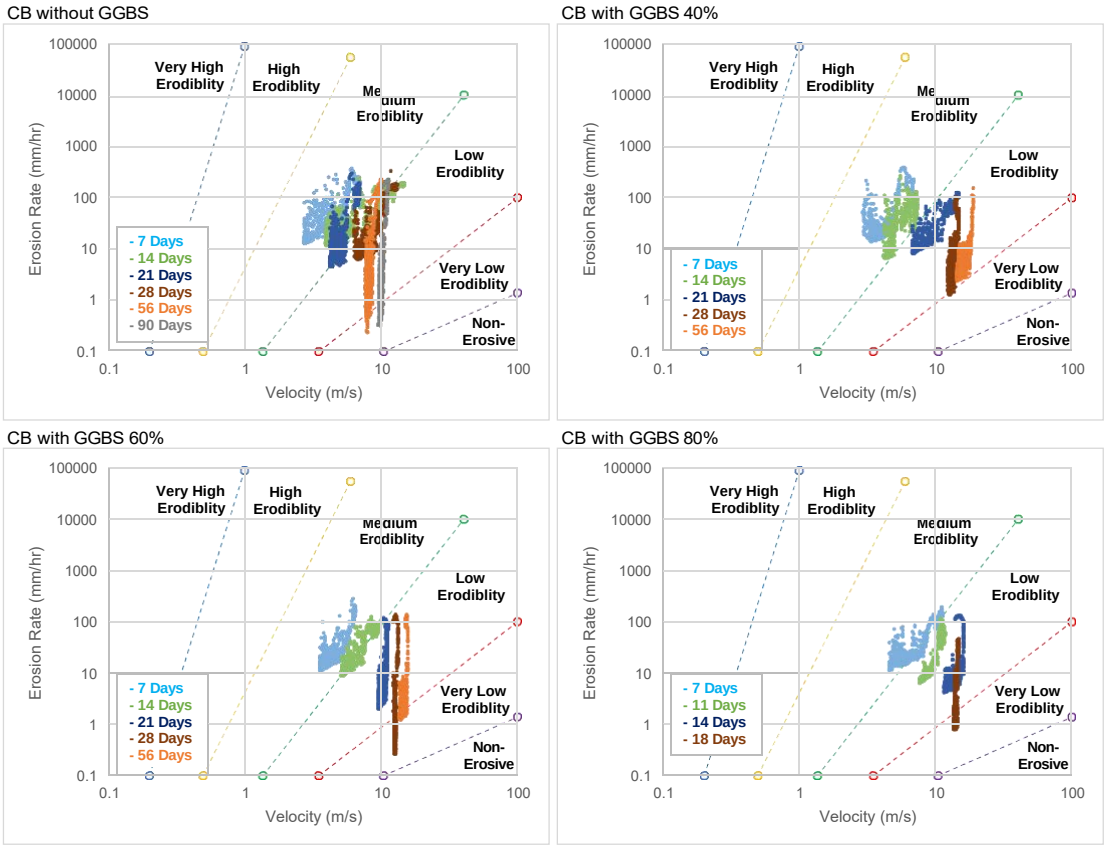


Figure 4.50 The erosion classification based on velocity (Briaud, 2008)

Table 4.4 Critical Hydraulic Shear Stress and Critical Velocity

Material	Age (Day)	Critical Hydraulic Shear Stress (Pa)			Critical Velocity (m/s)		
		Max	Min	Mean	Max	Min	Mean
CB without GGBS	7	56	78	37	2.93	3.18	2.59
	14	86	122	61	3.82	4.13	3.38
	21	176	235	130	4.17	4.31	3.97
	28	218	238	180	6.30	6.86	5.86
	56	462	496	432	8.13	8.99	6.93
	90	611	633	580	9.02	10.36	8.00
CB with GGBS 40%	7	117	155	96	3.03	3.32	2.78
	14	177	213	142	4.09	4.96	3.45
	21	311	364	236	6.64	7.03	6.09
	28	1662	1762	1574	13.28	14.63	11.89
	56	1810	1918	1734	13.70	14.42	13.18
CB with GGBS 60%	7	174	198	161	3.50	3.98	3.23
	14	420	523	265	5.46	6.74	4.39
	21	538	692	467	8.04	9.49	7.37
	28	1477	1614	1331	12.85	15.12	11.52
	56	1871	2145	1697	14.07	15.95	12.41
CB with GGBS 80%	7	248	298	175	4.49	4.68	4.12
	11	1397	1482	1313	12.06	15.67	7.62
	14	1527	1691	1445	12.08	14.87	9.73
	18	2116	2364	1996	14.09	16.17	12.73

Table 4.4 and Figure 4.49 summarise the relationship between critical hydraulic shear stress, velocity, and erosion rate. In general, the increase of critical hydraulic shear stress and velocity were related with the increase of curing duration. The percentage of GGBS added to the mix also influenced both parameters; the higher the GGBS percentage contributed in the higher hydraulic shear stress and velocity. This trend corresponded well with the trend in strength parameters (UCS and tensile strength) improvement with the increase of GGBS proportion and curing duration. The significant increase of critical hydraulic shear stress and velocity was observed during

the curing duration of 21 and 28 days for CB with 40% and 60% GGBS and the rate of increase considerably decreased from 28 to 56 days, whereas such significant increase was encountered from curing duration of 7 days for CB with GGBS 80%.

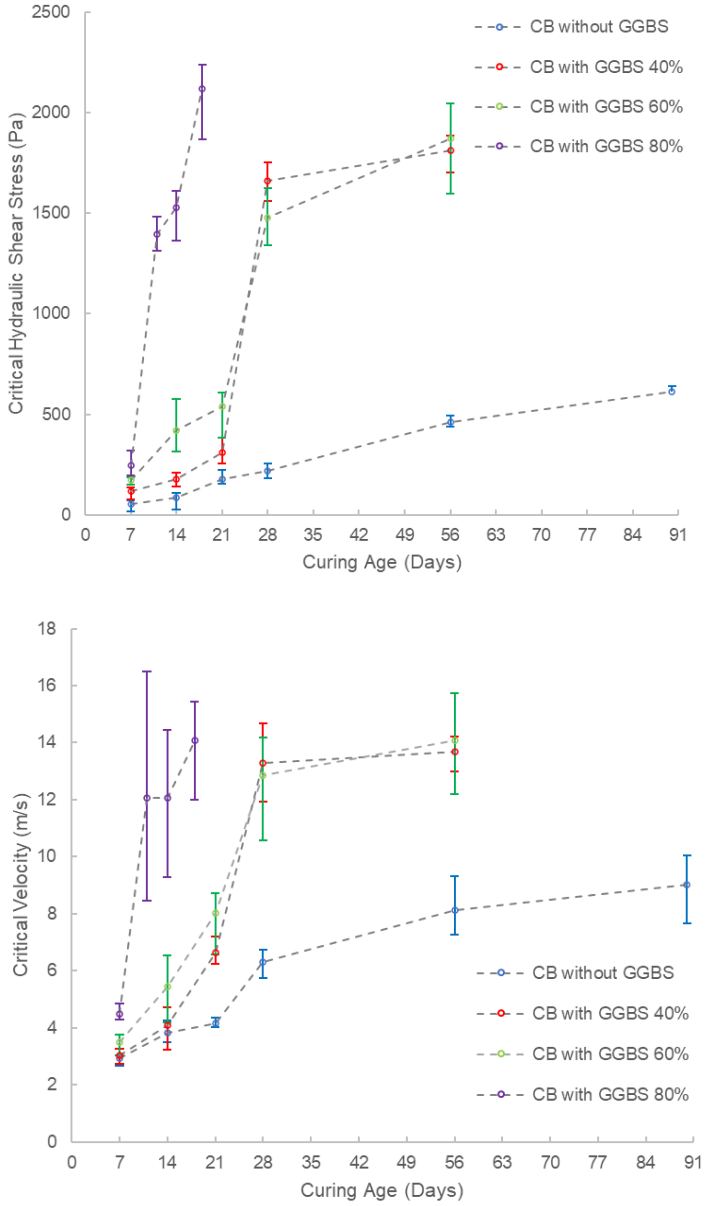


Figure 4.51 The relationship between curing age and critical hydraulic shear stress/velocity (5-6 sample per curing age)

Figure 4.52 shows the relationship between critical hydraulic shear stress and velocity. It was observed that the relationship was well represented by the logarithmic trendline; this suggested that both erodibility parameters were strongly correlated.

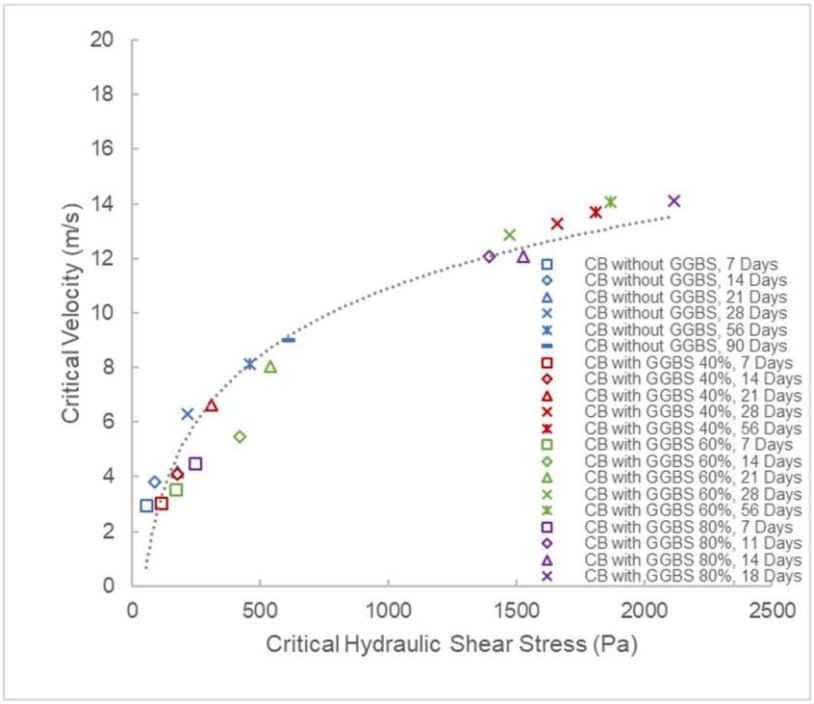


Figure 4.52 The relationship between critical hydraulic shear stress and critical velocity

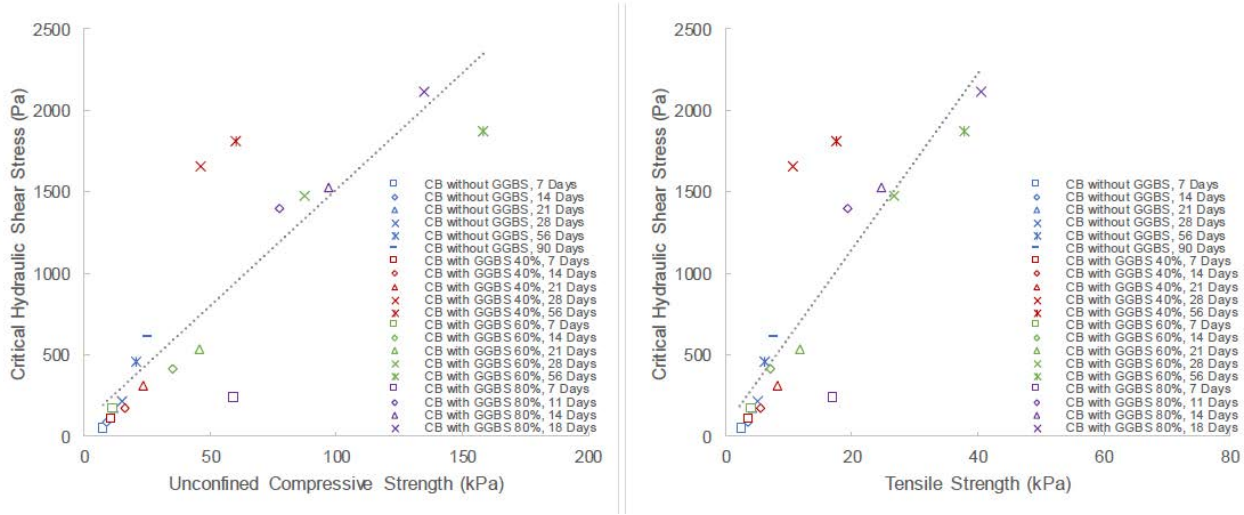


Figure 4.53 The relationship between unconfined compressive strength or tensile strength and critical hydraulic shear stress

Figure 4.53 and 4.54 show the relationship between erodibility parameters and strength parameters. The generated linear trend did not manage to establish a

correlation due to the spread of the plotted data especially those containing GGBS. Neither exponential nor logarithmic trendline could establish strong relationship between erodibility and strength parameters.

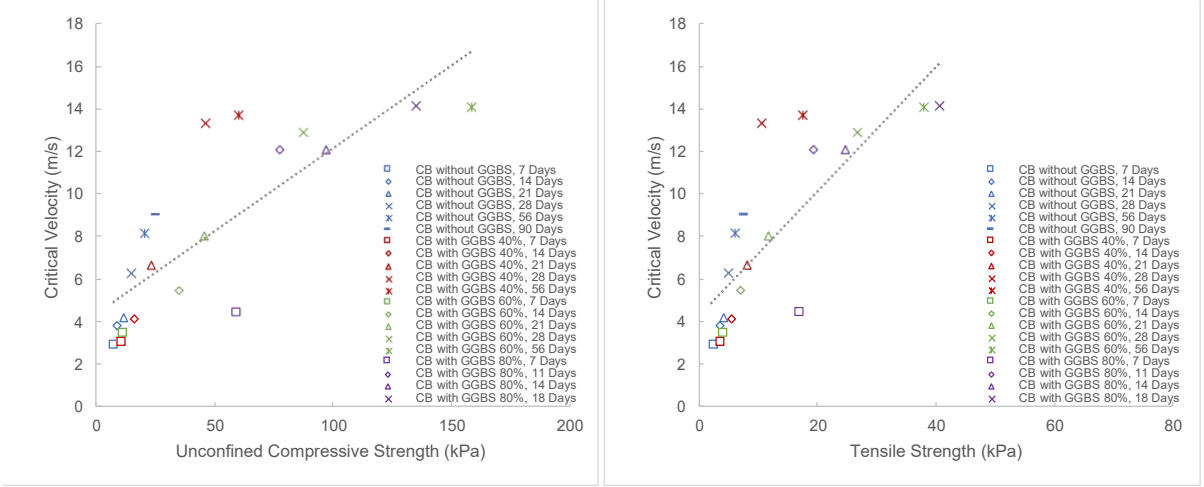


Figure 4.54 The relationship between unconfined compressive strength or tensile strength and critical velocity

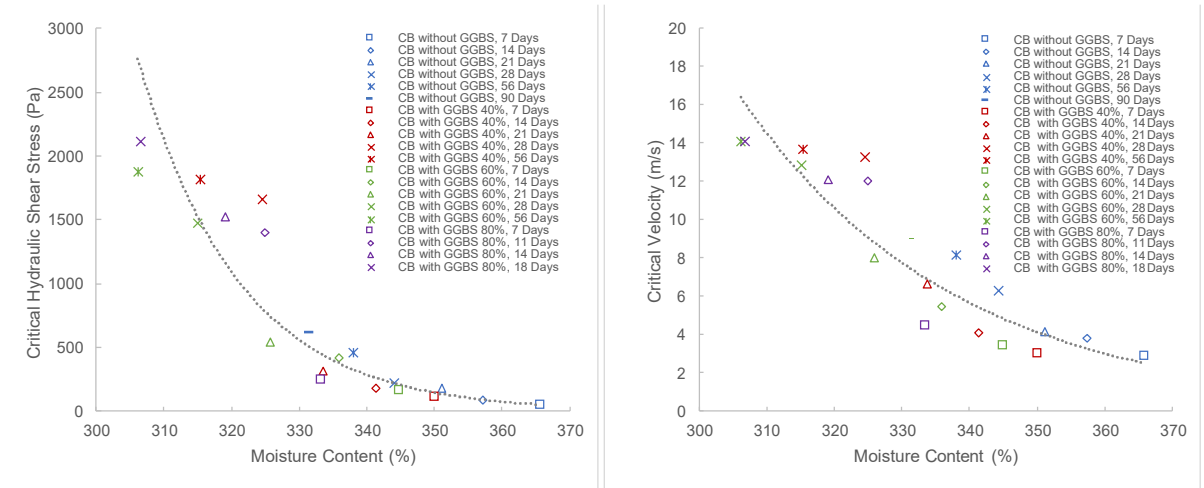


Figure 4.55 The relationship between moisture content and critical hydraulic shear stress or critical velocity

Figure 4.55 shows the relationship between erodibility parameters and moisture content. The relationship was represented by exponential trendline. For the critical hydraulic shear stress-moisture content relationship, the data plot was more spread for older sample or when the value of critical hydraulic shear stress was higher than

1000 Pa. For critical velocity-moisture content relationship, in general the spread was more consistent.

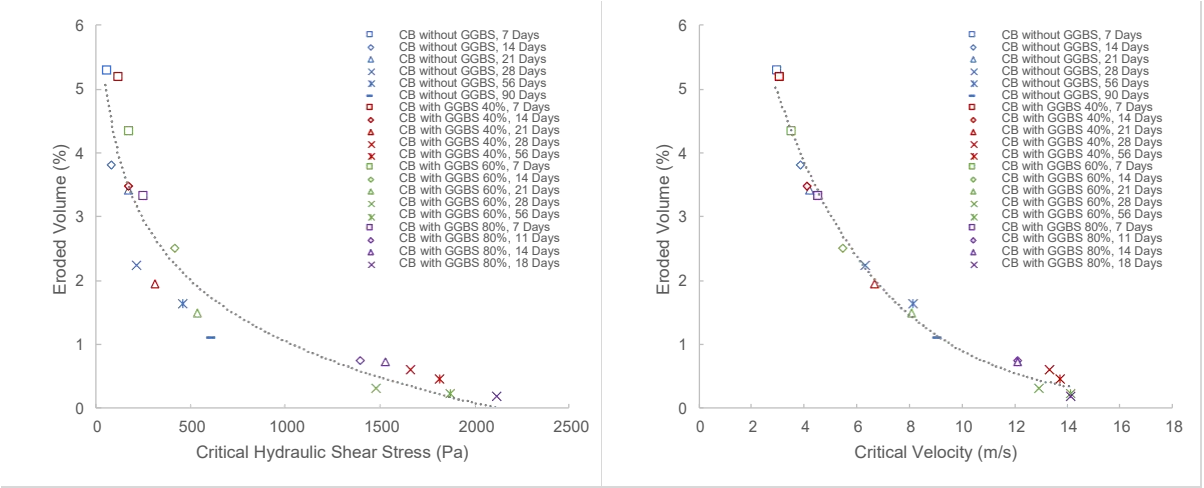


Figure 4.56 The relationship between critical hydraulic shear stress or critical velocity and eroded volume

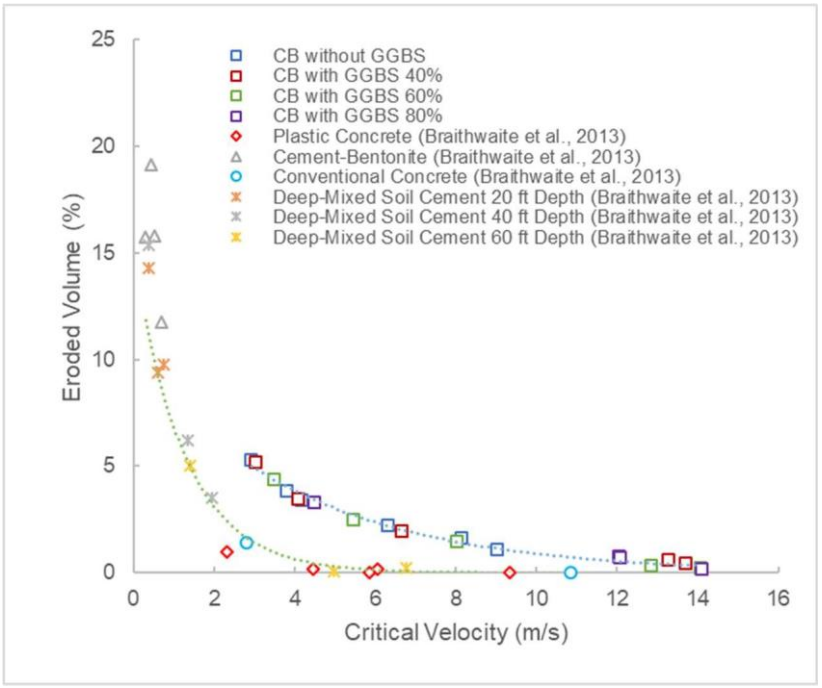


Figure 4.57 The comparison of the current and past studies on the relationship between critical velocity and eroded volume

Figure 4.56 shows the relationship between erodibility parameters and eroded volume. The calculation of eroded volume used average final hole diameter and assumed that the eroded hole was a cylinder; i.e. ignoring the angled-direction and irregular hole

shape. The exponential line well represented the relationship between critical velocity and eroded volume, whereas the critical hydraulic shear stress correlated well with eroded volume despite the spread for several data points. Figure 4.57 compared the result of the past (Braithwaite et al., 2013) and current study. It was observed the results of the current study yielded lower eroded volume for the higher critical velocity compared to the result by Braithwaite et al. (2013). This suggested that CB samples studied in the current study was more erosion resistant. In addition, the test duration for the currently lasted for 600 seconds at maximum while it lasted days (6 to 9 days) for Braithwaite et al. (2013). Wang et al. (2017) argued that the amount of the eroded volume was dependent upon the testing duration, i.e. the longer the duration, the higher the eroded volume. This completely ignored the fact that as the eroded hole enlarges due to erosion phenomenon, it leads to the decrease and increase of differential pressure and flowrate, which affected the hydraulic energy inside the hole. Therefore, the erosion process during the test is dominantly controlled by the hydraulic and erodibility parameters, as discussed in this study, instead of contingent upon the test duration.

4.3.2 Modified Triaxial Erosion Test

The test aimed to run erosion test under the varying confining pressure. The test was only conducted to samples containing GGBS because those without GGBS failed during the preparation stage. Unlike the HET, it was not possible to produce erodibility parameters such as hydraulic shear stresses and velocity due to the inability to back calculate the hole diameter expansion. This was due to the nature of post-test sample condition as the samples were damaged due to fracture and the presence of cracks prevented the hole to be casted by paraffin wax. The reading from flowmeter was disturbed for several major reasons: the fracture caused the massive enlargement of hole, the cracks caused the confining pressure and eroding fluid to be hydraulically connected, and the eroded material clogged the erosion channel. It should be noticed that the main feature of failure observed during the test was the fracture or formation of crack in the sample. Therefore, the result presented considered the peak and final differential pressure observed during and at end of the test. The selected results of the test are presented in Figure 4.58 and 4.59; complete result can be accessed from Appendix G. The data plotted the P1, P2, and ΔP which represented upstream pressure, downstream pressure and pressure differential (P1 – P2) against testing

duration. The result with confining pressure of 200 kPa was not presented as the sample destroyed after the application of the pressure to the sample (except for CB GGBS 40% as the delayed erosion was observe), therefore it failed before the erosion force got into the apparatus system.

Figure 4.60 and 4.61 show the relationship between confining pressure and peak/final differential pressure for each GGBS proportion and curing duration. The trend observed from the results suggested that the increase of confining pressure led to the increase of both peak and final differential pressure. The increase in GGBS proportion and curing age also contributed to the improvement of the peak and final differential pressure. This suggested that the increase confining pressure resulted in the higher erosive force threshold required to erode the sample, however this could also be interpreted as the threshold required to fracture the sample as the first mode of failure observed during the test was the crack/fracture formation then followed by the erosion. In addition, the varying mix proportion and curing age influenced how the material performed during the test.

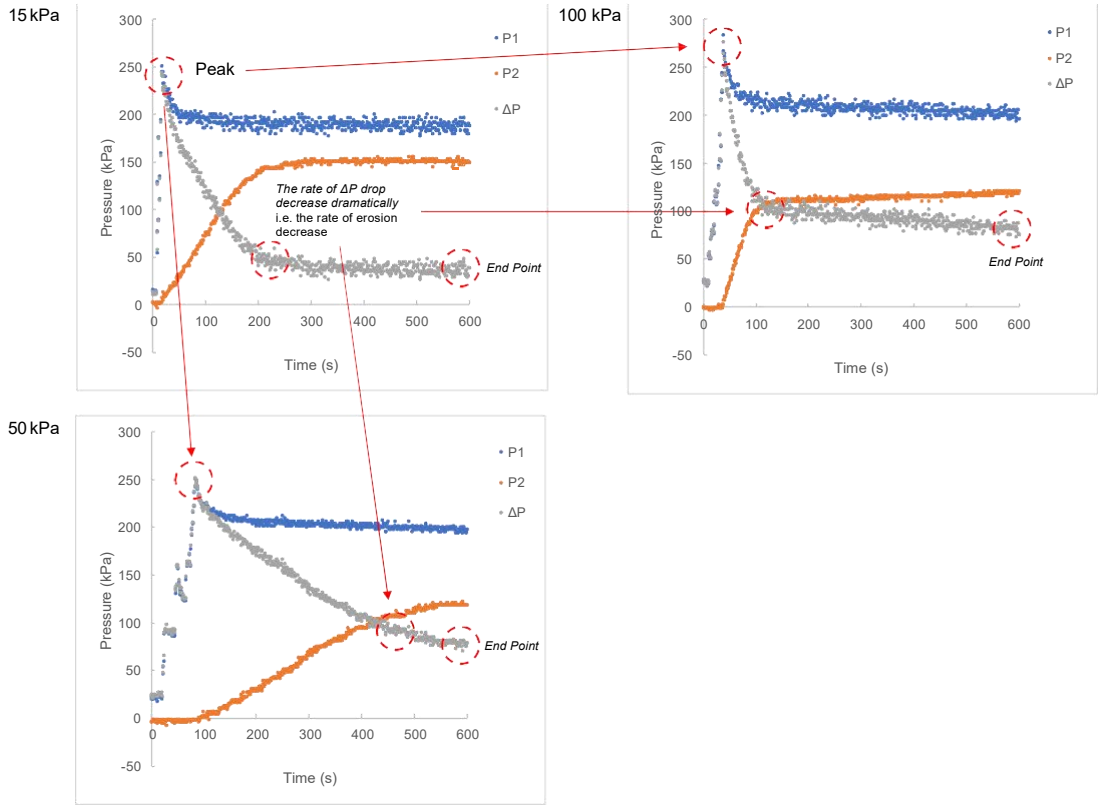


Figure 4.58 The modified triaxial erosion test result for CB with GGBS 40%, 21 Days

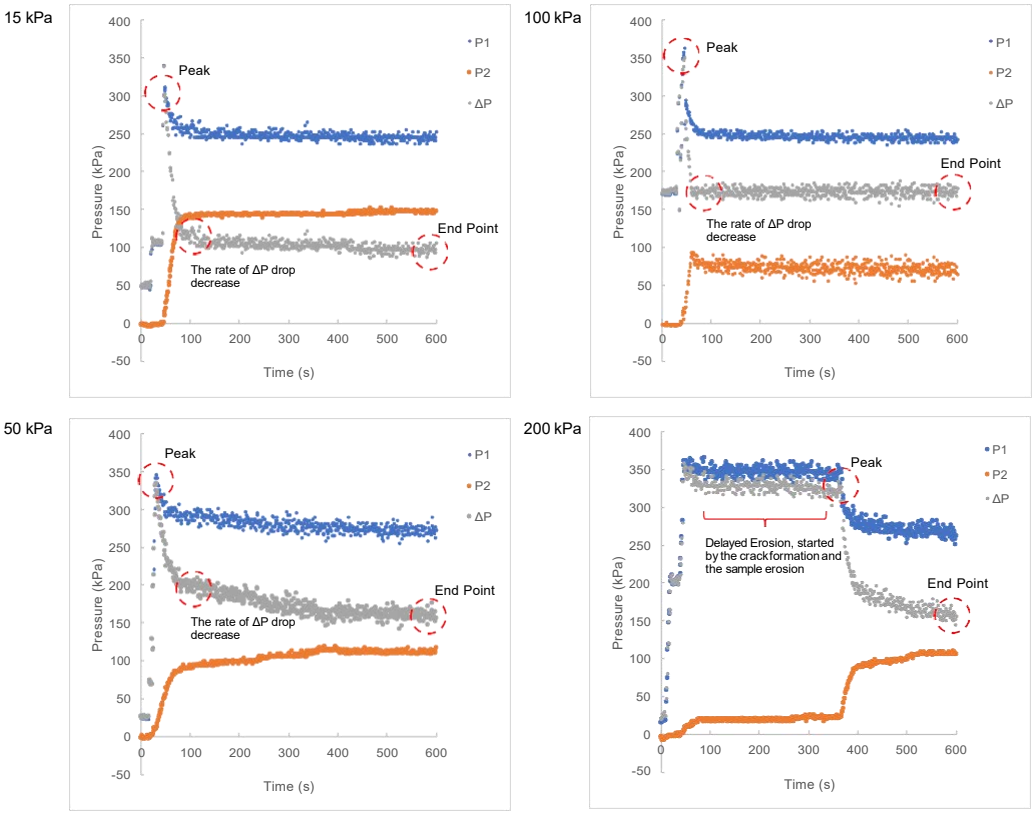


Figure 4.59 The modified triaxial erosion test result for CB with GGBS 40%, 56 Days

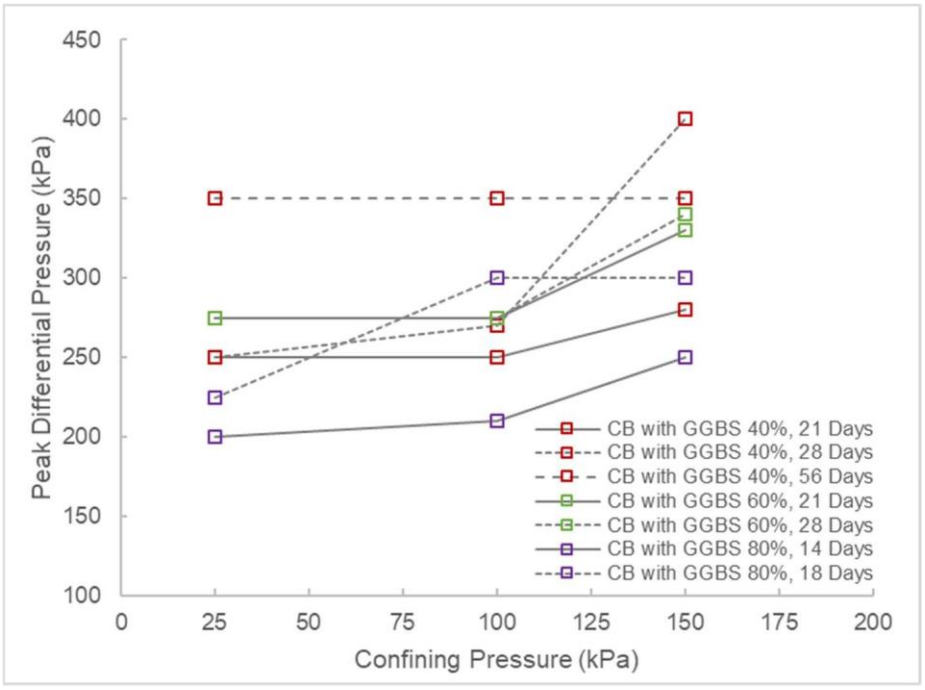


Figure 4.60 The impact of applied confining pressure in the peak differential pressure

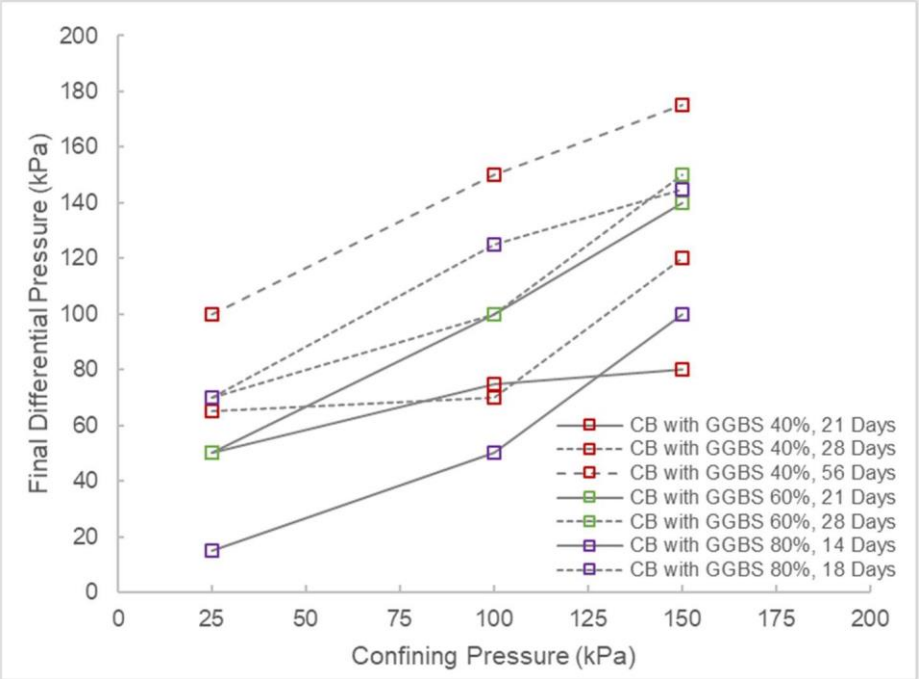


Figure 4.61 The impact of applied confining pressure in the final differential pressure

Figure 4.62 demonstrated the typical fracture/failure mode suffered from the sample after the test. It was visible that the fracture or crack dominantly featured at the upstream side of the sample. As the pressure projected from the pump was started from upstream therefore the pressure at that location was always higher compared to the downstream. The pressure loss was experienced when the eroding fluid travelled through the hole. This phenomenon suggested the failure mode due to the combination of pressure from eroding fluid and confining pressure was buckling failure. Although the erosion usually took place subsequently, the degree of buckling failure determined whether the erosion would commence or not. As discussed previously, when the failure occurred, there was a possibility of the damaged material to clog or disrupt the flow of the eroding fluid inside the hole. The flow disruption could lead to localised pressure build up. When the pressure concentrated, the further fracture could form and provided a channel for eroding fluid to flow which eventually led to the erosion phenomenon. The degree of initial buckling failure heavily influenced the sequence of the failure mechanism.

From the test, it suggested that under complex stress, the erodibility behaviour of CB samples changes in accordance to the change in confining pressure and eroding fluid pressure. Nonetheless, due to the limitation of the apparatus, it was not possible to

run the test under the condition that the samples are not damaged during the test further studies should be conducted to allow the possibility of the sample to not crack/fracture during the test in order to investigate how the confining pressure affect the erosion resistance of the sample.



Figure 4.62 The typical after test sample condition

4.4 Scanning Electron Microscopy Test

The results from Cryo-SEM were obtained from the microscope observation available from School of Metallurgy laboratory. In general, the change in microstructure of CB samples was observed with the change in GGBS replacement and curing age. Compared to the CB without GGBS, the samples containing GGBS are composed of finer fibre-like structures. The longer the curing, the more inter-connected the section in the structure. For this observation to be possible, the CB samples should be fracture beforehand which this could lead to underestimation of the connectivity of the structure and the observation of the CSH fibre. The selected result of the observation is presented in Figure 4.63-4.66 (samples cured for 56 days). The other results can be accessed from Appendix H.

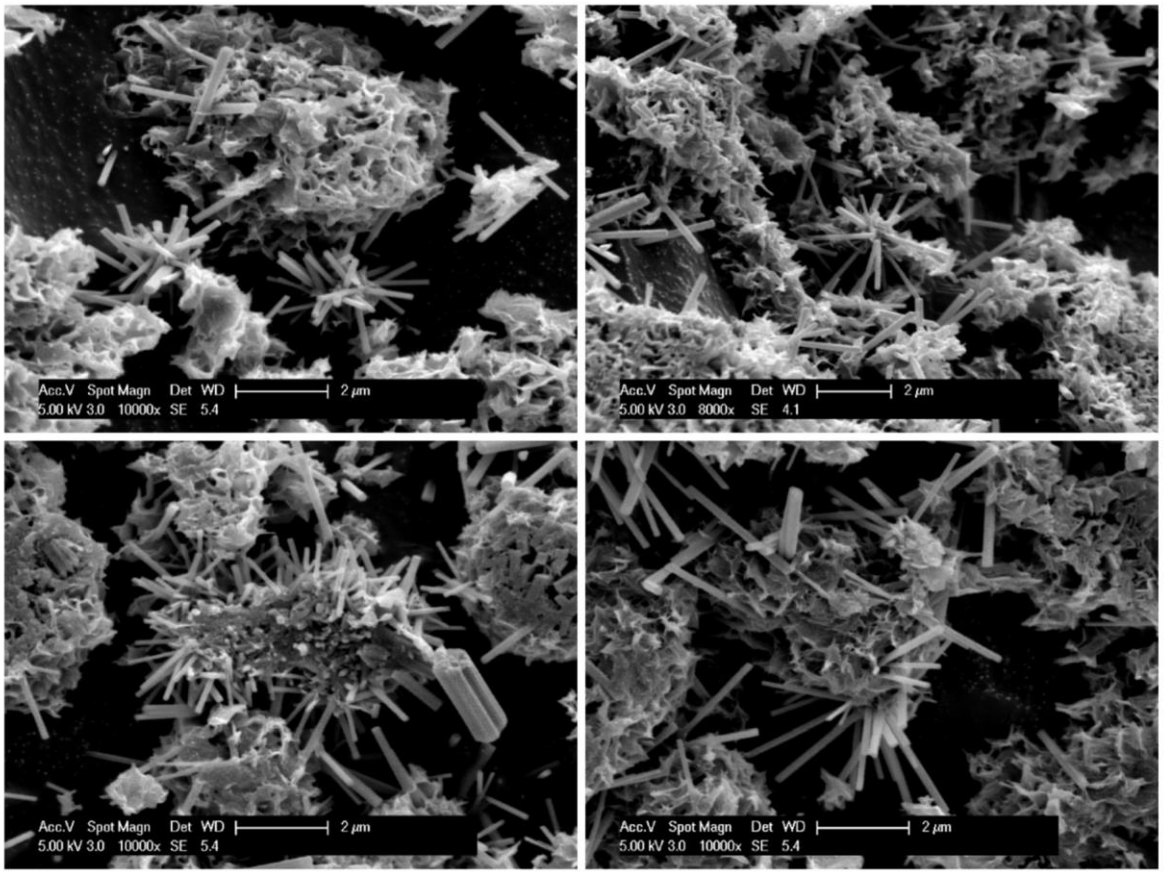


Figure 4.63 CB without GGBS, 56 Days

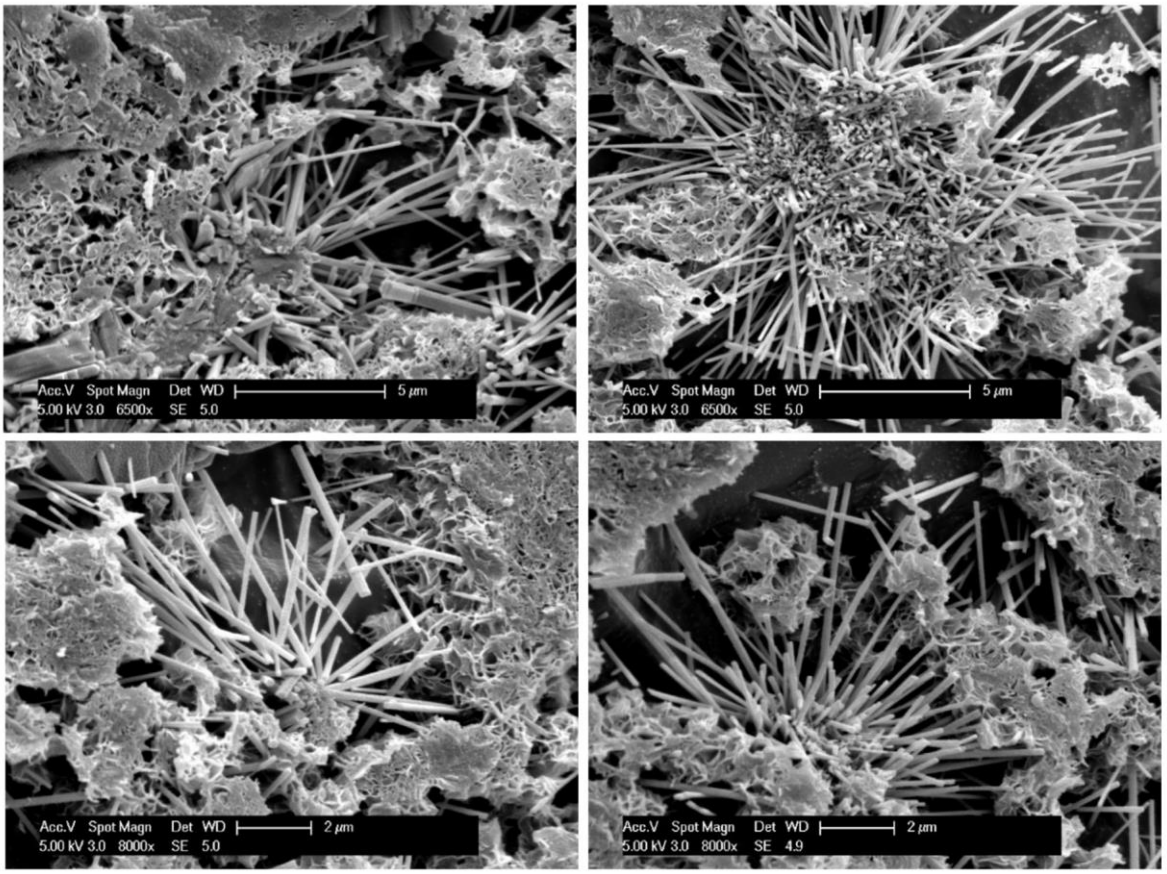


Figure 4.64 CB with GGBS 40%, 56 Days

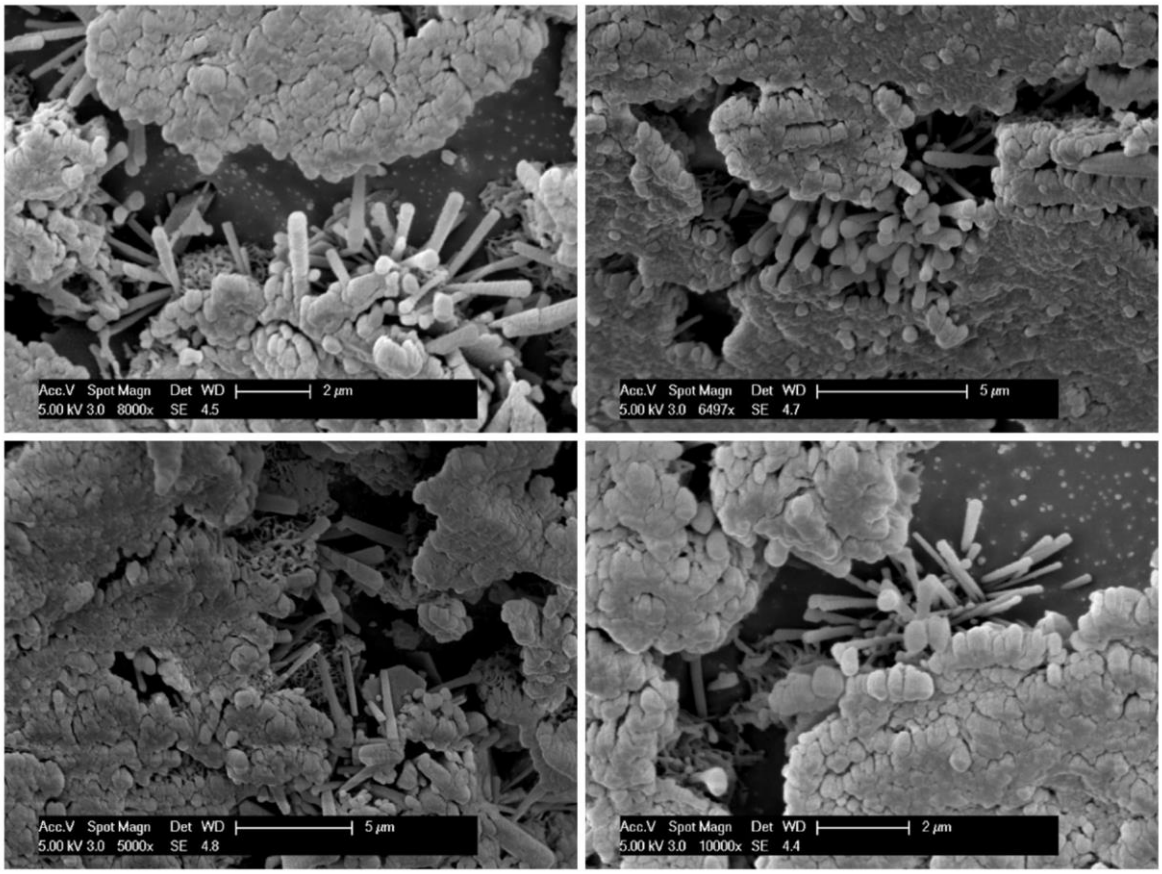


Figure 4.65 CB with GGBS 60%, 56 Days

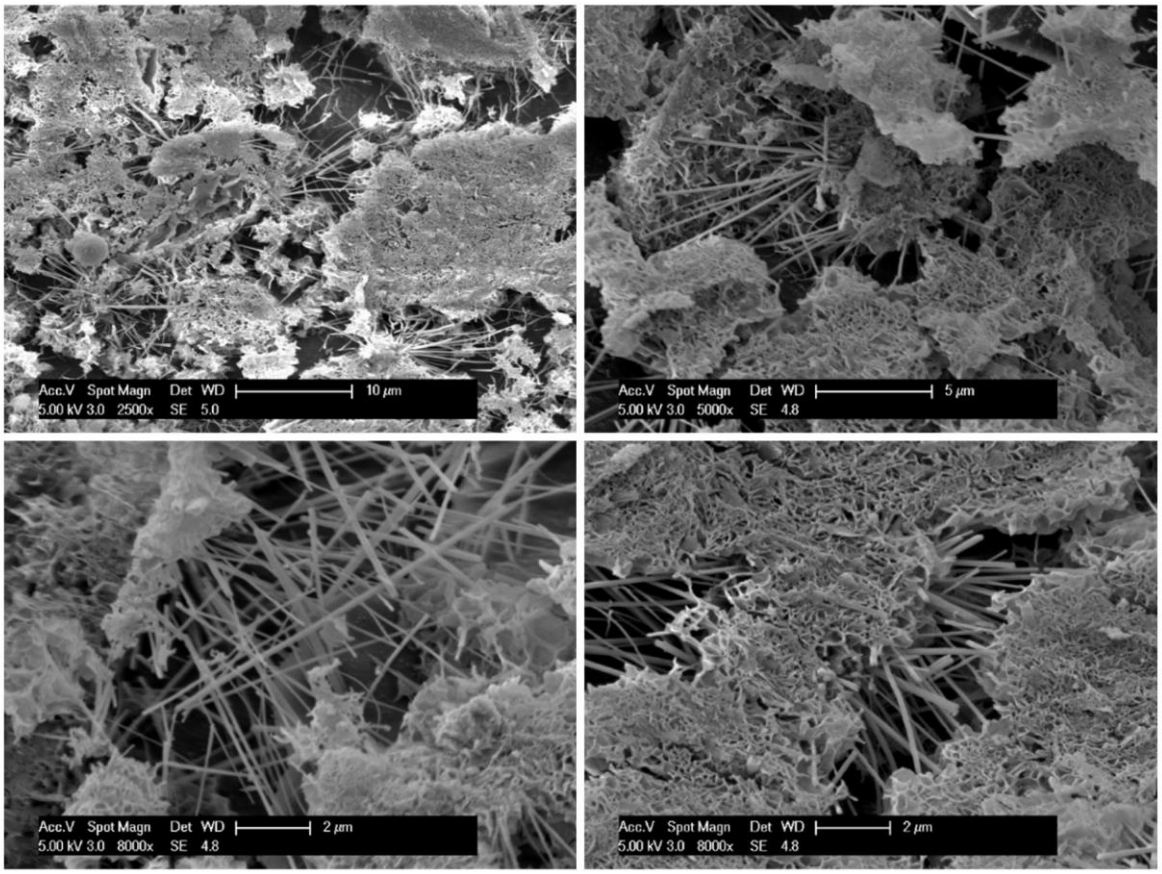


Figure 4.66 CB with GGBS 80%, 56 Days

Chapter 5
Summary

5.1 Conclusion and Future Work

Understanding the cause of the dam and embankment failure is critically important as it helps in identifying the necessary design and construction steps that should be considered as well as anticipating the possible source of failure. The failure of embankment and dams is still mainly dominated by piping erosion with considerably high percentage, 31% and 48 % (ICOLD, 1995; Foster et al., 2000). The cement-bentonite barrier is a potential solution to this problem as the barrier can be installed into an existing earth dam, that is considered vulnerable to internal erosion, and it will cure to form a cut-off wall that will renovate the low hydraulic core of the barrier and thus reduce the risk of dam failure via internal erosion. For the CBB to be used in such an application (or for environmental protection purposes when attempting to control contamination plumes), then it is important that these walls are resistant to internal erosion.

Laboratory based investigation using one of several techniques has proven a relatively simple way of assessing of the internal erosion resistance of various soils, including CB. However, insufficient research has been dedicated to furthering the understanding of how this material (CB) withstand the internal erosion. Therefore, it is important to investigate the erodibility of CB especially focusing on the hydraulic shear stress that is required to initiate erosion and the rate of erosion after the erosion commence. Further understanding on the behaviour of CB older than 28-days is also important in order to assess the resistance of CB against erosion over the time.

The behaviour of CB materials has been investigated and analysed in this thesis using laboratory experiments. The key aspects of CB behaviour studied is the following:

1. Basic properties
2. Strength
3. Erodibility
4. Microstructure

Material strength and basic properties test comprised of unconfined compressive strength, tensile strength, hydraulic fracturing, moisture content and specific gravity.

The erosion test was divided into two: hole erosion test and modified triaxial erosion test. The cryo-SEM test was performed to investigate the CB microstructure. Technical procedure and its limitation were discussed and justified. The data analysis mainly focused on the data obtained from the sensors/data loggers and they were used for the further analysis to understand the erodibility of CB samples.

The test conducted to CB samples with varying GGBS replacement and curing time. The strength of all samples improved over the time. The longer the samples cured, the higher the UCS and tensile strength of the samples. The UCS and tensile strength obtained from the samples with hole in the centre are lower than those without hole which suggest that the simulated crack/hole on samples affected the strength of the samples. In general, the result suggests that moisture content of the samples was highly linked to both curing age and mix proportion. The lower moisture content was obtained from sample with longer curing and higher GGBS percentage, and vice versa for higher moisture content.

In case of hydraulic fracturing, the increase of curing age and confining pressure contributed to the increase of internal pressure required for the fracture to occur in the samples. The samples containing higher GGBS replacement required higher internal pressure to trigger the failure. To better understand the role of test and condition and confining pressure, it is therefore suggested that further study using improved test apparatus should be conducted to investigate the CB material susceptibility to hydraulic under both test conditions for young samples and higher confining pressure ranges.

For erosion test, both peak and final differential pressure as well as final flow rate were highly dependent on the curing age and the mix proportion. The technical difficulties were encountered pertaining to simulating the erosion hole akin to the crack found in the field. This suggested that the possibility to non-invasive measurement method in measuring the diameter of eroded hole should be explored. Despite the limitations, the result provided an overview on the range of data noise should be expected from the apparatus and the relationship of hydraulic parameters.

The effect of the high-pressure application at the upstream caused the sample to be partially damaged for juvenile samples. As soon as the sequence of entrance damage ceased, the test was halted. Due to the damage caused, it was not possible to properly quantify the extent of the erosion and the test was considered not completed. Nonetheless, this phenomenon suggested that under the high-pressure difference, instead of causing erosion, it led to fracturing and followed by the flushing of the destroyed sample by the eroding fluid.

The longer the curing and the higher the GGBS percentage, the final differential pressure was higher and vice versa, while the final flow rate was lower and vice versa. Both critical hydraulic shear stress and velocity increased with the longer curing and increasing GGBS proportion. The samples without GGBS did not exceed the critical hydraulic shear stress and velocity higher than 1000 Pa and 10 m/s respectively although cured for 90 days. The samples containing GGBS exceeded both values after cured longer than 21 days for 40% and 60% GGBS replacement, while it only took 11 days for 80% replacement. For all samples containing GGBS, the critical hydraulic shear stress and velocity were within the range 1500-2000 Pa and 12-15 m/s after cured longer than 21 days and earlier for 80% replacement.

For test using modified triaxial erosion apparatus, the trend observed from the results suggested that the increase of confining pressure led to the increase of both peak and final differential pressure the increase in GGBS proportion and curing age also contributed to the improvement of the peak and final differential pressure. This suggested that the increase confining pressure resulted in the higher erosive force threshold required to erode the sample.

For cryo-SEM test, the change in microstructure of CB samples was observed with the change in GGBS replacement and curing age. Compared to the CB without GGBS, the samples containing GGBS are composed of finer fibre-like structures. The longer the curing, the more inter-connected the section in the structure.

References

Alzayani, N.J., Royal, A., Ghataora, G. and Jefferson, I. (2017) Cement-Bentonite in comparison with other Cemented Materials. Environmental Geotechnics. DOI: 10.1680/jenge.14.00050

ASTM D4647 / D4647M-13 (2013) Standard Test Methods for Identification and Classification of Dispersive Clay Soils by the Pinhole Test. ASTM International, West Conshohocken, PA

Batog, A., Hawrysz, M., Strózyk, J. (2007) Estimation of susceptibility to colloidal erosion of cohesive soils using the pinhole test. Geologos 11, pp. 421–427

Beier, H., and Strobl, T. (1985) Resistance against Internal Erosion of Various Types of Cutoff Walls in Dam Construction. Proceedings of 15th ICOLD Congress, Lausanne, Q. 58, R. 22, Vol. 3, pp. 417-428

Benahmed, N. and Bonelli, S. (2012) Investigating concentrated leak erosion behaviour of cohesive soils by performing Hole Erosion Tests. European Journal of Environmental and Civil Engineering, Vol, 16, No. 1, pp. 43-58

Bennabi, A., Karoui, T., Benamar, A., and Wang, H.Q. (2012) Some elements of comparison between two laboratory devices for soil erosion testing. Proceedings of 6th International Conference on Scour and Erosion Paris, pp. 1089-1096

BGS (2019) Ground source heat pumps. British Geological Survey. Accessed at https://www.bgs.ac.uk/reference/gshp/gshp_report.html#:~:text=Below%20this%20the%20ground%20temperature,about%207%20%2D%2015%C2%B0C.

Bonelli, S., and Benahmed, N. (2011) Piping flow erosion in water retaining structures. International Journal on Hydropower and Dams, 18(3), pp. 94-98

Boor, B., Kunstatsky, J., and Patocka, C. (1968) Hydraulics of water structures.SNTL Prague

Botschek, J., Krause, S., Abel, T., Skowronek, A., (2002) Piping and erodibility of loessicsoils in Bergischer Land, Nordrhein-Westfalen. Journal of Plant Nutrient Soil Science 165, pp. 241–246

Braithwaite, N., Rice, J., and Paul, D. (2013) Erodability of Seepage Barrier Materials. Proceedings of 33rd Annual U.S. Society on Dams Conference, pp. 345-356

Brandl, H. (1996) Slurry barrier walls for waste containment and contaminated land. Proceedings of 2nd International Congress on Environmental Geotechnics, Osaka, Vol. 1, pp. 459-466.

Briaud, J.L. (2008) Case histories in soil and rock erosion: Woodrow Wilson Bridge, Brazos River Meander, Normandy Cliffs, and New Orleans Levees. Journal of Geotechnical and Geoenvironmental Engineering, 134 (10), pp. 1425-1447

Briaud, J.L., Ting, F.C.K., Chen, H.C., Cao, Y., Han, S.W., and Kwak, K.W (2001) Erosion Function Apparatus for Scour Rate Predictions. Journal of Geotechnical and Geoenvironmental Engineering, 127(2), pp. 105-113

Brown, R.G. (1963) Smoothing, Forecasting and Prediction. Prentice-Hall: Englewood Cliffs

BS 1377-2 (1990) Methods of test for Soils for civil engineering purposes – Part 2: Classification tests. British Standard Institution.

Burns, B. (2006) Internal Erosion of Earth Embankments. Ph.D. Thesis. University of Birmingham

Carreto, J.M.R, Caldeira, L.M.M.S., and Maranha das Neves, E.J.L. (2016) Hydromechanical Characterization of Cement-Bentonite Slurries in the Context of Cutoff Wall Applications. Journal of Materials in Civil Engineering, 28 (2), 04015093

Chang, D. (2012) Internal Erosion and Overtopping Erosion of Earth Dams and Landslide Dams. Ph.D. Thesis. Hong Kong University of Science and Technology. Available at: http://repository.ust.hk/ir/Record/1783.1-7478

Chang, M. and Huang, R-C. (2015) Observations of hydraulic fracturing in soils through field testing and numerical simulations. Canadian Geotechnical Journal, Vol. 53, Number 2, pp. 343-359

Charles, J.A., and Boden, J.B. (1985) The failure of embankment dams in the United Kingdom. Failure in earthworks, pp. 181-202

Chevalier, C., Haghighi, I., and Herrier, G. (2012) Resistance to erosion of lime treated soils: a complete parametric study in laboratory. 6th International Conference on Scour and Erosion, Paris, France, pp. 1065-1072

Dascal, O. (1979) Structural behaviour of the Manicouagan 3 cutoff. Canadian Geotechnical Journal, 16(1), pp. 200–221

Deschênes, J.H., Massiéra, M., and Tournier, J.P. (1995) Testing of a cement- bentonite mix for a low-permeability plastic barrier. In Dredging, Remediation, and Contaminated Sediments (Demars, K.R., Richardson, G.N., Yong, R.N., and Chaney, R.C. (Editors)). ASTM STP 1293, ASTM, Philadelphia, PA, USA, pp. 252–270

Dinchak, W.G. (1985) Cement-Bentonite slurry walls limit seepage. [online] Available from http://www.concreteconstruction.net/concrete-articles/cement-bentonite- slurry-walls-limit-seepage.aspx

ECOCEM (2012) Material safety data sheet: Ground-granulated blast-furnace slag [online] Available from http://www.ecocem.ie/downloads/material_safety_sheet.pdf [Accessed 1 August 2018]

Eddleston, M. and Wan, C.F. (2014) Use of basic soil test data in internal erosion risk assessments. Dams and Reservoirs, 24(1), pp. 26-39

Escalante-Garcia, J.I. and Sharpe, J.H. (2004) The chemical composition and microstructure of hydration products in blended cements. ement and Concrete Composites, 26, pp. 967–p976

Evans, J.C. (1993) 'Vertical cutoff walls' in Daniel, D.E. Geotechnical Practice for Waste Disposal. Springer, pp. 430-454

Evans, J.C. (1994). Hydraulic Conductivity of Vertical Cutoff Walls. In Daniel, D. and Trautwein, S. (Eds.) STP1142-EB Hydraulic Conductivity and Waste Contaminant Transport in Soil, pp. 79-94

Fattahi, S. M., Soroush, A., and Shourijeh, P. T. (2017) The Hole Erosion Test: A Comparison of Interpretation Methods. Geotechnical Testing Journal, 40 (3)

Fauzilah, I., Zainab, M., Mukri, M. (2008) A study of the mechanism of internal erosion resistance to soil slope instability. The Electronic Journal of Geotechnical Engineering Vol. 13, Bundle A, pp. 12

Fell, R. and Fry, J.J. (2013) State of The Art on the Likelihood of Internal Erosion of Dams and Levees by Means of Testing, in Bonelli, S. and Nicot, F. (ed) Erosion in Geomechanics Applied to Dams and Levees. London: Taylor & Francis, pp. 1-99

Fell, R., MacGregor, P., Stapledon, D., Bell, G., and Foster, M. (2018) Geotechnical Engineering of Dams. London: CRC Press. 2nd Edition

Flores-Berrones, R. and Lopez-Acosta, N.P. (2011) Internal Erosion Due to Water Flow Through Earth Dams and Earth Structures. Soil Erosion Studies, Dr. Danilo Godone (Ed.), InTech.

Foster, M., Fell, R. and Spannagle, M. (2000). The statistics of embankment dam failures and accidents, Canadian Geotechnical Journal, 37 (5), National Research Council Canada, Ottawa, pp. 1000–1024

Fratalocchi, E., Manassero, M., Pasqualini, E., Roccato, M., and Spanna, C. (1996) Predicting hydraulic conductivity of cement-bentonite slurries. Proceedings of 2nd International Congress on Environmental Geotechnics, Osaka, Vol. 1, pp. 503-508

Fratalocchi, E., Pasqualini, E., Balboni, P., and Mozzi, R. (2006). Durability assessment of a confinement cutoff wall for a phosphogypsum landfill. Proceedings of the 16 th International Conference on Soil Mechanics and Geotechnical Engineering. Millpress Science Publishers, Rotterdam, The Netherlands, pp. 2257- 2260

Garand, P., Bigras, A., Rattue, D.A., Hammamji, Y., and Sauchet, J-P. (2006) Erosion Resistance of Plastic Concrete. Proceedings of 22nd ICOLD Congress, Barcelona. Q. 84, R. 25, Vol. 1, pp. 391-410

Garner, S.J. and Fannin, R.J. (2010) Understanding internal erosion: a decade of research following a sinkhole event. International Journal on Hydropower and Dams, Vol. 17, Issue 3, pp. 93-98

Garvin, S.L. and Hayles, C.S. (1999) The chemical compatibility of cement-bentonite cut-off wall material. Construction and Building Materials, 13, pp. 329-341

Ghanbari, A. and Rad, S.S. (2015) Development of an empirical criterion for predicting the hydraulic fracturing in the core of earth dams. Acta Geotecnica, Vol. 10, Issue 2, pp. 243-254

Guner, A. (1978) Properties and behaviour of bentonite-cement slurries. University of London PhD Thesis, pp. 279

Guyer, J.P. (2019) An Introduction to Embankment Dam Cutoff Walls. Independently published by J. Paul Guyer.

Haghighi, I., Chevalier, C., Duc, M., Guedon, S., and Reiffstech, P. (2013) Improvement of Hole Erosion Test and Results on Reference Soils. Journal of Geotechnical and Geoenvironmental Engineering, Vol. 139, No. 2, pp. 330-339

Hanson, G.J. (1991) Development of a jet index to characterize erosion resistance of soils in earthen spillways. Transactions of the ASAE, vol. 34, no. 5, pp. 2015-2020.

Hanson, G.J. (1992) Erosion resistance of compacted soils. Transportation Research Record 1369, pp. 16-30.

Hanson, G.J. and Cook, K.R. (2004) Apparatus, Test Procedures, and Analytical Methods to Measure Soil Erodibility in Situ. American Society of Agricultural Engineers. Vol. 20(4), pp. 455−462

Hanson, G.J. and Hunt, S.L. (2007) Lessons Learned Using Laboratory Jet Method to Measure Soil Erodibility of Compacted Soils. American Society of Agricultural and Biological Engineers, Vol. 23(3), pp. 305-312

Hark, M. (2019) A modified hole-erosion-test on high plastic clay with different soil structure. Scour and Erosion IX: Proceedings of the 9th International Conference on Scour and Erosion, Taipei, Taiwan, pp. 485-492

Head, K.H. (1982) Permeability, shear strength and compressibility tests. Manual of Soil Laboratory Testing Vol. 2

Henensal, P. and Duchatel, F. (1990) L'érodimètre à jets mobiles, Bull. Lab. Ponts et Chaussées, 167: pp. 47-53

Hinchberger, S., Weck, J., and Newson, T. (2010) Mechanical and hydraulic characterization of plastic concrete for seepage cut-off walls. Canadian Geotechnical Journal, 47(4), pp. 461-471.

ICOLD (1995) Bulletin 99: Dam Failures – Statistical Analysis. International Commission on Large Dams, Paris. Available from the Bulletins section of the ICOLD website: h ttp://www.icold-cigb.org

ICOLD (2011) ICOLD Constitution Status. Available from the ICOLD website: h ttp://www.icold-cigb.org

ICOLD (2013) Bulletin 150: Cutoffs for Dams. International Commission on Large Dams, Paris. Available from the Bulletins section of the ICOLD website: h ttp://www.icold-cigb.org

ICOLD (2015) Bulletin 164: Internal Erosion of Existing Dams, Levees and Dykes and their Foundations. International Commission on Large Dams, Paris. Available from the Bulletins section of the ICOLD website: h ttp://www.icold-cigb.org

Indraratna, B., Muttuvel, T., and Khabbaz, H. (2009) Modelling the erosion rate of chemically stabilized soil incorporating tensile force – deformation characteristics. Canadian Geotechnical Journal, 46(1), pp. 57-68

Indraratna, B., Muttuvel, T., Khabbaz, H. and Armstrong, R. (2008) Predicting the Erosion Rate of Chemically Treated Soil Using a Process Simulation Apparatus for Internal Crack Erosion. Journal of Geotechnical and Geoenvironmental Engineering, Vol. 134, No. 6, pp. 837-844

Institution of Civil Engineers (ICE) (1999) Specification for the construction of slurry trench cut-off walls. Thomas Telford, London

Jefferis, S. (2012) Cement-Bentonite Slurry Systems. Grouting and Deep Mixing 2012, pp. 1-24

Jefferis, S.A. (1981) Bentonite-cement slurries for hydraulic cut-offs, International Conference Soil Mechanics and Foundation Engineering Stockholm, June Vol 1, pp. 435-440

Jefferis, S.A. (1997) The origins of the slurry trench cut-off and a review of cement-bentonite cut-off walls in the UK. 1st International Containment Technology Conference and Exhibition, Florida, pp. 52-61

Jefferis, S.A. (2008) Reactive transport in cut-off walls and implications for wall durability. GeoCongress 2008, pp. 652–659

Jiang, L., Chirdchanin, M., and Katsutada, O. (2004) Stabilization effects of surplus soft clay with cement and GBF slag. Journal of Environmental Sciences (IOS Press), 2004, Vol.16 (3), p.397-404

Joshi, K., Kechavarzi, C., Sutherland, K., Ng, M.Y.A., Soga, K., and Tedd, P. (2010) Laboratory and In Situ Tests for Long-Term Hydraulic Conductivity of a Cement-Bentonite Cutoff Wall. Journal of Geotechnical and Geoenvironmental Engineering, Vol. 136, No. 4, pp. 562-572

Joshi, K., Soga, K., Ng, M.Y.A., and Kechavarzi, C. (2008) Durability study of eleven years old cement-betnonite cut-off wall material. Goecongress 2008, pp. 620–627

Ke and Takahashi (2014) Experimental investigations on suffusion characteristics and its mechanical consequences on saturated cohesionless soil. Soils and Foundations, 54 (4), pp. 713-730

Leonards, G.A., Huang, A.B., Ramos, J. (1991) Piping and erosion tests at Conner Run Dam. Journal of Geotechnical Engineering 117, pp. 108–117

Lim, S.S. (2006) Experimental investigation of erosion in variably saturated clay soil. Unpublished PhD Dissertation, Sydney: University of New South Wales

Luthi, M. (2011) A Modified Hole Erosion Test (HET-P) to Study Erosion Characteristics of Soil. Unpublished MSc Thesis, British Columbia: University of British Columbia

Luthi, M., Fannin, R.J., and Millar, R.G. (2012) A Modified Hole Erosion Test (HET-P) Device. Geotechnical Testing Journal, Vol. 35, No. 4, pp 1-5

Marot D, Le V, Garnier J, Thorel L, Audrain P. (2012) Study of scale effect in an internal erosion mechanism: centrifuge model and energy analysis. European Journal of Environmental and Civil Engineering, 16, pp. 1–19.

Marot, D., Reggazoni, P., and Wahl, T. (2011) An Energy-Based Method for Providing Soil Surface Erodibility Rankings. Journal of Geotechnical and Geoenvironmental Engineering, Vol. 137 (12), pp. 1290-1293

Marot, D., Rochim, A., Nguyen, H-H., Bendahmane, F., Sibille, L. (2016) Assessing the susceptibility of gap-graded soils to internal erosion: proposition of a new experimental methodology. Natural Hazards, Vol. 83(1), pp.365-388

Mattsson, H., Hellstrom, J.G.I, and Lundstrom, T.S. (2008) On Internal Erosion in Embankment Dams: A literature survey of the phenomenon and the prospect to model it numerically. Luleå University of Technology Research Report.

Mehenni, A., Cuisinier, O., and Masrouri, F. (2016) Impact of Lime, Cement, and Clay Treatments on the Internal Erosion of Compacted Soils. Journal of Materials in Civil Engineering, 04016071

Millet, R.A., Perez, J., and Davidson, R.R. (1992) USA Practice slurry wall specification 10 years later. In: Slurry Walls: Design, Construction, and Quality Control, D.B. Paul, R.R. Davidson and N.J. Cavalli, eds., STP 1129, ASTM, Philadelphia, PA, pp. 42-66

Mitchell, J.K. and Soga, K. (2005) Fundamentals of Soil Behavior. 3rd Edition, USA: John Wiley & Sons

Moody, L.F. (1944) Friction factors for pipe flow. Transactions of the American Society of Mechanical Engineers, 66 (8), pp. 671–684

Munson, B., Young, D. and Okiishi, T. (1998) Fundamentals of Fluid Mechanics. 3rd Edition, John Wiley & Sons, Inc., New York

Muttuvel, T. (2008) Erosion rate of chemically stabilized soils incorporating tensile stress-deformation behavior. Ph.D. Thesis, School of Civil, Mining and Environmental Engineering, University of Wollongong

Nadal-Romero, E., Verachtert, E., Poesen, J. (2011) Pinhole test for identifying susceptibility of different horizons in loess-derived soils to piping erosion. Geomorphology, 135, pp. 66-79

Nearing, M. (1991) A probabilistic model of soil detachment by shallow turbulent flow. Transactions of the American Society of Agricultural Engineers, Vol. 34, No. 1, pp. 81-85

Nearing, M.A. and Parker, S.C. (1994) Detachment of Soil by Flowing Water Under Turbulent and Laminar Conditions. Soil Science Society of America Journal, Vol. 58/No. 6, pp. 1612-1614

Nerincx, N., Bonelli, S., Puiatti, D., Herrier, G., Fry, J.J., Tourment, R. and Nicaise, S. (2016) Impact of lime treated soils performance on design of earthfill dikes. Proceeding of 3rd European Conference on Flood Risk Management

Ng, M.Y.A. (2009) Modelling of hydraulic fracturing in cement bentonite geomaterials. Unpublished PhD Dissertation, Cambridge: University of Cambridge

Opdyke, S.M., and Evans, J.C. (2005) Slag-cement-bentonite slurry walls. ASCE Journal of Geotechnical and Geoenvironmental Engineering, 131: pp. 673-681

Osouli, A., Karimpour, M., Zamiran, S., Ruholl, D., Behrends, B., Stendback, E., and Galle, K. (2014) Levee Erosion and Scour Potential Due to Floodwall Overtopping. Proceedings of 33rd Annual U.S. Society on Dams Conference, pp. 345-356

Regazzoni P, and Marot, D. (2013) A comparative analysis of interface erosion tests. Natural Hazards, 67, pp. 937–950.

Rice, J.D. (2007) A Study on the Long-Term Performance of Seepage Barriers in Dams. Unpublished PhD Dissertation, Blacksburg, Virginia: Virginia Polytechnic Institute and State University

Rice, J.D. and Duncan, J.M. (2010a) Findings of case histories on the long-term performance of seepage barriers in dams. Journal of Geotechnical and Geoenvironmental Engineering, Vol. 136, No. 1, pp. 2-15

Rice, J.D. and Duncan, J.M. (2010b) Deformation and cracking of seepage barriers in dams due to changes in the pore pressure regime. Journal of Geotechnical and Geoenvironmental Engineering, Vol. 136, No. 1, pp. 16–25.

Richards, K.S., and Reddy, K.R. (2007). Critical appraisal of piping phenomena in earth dams. Bulletin of Engineering Geology and the Environment. Vol. 66, No 4, pp. 381-402

Richardson IG, Groves GW (1992) Microstructure and microanalysis of hardened cement pastes involving ground granulated blast furnace slag. Journal of Materials Science, 27(22), pp. 6204 – 6212

Riha, J., and Jandora, J. (2015). Pressure conditions in the hole erosion test. Canadian Geotechnical Journal, 52, pp. 114-119

Rodney, B. (2008) Assessing the vulnerability of a typical British embankment dam to internal erosion. Ensuring reservoir safety into the future: Proceedings of the 15th Conference of the British Dam Society, pp. 13-28.

Royal, A. and Jefferson, I. (2017) Use of Wastes, Recycled Aggregates and Secondary Aggregates in Geotechnical Engineering Applications. in P Singh, V Singh, A Singh, D Kumbhakar & M Roy (eds), NexGen Technologies for Mining and Fuel Industries. vol. 1, Allied Publishers, New Delhi, India, pp. 719.

Royal, A.C.D., Makhover, Y., Moshirian, S. and Hesami, D. (2013) Investigation of cement-bentonite slurry samples containing PFA in the UCS and triaxial appartus. Geotech-nical and Geological Engineering 31: 767-781

Royal, A.C.D., Opukumo, A.W., Qadr, C.S., Perkins, L.M., and Walenna, M.A. (2018) Deformation and Compression Behaviour of a Cement-Bentonite Slurry for Groundwater Control Applications. Geotechnical and Geological Engineering.

Ryan, M. (2015) Internal Erosion in Cement-Bentonite using Pin-Hole Erosion Test. Unpublished MSc Project Report, Birmingham: University of Birmingham

Sezer, A., Inan, G., Yilmaz, H.R., and Ramyar, K. (2006) Utilization of a very high lime fly ash for improvement of Izmir clay. Building and Environment, Vol.41 (2), p.150- 156

Sharif, Y.A. (2013) Experimental Study on Piping Failure of Earthen Levee and Dams. Ph.D Thesis. University of South Carolina

Sherard, J.L., Dunningan, L., Decker, R.S., Steele, F. (1976) Pinhole test for identifying dispersive soils. Journal of the Geotechnical Engineering Division 102, pp. 69–85

Singh, A. K., Mishra, G. C., Samadhiya, N. K., and Ojha, C. S. P. (2006). Design of a Rigid Cutoff Wall. International Journal of Geomechanics, 6(4), pp. 215–225

Singh, V. (1996) Dam Breach Modeling Technology. Vol. 17, Netherlands, Springer

Sjodahl, P. (2006) Resistivity investigation and monitoring for detection of internal erosion and anomalous seepage in embankment dams. Ph.D Thesis. Lund University

Soga, K., Joshi, K., and Evans, J.C. (2013) Cement bentonite cutoff walls for polluted sites. In Coupled Phenomena in Environmental Geotechnics, 1st Edition. (Manassero, M., Dominijanni, A., Foti, S., and Musso, G. (Editors)). Taylor & Francis: London, UK.

Soroush, A., Shourijeh, P., and Fouladi, S. (2019) The Effects of Soil Erosion Characteristics on Critical Filter Design in Embankment Dams, Geotechnical Testing Journal, https://doi.org/10.1520/GTJ20170323. ISSN 0149-6115.

Talefirouz, D., Çokça, E., and Omer, J. (2016) Use of granulated blast furnace slag and lime in cement-bentonite slurry wall construction. International Journal of Geotechnical Engineering, 10(1), pp. 81-85

Tedd, P., Carter, I.C., Watts, K.S., and Charles, J.A. (2011) Investigating hydraulic fracture at a puddle clay core dam. Dams and Reservoirs, Vol. 21, Issue 3, pp. 123-135

TOLSA (2008) Technical Data Sheet: BerkbentBentonite 163. Madrid

Tosun, H., (1997) Comparative study on physical tests of dispersibility of soils used for earthfill dams in Turkey. Geotechnical Testing Journal 20, pp. 242–251

U.S. Department of the Interior Bureau of Reclamation (USBR) (2016) Teton Dam History and Facts. U.S. Department of the Interior Bureau of Reclamation.

U.S. Department of the Interior Bureau of Reclamation (USBR) (2014) Design Standards No. 13 Embankment Dams, Chapter 16: Cutoff Walls. U.S. Department of the Interior Bureau of Reclamation.

Walenna, M.A., Royal, A.C.D., Jefferson, I., and Ghataora, G.S. (2019) Investigating the erosion resistance of cement-bentonite barrier material using hole erosion test. Proceedings of the 9th International Conference on Scour and Erosion, pp. 103-109

Wan, C.F., and Fell, R. (2002) Investigation of internal erosion and piping of soils in embankment dams by the slot erosion test and the hole erosion test. UNICIV Report No R-412, University of New South Wales, Sydney.

Wan, C.F., and Fell, R. (2004) Investigation of rate of erosion of soils in embankment dams. Journal of Geotechnical and Geoenvironmental Engineering, 30, pp. 373– 380.

Wang, J-j., Zhang, H-p., Zhao, M-j., and Lin, X. (2009) Mechanisms of hydraulic fracturing in cohesive soil. Water Science and Engineering, Vol. 2, Issue 4, pp. 95- 102

Wang, Z., Zhao, B., and Royal, A.C.D. (2017) Investigation of Erosion of Cement-Bentonite via Piping. Advances in Materials Science and Engineering, ID 1762042

Warren, A. L. (2011). Investigation of dam incidents and failures. Proceedings of the Institution of Civil Engineers - Forensic Engineering, 164(1), 33–41.

Wen, L., Chai, J., Xu, Z., Qin, Y., and Li, Y. (2017) A statistical analysis on concrete cut-off wall behaviour. Proceedings of the Institution of Civil Engineers. 1700142

Xanthakos, P.P. (1979) Slurry Walls, McGraw-Hill Book Co., New York

Xu, Y., and Zhang, L.M. (2009) Breaching parameters of earth and rockfill dams. Journal of Geotechnical and Geoenvironmental Engineering, 135 (12), pp. 1957- 1970